ERROR BOUNDS OF COMPACT FINITE DIFFERENCE METHODS FOR SOME DISPERSIVE PDES AND APPLICATIONS

ZHANG TENG

NATIONAL UNIVERSITY OF SINGAPORE

2021

ERROR BOUNDS OF COMPACT FINITE DIFFERENCE METHODS FOR SOME DISPERSIVE PDES AND APPLICATIONS

ZHANG TENG

(B.Sc., Xi'an Jiaotong University)

A THESIS SUBMITTED

FOR THE DEGREE OF DOCTOR OF PHILOSOPHY

DEPARTMENT OF MATHEMATICS

NATIONAL UNIVERSITY OF SINGAPORE

2021

Supervisor:

Professor BAO Weizhu

Examiners:

Assistant Professor TONG Xin

Assistant Professor CAI Zhenning

Professor Christophe BESSE, Université Paul Sabatier Toulouse 3

DECLARATION

I hereby declare that the thesis is my original work and it has been written by me in its entirety. I have duly acknowledged all the sources of information which have been used in the thesis.

This thesis has also not been submitted for any degree in any university previously.

Zhang Teng

ZHANG Teng

April 12, 2021

Acknowledgements

It is my great honour here to thank those who made this thesis possible.

First and foremost, I wish to express my deepest gratitude to my supervisor Professor BAO Weizhu for his professional mentorship and guidance. Prof. BAO is a rigorous, brilliant and knowledgeable applied mathematician. He leads me to this exciting research field and his generous support and continuous encouragement pave the way for me to the research road.

I am fortunate to get involved in our research group and grateful to my colleagues, including but not limited to Prof. TANG Qinglin, Prof. WANG Tingchun, Dr. RUAN Xinran, Dr. SU Chunmei, Dr. ZHAO Quan, Dr. YIN Jia, Dr. LIN Bo, Dr. FENG Yue, Mr. GUO Yichen. Thanks for their help in research collaboration, seminar discussion, and help in life.

I also greatly appreciate NUS and Department of Mathematics for awarding me the scholarship and contributing to a great environment during my graduate study. I want to thank all of my peers in the office, Dr. QIAN lilong, Dr. WU Hao, Dr. XI Guojiang, Dr. YANG Ziyi, for good research atmosphere and valuable discussions.

Last but not least, thank my family for their encouragement and unconditional support. Without them, I would never have arrived at this stage of my life.

ZHANG Teng

MAR 2021

Contents

Summary

Dispersive partial differential equations (PDEs) have been arising widely from the fields of quantum mechanics, plasma physics and nonlinear optics. In many cases, the solutions of dispersive PDEs are highly oscillatory, which brings significant analytical and numerical difficulties. Thus, it is important to design efficient and accurate numerical methods for the oscillatory dispersive PDEs.

The aim of this thesis is to propose and analyse some fourth-order compact finite difference schemes (4cFDs) for approximating several highly oscillatory dispersive PDEs. Rigorous proofs of error estimates are presented and numerical results are reported to verify the error bounds. Finally, we apply the 4cFD to discretize the Laplace's equation satisfying nonstandard boundary conditions (BCs) for preparing the initial data in simulations of quantized vortex interactions of the nonlinear Schrödinger equation with periodic BCs.

This thesis mainly contains three parts. The first part considers the nonlinear Klein-Gordon equitation (NKGE) in the nonrelativistic regime with a dimensionless parameter $\varepsilon \in (0, 1]$ inversely proportional to the speed of light. Two 4cFDs including a Crank-Nicolson one and a semi-implicit one are derived for solving NKGE. Under proper assumption on the analytical solutions, error estimates of the two schemes are rigorously derived and they are at $O(h^4 + \tau^2/\varepsilon^6)$ with h mesh size and

τ time step. From the error bounds, the strategy in choosing time step and mesh size can be obtained. In addition, the energy conservation of the two schemes is also studied.

The second part is devoted to efficiently solving the Zakharov system (ZS) in the subsonic regime with a dimensionless parameter ε inversely proportional to the acoustic speed. The solutions of ZS have highly oscillatory waves and outgoing initial layers due to the perturbation from wave operator in ZS and the incompatibility of the initial data. The solutions propagate waves with $O(\varepsilon)$ wavelength in time, $O(1/\varepsilon)$ speed in space, and $O(\varepsilon^2)$ and $O(1)$ amplitudes for well-prepared and ill-prepared initial data, respectively. The high oscillation brings noticeable difficulties in analysing the error bounds of numerical methods to ZS. At first, a conservative semi-implicit 4cFD for ZS is given. For the well- and less-ill-prepared initial data, a uniform error bound at $O(h^4 + \tau^{2\alpha^\dagger/3})$ is derived, where $1 \leq \alpha^\dagger \leq 2$ is a parameter independent of ε determined by the illness of initial data of ZS; and for the ill-prepared initial data, an error bound at $O(h^4/\varepsilon^{1-\alpha^*} + \tau^2/\varepsilon^{3-\alpha^*})$ is derived with $0 \leq \alpha^* \leq 1$ a nonnegative parameter independent of ε describing the illness of initial data. Then, a 4cFD for ZS in an asymptotic consistent formulation is given to achieve uniform error bounds for both well- and ill-prepared initial data. The uniform error bound for the well prepared initial data is $O(h^4 + \tau^{4/3})$ and the error bound for the ill-prepared initial data is $O(h^4 + \tau^{(1+\alpha^*)/(2+\alpha^*)})$. The main tools in the proof include energy methods, cut-off techniques, and the error between ZS and its limiting equation. The compact schemes provide much better spatial resolution than standard second order finite difference methods. Thus, the computational cost can be reduced a lot, especially for cases with ill-prepared initial data. Since we have uniform error bounds, the mesh size can be chosen independently of ε.

The last part is an application of the compact finite difference scheme to a numerical simulation of interactions of quantized vortices under the nonlinear Schrödinger equation with periodic BCs in two dimensions. An efficient way of initial setups via solving the Laplace's equation with non-standard boundary condition by a 4cFD is proposed. The numerical simulation results confirm the existing reduced dynamical laws in the case that the initial data satisfy the zero momentum limit condition. We also study vortex dynamics for initial data with nonzero momentum limit and vortex interactions on rectangle domains. Based on our results, we formulate a conjecture on generalized reduced dynamical laws for vortex dynamics of NLSE with periodic BCs.

List of Tables

List of Figures

List of Symbols and Abbreviations

t	time variable
$\boldsymbol{x}$	spatial variable
i	imaginary unit
ε	a dimensionless parameter in $(0,1]$
$\mathbb{R}^d$	d-dimensional Euclidean space
$\mathbb{C}^d$	d-dimensional complex space
h	spatial mesh size
τ	time step size
∇	gradient
Δ	Laplace operator
$v \lesssim w$	for $v, w \geq 0$, $v \leq Cw$ for some generic constant $C \geq 0$
$\bar{u}$	conjugate of a complex number u
NKGE	nonlinear Klein-Gordon equation
ZS	Zakharov system
NLSE	nonlinear Schrödinger equation
4cFD	fourth-order compact finite difference scheme
CN-4cFD	Crank-Nicolson 4cFD
SI-4cFD	semi-implicit 4cFD

CSI-4cFD	conservative semi-implicit 4cFD
UA-4cFD	uniform accurate 4cFD
CNFD	Crank-Nicolson finite difference scheme
SIFD	semi-implicit finite difference scheme
RDLs	reduced dynamical laws

Chapter 1

Introduction

This chapter serves as an introduction of this thesis. Firstly, the background of dispersive partial differential equations (PDEs) and three typical nonlinear dispersive PDEs with high oscillations are introduced. Then, the compact finite difference methods are briefly reviewed, and the main contributions of this thesis are given.

1.1 Motivation

Dispersive partial differential equations refer to PDEs with solutions experiencing dispersion phenomena that waves of different wavelength propagate at different phase velocities [76]. Dispersive PDEs have been widely used in the modelling of quantum mechanics, plasma physics, and nonlinear optics [24,50,63]. Based on their vast applications, there are extensive studies on dispersive PDEs both analytically [1,76,92,107] and numerically [13,24,106].

In some singular limit regimes, such as nonrelativistic, subsonic, and semi-classical limit regimes, the oscillation in solutions of dispersive PDEs will give severe numerical burdens [16,116]. Without designing special solver based on the structure of the waves of the solutions, the Shannon sampling theorem [62] requires us to resolve the finest wavelength properly, i.e., using several grid points per wavelength, in order to get accurate numerical results. And, applications to real-world problems, especially in two or three dimensional space, give rise to a demand of the spatial discretization formulations with high resolution capacity as well as low computation and memory cost.

1.2 Some oscillatory dispersive PDEs

1.2.1 Nonlinear Klein-Gordon equation (NKGE)

The Klein-Gordon equation is the relativistic version of the Schrödinger equation, which describes the quantized version of the relativistic energy-momentum relation. It is prevalently adopted to model bosons without spin, such as the Higgs boson and the weakly-interacting massive particles. The nonlinear Klein-Gordon equation (NKGE) in d dimensions reads

$$\frac{\hbar^2}{mc^2}\partial_{tt}u(\mathbf{x},t) - \frac{\hbar^2}{m}\Delta u(\boldsymbol{x},t) + mc^2 u(\boldsymbol{x},t) + f(u(\boldsymbol{x},t)) = 0, \quad \mathbf{x} \in \mathbb{R}^d, t > 0, \quad (1.2.1)$$

where t is time, $\boldsymbol{x}$ is the spatial coordinate in d dimensions with $d = 1, 2, 3$, m is mass of the particles, c is the speed of light and $\hbar$ is the reduced Plank constant. Applying the change of variables: $t \to \frac{\hbar}{m\varepsilon^2 c^2}t$ and $\boldsymbol{x} \to \frac{\hbar}{m\varepsilon c}\boldsymbol{x}$ with $\varepsilon = \frac{1}{\sqrt{m}c}$, the NKGE (1.2.1) takes the following dimensionless form [9, 24, 48, 79, 99, 111]:

$$\varepsilon^2\partial_{tt}u(\boldsymbol{x},t) - \Delta u(\boldsymbol{x},t) + \frac{1}{\varepsilon^2}u(\boldsymbol{x},t) + f(u(\boldsymbol{x},t)) = 0, \quad \boldsymbol{x} \in \mathbb{R}^d, \ t > 0, \qquad (1.2.2)$$

with initial conditions

$$u(\boldsymbol{x},0) = u_0(\boldsymbol{x}), \ \partial_t u(\boldsymbol{x},0) = \frac{1}{\varepsilon^2}u_1(\boldsymbol{x}), \quad \boldsymbol{x} \in \mathbb{R}^d. \qquad (1.2.3)$$

Here, ε is a dimensionless parameter in $(0, 1]$ which is inversely proportional to the speed of light, $u = u(\boldsymbol{x}, t)$ is the unknown complex-valued wave function with temporal wavelength of $O(\varepsilon^2)$, u_0 and u_1 are $O(1)$ functions determining the initial data, $f(u) : \mathbb{C} \to \mathbb{C}$ is a given gauge invariant nonlinearity describing the nonlinear interaction [48], which is independent of ε and satisfies

$$f(e^{i\theta}u) = e^{i\theta}f(u), \quad \forall\theta \in [0, 2\pi].$$

In most applications and theoretical investigations of NKGE (1.2.2) , $f(u)$ is taken as the pure power nonlinearity [52, 53, 80, 81, 103], i.e.

$$f(u) = g(|u|^2)u, \text{ with } g(\rho) = \lambda\rho^p \text{ for some } \lambda \in \mathbb{R}, p \in \mathbb{N}.$$

When $p = 1$, the nonlinear term $f(u) = \lambda|u|^2u$ describes the standard cubic nonlinear interaction in real application on radiation theory, plasma physics, general relativity and quantum vortices [45, 59, 120]. An important feature of NKGE (1.2.2) is that it preserves the total energy [24, 79, 89]

$$\begin{aligned} E(t) &:= \int_{\mathbb{R}^d} \left[\varepsilon^2|\partial_t u|^2 + |\nabla u|^2 + \frac{1}{\varepsilon^2}|u|^2 + F(|u|^2)\right] \mathrm{d}\boldsymbol{x} \\ &\equiv E(0) = \int_{\mathbb{R}^d} \left[\frac{1}{\varepsilon^2}(|u_0|^2 + |u_1|^2) + |\nabla u_0|^2 + F(|u_0|^2)\right] \mathrm{d}\boldsymbol{x}, \quad t \geq 0, \end{aligned} \tag{1.2.4}$$

where

$$F(\rho) = \int_0^\rho g(s)\mathrm{d}s = \frac{\lambda}{p+1}\rho^{p+1}. \tag{1.2.5}$$

Since Klein-Gordon equation was proposed in 1920s, extensive analytical and numerical studies of the equation have been carried out in the literature. These studies include existence and uniqueness of analytical solutions [80, 81, 100, 103] as well as all kinds of different schemes for numerical solutions from finite difference time domain methods [9, 12, 24, 31, 43, 49, 87, 105] to spectral methods [8, 33, 46, 70] and time integrator methods [8,9,11,117]. A recent work of Bao and Zhao in [24] has reviewed lots of finite difference schemes including Crank-Nicolson, leap-frog, semi-implicit and explicit finite difference methods, which are all second order methods in space. However, there are few studies on designing high order finite difference schemes for NKGE in the nonrelativistic regime.

1.2.2 Zakharov system (ZS)

Consider the Zakharov system (ZS) in d dimensions describing the propagation of Langmuir waves in plasma,

$$
\begin{cases}
i\partial_t E^\varepsilon(\boldsymbol{x},t)+\Delta E^\varepsilon(\boldsymbol{x},t)-N^\varepsilon(\boldsymbol{x},t)E^\varepsilon(\boldsymbol{x},t)=0, & \boldsymbol{x}\in\mathbb{R}^d,\ \ t>0,\\
\varepsilon^2\partial_{tt}N^\varepsilon(\boldsymbol{x},t)-\Delta N^\varepsilon(\boldsymbol{x},t)-\Delta\left|E^\varepsilon(\boldsymbol{x},t)\right|^2=0, & \boldsymbol{x}\in\mathbb{R}^d,\ \ t>0,\\
E^\varepsilon(\boldsymbol{x},0)=E_0(\boldsymbol{x}),\ N^\varepsilon(\boldsymbol{x},0)=N_0^\varepsilon(\boldsymbol{x}),\ \partial_t N^\varepsilon(\boldsymbol{x},0)=N_1^\varepsilon(\boldsymbol{x}), & \boldsymbol{x}\in\mathbb{R}^d,
\end{cases}
\tag{1.2.6}
$$

where $E^\varepsilon(\boldsymbol{x},t)$ is a complex function describing the slowly varying envelope of a high-frequency plasma field, $N^\varepsilon(\boldsymbol{x},t)$ is a real function representing the plasma ion density fluctuation from its equilibrium position, $\boldsymbol{x}$ is the spatial coordinate, t is the temporal coordinate, and $\varepsilon\in(0,1]$ is a dimensionless parameter inversely proportional to the ion acoustic speed. $E_0(\boldsymbol{x})$, $N_0^\varepsilon(\boldsymbol{x})$ and $N_1^\varepsilon(\boldsymbol{x})$ are given initial data with $N_1^\varepsilon(\boldsymbol{x})$ satisfying $\int_{\mathbb{R}^d} N_1^\varepsilon(\boldsymbol{x})\mathrm{d}\boldsymbol{x}=0$.

The Zakharov system is a simplified model to describe the nonlinear interaction between the envelope of the electric field E^ε and the mean mode of the ionic fluctuations of density N^ε in plasma. The Schrödinger operator is three-scale approximation of Maxwell's equations and the wave operator is the classical long-wave approximation of the Euler equations [64,108]. There have been extensive theoretical and numerical studies on the ZS (1.2.6) since Zakharov described the propagation of Langmuir waves in plasma [122]. For the analytical part, the well-posedness of the Cauchy problem for ZS is discussed in [2, 30, 51]; the well-posedness of ZS in the subsonic regime and their convergence to a nonlinear Schrödinger equation are given in [30, 82, 91, 98]; blow-up solutions for ZS are considered in [54, 84]. For the numerical part, an energy preserving first order finite difference method was firstly given in [55, 56]. Then Chang, Guo and Jiang improved the estimate to the optimal second-order convergence [38]. For methods other than finite difference methods, Bao, Sun and Wei proposed exponential-wave-integrator spectral methods in [19]. Spectral time splitting methods are considered [18,63]. In [106], Su gave an overview of several pseudo-spectral and time-splitting methods. For other numerical methods, we refer to [10, 16, 17, 78, 112, 118] and references therein.

From the analytical analysis on ZS in [30, 51], we know that the ZS (1.2.6) conserves the wave energy

$$M^\varepsilon(t) = \|E^\varepsilon(\cdot,t)\|^2_{L^2(\mathbb{R}^d)} := \int_{\mathbb{R}^d} |E^\varepsilon(\boldsymbol{x},t)|^2 \,\mathrm{d}\boldsymbol{x} \equiv \int_{\mathbb{R}^d} |E_0(\boldsymbol{x})|^2 \,\mathrm{d}\boldsymbol{x} = M^\varepsilon(0), \quad t \geq 0, \tag{1.2.7}$$

and the Hamiltonian

$$H^\varepsilon(t) := \int_{\mathbb{R}^d} \left[|\nabla E^\varepsilon|^2 + N^\varepsilon |E^\varepsilon|^2 + \frac{1}{2}\left(\varepsilon^2 |\nabla U^\varepsilon|^2 + |N^\varepsilon|^2\right)\right] \mathrm{d}\boldsymbol{x} \equiv H^\varepsilon(0), \quad t \geq 0, \tag{1.2.8}$$

with $U^\varepsilon := U^\varepsilon(\boldsymbol{x},t)$ defined by

$$\begin{cases} \Delta U^\varepsilon(\boldsymbol{x},t) = -\partial_t N^\varepsilon(\boldsymbol{x},t), & \boldsymbol{x} \in \mathbb{R}^d, \\ \lim_{|\boldsymbol{x}|\to\infty} U^\varepsilon(\boldsymbol{x},t) = 0, & t \geq 0. \end{cases} \tag{1.2.9}$$

As pointed out in [2, 32, 82], under some proper assumptions on the compatible condition for the initial data, the ZS (1.2.6) converges to a cubic nonlinear Schrödinger equation (NLSE)

$$\begin{cases} i\partial_t E(\boldsymbol{x},t) + \Delta E(\boldsymbol{x},t) + |E(\boldsymbol{x},t)|^2 E(\boldsymbol{x},t) = 0, & \boldsymbol{x} \in \mathbb{R}, \quad t > 0, \\ E(\boldsymbol{x},0) = E_0(\boldsymbol{x}), & \boldsymbol{x} \in \mathbb{R}, \end{cases} \tag{1.2.10}$$

as $\varepsilon \downarrow 0$. The compatibility of the initial data between the ZS (1.2.6) and the NLSE (1.2.10) indicates that the initial values of (1.2.6) satisfy

$$N_0^\varepsilon(\boldsymbol{x}) = -|E_0(\boldsymbol{x})|^2 + \varepsilon^\alpha w_0(\boldsymbol{x}), \tag{1.2.11}$$

$$N_1^\varepsilon(\boldsymbol{x}) = 2\,\mathrm{Im}(\bar{E}_0(\boldsymbol{x})\Delta E_0(\boldsymbol{x})) + \varepsilon^{\beta-1} w_1(\boldsymbol{x}), \tag{1.2.12}$$

with $\alpha, \beta \geq 0$ non-negative parameters for $w_0(\boldsymbol{x})$ and $w_1(\boldsymbol{x})$ smooth enough $O(1)$ functions. The initial data are classified into well-prepared ($\alpha, \beta \geq 2$), less-ill-prepared ($\min\{\alpha,\beta\} \in [1,2)$), and ill-prepared ($\min\{\alpha,\beta\} \in [0,1)$) cases through considering the leading order oscillatory term in the density N^ε [2, 17, 32, 82]:

1. The leading order oscillation for the well-prepared initial data comes from the $\varepsilon^2\partial_{tt}N^\varepsilon$ term in equation with scale $O(\varepsilon^2)$;

2. The leading order oscillations for the less-ill-prepared initial data comes from the first initial layer with scale $O(\varepsilon^{\min\{\alpha,\beta\}})$ and bounded expansion term $\partial_t N^\varepsilon$;

3. The leading order oscillations for the ill-prepared initial data comes from the first $O(\varepsilon^{\min\{\alpha,\beta\}})$ initial layer of N^ε with unbounded $\partial_t N^\varepsilon$ of scale $O(\varepsilon^{\min\{\alpha,\beta\}-1})$.

Due to the fast out-going initial layer from the wave operator in (1.2.6), the computational domain should be of order $O(1/\varepsilon)$. The high oscillation in time and the large computational domain in space demand a spatial discretization formulation with high resolution to achieve a small memory and computational cost.

1.2.3 Nonlinear Schrödinger equation (NLSE)

The nonlinear Schrödinger equation (NLSE), also called the Gross-Pitaevskii equation, is a well-known mean-field model for the dynamics of a quantum system of weakly interacting identical bosons near absolute zero temperature, such as the Bose-Einstein condensation [6, 13, 28, 34]. It is a frequently used model for the simulation of quantized vortices in superfluids and Bose-Einstein condensation. Consider a NLSE with a dimensionless parameter $\varepsilon > 0$ in a two dimensional (2D) rectangular domain $\Omega = (0, a) \times (0, b)$:

$$i\partial_t \psi^\varepsilon(\boldsymbol{x}, t) = \Delta\psi^\varepsilon + \frac{1}{\varepsilon^2}(1 - |\psi^\varepsilon|^2)\psi^\varepsilon, \qquad \boldsymbol{x} = (x, y) \in \Omega, t > 0, \tag{1.2.13}$$

with initial condition

$$\psi^\varepsilon(\boldsymbol{x}, 0) = \psi_0^\varepsilon(\boldsymbol{x}), \quad \boldsymbol{x} \in \Omega, \tag{1.2.14}$$

and satisfying the periodic boundary conditions (BCs) on Ω.

As mentioned in [6, 15, 36], the NLSE (1.2.13) has properties of mass conservation, energy conservation and momentum conservation. With mass, energy and momentum defined as

$$M(t) = \int_\Omega |\psi^\varepsilon(\boldsymbol{x}, t)|^2 \mathrm{d}\boldsymbol{x}, \tag{1.2.15}$$

$$E(t) = \int_\Omega [\frac{1}{2}|\nabla\psi^\varepsilon(\boldsymbol{x}, t)|^2 + \frac{1}{4\varepsilon^2}(1 - |\psi^\varepsilon(\boldsymbol{x}, t)|^2)^2]\mathrm{d}\boldsymbol{x}, \tag{1.2.16}$$

$$\mathbf{P}(t) = \mathrm{Im}\left(\int_\Omega \bar{\psi}^\varepsilon(\boldsymbol{x}, t)\nabla\psi^\varepsilon(\boldsymbol{x}, t)\mathrm{d}\boldsymbol{x}\right). \tag{1.2.17}$$

When taking $\psi_0^\varepsilon(\boldsymbol{x}) = C$ as a constant initial, the (1.2.13) has an analytical solution

$$\psi^\varepsilon(\boldsymbol{x}, t) = C \exp(it(|C|^2 - 1)/\varepsilon^2). \tag{1.2.18}$$

The solution of (1.2.13) experiences high temporal oscillations even with simple constant initials as (1.2.18) showed.

Quantized vortex refers to a quantized flux circulation of some physical quantity, such as the circle of quantized super current carrying magnetic flux in the type II superconductors [39] and the quantized angular momentum in superfluid and Bose-Einstein condensate [25]. In the mathematical model, it is a topological defect of the order parameters ψ^ε with the distinguished property that the flux circulation $\int_\gamma \nabla \arg(\psi^\varepsilon) \cdot \mathrm{d}\vec{l}$ (with γ a closed curve in Ω) is quantized, which means the the flux circulation of a vortex can only take several fixed discrete numbers [25, 47, 65]. For example, the circulation of the velocity of superfluid governed by the dimensionless NLSE along any circle enclosing a vortex takes value of $2n\pi$, with $n \in \mathbb{Z}\backslash\{0\}$. In two dimensional space, the vortex center refers to a point where the value of ψ^ε is zero, which is a two dimensional simplification of rectilinear vortex lines in three dimensional space [39, 93]. The leading order of quantized vortex interactions of the superfluid governed by the nonlinear Schrödinger equation are summarized into some ODE system sketching the motion of vortex centers called reduced dynamical laws as described in [25, 41, 47, 61, 72–75].

1.3 Fourth-order compact finite difference (4cFD) methods

Compact finite difference schemes are frequently used in higher-order numerical solvers for the Navier-Stokes equations for their efficiency and stability [35, 44, 58, 69, 110, 123]. The key idea of compact finite schemes is to approximate the derivative with fewer grid points with implicit finite difference operator than the explicit central difference method. [68] gives a summary on systematic procedure to construct higher order compact schemes for first, second and third derivatives up to tenth order compact schemes. Among the compact finite difference schemes, the fourth-order compact finite difference scheme (4cFD) is a most commonly used one [113,114,116, 119,129]. We quote the derivation of fourth-order compact finite difference operator in [68] as follows.

Given a uniform spatial mesh h in one dimensional space with nodes denoted by $x_j = jh$, for a smooth function $f(x)$, let $f_j = f(x_j)$ and let f''_j be the finite difference approximation to $f''(x_j)$. Write the approximation in form

$$\begin{aligned}\beta f''_{j-2}+&\alpha f''_{j-1} + f''_j + \alpha f''_{j+1} + \beta f''_{j+2} \\ &= a\frac{f_{j+1} - 2f_j + f_{j-1}}{h^2} + b\frac{f_{j+2} - 2f_j + f_{j-2}}{4h^2} + c\frac{f_{j+3} - 2f_j + f_{j-3}}{9h^2},\end{aligned} \tag{1.3.1}$$

and balance the coefficients a, b, c and α, β by matching the coefficients of monomials of h from the Taylor expansions of $f(x)$ at $x'_j s$ from low degree to high. The first unmatched coefficient determines the order of the approximation in (1.3.1). The constraints on the coefficients for approximation orders are:

$$a + b + c = 1 + 2\alpha + 2\beta, \quad \text{(second order)} \tag{1.3.2}$$

$$a + 2^2 b + 2^2 c = \frac{4!}{2!}(\alpha + 2^2\beta), \quad \text{(fourth order)} \tag{1.3.3}$$

$$a + 2^4 b + 2^4 c = \frac{6!}{4!}(\alpha + 2^4\beta), \quad \text{(sixth order)} \tag{1.3.4}$$

$$\cdots\cdots$$

Equation (1.3.2) and (1.3.3) together provide the requirement for a fourth order approximation. In order to get a compact scheme with less stencil on both sides of (1.3.1), we choose $c = \beta = 0$. Then, we have

$$a = \frac{4}{3}(1 - \alpha), \; b = \frac{1}{3}(10\alpha - 1). \tag{1.3.5}$$

Let $b = 0$, we have three-node stencils on both sides of (1.3.1)

$$\frac{1}{10} f''_{j-1} + f''_j + \frac{1}{10} f''_{j+1} = \frac{6}{5}\frac{f_{j+1} - 2f_j + f_{j-1}}{h^2}. \tag{1.3.6}$$

Denote the finite difference operator $\delta_x^2 f_j = \frac{f_{j+1}-2f_j+f_{j-1}}{h^2}$ and $\mathcal{A}_h = I + \frac{h^2}{12}\delta_x^2$, then (1.3.6) can be expressed as

$$\mathcal{A}_h f_j'' = \delta_x^2 f_j. \tag{1.3.7}$$

We get the fourth order compact finite difference approximation to the second order derivatives of the form

$$f_j'' = \mathcal{A}_h^{-1}\delta_x^2 f_j. \tag{1.3.8}$$

1.4 Contributions

As pointed out in Section 1.2, although there has been much effort devoted to solve the above dispersive PDEs numerically, high resolution schemes and low computational cost methods are still in demand, and detailed error bound of the proposed schemes are worth studying.

By extending the second order finite difference operator to the fourth-order compact finite difference operator, we get two 4cFDs for NLKG, including a Crank-Nicolson one and a semi-implicit one. The optimal error estimates and the strategy in choosing time step are rigorously analysed, and the energy conservation in the discrete sense is also studied. With a proper smoothness and boundedness assumption on the analytical solutions, we can prove that errors of the two schemes are both of $O(h^4 + \frac{\tau^2}{\varepsilon^6})$ through the energy methods and cut-off techniques.

For the Zakharov system in the subsonic regime, we also provide two 4cFDs, including a conservative semi-implicit one and a uniform accurate one. The conservative semi-implicit 4cFD has error bounds independent of ε only for well and less-ill prepared initial data, and the uniform accurate 4cFD from an asymptotic consistent formulation of ZS achieves uniform error bounds for both well and ill prepared initial data. The uniform error bounds are constructed by the minimum of the error bounds from energy method and the error bounds from the limiting equation.

For the application of the 4cFD to the quantized vortices under the nonlinear Schrödinger equation with periodic BCs in 2D space. A method for initial setups via solving a Laplace's equation with non-standard BCs is proposed. The numerical simulation results coincide well with the existing reduced dynamical laws and further simulations provide a conjecture on the generalization of the existing reduced dynamical laws.

1.5 Organization of the thesis

This thesis is organized as follows.

In Chapter 2, two fourth-order compact finite difference schemes are given to NKGE in the nonrelativistic regime. Detailed proof of solvability, stability and error bounded of the schemes are given. Chapter 3 and 4 focus on the Zakharov system in the subsonic regime. A Hamilton conservative semi-implicit fourth-order compact finite difference scheme is given in Chapter 3; and a uniform accurate scheme from the discretization of ZS in asymptotic consistent formulation is considered in Chapter 4. Chapter 5 is a numerical application on the simulation of quantized vortex of NLSE in 2D with periodic BCs. Chapter 6 draws a conclusion of the thesis and discusses some possible future works.

Chapter 2

Error Bounds of 4cFDs for NKGE

In this chapter, we aim to derive and analyse two fourth-order compact finite difference schemes, a conservative Crank-Nicolson scheme and a semi-implicit scheme, for solving the complex nonlinear Klein-Gordon equation with power nonlinearity in the nonrelativistic limit regime

$$\varepsilon^2\partial_{tt}u(\boldsymbol{x},t) - \Delta u(\boldsymbol{x},t) + \frac{1}{\varepsilon^2}u(\boldsymbol{x},t) + \lambda|u(\boldsymbol{x},t)|^p u(\boldsymbol{x},t) = 0, \quad \boldsymbol{x} \in \mathbb{R}^d,\ t > 0, \tag{2.0.1}$$

with initial conditions

$$u(\boldsymbol{x},0) = u_0(\boldsymbol{x}),\ \partial_t u(\boldsymbol{x},0) = \frac{1}{\varepsilon^2}u_1(\boldsymbol{x}), \quad \boldsymbol{x} \in \mathbb{R}^d. \tag{2.0.2}$$

Solvability, stability, and proof of the error bounds of the schemes are given.

2.1 NKGE in the nonrelativistic regime and time oscillation

For simplicity, we only show the schemes and analysis in one spacial dimension. Generalizations to higher dimensions are straightforward. For numerical computation, we truncate our computational domain into an interval $\Omega = (a, b)$ with homogeneous Dirichlet boundary conditions. That is to say, we consider the initial-boundary value problem of NKGE as follows,

$$\varepsilon^2\partial_{tt}u(x,t) - \partial_{xx}u(x,t) + \frac{1}{\varepsilon^2}u(x,t) + \lambda|u(x,t)|^p u(x,t) = 0,\ x \in \Omega, t > 0, \tag{2.1.1}$$

$$u(a,t) = u(b,t) = 0, \quad t \geq 0, \tag{2.1.2}$$

$$u(x,0) = u_0(x),\ \partial_t u(x,0) = \frac{1}{\varepsilon^2}u_1(x), \quad x \in \bar{\Omega}. \tag{2.1.3}$$

The key point of the high-order compact finite difference method is to approximate the derivative with the fewest nodes to get the expected accuracy. The compact schemes draw great interest in numerical PDEs since they play an important role in the simulation of high frequency wave phenomena [26, 68, 86, 113, 130]. The fourth-order compact finite difference scheme is the most simple case to achieve higher spatial order with same amount of grids used in each spatial direction compared with the central difference method.

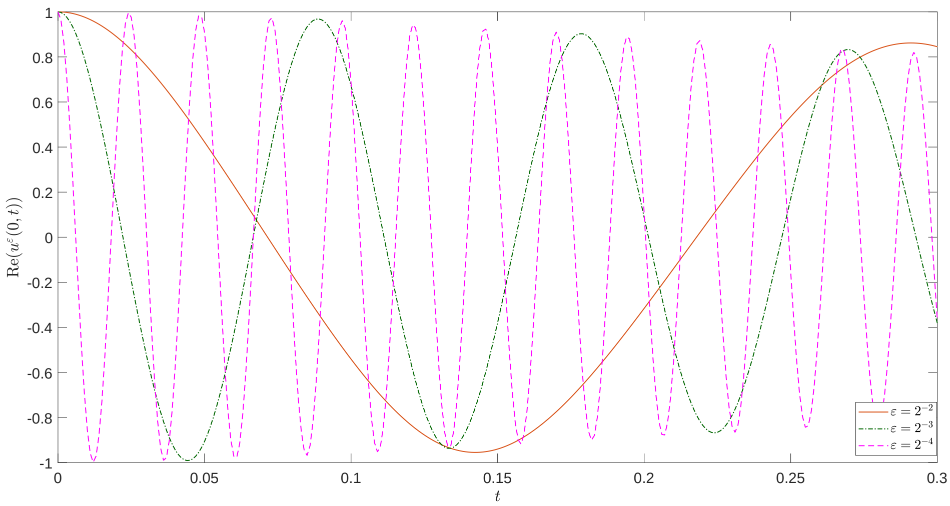

Figure 2.1: Oscillations at point $x = 0$ in time direction for different ε's.

Apart from the energy conservation in Chapter 1, the high oscillation in time is another key property of the NKGE in the nonrelativistic regime. As indicated in [8, 81, 88], the NKGE (2.0.1) has $O(\varepsilon^2)$ length waves propagating in time direction as $\varepsilon \downarrow 0$. We plot the real part of $u^\varepsilon(0,t)$ in Figure 2.1 for different ε's. The three simulations have the same u_0 and u_1 in initial data as stated in the beginning of Section 2.2.3. The figure contains nearly one period of wave for the case $\varepsilon = \frac{1}{4}$ and 4 waves for the case $\varepsilon = \frac{1}{8}$. In each interval that contains one wave of case $\varepsilon = \frac{1}{8}$, there are almost 4 waves for the case with $\varepsilon = \frac{1}{16}$. This supports the asymptotic analysis results and suggests that we need time step τ fine enough and also depending on ε to catch the oscillations in time direction. This also explains why we cannot get ride of the dependency on ε for the temporal error for the finite difference schemes.

The remainder of this chapter is organized as follows. In Section 2.2, the commonly used second order Crank-Nicolson scheme is extended to a fourth-order compact scheme, stability conditions and energy conservations are also discussed. The corresponding error bounds are analysed rigorously. In Section 2.3, the scheme of SI-4cFD is given. The solvability, error estimate and numerical simulation results are also provided. Several numerical simulation results and comparison with second order methods are reported in Section 2.4.

2.2 Conservative Crank-Nicolson 4cFD (CN-4cFD) for NKGE

In this section, we derive an implicit and a semi-implicit fourth-order compact finite difference schemes for NKGE and analyse their stability conditions. Define mesh size $h := (b-a)/J$ and time step $\tau := T/N$ with J, N two positive integers and $T > 0$ a fixed time we compute to. Denote the grid points and time steps as:

$$x_j := a + jh, j = 0, 1, \ldots, J;\ t_n := n\tau, n = 0, 1, \ldots, N.$$

Define $\mathcal{T}_J = \{1, 2, \cdots, J-1\}$ and $\mathcal{T}_J^0 = \{0, 1, 2, \cdots, J\}$ as the index sets of grid points. Let u_j^n denote the numerical approximation of $u(x_j, t_n)$ for $j \in \mathcal{T}_J^0$ and let X_J be a space of complex-valued grid functions defined as

$$X_J = \{u = \{u_j\} \mid j \in \mathcal{T}_J^0, u_0 = u_J = 0\} \subset \mathbb{C}^{J+1}. \tag{2.2.1}$$

We use the standard finite difference operators as noted in [9]:

$$\delta_t^+ u_j^n = \frac{u_j^{n+1}-u_j^n}{\tau}, \quad \delta_t^- u_j^n = \frac{u_j^n-u_j^{n-1}}{\tau}, \quad \delta_t^2 u_j^n = \delta_t^-\delta_t^+ u_j^n = \frac{u_j^{n+1}-2u_j^n+u_j^{n-1}}{\tau^2},$$
$$\delta_x^+ u_j^n = \frac{u_{j+1}^n-u_j^n}{h}, \quad \delta_x^- u_j^n = \frac{u_j^n-u_{j-1}^n}{h}, \quad \delta_x^2 u_j^n = \delta_x^-\delta_x^+ u_j^n = \frac{u_{j+1}^n-2u_j^n+u_{j-1}^n}{h^2}.$$

The spatial 4th-order compact finite difference operator $\mathcal{A}_h$ is defined as

$$\mathcal{A}_h u_j^n = \frac{1}{12}(u_{j-1}^n + 10u_j^n + u_{j+1}^n), \quad j \in \mathcal{T}_J. \tag{2.2.2}$$

This is directly from

$$\mathcal{A}_h u_j^n = (I + \frac{h^2}{12}\delta_x^2)u_j^n, \quad j \in \mathcal{T}_J, \tag{2.2.3}$$

where I denotes identical operator. As in [68,77,97], one can see that $\mathcal{A}_h u_{xx}(x_j,t_n) = \delta_x^2 u(x_j,t_n) + O(h^4)$ for $u(\cdot,t_n) \in C^6([a,b])$.

2.2.1 The numerical scheme

Firstly, let us consider the fully implicit 4th-order compact finite difference scheme (CN-4cFD) [126] from a variation of the second order Crank-Nicolson method [37], which reads

$$\varepsilon^2\delta_t^2 u_j^n - \frac{1}{2}\mathcal{A}_h^{-1}\delta_x^2\left(u_j^{n+1}+u_j^{n-1}\right) + \frac{1}{2\varepsilon^2}\left(u_j^{n+1}+u_j^{n-1}\right) + G\left(u_j^{n+1},u_j^{n-1}\right) = 0, \tag{2.2.4}$$

for $j \in \mathcal{T}_J$ and $n \geq 1$, where

$$G(w,v) = \begin{cases} \dfrac{F(w)-F(v)}{2(|w|^2-|v|^2)}(w+v), & \text{if } w \neq v, \\ \lambda|w|^p w, \ \text{if } w = v, \end{cases} \tag{2.2.5}$$

provides a numerical approximation of $\lambda|u|^p u$ with $F(u) = \frac{\lambda}{p+2}|u|^{p+2}$ as defined in (1.2.5). For the initial boundary conditions (2.1.2) and (2.1.3), we use the following discretization:

$$u_0^n = u_J^n = 0, \quad n \geq 0, \tag{2.2.6}$$
$$u_j^0 = u_0(x_j), \quad j \in \mathcal{T}_J^0, \tag{2.2.7}$$
$$\begin{aligned} u_j^1 =& u_j^0 + \sin\left(\frac{\tau}{\varepsilon^2}\right)u_1(x_j) + \frac{\tau}{2}\sin\left(\frac{\tau}{\varepsilon^2}\right)\left[\mathcal{A}_h^{-1}\delta_x^2 u_j^0 \right.\\ &\left. - \frac{1}{\tau}\sin\left(\frac{\tau}{\varepsilon^2}\right)u_j^0 - \lambda|u_j^0|^p u_j^0\right], \quad j \in \mathcal{T}_J. \end{aligned} \tag{2.2.8}$$

Here we use (2.2.8) to compute u_j^1 instead of the classical method

$$u_j^1 = u_j^0 + \frac{\tau}{\varepsilon^2} u_1(x_j) + \frac{\tau^2}{2\varepsilon^2}\left[\mathcal{A}_h^{-1}\delta_x^2 u_j^0 - \frac{1}{\varepsilon^2}u_j^0 - \lambda |u_j^0|^p u_j^0\right], \quad j \in \mathcal{T}_J, \tag{2.2.9}$$

by substituting $\frac{\tau}{\varepsilon^2}$ with $\sin(\frac{\tau}{\varepsilon^2})$. The benefit of this substitution is that u^1 is uniformly bounded for $\varepsilon \in (0,1]$ as mentioned in [8, 24].

Through out this chapter, we try to get as general as possible results with less restrictions on the parameters in (2.1.1). Although we show the existence of numerical solutions only for nonnegative λ as [105] pointed out the blow-ups of exact solutions for some nonlinearities with negative λ, we also consider the negative part of λ in the discussion of stability. The error bounds are proved for all power nonlinearities with real $p \geq 2$.

For any grid function $v \in X_J$, we define the standard discrete ℓ^2 norm, semi-H^1 norm and ℓ^∞ norm as

$$\|v\|_{\ell^2} = \sqrt{h\sum_{j=1}^{J-1} |v_j|^2}, \quad |v|_1 = \sqrt{h\sum_{j=0}^{J-1} |\delta_x^+ v_j|^2},$$
$$|v|_2 = \sqrt{h\sum_{j=1}^{J-1} |\delta_x^2 v_j|^2}, \quad \|v\|_{\ell^\infty} = \max_{1\leq j\leq J-1} |v_j|.$$

For grid functions $v, w \in X_J$, we introduce the discrete inner product as

$$\langle v, w\rangle = h\sum_{j=1}^{J-1} v_j \bar{w}_j.$$

Denote $\delta_x^2 v = (0, \delta_x^2 v_1, \cdots, \delta_x^2 v_{J-1}, 0) \in X_J$ as the finite difference approximation to the second order derivative with extended zero boundary. Then, it is easy to check that

$$\|v\|_{\ell^2}^2 = \langle v, v\rangle, \tag{2.2.10}$$
$$|v|_1^2 = -\langle v, \delta_x^2 v\rangle, \tag{2.2.11}$$

for any $v \in X_J$. Note that the (2.2.11) only holds for $v \in X_J$, in which vector has zero boundary elements.

Throughout the thesis, we denote C as generic positive constant which may be dependent on the regularity of exact solution and the given initial data but independent of the time step τ, the grid size h, and the dimensionless parameter ε; and we use the notation $w \lesssim v$ to present $w \le Cv$ with w, v two non-negative numbers.

Energy conservation for CN-4cFD method

Introducing two $(J-1)\times(J-1)$ matrices

$$A = \frac{1}{12}\begin{pmatrix} 10 & 1 & & & \\ 1 & 10 & 1 & & \\ & \ddots & \ddots & \ddots & \\ & & 1 & 10 & 1 \\ & & & 1 & 10 \end{pmatrix}, \quad \Lambda = -\frac{1}{h^2}\begin{pmatrix} -2 & 1 & & & \\ 1 & -2 & 1 & & \\ & \ddots & \ddots & \ddots & \\ & & 1 & -2 & 1 \\ & & & 1 & -2 \end{pmatrix},$$

which correspond to the linear operators $\mathcal{A}_h$ and $-\delta_x^2$, respectively, denote by $M = (m_{j,k})$ the product of A^{-1} and Λ, i.e., $M = A^{-1}\Lambda$, and denote by $W = (w_{j,k})$ the product of Λ and M, i.e., $W = \Lambda M = \Lambda A^{-1}\Lambda$. Under the above notations, one can easily verify that

$$\begin{aligned} |v|_1 &= \sqrt{h\sum_{j=1}^{J-1}\sum_{k=1}^{J-1}\bar{v}_j b_{j,k} v_k} = \sqrt{-h\sum_{j=1}^{J-1}\bar{v}_j\delta_x^2 v_j}, \\ |v|_2 &= \sqrt{h\sum_{j=1}^{J-1}\sum_{k=1}^{J-1}\bar{v}_j \tilde{b}_{j,k} v_k} = \sqrt{h\sum_{j=1}^{J-1}\delta_x^2\bar{v}_j\delta_x^2 v_j}, \end{aligned} \tag{2.2.12}$$

where $b_{j,k}$ and $\tilde{b}_{j,k}$ are the components in row j and column k of Λ and Λ^2 respectively.

By a direct computation, one can know that M is a real symmetric positive-definite matrix with eigenvalues $\lambda_{j,M} = \frac{1}{12}\left(10 + 2\cos\frac{j\pi}{J}\right)$ for $j \in \mathcal{T}_J$, hence, for any grid function $v \in X_J$, it makes sense to define semi-norms of v as

$$|v|_{1,*} = \sqrt{h\sum_{j=1}^{J-1}\sum_{k=1}^{J-1}\bar{v}_j m_{j,k} v_k}, \quad |v|_{2,*} = \sqrt{h\sum_{j=1}^{J-1}\sum_{k=1}^{J-1}\bar{v}_j w_{j,k} v_k}, \tag{2.2.13}$$

Similar to (2.2.12), one can prove that

$$|v|_{1,*} = \sqrt{-h\sum_{j=1}^{J-1} \bar{v}_j \mathcal{A}_h^{-1}\delta_x^2 v_j} = \sqrt{-h\sum_{j=1}^{J-1} v_j \mathcal{A}_h^{-1}\delta_x^2 \bar{v}_j}, \tag{2.2.14}$$

$$|v|_{2,*} = \sqrt{h\sum_{j=1}^{J-1} \delta_x^2\bar{v}_j \mathcal{A}_h^{-1}\delta_x^2 v_j} = \sqrt{h\sum_{j=1}^{J-1} \delta_x^2 v_j \mathcal{A}_h^{-1}\delta_x^2 \bar{v}_j}. \tag{2.2.15}$$

Furthermore, by a similar discussion in [116], we have the following equivalence relation of these norms:

$$|v|_1^2 \le |v|_{1,*}^2 \le \frac{3}{2}|v|_1^2, \quad |v|_2^2 \le |v|_{2,*}^2 \le \frac{9}{4}|v|_2^2. \tag{2.2.16}$$

Theorem 2.1. *The CN-4cFD method conserves the discrete energy defined by*

$$\begin{aligned} E^n =&\varepsilon^2\|\delta_t^+ u^n\|_{\ell^2}^2 + \frac{1}{2}(|u^{n+1}|_{1,*}^2 + |u^n|_{1,*}^2) + \frac{1}{2\varepsilon^2}(\|u^{n+1}\|_{\ell^2}^2 + \|u^n\|_{\ell^2}^2) \\ &+ \frac{h}{2}\sum_{j=1}^{J-1}(F(u_j^{n+1}) + F(u_j^n)), \quad 0 \le n \le N-1. \end{aligned} \tag{2.2.17}$$

Proof. As the proof for the Crank-Nicolson scheme of nonlinear Schrödinger equation in [116], for any $1 \le n \le N-1$, multiplying $h(\bar{u}_j^{n+1} - \bar{u}_j^{n-1})$ on scheme (2.2.4) and summing up the result for all $j \in \mathcal{T}_J$, we have

$$\begin{aligned} &\varepsilon^2 h\sum_{j=1}^{J-1}(|\delta_t^+ u_j^n|^2 - |\delta_t^+ u_j^{n-1}|^2) - \frac{1}{2}h\sum_{j=1}^{J-1}\left(\bar{u}_j^{n+1}\mathcal{A}_h^{-1}\delta_x^2 u_j^{n+1} - \bar{u}_j^{n-1}\mathcal{A}_h^{-1}\delta_x^2 u_j^{n-1}\right) \\ &+\frac{1}{2\varepsilon^2}h\sum_{j=1}^{J-1}\left(|u_j^{n+1}|^2 - |u_j^{n-1}|^2\right) + \frac{1}{2}h\sum_{j=1}^{J-1}\left(F(u_j^{n+1}) - F(u_j^{n-1})\right) = 0, \end{aligned} \tag{2.2.18}$$

where (2.2.14) and the summation-by-part formula being used. The above equation immediately indicates

$$E^n - E^{n-1} = 0, \quad 1 \le n \le N-1. \tag{2.2.19}$$

This completes the proof. □

Solvability of the difference equations

Lemma 2.1. (Solvability for CN-4cFD) *For any $u^n, u^{n-1} \in X_J$ $(1 \le n \le N-1)$, the solution u^{n+1} of CN-4cFD (2.2.4) exists. In addition, under the assumption that $\tau \lesssim h$ and $\lambda \ge 0$, there exists $h_0 > 0$ such that the solution is unique for $h \in (0, h_0)$.*

Proof. First, we prove the existence of the CN-4cFD (2.2.4). For simplicity, we define the average value of u^{n+1} and u^{n-1} as $\tilde{u}^n$, i.e.,

$$\tilde{u}_j^n = \frac{1}{2}(u_j^{n+1} + u_j^{n-1}), \quad \text{for} \quad j \in \mathcal{T}_J. \tag{2.2.20}$$

For any $j \in \mathcal{T}_J$, we can express (2.2.4) as

$$\tilde{u}^n = u^n + \frac{\tau^2}{2\varepsilon^2} F^n(\tilde{u}^n) \tag{2.2.21}$$

with $F^n : X_J \to X_J$ defined as

$$(F^n(v))_j = \left[\mathcal{A}_h^{-1}\delta_x^2 - \frac{1}{\varepsilon^2} - \frac{F(2v_j - u_j^{n-1}) - F(u_j^{n-1})}{(|2v_j - u_j^{n-1}|^2 - |u_j^{n-1}|^2)} \right] v_j, \ j \in \mathcal{T}_J. \tag{2.2.22}$$

Define a mapping $G^n : X_J \to X_J$ as

$$G^n(v) = v - u^n - \frac{\tau^2}{2\varepsilon^2} F^n(v), \ v \in X_J. \tag{2.2.23}$$

Then it is obvious that G^n is continuous. And for any $v \in X_J$, when $\lambda \geq 0$, we have

$$\begin{aligned} \mathrm{Re}\langle G^n(v), v\rangle &= \|v\|_{\ell^2}^2 - \mathrm{Re}\langle u^n, v\rangle - \mathrm{Re}\langle \frac{\tau^2}{2\varepsilon^2} F^n(v), v\rangle \\ &\geq \|v\|_{\ell^2}^2 - \mathrm{Re}\langle u^n, v\rangle \\ &\geq \|v\|_{\ell^2}(\|v\|_{\ell^2} - \|u^n\|_{\ell^2}), \end{aligned}$$

which implies,

$$\lim_{\|v\|_{\ell^2} \to \infty} \frac{|\,\mathrm{Re}\langle G^n(v), v\rangle|}{\|v\|_{\ell^2}} = \infty. \tag{2.2.24}$$

Therefore G^n is surjective. From the Brouwer fixed point theorem [7,66], we conclude that there exists a solution v^* such that $G^n(v^*) = 0$, witch provides a solution $2v^* - u^{n-1}$ to (2.2.4). Note the first inequality above is due to $\mathrm{Re}\langle \frac{\tau^2}{2\varepsilon^2} F^n(v), v\rangle = \frac{\tau^2}{2\varepsilon^2}\langle F^n(v), v\rangle \leq 0$ for non-negative λ:

$$\langle F^n(v), v\rangle = -|v|_{1,*}^2 - \frac{\|v\|_{\ell^2}^2}{\varepsilon^2} - \sum_{j=0}^{J} \frac{F(2v_j - u_j^{n-1}) - F(u_j^{n-1})}{(|2v_j - u_j^{n-1}|^2 - |u_j^{n-1}|^2)} |v_j|^2. \tag{2.2.25}$$

Considering the summand in last term of (2.2.25), for any $\alpha, \beta \in \mathbb{C}$ with $\alpha \neq \beta$, we have:

$$\frac{F(\alpha) - F(\beta)}{(|\alpha|^2 - |\beta|^2)} = \frac{2\lambda}{p+2} \frac{(|\alpha|^2)^{\frac{p}{2}+1} - (|\beta|^2)^{\frac{p}{2}+1}}{(|\alpha|^2 - |\beta|^2)} = \lambda \xi_{\alpha,\beta}^{\frac{p}{2}} \geq 0, \tag{2.2.26}$$

for some $\xi_{\alpha,\beta}$ between $|\alpha|^2$ and $|\beta|^2$ through the mean value theorem.

Next, we prove the uniqueness. Due to $u^{n+1} \in X_J$ for $n = 0, 1, 2, \cdots, N$, then we obtain from the inverse inequality [109] that

$$\|u^n\|_{\ell^\infty} \lesssim |u^n|_1, \quad n = 0, 1, 2, \cdots, N. \tag{2.2.27}$$

Considering (2.2.16) and the conservation of energy (2.2.17), we can extend (2.2.27) to

$$\left\|u^{n+1}\right\|_{\ell^\infty} \lesssim |u^{n+1}|_1 \lesssim |u^{n+1}|_{1,*} \lesssim E^n = E^0, \quad n = 0, 1, 2, \cdots, N-1. \tag{2.2.28}$$

For any given $u^n, u^{n-1} \in X_J$ $(n \geq 1)$, suppose that there exist two solutions $u^{n+1}, v^{n+1} \in X_J$ satisfying (2.2.4) and denote $w = u^{n+1} - v^{n+1}$. Then we have

$$\frac{\varepsilon^2}{\tau^2} w_j = \frac{1}{2}\mathcal{A}_h^{-1}\delta_x^2 w_j - \frac{1}{2\varepsilon^2} w_j - \left(G\left(u_j^{n+1}, u_j^{n-1}\right) - G\left(v_j^{n+1}, u_j^{n-1}\right)\right), \quad j \in \mathcal{T}_J. \tag{2.2.29}$$

Multiply $\bar{w}_j$ on both sides and sum up the equations for all $j \in \mathcal{T}_J$, noticing (2.2.28), we have

$$\|w\|_{\ell^2}^2 \lesssim \frac{\tau^2}{\varepsilon^2}(E^0)^2 \|w\|_{\ell^2}^2. \tag{2.2.30}$$

When h is small enough and $\tau \lesssim h$, we can have $\|w\|_{\ell^2}^2 \leq \frac{1}{2}\|w\|_{\ell^2}^2$ for some small enough $\tau \leq \tau_0$, which implies $\|w\|_{\ell^2}^2 = 0$ and the solution is unique. $\square$

Stability of CN-4cFD

Through a standard Von Neumann analysis [104], we have the following stability condition for the locally linearized CN-4cFD:

Theorem 2.2. (linear stability) *Suppose $p = 0$ and $\lambda > -\varepsilon^{-2}$, for the linear form of equation (2.1.1), the CN-4cFD method is unconditionally stable for any $\tau > 0$, and $h > 0$.*

Proof. Plugging

$$u_j^{n-1} = \sum_l \hat{U}_l e^{2ijl\pi/J}, \quad u_j^n = \sum_l \gamma_l \hat{U}_l e^{2ijl\pi/J}, \quad u_j^{n+1} = \sum_l \gamma_l^2 \hat{U}_l e^{2ijl\pi/J}, \tag{2.2.31}$$

into equation (2.2.4), with γ_l denoting the amplification factor of the l-th mode in phase space.

Then we have characteristic equation with structure of form

$$\gamma_l^2 - 2\theta_l\gamma_l + 1 = 0, \quad l = -\frac{J}{2}, \cdots, \frac{J}{2} - 1, \tag{2.2.32}$$

with θ_l determined by the corresponding schemes. The quadratic equation above has two solutions $\gamma_l = \theta_l \pm \sqrt{\theta_l^2 - 1}$. The stability conditions of the two schemes become

$$|\gamma_l| \leq 1 \Longleftrightarrow |\theta_l| \leq 1, \quad l = -\frac{J}{2}, \cdots, \frac{J}{2} - 1. \tag{2.2.33}$$

For the CN-4cFD, we have

$$\theta_l = \frac{2\varepsilon^4}{2\varepsilon^4 + \tau^2\left(\varepsilon^2\mu_l^2/\left(1 - \frac{1}{3}\sin^2(\frac{l\pi}{J})\right) + \varepsilon^2\lambda + 1\right)}, \tag{2.2.34}$$

where

$$\mu_l = \frac{2}{h}\sin\left(\frac{l\pi}{J}\right). \tag{2.2.35}$$

Since $\lambda > -\varepsilon^2$, we have the denominator of (2.2.34) is larger than the dominator, i.e., $|\theta_l| \leq 1$ unconditionally. $\square$

2.2.2 Error estimates

In order to get rigorous error estimates on our numerical methods, based on the theoretical analysis on NKGE given in [80, 89], we require the following assumption on the exact solution u of (2.1.1):

$$u \in C^5\left([0,T]; L^2\right) \cap C^4\left([0,T]; W^{2,\infty}\right) \cap C^3\left([0,T]; W^{4,\infty}\right) \cap C^1([0,T], W_0^{6,\infty} \cap H_0^1),$$

$$\|\partial_t^r \partial_x^s u(x,t)\|_{L^\infty(\Omega_T)} \lesssim \frac{1}{\varepsilon^{2r}}, \quad 0 \leq r \leq 5 \ \& \ 0 \leq r+s \leq 7. \tag{2.A}$$

Here, $\Omega_T = (a,b) \times (0,T)$ with T less than the maximum existence time of the solution.

Define the error function $e^n \in X_J$ for $n = 0, 1, \cdots, N$ as

$$e_j^n = u(x_j, t_n) - u_j^n, \quad j \in \mathcal{T}_J^0, \tag{2.2.36}$$

with $u(x_j,t_n)$ and u_j^n the exact solution and the numerical solution at the point (x_j,t_n).

We state the error estimate results of the proposed numerical schemes as follows.

Theorem 2.3. (Error estimates for CN-4cFD) *Assume $\tau \lesssim h$ and under the assumption (2.A), there exist $\tau_0, h_0 > 0$ sufficiently small and independent of ε such that for any $\varepsilon \in (0,1]$, we have the following error estimate of the CN-4cFD scheme for any $\tau \in (0,\tau_0], h \in (0,h_0]$:*

$$\|e^n\|_{\ell^2} + \left\|\delta_x^+ e^n\right\|_{\ell^2} \lesssim h^4 + \frac{\tau^2}{\varepsilon^6}, \quad 0 \le n \le N. \tag{2.2.37}$$

In this subsection, we aim to prove Theorem 2.3. Define the local truncation error $\xi^n \in X_h$ of the CN-4cFD scheme for $n = 0,1,2,\cdots,N-1$ as

$$\xi_j^0 :=\delta_t^+ u\left(x_j,0\right) - \frac{1}{\varepsilon^2}u_1(x_j) - \frac{\tau}{2\varepsilon^2}\left[\mathcal{A}_h^{-1}\delta_x^2 u_0(x_j) - \frac{1}{\varepsilon^2}u_0(x_j) - \lambda|u_0(x_j)|^2 u_0(x_j)\right], \tag{2.2.38}$$

$$\begin{aligned}\xi_j^n :=&\varepsilon^2\delta_t^2\left(u\left(x_j,t_n\right)\right) - \frac{1}{2}\mathcal{A}_h^{-1}\left[\delta_x^2\left(u\left(x_j,t_{n+1}\right)\right) + \delta_x^2\left(u\left(x_j,t_{n-1}\right)\right)\right] \\ &+ \frac{1}{2\varepsilon^2}\left[u\left(x_j,t_{n+1}\right) + u\left(x_j,t_{n-1}\right)\right] + G\left(u\left(x_j,t_{n+1}\right), u\left(x_j,t_{n-1}\right)\right), \quad n \ge 1.\end{aligned} \tag{2.2.39}$$

For the CN-4cFD method (2.2.4), we have following local truncation error and total error estimate.

Lemma 2.2. (Local truncation errors for CN-4cFD) *Assume $\tau \lesssim h$ and under the assumptions (2.A), we have*

$$\|\xi^n\|_{\ell^2} \lesssim h^4 + \frac{\tau^2}{\varepsilon^6}, \quad \left\|\delta_t^+\xi^n\right\|_{\ell^2} \lesssim \frac{1}{\varepsilon^2}(h^4 + \frac{\tau^2}{\varepsilon^6}), \quad 0 \le n \le N. \tag{2.2.40}$$

Proof. Taking Taylor series expansions of $u(x,t)$ at $(x_j,0)$ to approximate the values $u(x_{j\pm1},0)$ and $u(x_j,\tau)$, we have:

$$\begin{aligned}\xi_j^0 =&\frac{1}{\tau}\left(u\left(x_j,0\right) + \tau\partial_t u\left(x_j,0\right) + \frac{\tau^2}{2}\partial_t^2 u\left(x_j,0\right) + \frac{\tau^3}{6}\partial_t^3 u\left(x_j,\tau^*\right) - u\left(x_j,0\right)\right) - \frac{u_1(x_j)}{\varepsilon^2} \\ &- \frac{\tau}{2\varepsilon^2}\left[\mathcal{A}_h^{-1}\left(u_0^{(2)}(x_j) + \frac{h^2}{12}u_0^{(4)}(x_j) + \frac{h^4}{360}u_0^{(6)}\left(x_j^*\right)\right) - \frac{1}{\varepsilon^2}u_0(x_j) - \lambda|u_0(x_j)|^2 u_0(x_j)\right] \\ =&\frac{\tau^2}{6}\partial_t^3 u(x_j,\tau^*) + \frac{7\tau h^4}{1440\varepsilon^2}\mathcal{A}_h^{-1}u_0^{(6)}\left(x_j^{**}\right),\end{aligned}$$

for some $\tau^* \in (0,\tau)$ and $x_j^*, x_j^{**} \in (x_{j-1}, x_{j+1})$. Therefore,

$$|\xi_j^0| \lesssim \tau^2 \left\|\partial_t^3 u\right\|_{L^\infty(\Omega_T)} + \frac{h^4\tau}{\varepsilon^2}\left\|\partial_x^6 u_0\right\|_{L^\infty(\Omega_T)} \lesssim \frac{\tau^2}{\varepsilon^6} + \frac{h^4\tau}{\varepsilon^2} \lesssim \frac{\tau^2}{\varepsilon^6} + h^4. \tag{2.2.41}$$

Similarly, we can have:

$$\begin{aligned} |\xi_j^n| \lesssim & \varepsilon^2\tau^2 \left\|\partial_t^4 u\right\|_{L^\infty(\Omega_T)} + \tau^2 \left\|\partial_t^2\partial_x^2 u\right\|_{L^\infty(\Omega_T)} + h^4 \left\|\partial_x^6 u\right\|_{L^\infty(\Omega_T)} \\ & + \tau^2 \left[\left\|\partial_t^2 u\right\|_{L^\infty(\Omega_T)} + \left\|\partial_t u\right\|^2_{L^\infty(\Omega_T)} + \frac{1}{2\varepsilon^2}\left\|\partial_t^2 u\right\|_{L^\infty(\Omega_T)}\right] \\ \lesssim & \frac{\tau^2}{\varepsilon^6} + h^4; \end{aligned} \tag{2.2.42}$$

and

$$\begin{aligned} |\delta_t^+\xi_j^n| \lesssim & \varepsilon^2\tau^2 \left\|\partial_t^5 u\right\|_{L^\infty(\Omega_T)} + \tau^2 \left\|\partial_t^3\partial_x^2 u\right\|_{L^\infty(\Omega_T)} + h^4 \left\|\partial_t\partial_x^6 u\right\|_{L^\infty(\Omega_T)} \\ & + \tau^2 \left[\left\|\partial_t^3 u\right\|_{L^\infty(\Omega_T)} + \left\|\partial_t^2 u\right\|^2_{L^\infty(\Omega_T)} + \frac{1}{2\varepsilon^2}\left\|\partial_t^3 u\right\|_{L^\infty(\Omega_T)}\right] \\ \lesssim & \frac{1}{\varepsilon^2}\left(\frac{\tau^2}{\varepsilon^6} + h^4\right). \end{aligned} \tag{2.2.43}$$

This completes the proof. $\square$

Note that if we consider the local truncation error with first step scheme (2.2.8), then we have a new local truncation error $\tilde{\xi}^0$ for the first step: $\tilde{\xi}_j^0 = \delta_t^+ u(x_j, 0) - 1/\tau \sin(\frac{\tau}{\varepsilon^2}) u_1(x_j) - \frac{1}{2}\sin(\frac{\tau}{\varepsilon^2})\left[\mathcal{A}_h^{-1}\delta_x^2 u_0(x_j) - 1/\tau \sin(\frac{\tau}{\varepsilon^2}) u_0(x_j) - \lambda |u_0(x_j)|^2 u_0(x_j)\right]$. Then, $\left|\tilde{\xi}_j^0 - \xi_j^0\right| \leq \left|\xi_j^0\right| + \frac{\tau}{\varepsilon^2}\left|1 - \sin(\frac{\tau}{\varepsilon^2})/\frac{\tau}{\varepsilon^2}\right|(\|u_1\|_\infty + \|u_0\|_{w^{2,\infty}}) \lesssim \left|\xi_j^0\right| + \frac{\tau^3}{\varepsilon^6}$. Therefore, the error bounds for local truncation errors in (2.2.40) work for both (2.2.8) and (2.2.9) initial steps.

Since u is bounded under assumption (2.A), we adapt the standard cut-off technique [5,7] to truncate the nonlinearity into a global Lipschitz function with compact support.

Denote $M_0 = \|u\|_{L^\infty(\Omega_T)}$, $B = (1 + M_0)^2$, and choose a smooth function $\rho(\theta) \in C_0^\infty(\mathbb{R}^+)$ such that

$$\rho(\theta) = \begin{cases} 1, & 0 \leq \theta < 1, \\ \in [0,1], & 1 \leq \theta < 2, \\ 0, & \theta \geq 2, \end{cases} \tag{2.2.44}$$

and define

$$\rho_B(\theta) = \rho(\theta/B)\theta, \quad \theta \in \mathbb{R}^+. \tag{2.2.45}$$

Then $\rho_B(\theta)$ is a smooth function with compact support and therefore globally Lipschitz, i.e., there exists a positive constant $C_B > 0$, independent of ε, s.t.

$$|\rho_B(\theta_1) - \rho_B(\theta_2)| \le C_B|\sqrt{\theta_1} - \sqrt{\theta_2}|, \quad \forall \theta_1, \theta_2 \in \mathbb{R}^+ \tag{2.2.46}$$

Substituting the nonlinearity $\lambda|u|^p u$ in (2.1.1) by $\lambda\rho_B^{p/2}(|u|^2)u$ with $\rho_B^{p/2}(|u|^2) = (\rho_B(|u|^2))^{p/2}$, then for initial value $\hat{u}^0 = u^0, \hat{u}^1 = u^1$, the discretization of CN-4cFD scheme becomes

$$\varepsilon^2\delta_t^2\hat{u}_j^n - \frac{1}{2}\mathcal{A}_h^{-1}\delta_x^2\left(\hat{u}_j^{n+1} + \hat{u}_j^{n-1}\right) + \frac{1}{2\varepsilon^2}\left(\hat{u}_j^{n+1} + \hat{u}_j^{n-1}\right) + \hat{G}\left(\hat{u}_j^{n+1}, \hat{u}_j^{n-1}\right) = 0, \tag{2.2.47}$$

where

$$\hat{G}(w,v) = \begin{cases} \lambda\dfrac{\rho_B^{\frac{p}{2}+1}(|w|^2) - \rho_B^{\frac{p}{2}+1}(|v|^2)}{2(p+2)(\rho_B(|w|^2) - \_B(|v|^2))}(w+v), & \text{if } w \neq v, \\ \lambda|w|^p w, \ \text{if } w = v. \end{cases} \tag{2.2.48}$$

Noting

$$G\left(u\left(x_j, t_{n+1}\right), u\left(x_j, t_{n-1}\right)\right) = \hat{G}\left(u\left(x_j, t_{n+1}\right), u\left(x_j, t_{n-1}\right)\right),$$

we know that the local truncation error of the scheme (2.2.47) is the same as the CN-4cFD scheme (2.2.4). Hence, $\hat{u}_j^n$ can be viewed as another approximation of $u(x_j, t_n)$ with modified nonlinearity approximation. Notice that the scheme (2.2.47) is uniquely solvable for sufficiently small h and $\lambda \ge 0$, as the case of Lemma 2.1.

Define the error function $\hat{e}^n \in \mathcal{T}_J^0$ for $\hat{u}^n$ as

$$\hat{e}_j^n = u\left(x_j, t_n\right) - \hat{u}_j^n, \quad j \in \mathcal{T}_J^0, n \ge 0, \tag{2.2.49}$$

and

$$\eta_j^n = \hat{G}\left(u\left(x_j, t_{n+1}\right), u\left(x_j, t_{n-1}\right)\right) - \hat{G}\left(\hat{u}_j^{n+1}, \hat{u}_j^{n-1}\right), \quad j \in \mathcal{T}_J^0, \ 1 \le n \le N \tag{2.2.50}$$

then we have the following results.

Lemma 2.3. *Under assumption (2.A), there exist $h_0 > 0$ and $\tau_0 > 0$ sufficiently small, such that for $h \in (0, h_0], \tau \in (0, \tau_0]$ we have*

$$\|\hat{\eta}^n\|_{\ell^2}^2 \lesssim \left\|\hat{e}^{n-1}\right\|_{\ell^2}^2 + \left\|\hat{e}^{n+1}\right\|_{\ell^2}^2, \tag{2.2.51}$$

$$|\hat{\eta}^n|_1^2 \lesssim \left\|\hat{e}^{n-1}\right\|_{\ell^2}^2 + \left|\hat{e}^{n-1}\right|_1^2 + \left\|\hat{e}^{n+1}\right\|_{\ell^2}^2 + \left|\hat{e}^{n+1}\right|_1^2, \quad n \geq 1. \tag{2.2.52}$$

Proof. A direct calculation gives

$$\begin{aligned}
\hat{\eta}_j =& \frac{\lambda}{2(p+2)} \frac{\rho_B^{\frac{p}{2}+1}(|u(x_j,t_{n+1})|^2) - \rho_B^{\frac{p}{2}+1}(|u(x_j,t_{n-1})|^2)}{\rho_B(|u(x_j,t_{n+1})|^2) - \rho_B(|u(x_j,t_{n-1})|^2)}(u(x_j,t_{n+1}) + u(x_j,t_{n-1})) \\
&- \frac{\lambda}{2(p+2)} \frac{\rho_B^{\frac{p}{2}+1}(|\hat{u}_j^{n+1}|^2) - \rho_B^{\frac{p}{2}+1}(|\hat{u}_j^{n-1}|^2)}{\rho_B(|\hat{u}_j^{n+1}|^2) - \rho_B(|\hat{u}_j^{n-1}|^2)}(\hat{u}_j^{n+1} + \hat{u}_j^{n-1}) \\
=& \frac{\lambda(u(x_j,t_{n+1}) + u(x_j,t_{n-1}))}{2(p+2)} \left(\frac{\rho_B^{\frac{p}{2}+1}(|u(x_j,t_{n+1})|^2) - \rho_B^{\frac{p}{2}+1}(|u(x_j,t_{n-1})|^2)}{\rho_B(|u(x_j,t_{n+1})|^2) - \rho_B(|u(x_j,t_{n-1})|^2)} \right. \\
&\left. - \frac{\rho_B^{\frac{p}{2}+1}(|\hat{u}_j^{n+1}|^2) - \rho_B^{\frac{p}{2}+1}(|\hat{u}_j^{n-1}|^2)}{\rho_B(|\hat{u}_j^{n+1}|^2) - \rho_B(|\hat{u}_j^{n-1}|^2)} \right) \\
&+ \frac{\lambda}{2(p+2)} \frac{\rho_B^{\frac{p}{2}+1}(|\hat{u}_j^{n+1}|^2) - \rho_B^{\frac{p}{2}+1}(|\hat{u}_j^{n-1}|^2)}{\rho_B(|\hat{u}_j^{n+1}|^2) - \rho_B(|\hat{u}_j^{n-1}|^2)}(\hat{e}_j^{n+1} + \hat{e}_j^{n-1}).
\end{aligned} \tag{2.2.53}$$

$$\begin{aligned}
&\frac{\rho_B^{\frac{p}{2}+1}(|u(x_j,t_{n+1})|^2) - \rho_B^{\frac{p}{2}+1}(|u(x_j,t_{n-1})|^2)}{\rho_B(|u(x_j,t_{n+1})|^2) - \rho_B(|u(x_j,t_{n-1})|^2)} - \frac{\rho_B^{\frac{p}{2}+1}(|\hat{u}_j^{n+1}|^2) - \rho_B^{\frac{p}{2}+1}(|\hat{u}_j^{n-1}|^2)}{\rho_B(|\hat{u}_j^{n+1}|^2) - \rho_B(|\hat{u}_j^{n-1}|^2)} \\
=& \int_0^1 \left(\theta\rho_B(|u(x_j,t_{n+1})|^2) + (1-\theta)\rho_B(|u(x_j,t_{n-1})|^2)\right)^{\frac{p}{2}} \mathrm{d}\theta \\
&- \int_0^1 \left(\theta\rho_B(|\hat{u}_j^{n+1}|^2) + (1-\theta)\rho_B(|\hat{u}_j^{n-1}|^2)\right)^{\frac{p}{2}} \mathrm{d}\theta \\
=& \int_0^1 \zeta_{j\theta}^{\frac{p}{2}-1} \Big(\theta(\rho_B(|u(x_j,t_{n+1})|^2) - \rho_B(|\hat{u}_j^{n+1}|^2)) \\
&+ (1-\theta)(\rho_B(|u(x_j,t_{n+1})|^2) - \rho_B(|\hat{u}_j^{n+1}|^2))\Big) \mathrm{d}\theta,
\end{aligned} \tag{2.2.54}$$

for some $\zeta_{j\theta} \in (0, 2B)$ from the mean value theorem.

For the other part, applying the mean value theorem on function $g(x) = x^{\frac{p}{2}+1}$, we have

$$\frac{\rho_B^{\frac{p}{2}+1}(|\hat{u}_j^{n+1}|^2) - \rho_B^{\frac{p}{2}+1}(|\hat{u}_j^{n-1}|^2)}{\rho_B(|\hat{u}_j^{n+1}|^2) - \rho_B(|\hat{u}_j^{n-1}|^2)} = \frac{2}{p+2}\rho_B^{\frac{p}{2}}(\zeta_j^n), \tag{2.2.55}$$

for some $\zeta_j^n \in (0, 2B)$.

Combining (2.2.53),(2.2.54) and (2.2.55) together, we get:

$$|\hat{\eta}_j| \lesssim B^{\frac{p}{2}-1}(|\hat{e}_j^{n+1}| + |\hat{e}_j^{n-1}|) + B^{\frac{p}{2}}(|\hat{e}_j^{n+1}| + |\hat{e}_j^{n-1}|) \lesssim |\hat{e}_j^{n+1}| + |\hat{e}_j^{n-1}|. \tag{2.2.56}$$

This gives

$$h|\hat{\eta}_j|^2 \lesssim h(|\hat{e}_j^{n+1}|^2 + |\hat{e}_j^{n-1}|^2). \tag{2.2.57}$$

Sum up the above equations for all $j \in \mathcal{T}_J$, then we have:

$$\|\hat{\eta}^n\|_{\ell^2}^2 \lesssim \left\|\hat{e}^{n-1}\right\|_{\ell^2}^2 + \left\|\hat{e}^{n+1}\right\|_{\ell^2}^2.$$

Applying similar procedure to $\delta_x^+\hat{\eta}_j^n$, we can get the second inequality (2.2.52). This completes the proof. $\square$

Lemma 2.4. (Error estimate for CN-4cFD with cutoff nonlinearity) *Assume $\tau \lesssim h$ and under the assumption (2.A), there exist $\tau_0, h_0 > 0$ sufficient small and independent of ε such that for any $\varepsilon \in (0,1]$, we have the following estimates of the scheme (2.2.47) for any $\tau \in (0, \tau_0], h \in (0, h_0]$:*

$$\|\hat{e}^n\|_{\ell^2} + |\hat{e}^n|_1 \lesssim h^4 + \frac{\tau^2}{\varepsilon^6}, \tag{2.2.58}$$

$$\|\hat{u}^n\|_{\ell^\infty} \le M_0 + 1, \quad 0 \le n \le N. \tag{2.2.59}$$

Proof. Subtracting (2.2.47) and (2.2.9) from (2.2.39), we get the following error equations for CN-4cFD:

$$\begin{aligned} &\varepsilon^2\delta_t^2\hat{e}_j^n - \frac{1}{2}\left(\mathcal{A}_h^{-1}\delta_x^2\hat{e}_j^{n+1} + \mathcal{A}_h^{-1}\delta_x^2\hat{e}_j^{n-1}\right) \\ &+ \frac{1}{2\varepsilon^2}\left(\hat{e}_j^{n+1} + \hat{e}_j^{n-1}\right) = \xi_j^n - \hat{\eta}_j^n, \quad j \in \mathcal{T}_J, \ n \ge 2, \end{aligned} \tag{2.2.60}$$

with

$$\hat{e}_j^0 = 0, \quad \hat{e}_j^1 = \tau\hat{\xi}_j^0, \quad j \in \mathcal{T}_J. \tag{2.2.61}$$

Define the energy for the error function $\hat{e}^n$ as

$$S^n = \varepsilon^2\left\|\delta_t^+\hat{e}^n\right\|_{\ell^2}^2 + \frac{1}{2}\left(\left|\hat{e}^n\right|_{1,*}^2 + \left|\hat{e}^{n+1}\right|_{1,*}^2\right) + \frac{1}{2\varepsilon^2}\left(\left\|\hat{e}^n\right\|_{\ell^2}^2 + \left\|\hat{e}^{n+1}\right\|_{\ell^2}^2\right). \tag{2.2.62}$$

Multiplying both sides of (2.2.60) by $h\tau(\delta_t^+\bar{\hat{e}}_j^n + \delta_t^+\bar{\hat{e}}_j^{n-1})$ and summing up for all $j \in \mathcal{T}_J$, then we get

$$\begin{aligned}
S^n - S^{n-1} =& h\tau\sum_{j=1}^{J-1}(\xi_j^n - \hat{\eta}_j^n)(\delta_t^+\bar{\hat{e}}_j^n + \delta_t^+\bar{\hat{e}}_j^{n-1})\\
\le& h\tau\sum_{j=1}^{J-1}(|\xi_j^n| + |\hat{\eta}_j^n|)|\delta_t^+\hat{e}_j^n + \delta_t^+\hat{e}_j^{n-1}|\\
\le& \tau\left(\frac{1}{\varepsilon^2}(\|\xi^n\|_{\ell^2}^2 + \|\hat{\eta}^n\|_{\ell^2}^2) + \varepsilon^2(\left\|\delta_t^+\hat{e}^n\right\|_{\ell^2}^2 + \left\|\delta_t^+\hat{e}^{n-1}\right\|_{\ell^2}^2)\right)\\
\lesssim& \tau(S^n + S^{n-1}) + \frac{\tau}{\varepsilon^2}(h^4 + \frac{\tau^2}{\varepsilon^6})^2,\ n \ge 1,
\end{aligned}$$

where Lemma 2.2 and Lemma 2.3 were used. Therefore, there exists $\tau_0 > 0$ small enough and independent of ε and h such that for $\tau \in (0, \tau_0)$

$$S^n - S^{n-1} \lesssim \tau S^{n-1} + \frac{\tau}{\varepsilon^2}(h^4 + \frac{\tau^2}{\varepsilon^6})^2,\ n \ge 1. \tag{2.2.63}$$

The discrete Gronwall's inequality [40] indicates that

$$S^n \lesssim S^0 + \frac{T}{\varepsilon^2}(h^4 + \frac{\tau^2}{\varepsilon^6})^2,\ n \ge 1. \tag{2.2.64}$$

Noting the local truncation errors from Lemma 2.2 gives

$$S^0 = \varepsilon^2\left\|\xi^0\right\|_{\ell^2}^2 + \frac{\tau^2}{2}|\xi^0|_{1,*}^2 + \frac{\tau^2}{\varepsilon^2}\left\|\xi^0\right\|_{\ell^2}^2 \lesssim (h^4 + \frac{\tau^2}{\varepsilon^6})^2(\varepsilon^2 + \frac{\tau^2}{2} + \frac{\tau^2}{\varepsilon^2}). \tag{2.2.65}$$

Combining (2.2.65) and (2.2.64) gives

$$S^n \lesssim \frac{1}{\varepsilon^2}(h^4 + \frac{\tau^2}{\varepsilon^6})^2. \tag{2.2.66}$$

The definition of S^n (2.2.62) reveals that

$$\|\hat{e}^n\|_{\ell^2}^2 + \left\|\hat{e}^{n+1}\right\|_{\ell^2}^2 \le 2\varepsilon^2 S^n \lesssim (h^4 + \frac{\tau^2}{\varepsilon^6})^2. \tag{2.2.67}$$

For the H^1-semi norm error, by multiplying both sides of (2.2.60) by $h\delta_x^2(\bar{\hat{e}}_j^{n+1} - \bar{\hat{e}}_j^{n-1})$ and summing the resulting equation up for $j \in \mathcal{T}_J$, then we get

$$\begin{aligned}
&-\varepsilon^2\left(\left|\delta_t^+\hat{e}^n\right|_1^2 - \left|\delta_t^+\hat{e}^{n-1}\right|_1^2\right) - \frac{1}{2}\left(\left|\hat{e}^{n+1}\right|_{2,*}^2 - \left|\hat{e}^{n-1}\right|_{2,*}^2\right)\\
&-\frac{1}{2\varepsilon^2}\left(\left|\hat{e}^{n+1}\right|_{1,*}^2 - \left|\hat{e}^{n-1}\right|_{1,*}^2\right) = h\sum_{j=1}^{J-1}(\xi_j^n - \hat{\eta}_j^n)\delta_x^2(\bar{\hat{e}}_j^{n+1} - \bar{\hat{e}}_j^{n-1}).
\end{aligned} \tag{2.2.68}$$

Define energy

$$\tilde{S}^n = \varepsilon^2 \left|\delta_t^+ \hat{e}^n\right|_1^2 + \frac{1}{2}\left(\left|\hat{e}^{n+1}\right|_{2,*}^2 + |\hat{e}^n|_{2,*}^2\right) + \frac{1}{2\varepsilon^2}\left(\left|\hat{e}^{n+1}\right|_{1,*}^2 + |\hat{e}^n|_{1,*}^2\right), \tag{2.2.69}$$

and we have

$$\tilde{S}^n - \tilde{S}^{n-1} = -h\sum_{j=1}^{J-1}(\xi_j^n - \hat{\eta}_j^n)\delta_x^2(\bar{\hat{e}}_j^{n+1} - \bar{\hat{e}}_j^{n-1}). \tag{2.2.70}$$

Therefore,

$$\tilde{S}^n - \tilde{S}^0 = -h\sum_{k=1}^{n}\sum_{j=1}^{J-1}\xi_j^n\delta_x^2(\bar{\hat{e}}_j^{k+1} - \bar{\hat{e}}_j^{k-1}) + h\sum_{k=1}^{n}\sum_{j=1}^{J-1}\hat{\eta}_j^n\delta_x^2(\bar{\hat{e}}_j^{k+1} - \bar{\hat{e}}_j^{k-1}). \tag{2.2.71}$$

For the right parts of (2.2.71), by using the summation-by-part formula and the Cauchy-Schwarz inequality, we have the following estimates,

$$\begin{aligned}
&\left|-h\sum_{k=1}^{n}\sum_{j=1}^{J-1}\xi_j^n\delta_x^2(\bar{\hat{e}}_j^{k+1} - \bar{\hat{e}}_j^{k-1})\right| \\
=&\left|h\tau\sum_{k=1}^{n}\sum_{j=1}^{J-1}\delta_t^+\xi_j^n\delta_x^2(\bar{\hat{e}}_j^{k+1} + \bar{\hat{e}}_j^{k}) + h\sum_{j=1}^{J-1}\xi_j^1(\delta_x^2(\bar{\hat{e}}_j^{1} + \bar{\hat{e}}_j^{0})) - h\sum_{j=1}^{J-1}\xi_j^{n+1}(\delta_x^2(\bar{\hat{e}}_j^{n+1} + \bar{\hat{e}}_j^{n}))\right| \\
\lesssim&\tau\sum_{k=1}^{n}\left(\varepsilon^2\left\|\delta_t^+\xi^k\right\|_{\ell^2}^2 + \frac{1}{\varepsilon^2}|e^{k+1}|_2^2 + \frac{1}{\varepsilon^2}|e^k|_2^2\right) \\
&+\varepsilon^2\left\|\xi^1\right\|_{\ell^2}^2 + \frac{1}{\varepsilon^2}|e^1|_2^2 + \frac{1}{\varepsilon^2}|e^{n+1}|_2^2 + \frac{1}{\varepsilon^2}|e^n|_2^2 + \varepsilon^2\left\|\xi^{n+1}\right\|_{\ell^2}^2 \\
\lesssim&(h^4 + \frac{\tau^2}{\varepsilon^6})^2 + \frac{\tau}{\varepsilon^2}\sum_{k=1}^{n+1}|e^k|_2^2 \lesssim (h^4 + \frac{\tau^2}{\varepsilon^6})^2 + \frac{\tau}{\varepsilon^2}\sum_{k=1}^{n+1}|e^k|_{2,*}^2,
\end{aligned} \tag{2.2.72}$$

and

$$\begin{aligned}
&|h\sum_{k=1}^{n}\sum_{j=1}^{J-1}\hat{\eta}_j^n\delta_x^2(\bar{\hat{e}}_j^{k+1} - \bar{\hat{e}}_j^{k-1})| \\
=&| - h\tau\sum_{k=1}^{n}\sum_{j=0}^{J-1}\delta_x^+\hat{\eta}_j^k(\delta_x^+\delta_t^+\hat{e}_j^k + \delta_x^+\delta_t^+\hat{e}_j^{k-1})| \\
\lesssim&\tau\sum_{k=1}^{n}(\frac{1}{\varepsilon^2}|\hat{\eta}^k|_1^2 + \varepsilon^2(|\delta_t^+\hat{e}^k|_1^2 + |\delta_t^+\hat{e}^{k-1}|_1^2)) \\
\lesssim&\frac{1}{\varepsilon^2}(h^4 + \frac{\tau^2}{\varepsilon^6})^2 + \sum_{k=1}^{n}\varepsilon^2(|\delta_t^+\hat{e}^k|_1^2 + |\delta_t^+\hat{e}^{k-1}|_1^2),
\end{aligned} \tag{2.2.73}$$

where (2.2.16), Lemma 2.2 and Lemma 2.3 were used.

Combining (2.2.71), (2.2.72) and (2.2.73) together, we get

$$\tilde{S}^n \lesssim \tau \sum_{k=1}^{n} \tilde{S}^k + \tilde{S}^0 + \frac{1}{\varepsilon^2}(h^4 + \frac{\tau^2}{\varepsilon^6})^2. \tag{2.2.74}$$

Since $\tilde{S}^0 \lesssim \frac{1}{\varepsilon^2}(h^4 + \frac{\tau^2}{\varepsilon^6})^2$ for local truncation error, from the Gronwall's inequality we have

$$\tilde{S}^n \lesssim \frac{1}{\varepsilon^2}(h^4 + \frac{\tau^2}{\varepsilon^6})^2. \tag{2.2.75}$$

The definition of $\tilde{S}^n$ (2.2.69) and the inequality (2.2.16) indicate

$$|\hat{e}^n|_1^2 + \left|\hat{e}^{n+1}\right|_1^2 \leq |\hat{e}^n|_{1,*}^2 + \left|\hat{e}^{n+1}\right|_{1,*}^2 \leq 2\varepsilon^2 \tilde{S}^n \lesssim (h^4 + \frac{\tau^2}{\varepsilon^6})^2. \tag{2.2.76}$$

Combining (2.2.67) and (2.2.76), we obtain the error estimate (2.2.58) immediately.

When h is small enough and considering $\tau \lesssim h, \tau = o(\varepsilon^3)$, we have:

$$\|\hat{e}^n\|_{l^\infty} \leq C\,|\hat{e}^n|_1 \leq 1, \quad n = 1, 2, \cdots, N. \tag{2.2.77}$$

And we get the boundedness of $\hat{u}^n$ in (2.2.59):

$$\|\hat{u}^n\|_{l^\infty} \leq \|u(\cdot, t_n)\|_{L^\infty} + \|\hat{e}^n\|_{l^\infty} \leq M_0 + 1, \quad n = 1, 2, \cdots, N \tag{2.2.78}$$

This completes the proof. □

Based on the above analysis, we now give the proof of Theorem 2.3.

Proof. From (2.2.59) and the definition of ρ, we know that (2.2.47) and (2.2.4) share the same solution, since $\hat{G}(\hat{u}^{n+1}, \hat{u}^{n-1})$ equals to $G(\hat{u}^{n+1}, \hat{u}^{n-1})$ for $\|\hat{u}^n\|_{\ell^\infty}^2 \leq B$. From the unique solvability of the CN-4cFD scheme in Lemma 2.1, we have $u^n = \hat{u}^n$ for each $0 \leq n \leq N$. Therefore, Theorem 2.3 is a direct inference from Theorem 2.4. □

2.2.3 Numerical results

In this section, we show the numerical results to support our error estimates in section 2.2.2. We choose the initial data for all the numerical solutions in this section as follows,

$$\lambda = 4,\ p = 2,\ u_0(x) = \mathrm{sech}(x^2) + ie^{-x^2},\ u_1(x) = 0, \quad \text{for } x \in \mathbb{R}.$$

In order to quantify the convergence, we use following standard error functions as in [9] for the discrete ℓ^∞-error, ℓ^2-error and H^1-error,

$$e_{\ell^\infty} = \|e^n\|_{\ell^\infty}, \quad e_{\ell^2} = \|e^n\|_{\ell^2}, \quad e_{H^1} = \sqrt{\|e^n\|_{\ell^2}^2 + |e^n|_1^2}. \tag{2.2.79}$$

During our numerical simulation, we truncate our computational domain to be $(a, b) = (-8, 8)$ and $T = 0.4$. Since the wave speed for the linear problem is O(1), the domain is large enough for us to use the homogenous boundary condition to simulation the original whole space problem (2.0.1). The 'exact solution' is computed by a fine mesh with $h = 2^{-10}, \tau = 10^{-7}$ for comparison. The following four figures show that the spatial discretization errors of both methods converge in 4th order. The first two figures in Figure 2.2 are the log-log plots of errors for CN-4cFD methods with respect to spatial mesh size h for different ε's. The slope of each error line is the same as the dashed line for h^4, which indicates that the spatial error has 4-th order convergence rate. The errors are independent of ε since the error scale does not change as ε decreases.

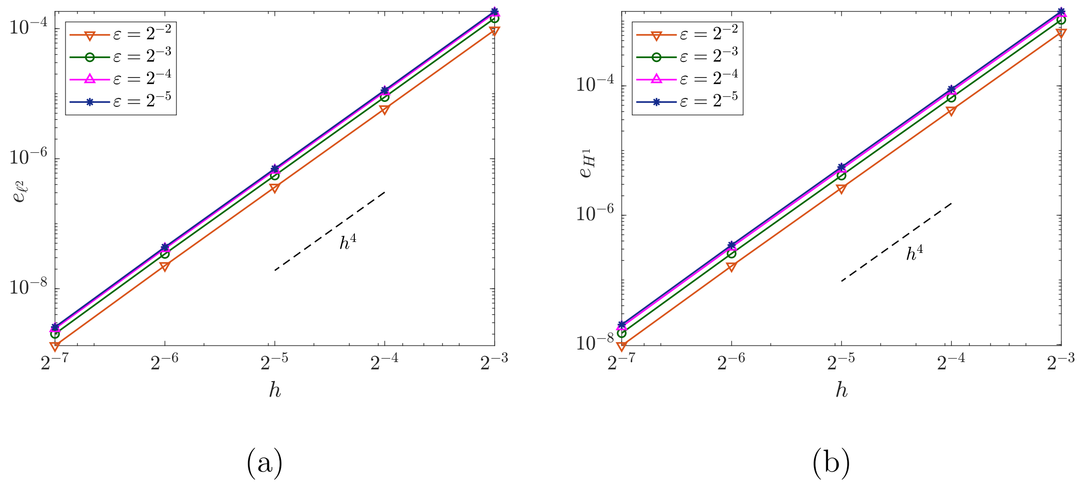

Figure 2.2: Log-log plots of ℓ^2 errors (a) and H^1 errors (b) w.r.t h for CN-4cFD.

Table 2.1: Temporal ℓ^∞ errors for CN-4cFD with $\tau_0 = \frac{1}{40}$, $\varepsilon_0 = \frac{1}{4}$ and $h = 2^{-8}$.

e_{H^1}	$\tau = \tau_0$	$\tau = \tau_0/4$	$\tau = \tau_0/4^2$	$\tau = \tau_0/4^3$	$\tau = \tau_0/4^4$	$\tau = \tau_0/4^5$
$\varepsilon = \varepsilon_0$	4.64E-1	**3.51E-2**	2.24E-3	1.40E-4	8.75E-6	5.18E-7
Order	-	**1.86**	1.98	1.99	2.00	2.04
$\varepsilon = \varepsilon_0/4^{\frac{1}{3}}$	8.81	3.55E-1	**2.27E-2**	1.42E-3	8.86E-5	5.22E-6
Order	-	0.66	**1.98**	2.00	2.00	2.04
$\varepsilon = \varepsilon_0/4^{\frac{2}{3}}$	5.77E-1	1.70	2.41E-1	**1.64E-2**	1.02E-3	6.02E-5
Order	-	-0.80	1.41	**1.94**	2.00	2.04
$\varepsilon = \varepsilon_0/4^{\frac{3}{3}}$	1.38	1.81E-1	2.24	1.44E-1	**8.43E-3**	4.94E-4
Order	-	1.47	-1.87	2.03	**2.05**	2.05
$\varepsilon = \varepsilon_0/4^{\frac{4}{3}}$	1.37	0.65	1.27	1.18	2.62E-1	**1.54E-2**
Order	-	0.54	-0.48	-0.05	1.08	**2.05**

Table 2.2: Temporal H^1 errors for CN-4cFD with $\tau_0 = \frac{1}{40}$, $\varepsilon_0 = \frac{1}{4}$ and $h = 2^{-8}$.

e_{H^1}	$\tau = \tau_0$	$\tau = \tau_0/4$	$\tau = \tau_0/4^2$	$\tau = \tau_0/4^3$	$\tau = \tau_0/4^4$	$\tau = \tau_0/4^5$
$\varepsilon = \varepsilon_0$	1.20	**9.19E-2**	5.87E-3	3.68E-4	2.30E-5	1.36E-6
Order	-	**1.85**	1.98	2.00	2.00	2.04
$\varepsilon = \varepsilon_0/4^{\frac{1}{3}}$	3.19	9.43E-1	**6.14E-2**	3.85E-3	2.40E-4	1.42E-5
Order	-	0.88	**1.97**	2.00	2.00	2.04
$\varepsilon = \varepsilon_0/4^{\frac{2}{3}}$	2.23	5.14	6.92E-1	**4.59E-2**	2.87E-3	1.69E-4
Order	-	-0.60	1.45	**1.95**	2.00	2.04
$\varepsilon = \varepsilon_0/4^{\frac{3}{3}}$	3.68	1.10	6.42	0.49	**2.97E-2**	1.75E-3
Order	-	0.87	-1.27	1.85	**2.02**	2.04
$\varepsilon = \varepsilon_0/4^{\frac{4}{3}}$	3.83	2.54	3.84	4.13	7.16E-1	**4.23E-2**
Order	-	0.29	-0.30	-0.05	1.26	**2.04**

2.3 Semi-implicit 4cFD (SI-4cFD) for NKGE

2.3.1 The numerical scheme

In practice, however, the conservative scheme could be difficult to use when $|u_j^{n+1}| - |u_j^{n-1}|$ is close to zero, and the nonlinear system (2.2.4) generally needs iterative solvers which are time consuming. Therefore, we consider the semi-implicit 4th-order compact finite difference scheme (SI-4cFD) as follows

$$\varepsilon^2\delta_t^2 u_j^n - \frac{1}{2}\mathcal{A}_h^{-1}\delta_x^2\left(u_j^{n+1}+u_j^{n-1}\right) + \frac{1}{2\varepsilon^2}\left(u_j^{n+1}+u_j^{n-1}\right) + f(u_j^n) = 0, \tag{2.3.1}$$

for $j \in \mathcal{T}_J$ and $n \geq 1$.

Lemma 2.5. (Solvability for SI-4cFD) *For any $u^n, u^{n-1} \in X_J$ $(1 \leq n \leq N-1)$, there exists a unique solution u^{n+1} of SI-4cFD* (2.3.1)*.*

The proof is similar to Lemma 2.1. The existence of a solution can be shown by the solvability of $\tilde{G}^n(v) = 0$ for the map $\tilde{G}^n : X_J \to X_J$ defined by

$$\tilde{G}^n(v) := v - u^n - \frac{\tau^2}{2\varepsilon^2}\left[(\mathcal{A}_h^{-1}\delta_x^2 - \frac{1}{\varepsilon^2})v - f(u^n)\right].$$

This can be proved by the Brouwer fixed point theorem similar as the procedure in lemma 2.1. The uniqueness of the solution is directly from the linearity of the SI-4cFD (2.3.1).

Theorem 2.4. (linear stability of SI-4cFD) *Suppose $p = 0$ and $\lambda > -\varepsilon^{-2}$, for the linear form of equation* (2.1.1)*, we have the following stability condition*

1. *when $-\varepsilon^{-2} \leq \lambda \leq \varepsilon^{-2}$ the SI-4cFD scheme is unconditionally stable for any $\tau, h > 0$;*

2. *when $\varepsilon^{-2} < \lambda$ the SI-4cFD scheme is stable under the condition*

$$\tau \leq \frac{2\varepsilon^2}{\sqrt{\varepsilon^2\lambda - 1}}. \tag{2.3.2}$$

Proof. Plugging (2.2.31) into equation (2.3.1), with γ_l denoting the the amplification factor of the l-th mode in phase space. Then, we have characteristic equation of form as in Theorem 2.2

$$\gamma_l^2 - 2\theta_l\gamma_l + 1 = 0, \quad l = -\frac{J}{2}, \cdots, \frac{J}{2} - 1,$$

with

$$\theta_l = \frac{2\varepsilon^4 - \tau^2\varepsilon^2\lambda}{2\varepsilon^4 + \tau^2\left(\varepsilon^2\mu_l^2/\left(1 - \frac{1}{3}\sin^2(\frac{l\pi}{J})\right) + 1\right)}. \tag{2.3.3}$$

When $-\varepsilon^{-2} \leq \lambda \leq \varepsilon^{-2}$, we have the denominator of (2.3.3) larger than the dominator, i.e., $|\theta_l| \leq 1$. When $\lambda \geq \varepsilon^{-2}$, we have $2\varepsilon^4 - \tau^2\varepsilon^2\lambda \geq -(2\varepsilon^4 + \tau^2) \Longrightarrow \theta_l \geq -1$. Therefore $|\theta_l| \leq 1$, which indicates $\tau \leq \frac{2\varepsilon^2}{\sqrt{\varepsilon^2\lambda - 1}}$. We obtain the stability condition for SI-4cFD as stated in Theorem 2.4. □

2.3.2 Error estimates

Theorem 2.5. (Error estimates for SI-4cFD) *Assume $\tau \lesssim h$ and under the assumption (2.A), there exist $\tau_0, h_0 > 0$ sufficient small and independent of ε such that for any $\varepsilon \in (0, 1]$, under the stability condition stated in theorem 2.2, we have the following error estimate of the SI-4cFD scheme for any $\tau \in (0, \tau_0], h \in (0, h_0]$:*

$$\|e^n\|_{\ell^2} + \left\|\delta_x^+ e^n\right\|_{\ell^2} \lesssim h^4 + \frac{\tau^2}{\varepsilon^6}, \quad 0 \leq n \leq N. \tag{2.3.4}$$

Substituting $u(x_j, t_n)$ into (2.2.9) and (2.3.1), we can have the following expression of local truncation errors for SI-4cFD scheme.

$$\begin{aligned} \xi_j^0 :=& \delta_t^+ u\left(x_j, 0\right) - \frac{1}{\varepsilon^2}u_1(x_j) \\ &- \frac{\tau}{2\varepsilon^2}\left[\mathcal{A}_h^{-1}\delta_x^2 u_0(x_j) - \frac{1}{\varepsilon^2}u_0(x_j) - \lambda|u_0(x_j)|^2 u_0(x_j)\right], \; j \in \mathcal{T}_J, \end{aligned} \tag{2.3.5}$$

$$\begin{aligned} \xi_j^n :=& \varepsilon^2\delta_t^2\left(u\left(x_j, t_n\right)\right) - \frac{1}{2}\mathcal{A}_h^{-1}\left[\delta_x^2\left(u\left(x_j, t_{n+1}\right)\right) + \delta_x^2\left(u\left(x_j, t_{n-1}\right)\right)\right] \\ &+ \frac{1}{2\varepsilon^2}\left[u\left(x_j, t_{n+1}\right) + u\left(x_j, t_{n-1}\right)\right] + \lambda|u(x_j, t_n)|^2 u(x_j, t_n), \quad j \in \mathcal{T}_J, \quad n \geq 1. \end{aligned} \tag{2.3.6}$$

Through Taylor expansions, we have the following error estimates for the local truncation errors as in Lemma 2.2,

$$\|\xi^n\|_{\ell^2} \lesssim h^4 + \frac{\tau^2}{\varepsilon^6}, \quad \left\|\delta_t^+\xi^n\right\|_{\ell^2} \lesssim \frac{1}{\varepsilon^2}(h^4 + \frac{\tau^2}{\varepsilon^6}), \quad 0 \leq n \leq N.$$

Define $\eta_j^n = \lambda|u(x_j,t_n)|^2u(x_j,t_n) - \lambda|u_j^n|^2u_j^n$, then the error equation for SI-4cFD method reads

$$\varepsilon^2\delta_t^2 e_j^n - \frac{1}{2}\left(\mathcal{A}_h^{-1}\delta_x^2 e_j^{n+1} + \mathcal{A}_h^{-1}\delta_x^2 e_j^{n-1}\right) + \frac{1}{2\varepsilon^2}\left(e_j^{n+1} + e_j^{n-1}\right) = \xi_j^n - \eta_j^n, \tag{2.3.7}$$

for $j \in \mathcal{T}_M, n \geq 2$, with

$$e_j^0 = 0, \quad e_j^1 = \tau\xi_j^0, \quad j \in \mathcal{T}_J. \tag{2.3.8}$$

The proof to Theorem 2.5 is similar to the case of CN-4cFD method by constructing 2 energy functions

$$S^n = \varepsilon^2\left\|\delta_t^+ e^n\right\|_{\ell^2}^2 + \frac{1}{2}\left(|e^n|_{1,*}^2 + \left|e^{n+1}\right|_{1,*}^2\right) + \frac{1}{2\varepsilon^2}\left(\|e^n\|_{\ell^2}^2 + \left\|e^{n+1}\right\|_{\ell^2}^2\right), \tag{2.3.9}$$

and

$$\tilde{S}^n = \varepsilon^2\left\|\delta_x^+\delta_t^+ e^n\right\|_{\ell^2}^2 + \frac{1}{2}\left(|e^n|_{2,*}^2 + \left|e^{n+1}\right|_{2,*}^2\right) + \frac{1}{2\varepsilon^2}\left(|e^n|_{1,*}^2 + \left|e^{n+1}\right|_{1,*}^2\right), \tag{2.3.10}$$

and using the discrete Gronwall's inequality and a mathematical induction argument.

2.3.3 Numerical results

We adopt the same initial data and mesh size for the numerical simulations of SI-4cFD. Figure 2.3 shows result on spatial errors of the SI-4cFD method quite similar to Figure 2.2. The slopes of each error line for different ε's are the same as the line h^4, which indicates that the convergence rate of spatial errors are of 4-th order. the error scale does not change with ε indicates that spatial errors are independent of ε. Although converging at the same order, the error for the SI-4cFD scheme is smaller than the CN-4cFD scheme under the same spatial mesh size especially for small h cases. This is because of the tolerance error in the iteration solver for CN-4cFD. In the numerical application of CN-4cFD, we choose the tolerance error of the iteration solver to be 10^{-12} which is much large than numerical error introduce by solving the SI-4cFD scheme, a conditional number of a normal matrix times the round-off error of double precision.

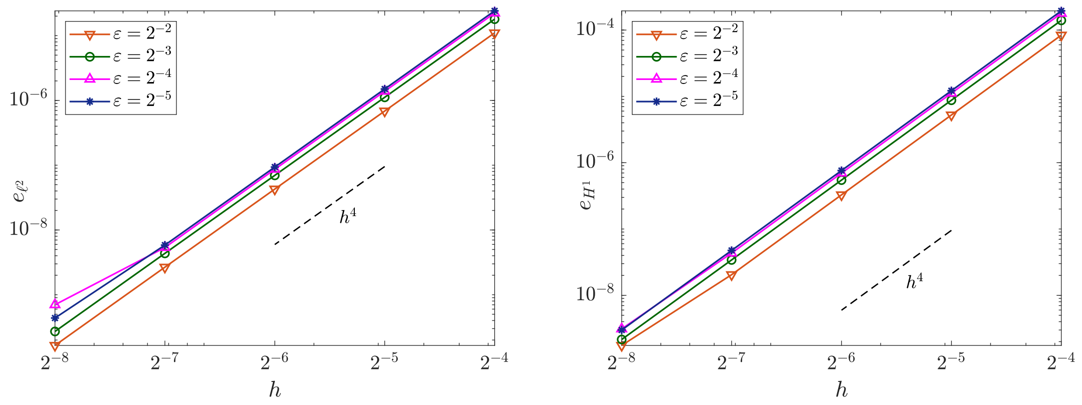

(a) (b)

Figure 2.3: Log-log plots of ℓ^2 errors (a) and H^1 errors (b) w.r.t h for SI-4cFD.

Table 2.3: Temporal ℓ^∞ errors for SI-4cFD with $\tau_0 = \frac{1}{40}$, $\varepsilon_0 = \frac{1}{4}$ and $h = 2^{-8}$.

e_{ℓ^∞}	$\tau = \tau_0$	$\tau = \tau_0/4$	$\tau = \tau_0/4^2$	$\tau = \tau_0/4^3$	$\tau = \tau_0/4^4$	$\tau = \tau_0/4^5$
$\varepsilon = \varepsilon_0$	2.71E-1	**1.87E-2**	1.18E-3	7.40E-5	4.58E-6	2.34E-7
Order	-	**1.93**	1.99	2.00	2.01	2.14
$\varepsilon = \varepsilon_0/4^{\frac{1}{3}}$	8.44E-1	2.68E-1	**1.71E-2**	1.07E-3	6.66E-5	3.92E-6
Order	-	8.27E-1	**1.99**	2.00	2.00	2.04
$\varepsilon = \varepsilon_0/4^{\frac{2}{3}}$	1.07	1.59	2.14E-1	**1.44E-2**	8.98E-4	5.29E-5
Order	-	-2.86E-1	1.45	**1.95**	2.00	2.04
$\varepsilon = \varepsilon_0/4^{\frac{3}{3}}$	2.41	1.80E-1	2.43	1.38E-1	**8.13E-3**	4.77E-4
Order	-	1.87	-1.88	2.07	**2.04**	2.05
$\varepsilon = \varepsilon_0/4^{\frac{4}{3}}$	1.61	1.56	1.28	1.18	2.57E-1	**1.51E-2**
Order	-	2.36E-2	1.42E-1	5.74E-2	1.10	**2.04**

From the Table 2.1–2.4 of temporal errors, we can see clearly that the temporal convergence rates of both methods are second order. The bold diagonals of these tables indicate that the temporal error has dependency on ε, which is of size $O(\frac{\tau^2}{\varepsilon^6})$: the data above each diagonal experience well second order convergence, while the errors below the diagonals do not have second order convergence. The errors for large time steps are always bounded, which coincides with our stability analysis in section 2.2.1 that both schemes have good stability. The ℓ^∞ errors for two methods also converge in second order, which is due to the special case of Sobolev embedding theorem that $H^1(\Omega) \subset L^\infty(\Omega)$ for $\Omega \subset \mathbb{R}$.

Table 2.4: Temporal H^1 errors for SI-4cFD with $\tau_0 = \frac{1}{40}$, $\varepsilon_0 = \frac{1}{4}$ and $h = 2^{-8}$.

e_{H^1}	$\tau = \tau_0$	$\tau = \tau_0/4$	$\tau = \tau_0/4^2$	$\tau = \tau_0/4^3$	$\tau = \tau_0/4^4$	$\tau = \tau_0/4^5$
$\varepsilon = \varepsilon_0$	7.79E-1	**5.40E-2**	3.42E-3	2.14E-4	1.32E-5	6.91E-7
Order	-	**1.93**	1.99	2.00	2.01	2.13
$\varepsilon = \varepsilon_0/4^{\frac{1}{3}}$	3.80	7.47E-1	**4.80E-2**	3.01E-3	1.87E-4	1.10E-5
Order	-	1.17	**1.98**	2.00	2.00	2.04
$\varepsilon = \varepsilon_0/4^{\frac{2}{3}}$	3.58	4.98	6.25E-1	**4.10E-2**	2.56E-3	1.51E-4
Order	-	-0.24	1.50	**1.96**	2.00	2.04
$\varepsilon = \varepsilon_0/4^{\frac{3}{3}}$	5.84	9.70E-1	6.56	4.73E-1	**2.88E-2**	1.69E-3
Order	-	1.30	-1.38	1.90	**2.02**	2.04
$\varepsilon = \varepsilon_0/4^{\frac{4}{3}}$	4.35	4.44	3.96	4.17	7.04E-1	**4.16E-2**
Order	-	-1.53E-2	8.33E-2	-3.82E-2	1.28	**2.04**

2.4 Comparison with existing methods

2.4.1 Comparison with second order methods

In this section, we compare the time consumption of the 4cFDs with the corresponding second order finite difference schemes. All algorithms are run on a single kernel of Intel Xeon Gold6132 CPU with frequency at 2.60GHz for a fair comparison. As introduced in [9], we adopt the following seconder order Crank-Nicolson finite difference scheme (CNFD)

$$\varepsilon^2 \delta_t^2 u_j^n - \frac{1}{2}\delta_x^2 \left(u_j^{n+1} + u_j^{n-1}\right) + \frac{1}{2\varepsilon^2}\left(u_j^{n+1} + u_j^{n-1}\right) + G\left(u_j^{n+1}, u_j^{n-1}\right) = 0, \qquad (2.4.1)$$

with $G(\cdot,\cdot)$ defined in (2.2.5), and the seconder order semi-implicit finite difference scheme (SIFD)

$$\varepsilon^2\delta_t^2 u_j^n - \frac{1}{2}\delta_x^2\left(u_j^{n+1}+u_j^{n-1}\right)+\frac{1}{2\varepsilon^2}\left(u_j^{n+1}+u_j^{n-1}\right)+f(u_j^n)=0. \tag{2.4.2}$$

We use the same numerical example as in Section 2.2.3. When comparing the time consumption between SI-4cFD and SIFD in Table 2.6 and 2.8, we can find that the time consumption for same mesh size are nearly equal for the two methods. However, the time consumption for CN-4cFD and CNFD mainly depends on the the number of iterations in each time step and therefore differs a lot as in Table 2.5 and 2.7. The semi-implicit methods use less time for both second-order and fourth-order schemes. In our numerical example, the average CPU time consumption for CN-4cFD is 2.4 times of SI-4cFD. The time consumption for CNFD is 5 times of SIFD.

When it comes to achieve a fix accuracy for numerical solutions, the higher order methods are much more efficient than second order methods. Considering the bold columns in the four tables, the two bold columns have $O(10^{-4})$ and $O(10^{-5})$ accuracy for all four methods respectively, but the time consumption for the second order methods have the same order as the square of the fourth-order methods, which imply the fourth-order methods can reduce the computational cost by a square root, especially for the cases that need high accuracy.

Table 2.5: Spatial errors and time consumptions for CN-4cFD at $t=1$ with $\varepsilon=\frac{1}{2^4}$.

h	$h_0=\frac{1}{4}$	$h_0/2$	$h_0/2^2$	$h_0/2^3$	$h_0/2^4$	$h_0/2^5$	$h_0/2^6$
$e^{\varepsilon}_{H^1}(t=1)$	8.24E-1	4.24E-1	**2.24E-4**	**1.43E-5**	8.99E-7	5.62E-8	5.12E-9
Order	-	9.58E-1	**1.09E1**	**3.97**	3.99	4.00	3.46
CPU time (s)	9.13	13.3	**20.3**	**34.4**	60.1	114	220

Table 2.6: Spatial errors and time consumptions for SI-4cFD at $t = 1$ with $\varepsilon = \frac{1}{2^4}$.

h	h_0	$h_0/2$	$h_0/2^2$	$h_0/2^3$	$h_0/2^4$	$h_0/2^5$	$h_0/2^6$
$e^{\varepsilon}_{H^1}(t = 1)$	8.24E-1	4.24E-1	**2.24E-4**	**1.43E-5**	8.99E-7	5.67E-8	3.52E-9
Order	-	9.58E-1	**1.09E1**	**3.97**	3.99	3.99	4.01
CPU time (s)	3.35	5.45	**8.15**	**14.2**	25.9	49.6	94.8

Table 2.7: Spatial errors and time consumptions for CNFD at $t = 1$ with $\varepsilon = \frac{1}{2^4}$.

h	$h_0/2$	$h_0/2^2$	$h_0/2^3$	$h_0/2^4$	$h_0/2^5$	$h_0/2^6$	$h_0/2^7$	$h_0/2^8$
$e^{\varepsilon}_{H^1}(t = 1)$	4.10E-1	2.08E-1	8.30E-3	2.10E-3	**5.26E-4**	1.32E-4	**3.28E-5**	8.11E-6
Order	-	9.83E-1	4.64	1.98	**2.00**	2.00	**2.00**	2.02
CPU time (s)	23.2	39.1	68.0	1.24E2	**2.42E2**	4.57E2	**8.90E2**	1.76E3

Table 2.8: Spatial errors and time consumptions for SIFD at $t = 1$ with $\varepsilon = \frac{1}{2^4}$.

h	$h_0/2$	$h_0/2^2$	$h_0/2^3$	$h_0/2^4$	$h_0/2^5$	$h_0/2^6$	$h_0/2^7$	$h_0/2^8$
$e^{\varepsilon}_{H^1}(t = 1)$	4.10E-1	2.08E-1	8.30E-3	2.10E-3	**5.26E-4**	1.32E-4	**3.28E-5**	8.11E-6
Order	-	9.83 E-1	4.64	1.98	**2.00**	2.00	**2.00**	2.02
CPU time (s)	4.52	6.94	12.8	24.1	**47.9**	92.8	**1.79E2**	3.46E2

2.4.2 Energy conservation of the 4cFDs

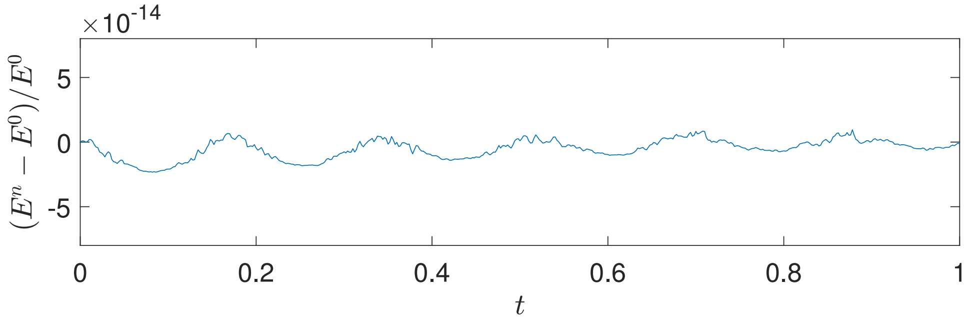

Figure 2.4: Variation of the discrete energy for CN-4cFD

During our iteration solver of the CN-4cFD, the computational error tolerance is taken as 10^{-12}. From the Figure 2.4 we can see the relative change of the discrete energy E^n in (2.2.17) is quite small and E^n is well conserved. Figure 2.5 shows a comparison of the discrete energies w.r.t. different ε's. The energy is the same order of $O(\frac{1}{\varepsilon^2})$ as the energy formula (1.2.4) shows. Therefore, we rescale each energy by a factor ε^2. In order to show the variation of the energy of SI-4cFD, the discrete energies are calculated with a coarse spatial mesh with $h = \frac{1}{8}$.

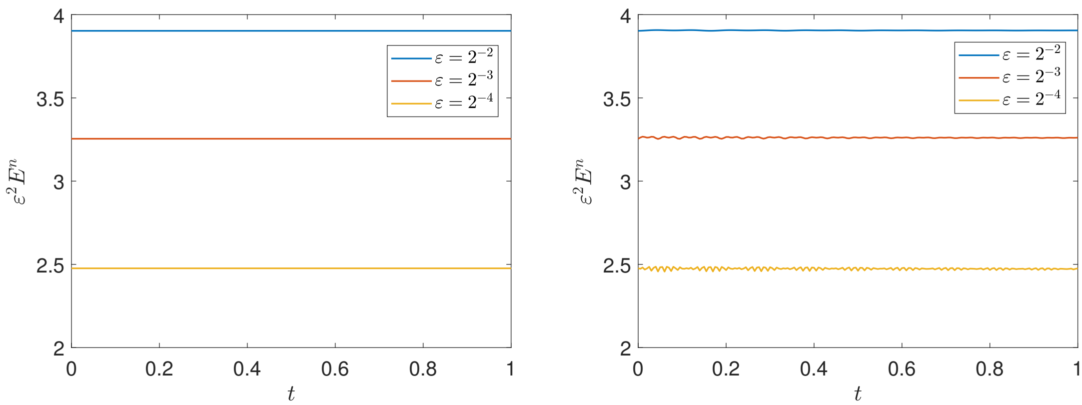

(a) (b)

Figure 2.5: Plot of scaled energies for CN-4cFD (a) and SI-4cFD (b).

Chapter 3

Error Estimate of a 4cFD for ZS

3.1 ZS in the subsonic regime

In their recent work [32], Cai and Yuan considered a semi-implicit conservative finite difference scheme to ZS in the subsonic regime. They got a rigorous uniform error bounds independent of the dimensionless parameter ε for suitable initial data. Due to the high speed outgoing wave from the initial layer [2, 17, 91], the numerical method needs a large spatial domain, which arouses large computational cost if we need small h to achieve a required accuracy. This situation can be severe for the ill-prepared initial data, whose error bound is inversely proportional to a power of ε, such as a spatial error of order $O(h^2/\varepsilon)$ for the scheme in [32]. Therefore, we adopt the fourth-order compact scheme [68, 116] to ZS, by approximating the spatial derivatives at a grid point with the same number of nodes as the second order method needs to achieve a higher accuracy, and the computational cost can be reduced with a coarser grid partition.

The rest of this chapter is organized as follows. In section 3.2, we introduce a semi-implicit fourth-order compact finite difference scheme for ZS. The solvability, stability, and conservation laws of both the discrete wave energy and the Hamiltonian are also discussed. In section 3.3, the error estimates of the scheme, especially the dependence of spatial and temporal errors on the small parameter ε, and a biased error estimate transferred by the nonlinear Schrödinger limit are analysed rigorously. Several numerical simulations are reported in section 3.4 to test the convergence rate from the theoretical analysis.

3.2 A conservative semi-implicit 4cFD (CSI-4cFD)

In this section, we present the conservative semi-implicit fourth order compact finite difference (CSI-4cFD) method to approximate the ZS. For simplicity, we only show the scheme and analysis in one spacial dimension. Generalizations to higher dimensions are straightforward. For numerical computation, we truncate our computational domain into an interval $\Omega = (a, b)$ with homogeneous Dirichlet boundary conditions. The ZS (1.2.6) now collapses to

$$\begin{cases} i\partial_t E^\varepsilon(x,t) + \partial_{xx} E^\varepsilon(x,t) - N^\varepsilon(x,t)E^\varepsilon(x,t) = 0, \quad x \in \Omega, \ \ t > 0, \\ \varepsilon^2 \partial_{tt} N^\varepsilon(x,t) - \partial_{xx} N^\varepsilon(x,t) - \partial_{xx} \left|E^\varepsilon(x,t)\right|^2 = 0, \quad x \in \Omega, \ \ t > 0, \\ E^\varepsilon(x,0) = E_0(x), N^\varepsilon(x,0) = N_0^\varepsilon(x), \partial_t N^\varepsilon(x,0) = N_1^\varepsilon(x), \ \ x \in \Omega, \\ E^\varepsilon(x,t)|_{\partial\Omega} = 0, \, N^\varepsilon(x,t)|_{\partial\Omega} = 0, \quad t > 0, \end{cases} \tag{3.2.1}$$

With initials

$$N_0^\varepsilon(x) = -|E_0(x)|^2 + \varepsilon^\alpha w_0(x), \tag{3.2.2}$$

$$N_1^\varepsilon(x) = 2\,\mathrm{Im}(\bar{E}_0(x)\Delta E_0(x)) + \varepsilon^{\beta-1} w_1(x), \tag{3.2.3}$$

where $E_0(x)$, $w_0(x)$, and $E_1(x)$ are smooth $O(1)$ initial data with compact support on Ω with parameter $\alpha, \beta \geq 0$. As the unbounded case in Section 1.2.2, we have the three type of initial data classified as well-prepared initial data ($\alpha, \beta \geq 2$), less-ill-prepared initial data ($\min\{\alpha,\beta\} \in [1,2)$), and ill-prepared initial data ($\min\{\alpha,\beta\} \in [0,1)$). The conserved wave energy and Hamiltonian for (3.2.1) are

$$M^\varepsilon(t) = \|E^\varepsilon(\cdot,t)\|^2_{L^2(\Omega)} := \int_\Omega \left|E^\varepsilon(\boldsymbol{x},t)\right|^2 \mathrm{d}\boldsymbol{x} \equiv \int_\Omega \left|E_0(\boldsymbol{x})\right|^2 \mathrm{d}\boldsymbol{x} = M^\varepsilon(0), \tag{3.2.4}$$

and

$$H^\varepsilon(t) := \int_\Omega \left(\left|\partial_x E^\varepsilon(x,t)\right|^2 + N^\varepsilon \left|E^\varepsilon\right|^2 + \frac{1}{2}\left(\varepsilon^2 \left|\partial_x U^\varepsilon\right|^2 + \left|N^\varepsilon(x,t)\right|^2\right) \right) \mathrm{d}x, \tag{3.2.5}$$

with potential function U^ε solves

$$-\partial_{xx}U^\varepsilon = N_t^\varepsilon, \quad U^\varepsilon|_{\partial\Omega} = 0. \tag{3.2.6}$$

3.2.1 The numerical scheme

Define mesh size $h := (b-a)/J$ and time step $\tau := T/N$, with J, N positive integers and $T > 0$ a fixed time less than the maximum common existence time for the solutions of (3.2.1). Denote the grid points and time steps as

$x_j := a + jh, j = 0, 1, \ldots, J; \quad t_n := n\tau,\ n = 0, 1, \ldots, N.$

Let $\mathcal{T}_J = \{1, 2, \cdots, J-1\}$ and $\mathcal{T}_J^0 = \{0, 1, 2, \cdots, J\}$ be the index sets of grid points. Let $E_j^{\varepsilon,n}$ and $N_j^{\varepsilon,n}$ be the numerical approximation of $E^\varepsilon(x_j, t_n)$ and $N^\varepsilon(x_j, t_n)$ for $j \in \mathcal{T}_J^0$ and denote the possible solution space as

$$X_J = \{u = (u_j)_{j\in\mathcal{T}_J^0} \mid u_0 = u_J = 0\} \subset \mathbb{C}^{J+1}. \tag{3.2.7}$$

We use the standard finite difference operators as noted in section 2.2:

$\delta_t^+ u_j^n = \frac{1}{\tau}\left(u_j^{n+1} - u_j^n\right),\ \delta_t^- u_j^n = \frac{1}{\tau}\left(u_j^n - u_j^{n-1}\right),\ \delta_t^2 u_j^n = \frac{1}{\tau^2}\left(u_j^{n+1} - 2u_j^n + u_j^{n-1}\right),$

$\delta_x^+ u_j^n = \frac{1}{h}\left(u_{j+1}^n - u_j^n\right),\ \delta_x^- u_j^n = \frac{1}{h}\left(u_j^n - u_{j-1}^n\right),\ \delta_x^2 u_j^n = \frac{1}{h^2}\left(u_{j+1}^n - 2u_j^n + u_{j-1}^n\right),$

for $u_j^n = E_j^{\varepsilon,n}$ or $N_j^{\varepsilon,n}$. Let $\mathcal{A}_h$ be the standard fourth order approximation of the discrete Laplacian as in Section 2.2:

$$\mathcal{A}_h u_j^n = u_j^n + \frac{h^2}{12}\delta_x^2 u_j^n. \tag{3.2.8}$$

Then we give the conservative SI-4cFD scheme [125] as

$$i\delta_t^- E_j^{\varepsilon,n} = \left[-\mathcal{A}_h^{-1}\delta_x^2 + \frac{N_j^{\varepsilon,n-1} + N_j^{\varepsilon,n}}{2}\right]\frac{E_j^{\varepsilon,n-1} + E_j^{\varepsilon,n}}{2}, \quad j \in \mathcal{T}_J, n \geq 1, \tag{3.2.9}$$

$$\varepsilon^2\delta_t^2 N_j^{\varepsilon,n} = \frac{1}{2}\mathcal{A}_h^{-1}\delta_x^2\left(N_j^{\varepsilon,n+1} + N_j^{\varepsilon,n-1}\right) + \mathcal{A}_h^{-1}\delta_x^2\left|E_j^{\varepsilon,n}\right|^2, \ j \in \mathcal{T}_J, n \geq 1, \tag{3.2.10}$$

with boundary and initial conditions

$$\begin{aligned} &E_0^{\varepsilon,n} = E_J^{\varepsilon,n} = 0, \quad N_0^{\varepsilon,n} = N_J^{\varepsilon,n} = 0, \\ &E_j^{\varepsilon,0} = E_0(x_j), \quad N_j^{\varepsilon,0} = -\left|E_0(x_j)\right|^2 + \varepsilon^\alpha w_0(x_j), \end{aligned} \tag{3.2.11}$$

and

$$\begin{aligned} N_j^{\varepsilon,1} &\approx N_0^{\varepsilon}(x_j) + \tau\partial_t N^{\varepsilon}(x_j,0) + \frac{\tau^2}{2}\partial_{tt}N^{\varepsilon}(x_j,0) \\ &\approx N_0^{\varepsilon}(x_j) + \tau\left(2\operatorname{Im}\left(\mathcal{A}_h^{-1}\bar{E}_0(x_j)\,\delta_x^2 E_0(x_j)\right) + \varepsilon^{\beta-1}w_1(x_j)\right) \\ &+ \frac{\tau^2}{2}\varepsilon^{\alpha-2}\mathcal{A}_h^{-1}\delta_x^2 w_0(x_j). \end{aligned} \tag{3.2.12}$$

Note that the equations for initial conditions in (3.2.11) are from the discretization of (3.2.2) and (3.2.3). In order to ensure the boundedness of $N^{\varepsilon,1}$ for $\alpha,\beta \geq 0$, we adopt the method in [32] and [24] to bound the terms containing $\varepsilon^{\beta-1}$ and $\varepsilon^{\alpha-2}$ in (3.2.12), using the trigonometric function $\sin(\tau/\varepsilon)$ which is uniformly bounded for $\varepsilon \in (0,1]$, and substitute (3.2.12) by:

$$\begin{aligned} N_j^{\varepsilon,1} = N_0^{\varepsilon}(x_j) &+ 2\tau\operatorname{Im}\left(\mathcal{A}_h^{-1}\bar{E}_0(x_j)\,\delta_x^2 E_0(x_j)\right) + \varepsilon^{\beta}\sin\left(\frac{\tau}{\varepsilon}\right)w_1(x_j) \\ &+ \frac{\varepsilon^{\alpha}}{2}\sin^2\left(\frac{\tau}{\varepsilon}\right)\mathcal{A}_h^{-1}\delta_x^2 w_0(x_j). \end{aligned} \tag{3.2.13}$$

For any grid function $u \in X_J$, we recall the standard discrete L^2 norm $\|\cdot\|_{\ell^2}$, semi-H^1 norm $|\cdot|_1$, the equivalent semi-H^1 norm $|\cdot|_{1,*}$ and ℓ^∞ norm $\|\cdot\|_{\ell^\infty}$ respectively as

$$\|u\|_{\ell^2} = \sqrt{h\sum_{j=1}^{J-1}|u_j|^2}, \quad |u|_1 = \sqrt{h\sum_{j=0}^{J-1}|\delta_x^+ u_j|^2},$$
$$|v|_{1,*} = \sqrt{-h\sum_{j=1}^{J-1}\bar{v}_j\mathcal{A}_h^{-1}\delta_x^2 v_j}, \quad \|u\|_{\ell^\infty} = \max_{1\le j\le J-1}|u_j|.$$

3.2.2 Energy conservation

Theorem 3.1. *The CSI-4cFD scheme preserves the discrete wave energy and Hamiltonian defined by*

$$M^{\varepsilon,n} = \|E^{\varepsilon,n}\|_{\ell^2}^2, \quad 0 \le n \le N, \tag{3.2.14}$$

$$\begin{aligned} H^{\varepsilon,n+\frac12} =& \frac12\left(\left|E^{\varepsilon,n+1}\right|_{1,*}^2 + \left|E^{\varepsilon,n}\right|_{1,*}^2\right) + \frac{\varepsilon^2}{2}\left|U^{\varepsilon,n+\frac12}\right|_{1,*}^2 + \frac14\left(\left\|N^{\varepsilon,n+1}\right\|_{\ell^2}^2 + \|N^{\varepsilon,n}\|_{\ell^2}^2\right) \\ &+ \frac{h}{4}\sum_{j=1}^{J-1}(N_j^{\varepsilon,n+1} + N_j^{\varepsilon,n})(|E_j^{\varepsilon,n+1}|^2 + |E_j^{\varepsilon,n}|^2), \quad 0 \le n \le N-1, \end{aligned} \tag{3.2.15}$$

where $U_j^{\varepsilon,n+\frac{1}{2}}$ *solves* $-\mathcal{A}_h^{-1}\delta_x^2 U_j^{\varepsilon,n+\frac{1}{2}} = \delta_t^+ N_j^{\varepsilon,n}$ *with homogeneous Dirichlet boundary* $U_0^{\varepsilon,n} = U_J^{\varepsilon,n} = 0$*, for* $0 \le n \le N$*.*

Proof. For proof of (3.2.14), multiplying $h(\bar{E}_j^{\varepsilon,n} + \bar{E}_j^{\varepsilon,n-1})$ on both side of (3.2.9), and summing them up for all $j \in \mathcal{T}_J$, we have:

$$\begin{aligned} &\frac{i}{\tau}\left(\|E^{\varepsilon,n}\|_{\ell^2}^2 - \left\|E^{\varepsilon,n-1}\right\|_{\ell^2}^2 + 2i\,\mathrm{Im}(\sum_{j=1}^{J-1} E_j^{\varepsilon,n}\bar{E}_j^{\varepsilon,n-1})\right) \\ &= \left|E^{\varepsilon,n} + E^{\varepsilon,n-1}\right|_{1,*}^2 + h\sum_{j=1}^{J-1} N_j^{\varepsilon,n-\frac{1}{2}}\left|E_j^{\varepsilon,n} + E_j^{\varepsilon,n-1}\right|^2, \quad 1 \le n \le N, \end{aligned} \tag{3.2.16}$$

where $N_j^{\varepsilon,n-\frac{1}{2}} = \frac{1}{2}(N_j^{\varepsilon,n} + N_j^{\varepsilon,n-1})$ is real-valued. The imaginary part of the above equation indicates

$$\frac{i}{\tau}\left(\|E^{\varepsilon,n}\|_{\ell^2}^2 - \left\|E^{\varepsilon,n-1}\right\|_{\ell^2}^2\right) = 0, \quad 1 \le n \le N, \tag{3.2.17}$$

i.e.,

$$\|E^{\varepsilon,n}\|_{\ell^2}^2 = \left\|E^{\varepsilon,n-1}\right\|_{\ell^2}^2, \quad 1 \le n \le N. \tag{3.2.18}$$

For proof of (3.2.15), multiplying $h(\bar{E}_j^{\varepsilon,n} - \bar{E}_j^{\varepsilon,n-1})$ on both side of (3.2.9), summing them up for all $j \in \mathcal{T}_J$, and considering the real parts, we have

$$\frac{1}{2}|E^{\varepsilon,n}|_{1,*} - \frac{1}{2}\left|E^{\varepsilon,n-1}\right|_{1,*} + \frac{1}{2}\langle N^{\varepsilon,n-\frac{1}{2}}, |E^{\varepsilon,n}|^2 - |E^{\varepsilon,n-1}|^2\rangle = 0, \quad 1 \le n \le N. \tag{3.2.19}$$

Multiplying $\tau h(U_j^{\varepsilon,n+\frac{1}{2}} + U_j^{\varepsilon,n-\frac{1}{2}})$ on both side of (3.2.10), and summing them up for all $j \in \mathcal{T}_J$, we have

$$\begin{aligned} &\varepsilon^2\left|U^{\varepsilon,n+\frac{1}{2}}\right|_{1,*} - \varepsilon^2\left|U^{\varepsilon,n-\frac{1}{2}}\right|_{1,*} + \frac{1}{2}\|N^{\varepsilon,n+1}\|_{\ell^2}^2 - \frac{1}{2}\left\|N^{\varepsilon,n-1}\right\|_{\ell^2}^2 \\ &+ \langle |E^{\varepsilon,n}|^2, N^{\varepsilon,n+1} - N^{\varepsilon,n-1}\rangle = 0, \quad 1 \le n \le N-1. \end{aligned} \tag{3.2.20}$$

(3.2.19)+$\frac{1}{2}$(3.2.20) reveals

$$\begin{aligned}
&\frac{1}{2}\left(\left|E^{\varepsilon,n+1}\right|_{1,*}^2+\left|E^{\varepsilon,n}\right|_{1,*}^2\right)+\frac{\varepsilon^2}{2}\left|U^{\varepsilon,n+\frac{1}{2}}\right|_{1,*}^2+\frac{1}{4}\left(\left\|N^{\varepsilon,n+1}\right\|_{\ell^2}^2+\left\|N^{\varepsilon,n}\right\|_{\ell^2}^2\right)\\
&+\frac{h}{4}\sum_{j=0}^{J}(N_j^{\varepsilon,n+1}+N_j^{\varepsilon,n})(|E_j^{\varepsilon,n+1}|^2+|E_j^{\varepsilon,n}|^2)\\
=&\frac{1}{2}\left(\left|E^{\varepsilon,n-1}\right|_{1,*}^2+\left|E^{\varepsilon,n}\right|_{1,*}^2\right)+\frac{\varepsilon^2}{2}\left|U^{\varepsilon,n-\frac{1}{2}}\right|_{1,*}^2+\frac{1}{4}\left(\left\|N^{\varepsilon,n-1}\right\|_{\ell^2}^2+\left\|N^{\varepsilon,n}\right\|_{\ell^2}^2\right)\\
&+\frac{h}{4}\sum_{j=0}^{J}(N_j^{\varepsilon,n-1}+N_j^{\varepsilon,n})(|E_j^{\varepsilon,n-1}|^2+|E_j^{\varepsilon,n}|^2),\quad 1\le n\le N-1,
\end{aligned}\tag{3.2.21}$$

i.e.,

$$H^{\varepsilon,n+\frac{1}{2}}=H^{\varepsilon,n-\frac{1}{2}},\quad 1\le n\le N-1.\tag{3.2.22}$$

This completes the proof. □

3.2.3 Solvability of the difference equations

Lemma 3.1. (Solvability for the CSI-4cFD) *For any given initial data $E^{\varepsilon,0}, N^{\varepsilon,0}, N^{\varepsilon,1}\in X_J$, there exists a unique set of solutions $E^{\varepsilon,n}$ and $N^{\varepsilon,n}$ to the CSI-4cFD* (3.2.9) *and* (3.2.10) *for $n>1$.*

Proof. The lemma can be proof by induction. During the sequential update of the numerical solutions:

$$E^{\varepsilon,1}\to N^{\varepsilon,2}\to E^{\varepsilon,2}\to N^{\varepsilon,3}\to\cdots,\tag{3.2.23}$$

a linear system is solved at each step. Therefore, the solution exists and is unique since two non-degenerated linear systems are solved consecutively in each iteration.

□

3.3 Error estimates

Let T^* be the maximum common existence time for the solutions $(E^\varepsilon(x,t),N^\varepsilon(x,t))$ and $E(x,t)$ to the ZS (3.2.1) and the corresponding cubic NLSE (1.2.10) respectively. For any $T\in(0,T^*]$, as the asymptotic analysis showed, we may assume that the exact solutions $(E^\varepsilon(x,t), N^\varepsilon(x,t))$ and $E(x,t)$ are smooth enough and satisfying the homogeneous Dirichlet boundary conditions and the following boundedness assumptions:

$$\begin{aligned}
&\|E^\varepsilon\|_{L^\infty([0,T];W^{7,\infty}(\Omega))} + \|E^\varepsilon\|_{W^{1,\infty}([0,T];W^{4,\infty}(\Omega))} + \varepsilon^{1-\alpha^*}\|E^\varepsilon\|_{W^{2,\infty}([0,T];W^{3,\infty}(\Omega))}\\
&+ \varepsilon^{2-\alpha^\dagger}\|E^\varepsilon\|_{W^{3,\infty}([0,T];W^{1,\infty}(\Omega))} \lesssim 1,\\
&\|N^\varepsilon\|_{L^\infty([0,T];W^{7,\infty}(\Omega))} + \varepsilon^{1-\alpha^*}\|N^\varepsilon\|_{W^{1,\infty}([0,T];W^{6,\infty}(\Omega))} + \varepsilon^{2-\alpha^\dagger}\|N^\varepsilon\|_{W^{2,\infty}([0,T];W^{2,\infty}(\Omega))}\\
&+ \varepsilon^{3-\alpha^\dagger}\|N^\varepsilon\|_{W^{3,\infty}([0,T];W^{2,\infty}(\Omega))} + \varepsilon^{4-\alpha^\dagger}\|N^\varepsilon\|_{W^{4,\infty}([0,T];W^{1,\infty}(\Omega))} \lesssim 1,
\end{aligned} \tag{3.A}$$

with the convergence

$$\|E^\varepsilon - E\|_{L^\infty([0,T],H^1(\Omega))} \lesssim \varepsilon^{1+\alpha^*}, \ \left\|N^\varepsilon - |E|^2\right\|_{L^\infty([0,T],L^2(\Omega))} \lesssim \varepsilon^{\alpha^\dagger}, \tag{3.B}$$

under a good initial data assumption

$$\|E_0\|_{H^6(\Omega)} + \|w_0\|_{H^4(\Omega)} + \|w_1\|_{H^4(\Omega)} \lesssim 1, \tag{3.C}$$

where

$$\alpha^* = \min(1,\alpha,\beta), \quad \alpha^\dagger = \min(\alpha,\beta,2). \tag{3.3.1}$$

Define the error functions $e^{\varepsilon,n}, \nu^{\varepsilon,n} \in X_J$ for $n \geq 0$ as

$$e_j^{\varepsilon,n} = E^\varepsilon(x_j,t_n) - E_j^{\varepsilon,n}, \quad \nu_j^{\varepsilon,n} = N^\varepsilon(x_j,t_n) - N_j^{\varepsilon,n}, \quad j \in \mathcal{T}_J^0, \tag{3.3.2}$$

3.3.1 Main results

For the CSI-4cFD (3.2.9), we have the following error estimates.

Theorem 3.2. (Error estimates for well-prepared and less-ill-prepared initial data) *Assume $\tau \lesssim h$ and under the assumption (3.A), there exist $\tau_0, h_0 > 0$ sufficiently small and independent of ε such that for any $\varepsilon \in (0,1]$, we have the following error estimate of the CSI-4cFD scheme with well-prepared and less-ill-prepared initial data ($\alpha, \beta \geq 1$) for any $\tau \in (0,\tau_0], h \in (0,h_0]$:*

$$\|e^{\varepsilon,n}\|_{\ell^2} + |e^{\varepsilon,n}|_1 + \|\nu^{\varepsilon,n}\|_{\ell^2} \lesssim h^4 + \frac{\tau^2}{\varepsilon^{3-\alpha^\dagger}}, \quad 0 \leq n \leq \frac{T}{\tau}, \tag{3.3.3}$$

$$\|e^{\varepsilon,n}\|_{\ell^2} + |e^{\varepsilon,n}|_1 + \|\nu^{\varepsilon,n}\|_{\ell^2} \lesssim h^4 + \tau^2 + \varepsilon^{\alpha^\dagger}, \ \ 0 \le n \le \frac{T}{\tau}. \tag{3.3.4}$$

Furthermore, combining (3.3.3) *and* (3.3.4) *together, we have the following uniform error estimate independent of* ε*:*

$$\|e^{\varepsilon,n}\|_{\ell^2} + |e^{\varepsilon,n}|_1 + \|\nu^{\varepsilon,n}\|_{\ell^2} \lesssim h^4 + \tau^{2\alpha^\dagger/3}, \ \ 0 \le n \le \frac{T}{\tau}. \tag{3.3.5}$$

Particularly, for the well-prepared initial data case ($\alpha, \beta \ge 2$)*, we have* $\alpha^\dagger = 2$ *and*

$$\|e^{\varepsilon,n}\|_{\ell^2} + |e^{\varepsilon,n}|_1 + \|\nu^{\varepsilon,n}\|_{\ell^2} \lesssim h^4 + \tau^{4/3}, \ \ 0 \le n \le \frac{T}{\tau}. \tag{3.3.6}$$

Theorem 3.3. (Error estimates for ill-prepared initial data) *Assume* $\tau \lesssim h$ *and under the assumption* (3.A)*, there exist* τ_0*,* $h_0 > 0$ *sufficiently small and independent of* ε *such that for any* $\varepsilon \in (0, 1]$*, we have the following error estimate of the CSI-4cFD scheme with ill-prepared initial data* ($\min\{\alpha, \beta\} \in [0, 1)$) *for any* $\tau \in (0, \tau_0]$*,* $h \in (0, h_0]$ *:*

$$\|e^{\varepsilon,n}\|_{\ell^2} + |e^{\varepsilon,n}|_1 + \|\nu^{\varepsilon,n}\|_{\ell^2} \lesssim \frac{h^4}{\varepsilon^{1-\alpha^*}} + \frac{\tau^2}{\varepsilon^{3-\alpha^*}}, \quad 0 \le n \le \frac{T}{\tau}. \tag{3.3.7}$$

Note that the uniform error bound (3.3.5) in Theorem 3.2 can be illustrated in the following triangle diagram with error scales labelled on each arrow connecting two terms:

$$\begin{tikzcd}
(E^{\varepsilon,n}, N^{\varepsilon,n}) \arrow[rr, "O(h^4+\frac{\tau^2}{\varepsilon^{3-\alpha^\dagger}})"] \arrow[dr, "O(h^4+\tau^2+\varepsilon^{\alpha^\dagger})"'] & & (E^\varepsilon, N^\varepsilon). \\
& (E, -|E|^2) \arrow[ur, "O(\varepsilon^{1+\alpha^*}+\varepsilon^{\alpha^\dagger})"'] &
\end{tikzcd}$$

Define the local truncation errors $\eta^{\varepsilon,n}, \xi^{\varepsilon,n} \in X_J$ of CSI-4cFD (3.2.9) and (3.2.10) as

$$\eta_j^{\varepsilon,n} = i\delta_t^- E^\varepsilon(x_j, t_n) + \left[\mathcal{A}_h^{-1}\delta_x^2 - \frac{N^\varepsilon(x_j, t_{n-1}) + N^\varepsilon(x_j, t_n)}{2}\right] \frac{E^\varepsilon(x_j, t_{n-1}) + E^\varepsilon(x_j, t_n)}{2}, \tag{3.3.8}$$

$$\xi_j^{\varepsilon,n} = \varepsilon^2\delta_t^2 N^\varepsilon(x_j, t_n) - \mathcal{A}_h^{-1}\delta_x^2\left(\frac{N^\varepsilon(x_j, t_{n+1}) + N^\varepsilon(x_j, t_{n-1})}{2} + |E^\varepsilon(x_j, t_n)|^2\right), \tag{3.3.9}$$

for $j \in \mathcal{T}_J$, $n \ge 1$.

Lemma 3.2. *Under assumption* (3.A)*, we have*

$$\|\eta^{\varepsilon,n}\|_{\ell^2} + \|\xi^{\varepsilon,n}\|_{\ell^2} + |\eta^{\varepsilon,n}|_1 \lesssim h^4 + \frac{\tau^2}{\varepsilon^{2-\alpha^\dagger}}, \tag{3.3.10}$$

$$\|\delta_t \xi^{\varepsilon,n}\|_{\ell^2} \lesssim \frac{h^4}{\varepsilon^{1-\alpha^*}} + \frac{\tau^2}{\varepsilon^{3-\alpha^\dagger}}. \tag{3.3.11}$$

Proof. For each $n \geq 1$ and $j \in \mathcal{T}_J$, take Taylor expansion of $E^\varepsilon(x,t)$ at point $(x_j, t_n - \frac{\tau}{2})$, and $E^\varepsilon_{xx}(x,t)$ at points (x_j,t_n) and (x_j,t_{n-1}) we have

$$\begin{aligned}
\eta_j^{\varepsilon,n} =& i\delta_t^- E^\varepsilon(x_j,t_n) + \left[\mathcal{A}_h^{-1}\delta_x^2 - \frac{N^\varepsilon(x_j,t_{n-1}) + N^\varepsilon(x_j,t_n)}{2}\right]\frac{E^\varepsilon(x_j,t_{n-1}) + E^\varepsilon(x_j,t_n)}{2}\\
&- \left(i\partial_t E^\varepsilon(x_j,t_{n-\frac12}) + \partial_x^2 E^\varepsilon(x_j,t_{n-\frac12}) - N^\varepsilon(x_j,t_{n-\frac12})E^\varepsilon(x_j,t_{n-\frac12})\right)\\
=& i\left(\delta_t^- E^\varepsilon(x_j,t_n) - \partial_t E^\varepsilon(x_j,t_{n-\frac12})\right) + \left(\frac{\partial_x^2 E^\varepsilon(x_j,t_{n-1}) + \partial_x^2 E^\varepsilon(x_j,t_n)}{2} - \partial_x^2 E^\varepsilon(x_j,t_{n-\frac12})\right)\\
&+ \left(\mathcal{A}_h^{-1}\delta_x^2\frac{E^\varepsilon(x_j,t_{n-1}) + E^\varepsilon(x_j,t_n)}{2} - \frac{\partial_x^2 E^\varepsilon(x_j,t_{n-1}) + \partial_x^2 E^\varepsilon(x_j,t_n)}{2}\right)\\
&+ \frac{N^\varepsilon(x_j,t_{n-1}) + N^\varepsilon(x_j,t_n)}{2}\left(E^\varepsilon(x_j,t_{n-\frac12}) - \frac{E^\varepsilon(x_j,t_{n-1}) + E^\varepsilon(x_j,t_n)}{2}\right)\\
&+ \left(N^\varepsilon(x_j,t_{n-\frac12}) - \frac{N^\varepsilon(x_j,t_{n-1}) + N^\varepsilon(x_j,t_n)}{2}\right)E^\varepsilon(x_j,t_{n-\frac12}) \qquad (3.3.12)\\
=& \frac{i\tau^2}{8}\int_0^1\int_0^\theta\int_{-s}^s \partial_t^3 E^\varepsilon\left(x_j, \frac{\sigma\tau}{2} + t_{n-\frac12}\right)\mathrm{d}\sigma\mathrm{d}s\mathrm{d}\theta + \frac{\tau^2}{8}\int_0^1\int_{-\theta}^\theta \partial_t^2\partial_x^2 E^\varepsilon\left(x_j, \frac{s\tau}{2} + t_{n-\frac12}\right)\mathrm{d}s\mathrm{d}\theta\\
&+ \left(\mathcal{A}_h^{-1}\delta_x^2\frac{E^\varepsilon(x_j,t_{n-1}) + E^\varepsilon(x_j,t_n)}{2} - \frac{\partial_x^2 E^\varepsilon(x_j,t_{n-1}) + \partial_x^2 E^\varepsilon(x_j,t_n)}{2}\right)\\
&- \frac{\tau^2}{16}\left(N^\varepsilon(x_j,t_{n-1}) + N^\varepsilon(x_j,t_n)\right)\int_0^1\int_{-\theta}^\theta \partial_t^2 E^\varepsilon\left(x_j, s\tau/2 + t_{n-1/2}\right)\mathrm{d}s\mathrm{d}\theta\\
&- \frac{\tau^2}{8}E^\varepsilon\left(x_j,t_{n-1/2}\right)\int_0^1\int_{-\theta}^\theta \partial_t^2 N^\varepsilon\left(x_j, s\tau/2 + t_{n-1/2}\right)\mathrm{d}s\mathrm{d}\theta.
\end{aligned}$$

For the third term in the last equality of (3.3.12), we have

$$\begin{aligned}
\mathcal{A}_h\left(\mathcal{A}_h^{-1}\delta_x^2 E^\varepsilon(x_j,t_n) - \partial_x^2 E^\varepsilon(x_j,t_n)\right) &= \delta_x^2 E^\varepsilon(x_j,t_n) - \mathcal{A}_h\partial_x^2 E^\varepsilon(x_j,t_n)\\
&= -\frac{h^4}{240}\partial_x^6 E^\varepsilon(\zeta_j,t_n),
\end{aligned} \tag{3.3.13}$$

for some $\zeta_j \in (x_{j-1}, x_{j+1})$. Therefore, we have the following bound

$$\left|\mathcal{A}_h^{-1}\delta_x^2\frac{E^\varepsilon(x_j,t_{n-1}) + E^\varepsilon(x_j,t_n)}{2} - \frac{\partial_x^2 E^\varepsilon(x_j,t_{n-1}) + \partial_x^2 E^\varepsilon(x_j,t_n)}{2}\right| \lesssim h^4\left\|\partial_x^6 E^\varepsilon\right\|_{L^\infty(\Omega_T)}.$$

Under assumption (3.A), we have

$$
\begin{aligned}
|\eta_j^{\varepsilon,n}| \lesssim & h^4\left\|\partial_x^6 E^\varepsilon\right\|_\infty + \tau^2\left(\left\|\partial_t^3 E^\varepsilon\right\|_\infty + \left\|\partial_t^2\partial_x^2 E^\varepsilon\right\|_\infty\right. \\
& \left. + \|N^\varepsilon\|_\infty\left\|\partial_t^2 E^\varepsilon\right\|_\infty + \|E^\varepsilon\|_\infty\left\|\partial_t^2 N^\varepsilon\right\|_\infty\right) \\
\lesssim & h^4 + \frac{\tau^2}{\varepsilon^{2-\alpha^\dagger}}.
\end{aligned} \tag{3.3.14}
$$

Similarly, we have

$$
\begin{aligned}
|\xi_j^{\varepsilon,n}| \lesssim & h^4\left(\left\|\partial_x^6 N^\varepsilon\right\|_\infty + \left\|\partial_x^6 |E^\varepsilon|^2\right\|_\infty\right) + \tau^2\left(\varepsilon^2\left\|\partial_t^4 N^\varepsilon\right\|_\infty + \left\|\partial_t^2\partial_x^2 N^\varepsilon\right\|_\infty\right) \\
\lesssim & h^4 + \frac{\tau^2}{\varepsilon^{2-\alpha^\dagger}}.
\end{aligned} \tag{3.3.15}
$$

Apply δ_x^+ and δ_t to (3.3.8) and (3.3.9) respectively, we have

$$
\begin{aligned}
|\delta_x^+\eta_j^{\varepsilon,n}| \lesssim & h^4\left\|\partial_x^7 E^\varepsilon\right\|_\infty + \tau^2\left(\left\|\partial_t^3\partial_x E^\varepsilon\right\|_\infty + \left\|\partial_t^2\partial_x^3 E^\varepsilon\right\|_\infty + \|\partial_x N^\varepsilon\|_\infty\left\|\partial_t^2 E^\varepsilon\right\|_\infty\right. \\
& \left. + \|N^\varepsilon\|_\infty\left\|\partial_t^2\partial_x E^\varepsilon\right\|_\infty + \|\partial_x E^\varepsilon\|_\infty\left\|\partial_t^2 N^\varepsilon\right\|_\infty + \|E^\varepsilon\|_\infty\left\|\partial_t^2\partial_x N^\varepsilon\right\|_\infty\right) \\
\lesssim & h^4 + \frac{\tau^2}{\varepsilon^{2-\alpha^\dagger}},
\end{aligned}
$$

$$
\begin{aligned}
|\delta_t\xi_j^{\varepsilon,n}| \lesssim & h^4\left(\left\|\partial_x^6\partial_t N^\varepsilon\right\|_\infty + \left\|\partial_x^6\partial_t |E^\varepsilon|^2\right\|_\infty\right) + \tau^2\left(\varepsilon^2\left\|\partial_t^5 N^\varepsilon\right\|_\infty + \left\|\partial_t^3\partial_x^2 N^\varepsilon\right\|_\infty\right) \\
\lesssim & \frac{h^4}{\varepsilon^{1-\alpha^*}} + \frac{\tau^2}{\varepsilon^{3-\alpha^\dagger}}.
\end{aligned}
$$

□

Lemma 3.3. *Under assumption (3.A) and (3.C), we have the following estimates for the first step error:*

$$
\left\|\nu^{\varepsilon,1}\right\|_{\ell^2} \lesssim \frac{\tau h^4}{\varepsilon^{1-\alpha^*}} + \frac{\tau^3}{\varepsilon^{3-\alpha^\dagger}}, \quad \left\|\delta_t^-\nu^{\varepsilon,1}\right\|_{\ell^2} \lesssim \frac{h^4}{\varepsilon^{1-\alpha^*}} + \frac{\tau^2}{\varepsilon^{3-\alpha^\dagger}}. \tag{3.3.16}
$$

The first estimation in (3.3.16) is from a direct Taylor expansion of $N^\varepsilon(x,t)$ at $(x_j, 0)$ for (3.2.13). The second estimation is a direct induction of the first one.

In order to give a rigorous error estimate without presumption on the boundedness of the numerical solutions, we adopt the cut-off technique to the nonlinear terms in ZS (3.2.1) as [5, 7, 32] did. We apply the cut-off function onto E^ε for the nonlinear terms $N^\varepsilon E^\varepsilon, \Delta|E^\varepsilon|^2$ in (3.2.1) as in [32]. Choose a sooth function

$\rho(s) \in C^\infty([0,+\infty))$ such that

$$\rho(s) = \begin{cases} 1, & 0 \le s < 1, \\ \in [0,1], & 1 \le s < 2, \\ 0, & s \ge 2. \end{cases} \tag{3.3.17}$$

Let M_0 be a uniform upper bound of $E(x,t)$ and $E^\varepsilon(x,t)$ for all $\varepsilon \in (0,1]$ on $\Omega_T = \Omega \times (0,T)$. For example, choose

$$M_0 = \max\{\|E(x,t)\|_{L^\infty(\Omega_T)}, \sup_{\varepsilon\in(0,1]} \|E^\varepsilon(x,t)\|_{L^\infty(\Omega_T)}\}, \tag{3.3.18}$$

Define the cut-off function for norms

$$\rho_B(s) = s\rho(s/B), \quad s \ge 0, \tag{3.3.19}$$

where $B = (1+M_0)^2$. Let

$$g(u,v) = \int_0^1 \rho_B'(\theta|u|^2 + (1-\theta)|v|^2)\mathrm{d}\theta. \tag{3.3.20}$$

Let $\hat{E}^{\varepsilon,0} = E^{\varepsilon,0}$, $\hat{N}^{\varepsilon,0} = N^{\varepsilon,0}$, $\hat{N}^{\varepsilon,1} = N^{\varepsilon,1}$ and let $(\hat{E}^{\varepsilon,n}, \hat{N}^{\varepsilon,n})$ be the solution of a variation of the CSI-4cFD scheme (3.2.9) and (3.2.10):

$$i\delta_t^- \hat{E}_j^{\varepsilon,n} = \left[-\mathcal{A}_h^{-1}\delta_x^2 + \frac{\hat{N}_j^{\varepsilon,n} + \hat{N}_j^{\varepsilon,n-1}}{2} g(\hat{E}_j^{\varepsilon,n}, \hat{E}_j^{\varepsilon,n-1})\right] \frac{\hat{E}_j^{\varepsilon,n} + \hat{E}_j^{\varepsilon,n-1}}{2}, \tag{3.3.21}$$

$$\varepsilon^2\delta_t^2 \hat{N}_j^{\varepsilon,n} = \frac{1}{2}\mathcal{A}_h^{-1}\delta_x^2\left(\hat{N}_j^{\varepsilon,n+1} + \hat{N}_j^{\varepsilon,n-1}\right) + \mathcal{A}_h^{-1}\delta_x^2 f\left(|\hat{E}_j^{\varepsilon,n}|^2\right), \tag{3.3.22}$$

for $j \in \mathcal{T}_J, n \ge 1$. Notice that $(\hat{E}^{\varepsilon,n}, \hat{N}^{\varepsilon,n})$ is another numerical approximation of $(E^\varepsilon(x_j,t_n), N^\varepsilon(x_j,t_n))$ and is equal to $(E^{\varepsilon,n}, N^{\varepsilon,n})$ if the function $g(\hat{E}_j^{\varepsilon,n}, \hat{E}_j^{\varepsilon,n-1}) = 1$ in (3.3.21) and $\rho_B\left(|\hat{E}_j^{\varepsilon,n}|^2\right) = |\hat{E}_j^{\varepsilon,n}|^2$ in (3.3.22) for all j,n. Since ρ_B' is bounded, we know ρ_B and g are Lipschitz functions. Therefore, the system composed by (3.3.21) and (3.3.22) is uniquely solvable for small time step τ. In the following context, we will prove the theorem 3.2 and 3.3 type error estimates for $(\hat{E}^{\varepsilon,n}, \hat{N}^{\varepsilon,n})$ at first.

3.3.2 An error bound via the energy method

We will show (3.3.3) type error estimate for $(\hat{E}^{\varepsilon,n}, \hat{N}^{\varepsilon,n})$. Define new error function $\hat{e}^{\varepsilon,n}, \hat{\nu}^{\varepsilon,n} \in X_J$ for $n \geq 0$ as

$$\hat{e}_j^{\varepsilon,n} = E^\varepsilon(x_j, t_n) - \hat{E}_j^{\varepsilon,n},\ \hat{\nu}_j^{\varepsilon,n} = N^\varepsilon(x_j, t_n) - \hat{N}_j^{\varepsilon,n},\ j \in \mathcal{T}_J^0, \tag{3.3.23}$$

and local truncation error $\hat{\eta}^{\varepsilon,n}, \hat{\xi}^{\varepsilon,n} \in X_J$ for the new scheme (3.3.21) and (3.3.22).

$$\begin{aligned}\hat{\eta}_j^{\varepsilon,n} =& i\delta_t^- E^\varepsilon(x_j,t_n) + \left[\mathcal{A}_h^{-1}\delta_x^2 - \frac{N^\varepsilon(x_j,t_{n-1}) + N^\varepsilon(x_j,t_n)}{2} g(E^\varepsilon(x_j,t_{n-1}), E^\varepsilon(x_j,t_n))\right] \\ & \times \frac{E^\varepsilon(x_j,t_{n-1}) + E^\varepsilon(x_j,t_n)}{2}, \\ \hat{\xi}_j^{\varepsilon,n} =& \varepsilon^2\delta_t^2 N^\varepsilon(x_j,t_n) - \mathcal{A}_h^{-1}\delta_x^2\left(\frac{N^\varepsilon(x_j,t_n) + N^\varepsilon(x_j,t_{n-1})}{2} + f\left(|E^\varepsilon(x_j,t_n)|^2\right)\right),\end{aligned}$$

for $j \in \mathcal{T}_J$, $n \geq 1$.

Under assumption (3.A), we have $g(E^\varepsilon(x_j,t_{n-1}), E^\varepsilon(x_j,t_n)) = 1$ and $\rho_B\left(|E^\varepsilon(x_j,t_n)|^2\right) = |E^\varepsilon(x_j,t_n)|^2$. Therefore, $\hat{\eta}_j^{\varepsilon,n} = \eta_j^{\varepsilon,n}$ and $\hat{\xi}_j^{\varepsilon,n} = \xi_j^{\varepsilon,n}$. As in Lemma 3.2, we have the following error bounds for $\hat{\eta}^{\varepsilon,n}, \hat{\xi}^{\varepsilon,n} \in X_J$:

$$\begin{aligned}\|\hat{\eta}^{\varepsilon,n}\|_{\ell^2} + \left\|\hat{\xi}^{\varepsilon,n}\right\|_{\ell^2} + |\hat{\eta}^{\varepsilon,n}|_1 \lesssim h^4 + \frac{\tau^2}{\varepsilon^{2-\alpha^\dagger}},\ \left\|\delta_t\hat{\xi}^{\varepsilon,n}\right\|_{\ell^2} \lesssim \frac{h^4}{\varepsilon^{1-\alpha^*}} + \frac{\tau^2}{\varepsilon^{3-\alpha^\dagger}},& \\ \left\|\hat{\nu}^{\varepsilon,1}\right\|_{\ell^2} \lesssim \frac{\tau h^4}{\varepsilon^{1-\alpha^*}} + \frac{\tau^3}{\varepsilon^{3-\alpha^\dagger}},\ \left\|\delta_t^-\hat{\nu}^{\varepsilon,1}\right\|_{\ell^2} \lesssim \frac{h^4}{\varepsilon^{1-\alpha^*}} + \frac{\tau^2}{\varepsilon^{3-\alpha^\dagger}}.&\end{aligned} \tag{3.3.24}$$

As in the conservation proof of the discrete Hamilton, we introduce the discrete potential function $\hat{u}^{\varepsilon,n-\frac{1}{2}} \in X_J$ such that

$$-\mathcal{A}_h^{-1}\delta_x^2\hat{u}_j^{\varepsilon,n-\frac{1}{2}} = \delta_t^-\hat{\nu}_j^{\varepsilon,n}, \tag{3.3.25}$$

for $j = 1, \cdots, J-1,\ n \geq 1$. Note that (3.3.25) and (3.3.24) give the bound of first layer of $\hat{u}^\varepsilon$

$$\left\|\hat{u}^{\varepsilon,1}\right\|_{\ell^2} \lesssim \left\|\delta_t^-\hat{\nu}^{\varepsilon,1}\right\|_{\ell^2} \lesssim \frac{h^4}{\varepsilon^{1-\alpha^*}} + \frac{\tau^2}{\varepsilon^{3-\alpha^\dagger}}. \tag{3.3.26}$$

Subtracting (3.3.21) from (3.3.8) and (3.3.22) from (3.3.9), we get the following error equations:

$$i\delta_t^-\hat{e}_j^{\varepsilon,n} = -\frac{1}{2}\mathcal{A}_h^{-1}\delta_x^2(\hat{e}_j^{\varepsilon,n} + \hat{e}_j^{\varepsilon,n-1}) + \hat{R}_j^n + \hat{\eta}_j^{\varepsilon,n}, \tag{3.3.27}$$

$$\varepsilon^2\delta_t^2\hat{\nu}_j^{\varepsilon,n} = \mathcal{A}_h^{-1}\delta_x^2\left(\frac{\hat{\nu}_j^{\varepsilon,n} + \hat{\nu}_j^{\varepsilon,n-1}}{2} + \hat{P}_j^n\right) + \hat{\xi}_j^{\varepsilon,n}, \tag{3.3.28}$$

for $j \in \mathcal{T}_J, n \geq 1$, with

$$\begin{aligned}
\hat{R}_j^n =&\frac{1}{4}\left(N^\varepsilon\left(x_j,t_n\right)+N^\varepsilon\left(x_j,t_{n-1}\right)\right)\\
&\times g\left(E^\varepsilon\left(x_j,t_n\right),E^\varepsilon\left(x_j,t_{n-1}\right)\right)\left(E^\varepsilon\left(x_j,t_n\right)+E^\varepsilon\left(x_j,t_{n-1}\right)\right)\\
&-\frac{1}{4}(N_j^{\varepsilon,n}+N_j^{\varepsilon,n-1})g(\hat{E}_j^{\varepsilon,n},\hat{E}_j^{\varepsilon,n-1})(\hat{E}_j^{\varepsilon,n}+\hat{E}_j^{\varepsilon,n-1}),
\end{aligned} \tag{3.3.29}$$

$$\hat{P}_j^n = \rho_B(|E^\varepsilon(x_j,t_n)|^2) - \rho_B(|\hat{E}_j^{\varepsilon,n}|^2). \tag{3.3.30}$$

In order to bound $\hat{R}_j^n$ by $|\hat{e}_j^{\varepsilon,n}|$ and $|\hat{\nu}_j^{\varepsilon,n}|$'s, we rewrite $\hat{R}_j^n$ as a summation of three differences:

$$\begin{aligned}
\hat{R}_j^n =&\frac{1}{4}(\hat{\nu}_j^{\varepsilon,n}+\hat{\nu}_j^{\varepsilon,n-1})g(\hat{E}_j^{\varepsilon,n},\hat{E}_j^{\varepsilon,n-1})(\hat{E}_j^{\varepsilon,n}+\hat{E}_j^{\varepsilon,n-1})\\
&+\frac{1}{4}(N^\varepsilon(x_j,t_n)+N^\varepsilon(x_j,t_{n-1}))g(\hat{E}_j^{\varepsilon,n},\hat{E}_j^{\varepsilon,n-1})(\hat{e}_j^{\varepsilon,n}+\hat{e}_j^{\varepsilon,n-1})\\
&+\frac{1}{4}(g(E^\varepsilon(x_j,t_n),E^\varepsilon(x_j,t_{n-1}))-g(\hat{E}_j^{\varepsilon,n},\hat{E}_j^{\varepsilon,n-1}))\\
&\times(N^\varepsilon(x_j,t_n)+N^\varepsilon(x_j,t_{n-1}))(E^\varepsilon(x_j,t_n)+E^\varepsilon(x_j,t_{n-1})).
\end{aligned} \tag{3.3.31}$$

From the construction of f and g, we know $\|f'\|_\infty, \|f''\|_\infty$ are bounded. Therefore we have

$$|\rho_B(|E^\varepsilon(x_j,t_n)|^2)-\rho_B(|\hat{E}_j^{\varepsilon,n}|^2)| \leq \sqrt{C_B}|\hat{e}_j^n|, \tag{3.3.32}$$

$$|g(E^\varepsilon(x_j,t_n),E^\varepsilon(x_j,t_{n-1}))-g(\hat{E}_j^{\varepsilon,n},\hat{E}_j^{\varepsilon,n-1})| \lesssim |\hat{e}_j^n|+|\hat{e}_j^{n-1}|, \tag{3.3.33}$$

$$|g_e(E^\varepsilon(x_j,t_n),E^\varepsilon(x_j,t_{n-1}))-g_e(\hat{E}_j^{\varepsilon,n},\hat{E}_j^{\varepsilon,n-1})| \lesssim |\hat{e}_j^n|+|\hat{e}_j^{n-1}|, \tag{3.3.34}$$

$$|\delta_x^+(g_e(E^\varepsilon(x_j,t_n),E^\varepsilon(x_j,t_{n-1}))-g_e(\hat{E}_j^{\varepsilon,n},\hat{E}_j^{\varepsilon,n-1}))| \lesssim \sum_{m=n-1}^{n}(|\hat{e}_j^m|+|\hat{e}_{j+1}^m|+|\delta_x^+\hat{e}_j^m|), \tag{3.3.35}$$

where $g_e(u,v)=g(u,v)(u+v)$, for $u,v\in\mathbb{C}$, and C_B is a number depending on B and $\rho(\cdot)$. After combining (3.3.31), (3.3.33) and (3.3.34) and using Cauchy inequality, we have

$$\left|\hat{R}_j^n\right| \lesssim \left|\hat{e}_j^{\varepsilon,n}\right|+\left|\hat{e}_j^{\varepsilon,n-1}\right|+\left|\hat{\nu}_j^{\varepsilon,n}\right|+\left|\hat{\nu}_j^{\varepsilon,n-1}\right|. \tag{3.3.36}$$

In order to bound the $\|\hat{e}_j^{\varepsilon,n}\|_{\ell^2}$ term, multiplying $h\tau(\bar{\hat{e}}_j^{\varepsilon,n}+\bar{\hat{e}}_j^{\varepsilon,n-1})$ on both side of (3.3.27), summing up for all j, and taking the imaginary part, we have:

$$\|\hat{e}^{\varepsilon,n}\|_{\ell^2}-\|\hat{e}^{\varepsilon,n-1}\|_{\ell^2}=\tau\,\mathrm{Im}\langle\hat{R}^n,\hat{e}^{\varepsilon,n}+\hat{e}^{\varepsilon,n-1}\rangle+\tau\,\mathrm{Im}\langle\hat{\eta}^{\varepsilon,n},\hat{e}^{\varepsilon,n}+\hat{e}^{\varepsilon,n-1}\rangle. \tag{3.3.37}$$

In order to bound the $|\hat{e}_j^{\varepsilon,n}|_1$ term, which is equivalent to $|\hat{e}_j^{\varepsilon,n}|_{1,*}$ as showed in (2.2.16), multiplying $h(\bar{\hat{e}}_j^{\varepsilon,n} - \bar{\hat{e}}_j^{\varepsilon,n-1})$ on both side of (3.3.27), summing up for all j, and taking the real part, we have:

$$\frac{1}{2}\left(|\hat{e}^{\varepsilon,n}|_{1,*} - |\hat{e}^{\varepsilon,n-1}|_{1,*}\right) = -\operatorname{Re}\langle \hat{R}^n, \hat{e}^{\varepsilon,n} + \hat{e}^{\varepsilon,n-1}\rangle - \operatorname{Re}\langle \hat{\eta}^{\varepsilon,n}, \hat{e}^{\varepsilon,n} - \hat{e}^{\varepsilon,n-1}\rangle. \quad (3.3.38)$$

In order to bound the $\|\hat{\nu}_j^{\varepsilon,n}\|_{\ell^2}$ term, multiplying $h\tau(\hat{u}_j^{\varepsilon,n+\frac{1}{2}} + \hat{u}_j^{\varepsilon,n-\frac{1}{2}})$ on both side of (3.3.27) and summing up for all j, we have:

$$\begin{aligned} &\varepsilon^2\left(|\hat{u}^{\varepsilon,n+\frac{1}{2}}|_{1,*} - |\hat{u}^{\varepsilon,n-\frac{1}{2}}|_{1,*}\right) + \frac{1}{2}\left(\|\hat{\nu}^{\varepsilon,n+1}\|_{\ell^2} - \|\hat{\nu}^{\varepsilon,n-1}\|_{\ell^2}\right) \\ &\quad + \langle \hat{P}^n, \hat{\nu}^{\varepsilon,n+1} - \hat{\nu}^{\varepsilon,n-1}\rangle = -\tau\langle \hat{\xi}^{\varepsilon,n}, \hat{u}^{\varepsilon,n+\frac{1}{2}} + \hat{u}^{\varepsilon,n-\frac{1}{2}}\rangle. \end{aligned} \quad (3.3.39)$$

For energy $\hat{S}^n$ defined by

$$\begin{aligned} \hat{S}^n =& 3C_B\|\hat{e}^{\varepsilon,n}\|_{\ell^2}^2 + 2|\hat{e}^{\varepsilon,n}|_{1,*}^2 + \varepsilon^2|\hat{u}^{\varepsilon,n+\frac{1}{2}}|_{1,*}^2 \\ &+ \frac{1}{2}\|\hat{\nu}^{\varepsilon,n+1}\|_{\ell^2}^2 + \frac{1}{2}\|\hat{\nu}^{\varepsilon,n}\|_{\ell^2}^2 + \langle \hat{P}^n, \hat{\nu}^{\varepsilon,n+1} + \hat{\nu}^{\varepsilon,n}\rangle, \end{aligned} \quad (3.3.40)$$

$3C_B$(3.3.37) + 4(3.3.38) + (3.3.39) indicates

$$\begin{aligned} \hat{S}^n - \hat{S}^{n-1} =& 3C_B\tau\operatorname{Im}\langle \hat{R}^n, \hat{e}^{\varepsilon,n} + \hat{e}^{\varepsilon,n-1}\rangle + 3C_B\tau\operatorname{Im}\langle \hat{\eta}^{\varepsilon,n}, \hat{e}^{\varepsilon,n} + \hat{e}^{\varepsilon,n-1}\rangle \\ &+ \left(\langle \hat{P}^n - \hat{P}^{n-1}, \hat{\nu}^{\varepsilon,n} + \hat{\nu}^{\varepsilon,n-1}\rangle - 4\operatorname{Re}\langle \hat{R}^n, \hat{e}^{\varepsilon,n} + \hat{e}^{\varepsilon,n-1}\rangle\right) \\ &- 4\operatorname{Re}\langle \hat{\eta}^{\varepsilon,n}, \hat{e}^{\varepsilon,n} - \hat{e}^{\varepsilon,n-1}\rangle - \tau\langle \hat{\xi}^{\varepsilon,n}, \hat{u}^{\varepsilon,n+\frac{1}{2}} + \hat{u}^{\varepsilon,n-\frac{1}{2}}\rangle. \end{aligned} \quad (3.3.41)$$

Note that the coefficient $3C_B$ in $\hat{S}^n$ is designed to make sure

$$\hat{S}^n \geq C\left(\|\hat{e}^{\varepsilon,n}\|_{\ell^2} + |\hat{e}^{\varepsilon,n}|_{1,*} + \|\hat{\nu}^{\varepsilon,n}\|_{\ell^2}\right)^2$$

for some positive constant C. We have the following lemma to bound each term on the RHS of (3.3.41).

Lemma 3.4. *Under assumption* (3.A), *we have the following estimates*

$$\left|\operatorname{Im}\langle \hat{R}^n, \hat{e}^{\varepsilon,n} + \hat{e}^{\varepsilon,n-1}\rangle\right| \lesssim \|\hat{e}^{\varepsilon,n}\|_{\ell^2}^2 + \|\hat{\nu}^{\varepsilon,n}\|_{\ell^2}^2 + \left\|\hat{e}^{\varepsilon,n-1}\right\|_{\ell^2}^2 + \left\|\hat{\nu}^{\varepsilon,n-1}\right\|_{\ell^2}^2, \quad (3.3.42)$$

$$\left|\operatorname{Im}\langle \hat{\eta}^{\varepsilon,n}, \hat{e}^{\varepsilon,n} + \hat{e}^{\varepsilon,n-1}\rangle\right| \lesssim \|\hat{\eta}^{\varepsilon,n}\|_{\ell^2}^2 + \|\hat{e}^{\varepsilon,n}\|_{\ell^2}^2 + \left\|\hat{e}^{\varepsilon,n-1}\right\|_{\ell^2}^2, \quad (3.3.43)$$

$$\left|\langle \hat{P}^n, \hat{\nu}^{\varepsilon,n} + \hat{\nu}^{\varepsilon,n+1}\rangle\right| \leq 2\left\|\hat{P}^n\right\|_{\ell^2}^2 + \frac{1}{4}\left(\|\hat{\nu}^{\varepsilon,n}\|_{\ell^2}^2 + \left\|\hat{\nu}^{\varepsilon,n+1}\right\|_{\ell^2}^2\right), \quad (3.3.44)$$

$$\left|\operatorname{Re}\langle \hat{\eta}^{\varepsilon,n}, \hat{e}^{\varepsilon,n} - \hat{e}^{\varepsilon,n-1}\rangle\right| \lesssim \tau\left(|\hat{\eta}^{\varepsilon,n}|_{1,*}^2 + \|\hat{\eta}^{\varepsilon,n}\|_{\ell^2}^2 + \sum_{n-1}^{n}(\|\hat{e}^{\varepsilon,m}\|_{\ell^2}^2 + |\hat{e}^{\varepsilon,m}|_{1,*}^2 + \|\hat{\nu}^{\varepsilon,m}\|_{\ell^2}^2)\right), \quad (3.3.45)$$

$$\begin{aligned}
&\left|\langle \hat{P}^n - \hat{P}^{n-1}, \hat{\nu}^{\varepsilon,n} + \hat{\nu}^{\varepsilon,n-1}\rangle - 4\,\mathrm{Re}\langle \hat{R}^n, \hat{e}^{\varepsilon,n} + \hat{e}^{\varepsilon,n-1}\rangle\right| \\
\lesssim&\tau\left(\|\hat{\eta}^{\varepsilon,n}\|_{\ell^2}^2 + \sum_{m=n-1}^{n}\left(\|\hat{e}^{\varepsilon,m}\|_{\ell^2}^2 + |\hat{e}^{\varepsilon,m}|_{1,*}^2 + \|\hat{\nu}^{\varepsilon,m}\|_{\ell^2}^2\right)\right),
\end{aligned} \tag{3.3.46}$$

and

$$\begin{aligned}
&\left|\tau\sum_{m=1}^{n}\langle \hat{\xi}^{\varepsilon,m}, \hat{u}^{\varepsilon,m+\frac{1}{2}} + \hat{u}^{\varepsilon,m-\frac{1}{2}}\rangle\right| \le \tau\sum_{m=1}^{n-1}\left(C\left\|\delta_t\hat{\xi}^{\varepsilon,m}\right\|_{\ell^2}^2 + \|\hat{\nu}^{\varepsilon,m}\|_{\ell^2}^2\right) \\
&+\sum_{m=0}^{1}\left(C\left\|\hat{\xi}^{\varepsilon,m}\right\|_{\ell^2}^2 + C\left\|\hat{\xi}^{\varepsilon,n+1-m}\right\|_{\ell^2}^2 + \|\hat{\nu}^{\varepsilon,m}\|_{\ell^2}^2 + \left\|\hat{\nu}^{\varepsilon,n+m}\right\|_{\ell^2}^2\right),
\end{aligned} \tag{3.3.47}$$

with C a constant independent of h, τ and ε.

Proof. The first 4 inequalities are direct from the Cauchy inequality. For any $u, v \in X_J$ and any positive constant C, we have

$$|\langle u, v\rangle| \le \frac{C}{2}\|u\|_{\ell^2}^2 + \frac{1}{2C}\|v\|_{\ell^2}^2. \tag{3.3.48}$$

Substituting the error equation (3.3.27) into (3.3.44), we have

$$\mathrm{Re}\langle \hat{\eta}^{\varepsilon,n}, \hat{e}^{\varepsilon,n} - \hat{e}^{\varepsilon,n-1}\rangle = \tau\,\mathrm{Im}\langle \hat{\eta}^{\varepsilon,n}, -\frac{1}{2}\mathcal{A}_h^{-1}\delta_x^2(\hat{e}^{\varepsilon,n} + \hat{e}^{\varepsilon,n-1}) + \hat{R}^n + \hat{\eta}^{\varepsilon,n}\rangle. \tag{3.3.49}$$

Then, (3.3.42)-(3.3.45) are direct inference of (3.3.48).

For (3.3.46), from the definition of $\hat{R}_j^n$ and $\hat{P}_j^n$ in (3.3.31) and (3.3.30), we have

$$\begin{aligned}
\langle \hat{P}^n - \hat{P}^{n-1}, &\hat{\nu}^{\varepsilon,n} + \hat{\nu}^{\varepsilon,n-1}\rangle - 4\,\mathrm{Re}\langle \hat{R}^n, \hat{e}^{\varepsilon,n} + \hat{e}^{\varepsilon,n-1}\rangle \\
&= \mathrm{Re}\langle(\hat{\nu}^{\varepsilon,n} + \hat{\nu}^{\varepsilon,n-1})G_e^n, E^\varepsilon(\mathbf{x}, t_n) - E^\varepsilon(\mathbf{x}, t_{n-1})\rangle \\
&\quad - \mathrm{Re}\langle(N^\varepsilon(\mathbf{x}, t_n) + N^\varepsilon(\mathbf{x}, t_{n-1}))G_e^n, \hat{e}^{\varepsilon,n} + \hat{e}^{\varepsilon,n-1}\rangle,
\end{aligned} \tag{3.3.50}$$

where $\mathbf{x} = (x_0 = a, x_1, x_2, \cdots, x_J = b)$ is the vector of all spatial grid points, and

$$G_e^n = g_e(E^\varepsilon(\mathbf{x}, t_n), E^\varepsilon(\mathbf{x}, t_{n-1})) - g_e(\hat{E}^{\varepsilon,n}, \hat{E}^{\varepsilon,n-1}).$$

From (3.3.34), we have $\|G_e^n\|_{\ell^2} \lesssim \|\hat{e}^{\varepsilon,n}\|_{\ell^2} + \|\hat{e}^{\varepsilon,n-1}\|_{\ell^2}$. From Cauchy inequality and mean value theorem, we get

$$\begin{aligned}
&|\operatorname{Re}\langle(\hat{\nu}^{\varepsilon,n}+\hat{\nu}^{\varepsilon,n-1})G_e^n, E^\varepsilon(\mathbf{x},t_n)-E^\varepsilon(\mathbf{x},t_{n-1})\rangle| \\
\lesssim&\tau\|\partial_t E^\varepsilon(\mathbf{x},t)\|_\infty\left(\|\hat{e}^{\varepsilon,n}\|_{\ell^2}^2+\|\hat{\nu}^{\varepsilon,n}\|_{\ell^2}^2+\left\|\hat{e}^{\varepsilon,n-1}\right\|_{\ell^2}^2+\left\|\hat{\nu}^{\varepsilon,n-1}\right\|_{\ell^2}^2\right) \\
\lesssim&\tau\left(\|\hat{e}^{\varepsilon,n}\|_{\ell^2}^2+\|\hat{\nu}^{\varepsilon,n}\|_{\ell^2}^2+\left\|\hat{e}^{\varepsilon,n-1}\right\|_{\ell^2}^2+\left\|\hat{\nu}^{\varepsilon,n-1}\right\|_{\ell^2}^2\right),
\end{aligned} \tag{3.3.51}$$

$$\begin{aligned}
&|\operatorname{Re}\langle(N^\varepsilon(\mathbf{x},t_n)+N^\varepsilon(\mathbf{x},t_{n-1}))G_e^n, \hat{e}^{\varepsilon,n}+\hat{e}^{\varepsilon,n-1}\rangle| \\
=&|\tau\operatorname{Im}\langle(N^\varepsilon(\mathbf{x},t_n)+N^\varepsilon(\mathbf{x},t_{n-1}))G_e^n,-\frac{1}{2}\mathcal{A}_h^{-1}\delta_x^2(\hat{e}^{\varepsilon,n}+\hat{e}^{\varepsilon,n-1})+\hat{R}^n+\hat{\eta}^{\varepsilon,n}\rangle| \\
\lesssim&\tau\left(\|\hat{\eta}^{\varepsilon,n}\|_{\ell^2}+\sum_{m=n-1}^{n}\left(\|\hat{e}^{\varepsilon,m}\|_{\ell^2}^2+\|\hat{\nu}^{\varepsilon,m}\|_{\ell^2}^2+|\hat{e}^{\varepsilon,m}|_{1,*}^2\right)\right).
\end{aligned} \tag{3.3.52}$$

Combining (3.3.51) and (3.3.52) together, then we have the bound in (3.3.46).

For (3.3.47), we have the Abel summation:

$$-\tau\sum_{m=1}^{n}\langle\hat{\xi}^{\varepsilon,m},\hat{u}^{\varepsilon,m+\frac{1}{2}}+\hat{u}_j^{\varepsilon,m-\frac{1}{2}}\rangle=\sum_{m=1}^{n}\langle(\delta_x^2)^{-1}\mathcal{A}_h\hat{\xi}^{\varepsilon,m},\hat{\nu}^{\varepsilon,m+1}-\hat{\nu}^{\varepsilon,m-1}\rangle \tag{3.3.53}$$

$$=\tau\sum_{m=2}^{n-1}\langle\delta_t(\delta_x^2)^{-1}\mathcal{A}_h\hat{\xi}^{\varepsilon,m},\hat{\nu}^{\varepsilon,m}\rangle+\sum_{m=0}^{1}\langle(\delta_x^2)^{-1}\mathcal{A}_h\hat{\xi}^{\varepsilon,m},\hat{\nu}^{\varepsilon,m}\rangle+\sum_{m=n}^{n+1}\langle(\delta_x^2)^{-1}\mathcal{A}_h\hat{\xi}^{\varepsilon,m},\hat{\nu}^{\varepsilon,m}\rangle.$$

Since $(\delta_x^2)^{-1}\mathcal{A}_h\hat{\xi}^{\varepsilon,n}\in X_J$ has zero boundary, there exists a positive constant C independent of h,τ and ε, based on the discrete Poincaré inequality such that

$$\left\|(\delta_x^2)^{-1}\mathcal{A}_h\hat{\xi}^{\varepsilon,n}\right\|_{\ell^2}\leq C\left\|\hat{\xi}^{\varepsilon,n}\right\|_{\ell^2}. \tag{3.3.54}$$

The estimate (3.3.47) holds for a direct application of Cauchy inequality (3.3.48) to (3.3.53). □

From (3.3.44) and (3.3.32), we get

$$\left|\langle\hat{P}^n,\hat{\nu}^{\varepsilon,n}+\hat{\nu}^{\varepsilon,n+1}\rangle\right|\leq 2C_B\|\hat{e}^{\varepsilon,n}\|_{\ell^2}^2+\frac{1}{4}\left(\|\hat{\nu}^{\varepsilon,n}\|_{\ell^2}^2+\left\|\hat{\nu}^{\varepsilon,n+1}\right\|_{\ell^2}^2\right). \tag{3.3.55}$$

Therefore, the $\hat{S}^n$ defined in (3.3.40) has a lower bound

$$\hat{S}^n\geq C_B\|\hat{e}^{\varepsilon,n}\|_{\ell^2}^2+|\hat{e}^{\varepsilon,n}|_{1,*}^2+\frac{1}{4}\|\hat{\nu}^{\varepsilon,n}\|_{\ell^2}^2\geq 0. \tag{3.3.56}$$

Summing up (3.3.41) for time steps from 1 to $n < \frac{T}{\tau}$ and applying the estimations in Lemma 3.4, we obtain

$$\begin{aligned}\hat{S}^n \leq &\hat{S}^0 + \sum_{m=0}^{1}\left(C\left\|\hat{\xi}^{\varepsilon,m}\right\|_{\ell^2}^2 + C\left\|\hat{\xi}^{\varepsilon,n+1-m}\right\|_{\ell^2}^2 + \|\hat{\nu}^{\varepsilon,m}\|_{\ell^2}^2 + \left\|\hat{\nu}^{\varepsilon,n+m}\right\|_{\ell^2}^2\right)\\ &+ C\tau\sum_{m=1}^{n}\left(\|\hat{e}^{\varepsilon,n}\|_{\ell^2}^2 + |\hat{e}^{\varepsilon,n}|_{1,*}^2 + \|\hat{\nu}^{\varepsilon,n}\|_{\ell^2}^2 + \|\hat{\eta}^{\varepsilon,n}\|_{\ell^2}^2 + |\hat{\eta}^{\varepsilon,n}|_{1,*}^2 + \left\|\hat{\xi}^{\varepsilon,n}\right\|_{\ell^2}^2\right)\\ \lesssim &\left(\frac{h^4}{\varepsilon^{1-\alpha*}} + \frac{\tau^2}{\varepsilon^{3-\alpha^\dagger}}\right)^2 + \tau\sum_{m=1}^{n}\hat{S}^m, \end{aligned} \tag{3.3.57}$$

with C a large enough positive number independent of h, τ, and ε. The last inequality above depends on

$$\begin{aligned}\hat{S}^0 =&2|\hat{e}^{\varepsilon,0}|_{1,*}^2 + \varepsilon^2|\hat{u}^{\varepsilon,\frac{1}{2}}|_{1,*}^2 + \frac{1}{2}\|\hat{\nu}^{\varepsilon,1}\|_{\ell^2}^2 + \langle\hat{P}^n, \hat{\nu}^{\varepsilon,1} + \hat{\nu}^{\varepsilon,0}\rangle\\ \lesssim &\left(\frac{h^4}{\varepsilon^{1-\alpha*}} + \frac{\tau^2}{\varepsilon^{3-\alpha^\dagger}}\right)^2.\end{aligned} \tag{3.3.58}$$

From the discrete Gronwall's inequality, for sufficiently small $\tau > 0$, we have

$$\hat{S}^n \lesssim \left(\frac{h^4}{\varepsilon^{1-\alpha*}} + \frac{\tau^2}{\varepsilon^{3-\alpha^\dagger}}\right)^2. \tag{3.3.59}$$

Combining (2.2.16), (3.3.56) and (3.3.59), we get

$$\|\hat{e}^{\varepsilon,n}\|_{\ell^2} + |\hat{e}^{\varepsilon,n}|_1 + \|\hat{\nu}^{\varepsilon,n}\|_{\ell^2} \lesssim \|\hat{e}^{\varepsilon,n}\|_{\ell^2} + |\hat{e}^{\varepsilon,n}|_{1,*} + \|\hat{\nu}^{\varepsilon,n}\|_{\ell^2} \lesssim \frac{h^4}{\varepsilon^{1-\alpha*}} + \frac{\tau^2}{\varepsilon^{3-\alpha^\dagger}}. \tag{3.3.60}$$

3.3.3 Another error bound via the limiting equation

We will show (3.3.4) type error estimate for $(\hat{E}^{\varepsilon,n}, \hat{N}^{\varepsilon,n})$ in this subsection. Define the biased error function as

$$\tilde{e}_j^{\varepsilon,n} = E(x_j, t_n) - \hat{E}_j^{\varepsilon,n},\ \tilde{\nu}_j^{\varepsilon,n} = N(x_j, t_n) - \hat{N}_j^{\varepsilon,n}, \quad j \in \mathcal{T}_J^0, n \geq 1, \tag{3.3.61}$$

where $N(x_j, t_n) = -|E(x_j, t_n)|^2$. Also define the discrete potential $\tilde{u}^{\varepsilon,n-\frac{1}{2}} \in X_J$ satisfying $\tilde{u}^{\varepsilon,n-\frac{1}{2}} = -(\delta_x^2)^{-1}\mathcal{A}_h\delta_t^-\tilde{\nu}_j^{\varepsilon,n}$ and define local truncation errors $\tilde{\eta}^{\varepsilon,n}, \tilde{\xi}^{\varepsilon,n} \in$

X_J as

$$\tilde{\eta}_j^{\varepsilon,n} = i\delta_t^- E(x_j,t_n) + \left[\mathcal{A}_h^{-1}\delta_x^2 - \frac{N(x_j,t_{n-1})+N(x_j,t_n)}{2} g(E(x_j,t_{n-1}),E(x_j,t_n))\right] \times \frac{E(x_j,t_{n-1})+E(x_j,t_n)}{2}, \tag{3.3.62}$$

$$\tilde{\xi}_j^{\varepsilon,n} = \varepsilon^2\delta_t^2 N(x_j,t_n) - \mathcal{A}_h^{-1}\delta_x^2\left(\frac{N(x_j,t_n)+N(x_j,t_{n-1})}{2} + f\left(|E(x_j,t_n)|^2\right)\right). \tag{3.3.63}$$

As proved in Lemma 3.2 and 3.3, under assumption (3.A) and (3.B), we have the following local truncation errors

$$\|\tilde{\eta}^{\varepsilon,n}\|_{\ell^2} + \left\|\delta_x^+\tilde{\eta}^{\varepsilon,n}\right\|_{\ell^2} \lesssim h^4+\tau^2, \quad \left\|\tilde{\xi}^{\varepsilon,n}\right\|_{\ell^2} + \left\|\delta_t\tilde{\xi}^{\varepsilon,n}\right\|_{\ell^2} \lesssim h^4+\tau^2+\varepsilon^2, \tag{3.3.64}$$

and

$$\left\|\tilde{\nu}^{\varepsilon,1}\right\|_{\ell^2} \lesssim \tau h^4+\tau^2+\varepsilon^\alpha+\varepsilon^\beta, \ \left\|\tilde{u}^{\varepsilon,\frac{1}{2}}\right\|_{\ell^2} \lesssim \left\|\delta_t^-\tilde{\nu}^{\varepsilon,1}\right\|_{\ell^2} \lesssim h^4+\tau+\varepsilon^{\alpha-1}+\varepsilon^{\beta-1}. \tag{3.3.65}$$

The differences between (3.3.62),(3.3.63) and (3.3.21),(3.3.22) yield the error functions

$$i\delta_t^-\tilde{e}_j^{\varepsilon,n} = -\frac{1}{2}\mathcal{A}_h^{-1}\delta_x^2(\tilde{e}_j^{\varepsilon,n}+\tilde{e}_j^{\varepsilon,n-1}) + \tilde{R}_j^n + \tilde{\eta}_j^{\varepsilon,n}, \tag{3.3.66}$$

$$\varepsilon^2\delta_t^2\tilde{\nu}_j^{\varepsilon,n} = \mathcal{A}_h^{-1}\delta_x^2\left(\frac{\tilde{\nu}_j^{\varepsilon,n}+\tilde{\nu}_j^{\varepsilon,n-1}}{2} + \tilde{P}_j^n\right) + \tilde{\xi}_j^{\varepsilon,n}, \tag{3.3.67}$$

for $j\in\mathcal{T}_J, n\geq 1$, with $\tilde{R}_j^n$ and $\tilde{P}_j^n$ defined similarly as $\hat{R}_j^n$ and $\hat{P}_j^n$ in Section 3.3.2:

$$\begin{aligned}\tilde{R}_j^n =& \frac{1}{4}\left(N\left(x_j,t_{n-1}\right)+N\left(x_j,t_n\right)\right)\\ &\times g\left(E\left(x_j,t_n\right),E\left(x_j,t_{n-1}\right)\right)\left(E\left(x_j,t_{n-1}\right)+E\left(x_j,t_n\right)\right)\\ &-\frac{1}{4}(N_j^{\varepsilon,n-1}+N_j^{\varepsilon,n})g(\hat{E}_j^{\varepsilon,n},\hat{E}_j^{\varepsilon,n-1})(\hat{E}_j^{\varepsilon,n-1}+\hat{E}_j^{\varepsilon,n}),\end{aligned} \tag{3.3.68}$$

$$\tilde{P}_j^n = f(|E(x_j,t_n)|^2) - f(|\hat{E}_j^{\varepsilon,n}|^2). \tag{3.3.69}$$

Define a discrete energy function

$$\begin{aligned}\tilde{S}^n =& 3C_B\|\tilde{e}^{\varepsilon,n}\|_{\ell^2}^2 + 2|\tilde{e}^{\varepsilon,n}|_{1,*}^2 + \varepsilon^2\left|\tilde{u}^{\varepsilon,n+\frac{1}{2}}\right|_{1,*}^2\\ &+\frac{1}{2}\|\tilde{\nu}^{\varepsilon,n+1}\|_{\ell^2}^2 + \frac{1}{2}\|\tilde{\nu}^{\varepsilon,n}\|_{\ell^2}^2 + \langle\tilde{P}^n,\tilde{\nu}^{\varepsilon,n+1}+\tilde{\nu}^{\varepsilon,n}\rangle.\end{aligned} \tag{3.3.70}$$

Similar to the procedure in Section 3.3.1, with the discrete Gronwall's inequality, we have

$$\left(\|\tilde{e}^{\varepsilon,n}\|_{\ell^2} + |\tilde{e}^{\varepsilon,n}|_{1,*} + \|\tilde{\nu}^{\varepsilon,n}\|_{\ell^2}\right)^2 \lesssim \tilde{S}^n \lesssim (h^4 + \tau^2 + \varepsilon^\alpha + \varepsilon^\beta + \varepsilon^2)^2. \tag{3.3.71}$$

Combining (3.3.71) with assumption (3.B) and we have

$$\begin{aligned}
&\|\hat{e}^{\varepsilon,n}\|_{\ell^2} + |\hat{e}^{\varepsilon,n}|_{1,*} + \|\hat{\nu}^{\varepsilon,n}\|_{\ell^2} \\
\le&\|\tilde{e}^{\varepsilon,n}\|_{\ell^2} + |\tilde{e}^{\varepsilon,n}|_{1,*} + \|E(\cdot,t_n) - E^\varepsilon(\cdot,t_n)\|_{H^1} + \|N(\cdot,t_n) - N^\varepsilon(\cdot,t_n)\|_{L^2} \\
\lesssim&h^4 + \tau^2 + \varepsilon^{\alpha^\dagger}.
\end{aligned} \tag{3.3.72}$$

3.3.4 Proof of the main results

Based on the above analysis, we now give the proof of (3.3.3) in Theorem 3.2 and (3.3.7) in Theorem 3.3. For any $u \in X_J$, from the discrete Sobolev inequality, there exists a constant C_Ω depending on the domain Ω such that

$$\|u\|_\infty \le C_\Omega |u|_1. \tag{3.3.73}$$

Under assumption (3.A) and (3.C) and from (3.3.60), we have

$$\left\|\hat{E}^{\varepsilon,n}\right\|_\infty \le \|E^\varepsilon(x,t)\|_\infty + \|\hat{e}^{\varepsilon,n}\|_\infty \le M_0 + 1, \tag{3.3.74}$$

for small enough h and τ. Then we have $\hat{E}^{\varepsilon,n} = E^{\varepsilon,n}$ and $\hat{N}^{\varepsilon,n} = N^{\varepsilon,n}$, since the equations for $\hat{E}^{\varepsilon,n}$ and $\hat{N}^{\varepsilon,n}$ collapse to (3.2.9) and (3.2.10). From the uniqueness of the solution of the CSI-4cFD method in Lemma 3.1, we have the boundedness of the original numerical solutions $(E^{\varepsilon,n}, N^{\varepsilon,n})$. Applying the whole estimating procedure of Section 3.3.1 to $e^{\varepsilon,n}$ and $\nu^{\varepsilon,n}$, we have the error bound

$$\|e^{\varepsilon,n}\|_{\ell^2} + |e^{\varepsilon,n}|_1 + \|\nu^{\varepsilon,n}\|_{\ell^2} \lesssim \frac{h^4}{\varepsilon^{1-\alpha^*}} + \frac{\tau^2}{\varepsilon^{3-\alpha^\dagger}}, \quad 0 \le n \le \frac{T}{\tau}, \tag{3.3.75}$$

as in (3.3.60).

For well- and less-ill prepared initial data cases, (3.3.75) becomes (3.3.3) since $\alpha^* = 1$. Applying the procedure in Section 3.3.2 to $e^{\varepsilon,n}$ and $\nu^{\varepsilon,n}$ as above, we obtain the error bound (3.3.4) in Theorem 3.2 as (3.3.72) with the extra assumption (3.B). Taking the minimum of (3.3.3) and (3.3.4), followed by taking the supreme for $\varepsilon \in (0,1]$, we have an ε independent error bound:

$$\|e^{\varepsilon,n}\|_{\ell^2} + \left\|\delta_x^+ e^{\varepsilon,n}\right\|_{\ell^2} + \|\nu^{\varepsilon,n}\|_{\ell^2} \lesssim h^4 + \sup_{\varepsilon\in(0,1]} \min\{\tau^2 + \varepsilon^{\alpha^\dagger}, \frac{\tau^2}{\varepsilon^{3-\alpha^\dagger}}\}, \quad 0 \le n \le \frac{T}{\tau}.$$

The two terms $\tau^2 + \varepsilon^{\alpha^\dagger}$ and $\frac{\tau^2}{\varepsilon^{3-\alpha^\dagger}}$ have the same order when $\tau^2 \sim \varepsilon^3$, therefore

$$\sup_{\varepsilon\in(0,1]} \min\{\tau^2 + \varepsilon^{\alpha^\dagger}, \frac{\tau^2}{\varepsilon^{3-\alpha^\dagger}}\} \lesssim \tau^{2\alpha^\dagger/3}. \tag{3.3.76}$$

For the ill-prepared initial date case, $\alpha^\dagger = \alpha^* = \min\{\alpha, \beta\} < 1$, and we get (3.3.7) from (3.3.75).

3.4 Numerical results

In this section, we present numerical results of the CSI-4cFD scheme (3.2.9) and (3.2.10) for the ZS (3.2.1). The initial data is chosen as [32]:

$$E_0(x) = \mathrm{e}^{-x^2/2}, w_0(x) = \mathrm{e}^{-x^2/4}, w_1(x) = x\mathrm{e}^{-x^2/4}. \tag{3.4.1}$$

The parameter α and β are taken several typical cases:

Case I. A well-prepared initial data, $\alpha = 2$ and $\beta = 2$;

Case II. A less-ill-prepared initial data, $\alpha = 1$ and $\beta = 1$;

Case III. An ill-prepared initial data, $\alpha = 0$ and $\beta = 0$;

Case IV. An ill-prepared initial data, $\alpha = 0$ and $\beta = 2$;

Case V. An ill-prepared initial data, $\alpha = 1$ and $\beta = 0.5$.

During our numerical simulation, the computational domain is fixed to $\Omega = (200, 200)$, such that the error due to the truncation with homogeneous Dirichlet boundary condition is negligible. The 'exact solution' is computed by a finer mesh or by the time splitting spectral method introduced in [18] with a fine enough mesh $h = 1/32, \tau = 10^{-7}$.

In order to quantify the convergence, we use following standard error functions for the discrete ℓ^2-error and H^1-error at $t_n = n\tau$:

$$e^{\varepsilon}_{\ell^2}(t_n) = \|e^{\varepsilon,n}\|_{\ell^2},\ e^{\varepsilon}_{H^1}(t_n) = \|e^{\varepsilon,n}\|_{\ell^2} + |e^{\varepsilon,n}|_1,\ \nu^{\varepsilon}_{\ell^2}(t_n) = \|\nu^{\varepsilon,n}\|_{\ell^2}. \tag{3.4.2}$$

Tables 3.1-3.5 and Figures 3.1-3.5 show the spatial errors of the 5 cases all converge at 4-th order. As Table 3.1 and Figure 3.1 show, the spatial convergence rate is independent of the dimensionless parameter ε for well-prepared initial data, which coincides well with theorem 3.2. This is also true for the less-ill-prepared initial data with example Case II showed in Table 3.2 and Figure 3.2. For the ill-prepared initial data with $\alpha = \beta = 0$ in Case III, the convergence rate of ν^{ε} is reciprocal to ε as showed in Figure 3.3 (b).

In Figure 3.1 (a), the L^2 error lines for N^{ε} are parallel to the dashed reference line h^4, which shows the spatial convergence rates are of fourth order. In the plot of $\nu^{\varepsilon}_{\ell^2}$ v.s. ε, the error lines become parallel to horizontal axis as ε decreases to zero, which shows the converge in space is uniform of ε. The error lines for E^{ε} are not well separated, therefore, we list the convergence tables of the H^1 Errors for E^{ε}'s. In Table 3.1, apart form the fourth order convergence rate detected in each row, the error in each column will not increase as $\varepsilon \downarrow 0$, which shows the spatial error is uniform of ε. The analysis for the other four groups of initial cases is similar.

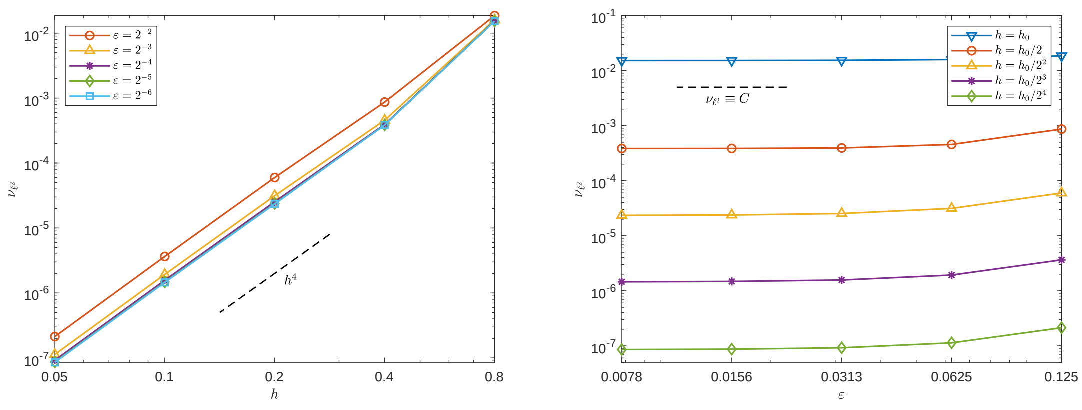

(a) (b)

Figure 3.1: Log-log plots of ℓ^2 errors of N^ε w.r.t h (a) and ε (b) with Case I initial data.

Table 3.1: Spatial errors of CSI-4cFD at $t = 1$ for the well-prepared initial data Case I with $\varepsilon_0 = 1/4, h_0 = 0.8$ at $t = 1$.

$e^\varepsilon_{H^1}(t=1)$	$h = h_0$	$h = h_0/2$	$h = h_0/2^2$	$h = h_0/2^3$	$h = h_0/2^4$
$\varepsilon = \varepsilon_0$	9.85E-2	7.85E-3	5.27E-4	3.29E-5	2.05E-6
Order	-	3.65	3.90	4.00	4.01
$\varepsilon = \varepsilon_0/2$	1.01E-1	8.43E-3	5.42E-4	3.38E-5	2.10E-6
Order	-	3.59	3.96	4.00	4.01
$\varepsilon = \varepsilon_0/2^2$	1.00E-1	8.62E-3	5.58E-4	3.48E-5	2.16E-6
Order	-	3.54	3.95	4.00	4.01
$\varepsilon = \varepsilon_0/2^3$	1.00E-1	8.64E-3	5.60E-4	3.50E-5	2.17E-6
Order	-	3.53	3.95	4.00	4.01
$\varepsilon = \varepsilon_0/2^4$	1.00E-1	8.65E-3	5.61E-4	3.50E-5	2.18E-6
Order	-	3.53	3.95	4.00	4.01
$\varepsilon = \varepsilon_0/2^5$	9.99E-2	8.65E-3	5.61E-4	3.50E-5	2.18E-6
Order	-	3.53	3.95	4.00	4.01

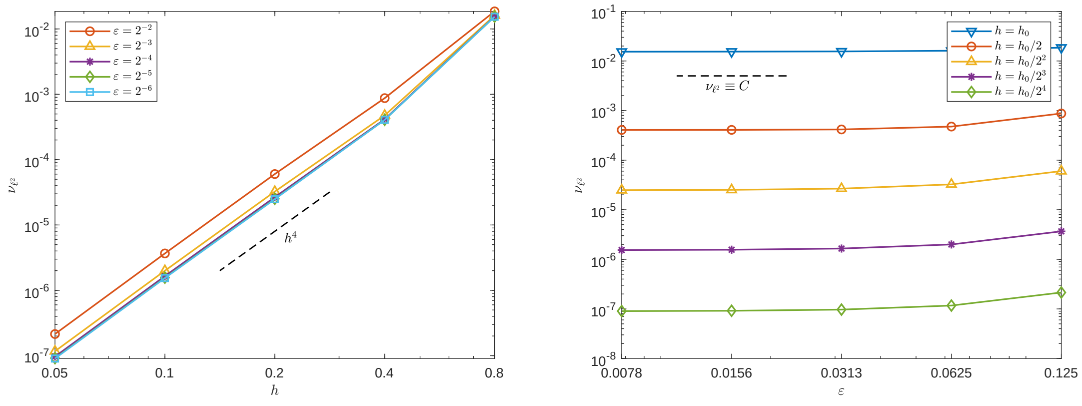

(a) (b)

Figure 3.2: Log-log plots of ℓ^2 errors of N^ε w.r.t h (a) and ε (b) with Case II initial data.

Table 3.2: Spatial errors of CSI-4cFD at $t = 1$ for the less-ill-prepared initial data Case II with $\varepsilon_0 = 1/4, h_0 = 0.8$ at $t = 1$.

$e^{\varepsilon}_{H^1}(t=1)$	$h = h_0$	$h = h_0/2$	$h = h_0/2^2$	$h = h_0/2^3$	$h = h_0/2^4$
$\varepsilon = \varepsilon_0 =$	9.80E-2	8.02E-3	5.40E-4	3.37E-5	2.10E-6
Order	-	3.61	3.89	4.00	4.01
$\varepsilon = \varepsilon_0/2$	1.01E-1	8.45E-3	5.46E-4	3.40E-5	2.12E-6
Order	-	3.58	3.95	4.00	4.01
$\varepsilon = \varepsilon_0/2^2$	1.00E-1	8.60E-3	5.56E-4	3.47E-5	2.16E-6
Order	-	3.54	3.95	4.00	4.01
$\varepsilon = \varepsilon_0/2^3$	1.00E-1	8.64E-3	5.60E-4	3.49E-5	2.17E-6
Order	-	3.53	3.95	4.00	4.01
$\varepsilon = \varepsilon_0/2^4$	1.00E-1	8.65E-3	5.61E-4	3.50E-5	2.18E-6
Order	-	3.53	3.95	4.00	4.01
$\varepsilon = \varepsilon_0/2^5$	9.99E-2	8.65E-3	5.61E-4	3.50E-5	2.18E-6
Order	-	3.53	3.95	4.00	4.01

Table 3.3: Spatial errors of CSI-4cFD at $t = 1$ for the ill-prepared initial data Case III with $\varepsilon_0 = 1/4, h_0 = 0.8$ at $t = 1$.

$e^{\varepsilon}_{H^1}(t = 1)$	$h = h_0$	$h = h_0/2$	$h = h_0/2^2$	$h = h_0/2^3$	$h = h_0/2^4$
$\varepsilon = \varepsilon_0$	1.20E-1	1.06E-2	7.00E-4	4.37E-5	2.72E-6
Order	-	3.50	3.92	4.00	4.01
$\varepsilon = \varepsilon_0/2$	1.01E-1	9.95E-3	6.90E-4	4.32E-5	2.69E-6
Order	-	3.34	3.85	4.00	4.01
$\varepsilon = \varepsilon_0/2^2$	9.93E-2	8.50E-3	5.53E-4	3.45E-5	2.15E-6
Order	-	3.55	3.94	4.00	4.01
$\varepsilon = \varepsilon_0/2^3$	9.97E-2	8.61E-3	5.59E-4	3.48E-5	2.17E-6
Order	-	3.53	3.95	4.00	4.01
$\varepsilon = \varepsilon_0/2^4$	9.99E-2	8.64E-3	5.61E-4	3.50E-5	2.18E-6
Order	-	3.53	3.95	4.00	4.01
$\varepsilon = \varepsilon_0/2^5$	9.99E-2	8.65E-3	5.61E-4	3.50E-5	2.18E-6
Order	-	3.53	3.95	4.00	4.01

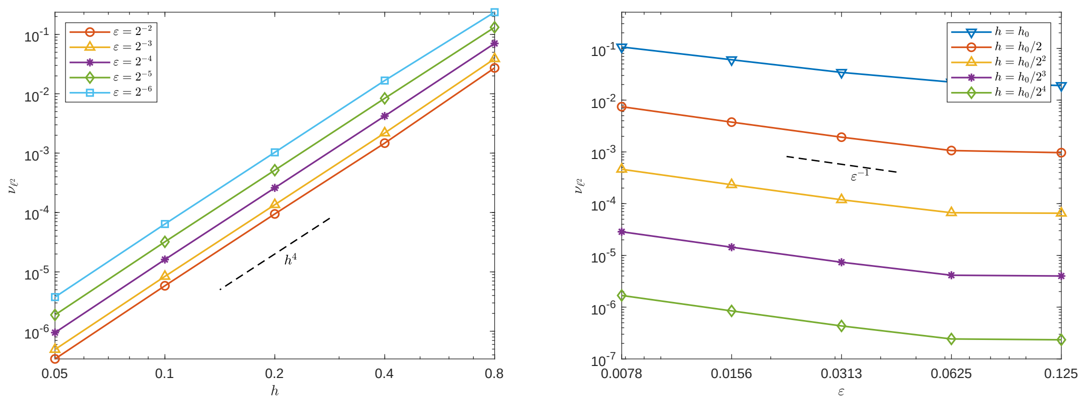

(a) (b)

Figure 3.3: Log-log plots of ℓ^2 errors of N^{ε} w.r.t h (a) and ε (b) with Case III initial data.

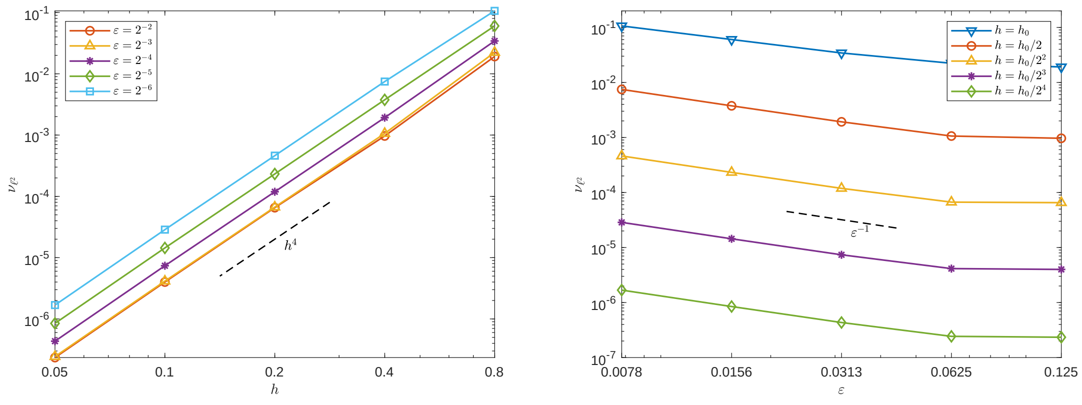

(a) (b)

Figure 3.4: Log-log plots of ℓ^2 errors of N^ε w.r.t h (a) and ε (b) with Case IV initial data.

Table 3.4: Spatial errors of CSI-4cFD at $t = 1$ for the ill-prepared initial data Case IV with $\varepsilon_0 = 1/4, h_0 = 0.8$ at $t = 1$.

$e^\varepsilon_{H^1}(t=1)$	$h = h_0$	$h = h_0/2$	$h = h_0/2^2$	$h = h_0/2^3$	$h = h_0/2^4$
$\varepsilon = \varepsilon_0$	9.34E-2	8.50E-3	5.79E-4	3.61E-5	2.25E-6
Order	-	3.46	3.88	4.00	4.01
$\varepsilon = \varepsilon_0/2$	9.64E-2	8.87E-3	5.96E-4	3.72E-5	2.32E-6
Order	-	3.44	3.90	4.00	4.01
$\varepsilon = \varepsilon_0/2^2$	9.82E-2	8.29E-3	5.32E-4	3.31E-5	2.06E-6
Order	-	3.57	3.96	4.00	4.01
$\varepsilon = \varepsilon_0/2^3$	9.94E-2	8.57E-3	5.55E-4	3.46E-5	2.15E-6
Order	-	3.54	3.95	4.00	4.01
$\varepsilon = \varepsilon_0/2^4$	9.98E-2	8.63E-3	5.60E-4	3.49E-5	2.17E-6
Order	-	3.53	3.95	4.00	4.01
$\varepsilon = \varepsilon_0/2^5$	9.99E-2	8.64E-3	5.61E-4	3.50E-5	2.18E-6
Order	-	3.53	3.95	4.00	4.01

Table 3.5: Spatial errors of CSI-4cFD at $t = 1$ for the ill-prepared initial data Case V with $\varepsilon_0 = 1/4, h_0 = 0.8$ at $t = 1$.

$e^{\varepsilon}_{H^1}(t=1)$	$h = h_0$	$h = h_0/2$	$h = h_0/2^2$	$h = h_0/2^3$	$h = h_0/2^4$
$\varepsilon = \varepsilon_0$	1.03E-1	8.37E-3	5.60E-4	3.49E-5	2.17E-6
Order	-	3.63	3.90	4.00	4.01
$\varepsilon = \varepsilon_0/2$	1.01E-1	8.57E-3	5.55E-4	3.46E-5	2.16E-6
Order	-	3.56	3.95	4.00	4.01
$\varepsilon = \varepsilon_0/2^2$	1.00E-1	8.61E-3	5.58E-4	3.48E-5	2.16E-6
Order	-	3.54	3.95	4.00	4.01
$\varepsilon = \varepsilon_0/2^3$	1.00E-1	8.64E-3	5.60E-4	3.49E-5	2.17E-6
Order	-	3.53	3.95	4.00	4.01
$\varepsilon = \varepsilon_0/2^4$	1.00E-1	8.65E-3	5.61E-4	3.50E-5	2.18E-6
Order	-	3.53	3.95	4.00	4.01
$\varepsilon = \varepsilon_0/2^5$	9.99E-2	8.65E-3	5.61E-4	3.50E-5	2.18E-6
Order	-	3.53	3.95	4.00	4.01

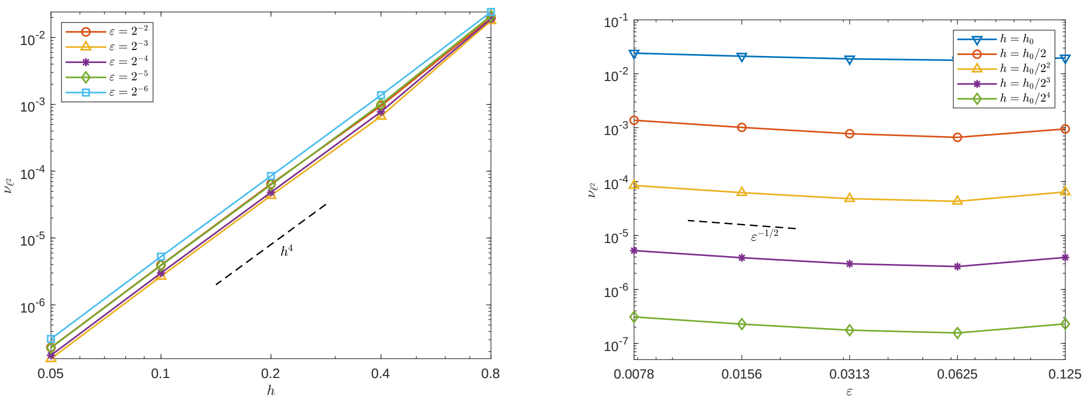

(a) (b)

Figure 3.5: Log-log plots of ℓ^2 errors of N^ε w.r.t h (a) and ε (b) with Case V initial data.

The left part of Figure 3.1-3.5 shows that the spatial error converges in 4-th order for all types of initial data when ε is fixed. The right part of the figures shows that only the ill-prepared initial data has spatial errors depending on the dimensionless parameter ε. These numerical results verify our statements in Theorem 3.2 and 3.3. Furthermore, the error scales showed in Figures 3.3(b), 3.4(b), 3.5(b) have different dependent rate $-1, -1$, and $-\frac{1}{2}$ on ε. This coincides with the $O(\frac{h^4}{\varepsilon^{1-\alpha*}})$ spatial error bounds given in Theorem 3.3, which is a tight spatial error bound depending on ε.

The time convergence test corresponding to Case I-V is showed in Tables 3.6-3.10. For a fixed ε, the temporal error of each case converges in second order. When ε decreases to 0, the error $e^{\varepsilon}_{H^1}$ of $E^{\varepsilon}(x,t)$ remains the same scale, but the error $\nu^{\varepsilon}_{\ell^2}$ of $N^{\varepsilon}(x,t)$ starts to increase. This situation is more clear for the ill-prepared data. In Table 3.8, for the last three columns of $\nu^{\varepsilon}_{\ell^2}$, the error in each row is approximate 8 times of the value of the above row form the line of $\varepsilon = \frac{1}{4}$, which shows the temporal error is of order $O(\tau^2/\varepsilon^3)$ and coincides with Theorem 3.3.

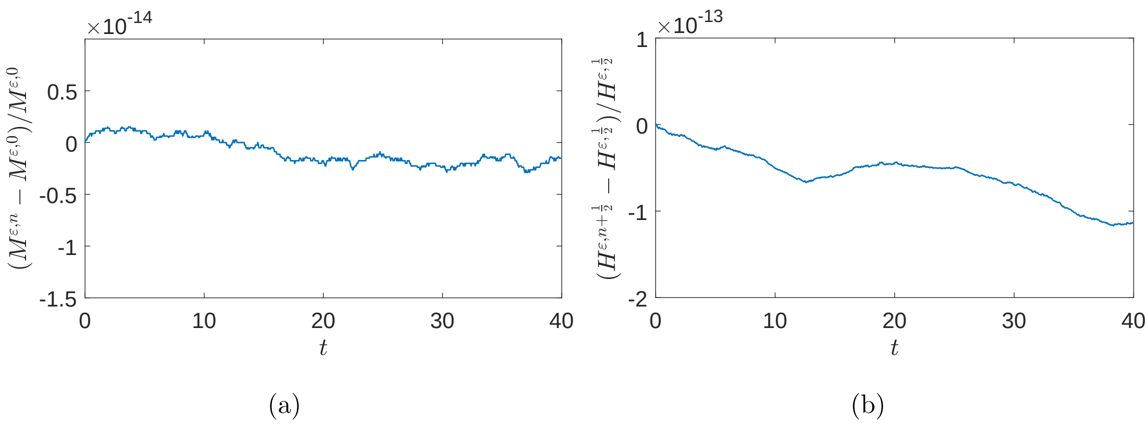

Figure 3.6: Wave energy (a) and Hamiltonian (b) variation w.r.t. t.

Figure 3.6 shows the variations of discrete wave energy and Hamiltonian for Case III initials with $\varepsilon = \frac{1}{32}$, $J = 128$, and $\tau = 0.05$. We run the simulation to a long time $T = 40$. The variations of wave energy and Hamiltonian are close to the round-off error of the double precision, which verifies the conservation numerically.

Table 3.6: Temporal errors of CSI-4cFD at $t = 1$ for the well-prepared initial data Case I with $\varepsilon_0 = 1, \tau_0 = 0.05$ at $t = 1$.

$e^{\varepsilon}_{H^1}$	τ_0	$\tau_0/2$	$\tau_0/2^2$	$\tau_0/2^2$	$\tau_0/2^3$	$\tau_0/2^4$	$\tau_0/2^5$
$\varepsilon = \varepsilon_0$	1.62E-2	4.77E-3	1.24E-3	3.12E-4	7.81E-5	1.95E-5	4.87E-6
Order	-	1.77	1.95	1.99	2.00	2.00	2.00
$\varepsilon = \varepsilon_0/2$	1.39E-2	4.10E-3	1.06E-3	2.68E-4	6.71E-5	1.68E-5	4.18E-6
Order	-	1.76	1.95	1.99	2.00	2.00	2.00
$\varepsilon = \varepsilon_0/2^2$	1.36E-2	3.97E-3	1.03E-3	2.58E-4	6.45E-5	1.61E-5	4.02E-6
Order	-	1.78	1.95	1.99	2.00	2.00	2.00
$\varepsilon = \varepsilon_0/2^3$	1.44E-2	4.03E-3	1.04E-3	2.62E-4	6.55E-5	1.64E-5	4.08E-6
Order	-	1.83	1.95	1.99	2.00	2.00	2.00
$\varepsilon = \varepsilon_0/2^4$	1.43E-2	4.06E-3	1.05E-3	2.63E-4	6.58E-5	1.65E-5	4.10E-6
Order	-	1.82	1.96	1.99	2.00	2.00	2.00
$\varepsilon = \varepsilon_0/2^5$	1.43E-2	4.07E-3	1.05E-3	2.64E-4	6.60E-5	1.65E-5	4.11E-6
Order	-	1.82	1.96	1.99	2.00	2.00	2.00

$\nu^{\varepsilon}_{\ell^2}$	τ_0	$\tau_0/2$	$\tau_0/2^2$	$\tau_0/2^2$	$\tau_0/2^3$	$\tau_0/2^4$	$\tau_0/2^5$
$\varepsilon = \varepsilon_0$	1.67E-3	4.18E-4	1.04E-4	2.61E-5	6.52E-6	1.63E-6	4.09E-7
Order	-	2.00	2.00	2.00	2.00	2.00	2.00
$\varepsilon = \varepsilon_0/2$	4.69E-3	1.20E-3	3.01E-4	7.53E-5	1.88E-5	4.70E-6	1.17E-6
Order	-	1.97	1.99	2.00	2.00	2.00	2.00
$\varepsilon = \varepsilon_0/2^2$	1.29E-2	3.85E-3	9.96E-4	2.51E-4	6.27E-5	1.57E-5	3.91E-6
Order	-	1.75	1.95	1.99	2.00	2.00	2.00
$\varepsilon = \varepsilon_0/2^3$	9.74E-3	3.46E-3	1.38E-3	3.77E-4	9.51E-5	2.38E-5	5.93E-6
Order	-	1.50	1.33	1.87	1.99	2.00	2.00
$\varepsilon = \varepsilon_0/2^4$	8.76E-3	3.97E-3	1.30E-3	4.83E-4	1.52E-4	3.91E-5	9.77E-6
Order	-	1.14	1.61	1.43	1.66	1.96	2.00
$\varepsilon = \varepsilon_0/2^5$	4.30E-3	2.68E-3	1.48E-3	5.87E-4	1.83E-4	6.86E-5	1.86E-5
Order	-	6.83E-1	8.55E-1	1.33	1.68	1.42	1.88

Table 3.7: Temporal errors of CSI-4cFD at $t = 1$ for the less-ill-prepared initial data Case II with $\varepsilon_0 = 1, \tau_0 = 0.05$ at $t = 1$.

$e^{\varepsilon}_{H^1}$	τ_0	$\tau_0/2$	$\tau_0/2^2$	$\tau_0/2^2$	$\tau_0/2^3$	$\tau_0/2^4$	$\tau_0/2^5$
$\varepsilon = \varepsilon_0$	1.62E-2	4.77E-3	1.24E-3	3.12E-4	7.81E-5	1.95E-5	4.87E-6
Order	-	1.77	1.95	1.99	2.00	2.00	2.00
$\varepsilon = \varepsilon_0/2$	1.45E-2	4.29E-3	1.11E-3	2.80E-4	7.02E-5	1.75E-5	4.37E-6
Order	-	1.76	1.95	1.99	2.00	2.00	2.00
$\varepsilon = \varepsilon_0/2^2$	1.46E-2	4.23E-3	1.09E-3	2.74E-4	6.87E-5	1.72E-5	4.28E-6
Order	-	1.79	1.95	1.99	2.00	2.00	2.00
$\varepsilon = \varepsilon_0/2^3$	1.49E-2	4.17E-3	1.08E-3	2.71E-4	6.77E-5	1.69E-5	4.22E-6
Order	-	1.83	1.95	1.99	2.00	2.00	2.00
$\varepsilon = \varepsilon_0/2^4$	1.47E-2	4.13E-3	1.06E-3	2.67E-4	6.67E-5	1.67E-5	4.15E-6
Order	-	1.83	1.96	1.99	2.00	2.00	2.00
$\varepsilon = \varepsilon_0/2^5$	1.49E-2	4.15E-3	1.06E-3	2.67E-4	6.69E-5	1.67E-5	4.17E-6
Order	-	1.84	1.96	1.99	2.00	2.00	2.00

$\nu^{\varepsilon}_{\ell^2}$	τ_0	$\tau_0/2$	$\tau_0/2^2$	$\tau_0/2^2$	$\tau_0/2^3$	$\tau_0/2^4$	$\tau_0/2^5$
$\varepsilon = \varepsilon_0$	1.67E-3	4.18E-4	1.04E-4	2.61E-5	6.52E-6	1.63E-6	4.09E-7
Order	-	2.00	2.00	2.00	2.00	2.00	2.00
$\varepsilon = \varepsilon_0/2$	5.73E-3	1.45E-3	3.65E-4	9.12E-5	2.28E-5	5.70E-6	1.42E-6
Order	-	1.98	1.99	2.00	2.00	2.00	2.01
$\varepsilon = \varepsilon_0/2^2$	1.67E-2	4.69E-3	1.20E-3	3.02E-4	7.55E-5	1.89E-5	4.71E-6
Order	-	1.83	1.96	1.99	2.00	2.00	2.00
$\varepsilon = \varepsilon_0/2^3$	4.12E-2	1.12E-2	3.02E-3	7.73E-4	1.94E-4	4.85E-5	1.21E-5
Order	-	1.88	1.89	1.97	2.00	2.00	2.00
$\varepsilon = \varepsilon_0/2^4$	9.59E-2	3.68E-2	1.03E-2	2.65E-3	6.70E-4	1.68E-4	4.18E-5
Order	-	1.38	1.84	1.96	1.98	2.00	2.00
$\varepsilon = \varepsilon_0/2^5$	9.55E-2	6.30E-2	3.11E-2	9.87E-3	2.56E-3	6.44E-4	1.61E-4
Order	-	6.00E-1	1.02	1.66	1.95	1.99	2.00

Table 3.8: Temporal errors of CSI-4cFD at $t = 1$ for the ill-prepared initial data Case III with $\varepsilon_0 = 1, \tau_0 = 0.05$ at $t = 1$.

$e^{\varepsilon}_{H^1}$	τ_0	$\tau_0/2$	$\tau_0/2^2$	$\tau_0/2^2$	$\tau_0/2^3$	$\tau_0/2^4$	$\tau_0/2^5$
$\varepsilon = \varepsilon_0$	1.62E-2	4.77E-3	1.24E-3	3.12E-4	7.81E-5	1.95E-5	4.87E-6
Order	-	1.77	1.95	1.99	2.00	2.00	2.00
$\varepsilon = \varepsilon_0/2$	1.71E-2	4.98E-3	1.29E-3	3.25E-4	8.13E-5	2.03E-5	5.07E-6
Order	-	1.78	1.95	1.99	2.00	2.00	2.00
$\varepsilon = \varepsilon_0/2^2$	2.70E-2	7.27E-3	1.85E-3	4.64E-4	1.16E-4	2.90E-5	7.23E-6
Order	-	1.90	1.97	2.00	2.00	2.00	2.00
$\varepsilon = \varepsilon_0/2^3$	2.73E-2	7.72E-3	2.00E-3	5.05E-4	1.26E-4	3.16E-5	7.87E-6
Order	-	1.82	1.95	1.99	2.00	2.00	2.00
$\varepsilon = \varepsilon_0/2^4$	4.28E-2	1.07E-2	2.67E-3	6.67E-4	1.67E-4	4.16E-5	1.04E-5
Order	-	2.00	2.00	2.00	2.00	2.00	2.00
$\varepsilon = \varepsilon_0/2^5$	8.87E-2	2.04E-2	4.99E-3	1.24E-3	3.09E-4	7.72E-5	1.92E-5
Order	-	2.12	2.03	2.01	2.00	2.00	2.00

$\nu^{\varepsilon}_{\ell^2}$	τ_0	$\tau_0/2$	$\tau_0/2^2$	$\tau_0/2^2$	$\tau_0/2^3$	$\tau_0/2^4$	$\tau_0/2^5$
$\varepsilon = \varepsilon_0$	1.67E-3	4.18E-4	1.04E-4	2.61E-5	6.52E-6	1.63E-6	4.09E-7
Order	-	2.00	2.00	2.00	2.00	2.00	2.00
$\varepsilon = \varepsilon_0/2$	8.61E-3	2.17E-3	5.44E-4	1.36E-4	3.40E-5	8.49E-6	2.11E-6
Order	-	1.99	2.00	2.00	2.00	2.00	2.01
$\varepsilon = \varepsilon_0/2^2$	4.34E-2	1.12E-2	2.82E-3	7.07E-4	1.77E-4	4.42E-5	1.10E-5
Order	-	1.96	1.99	2.00	2.00	2.00	2.00
$\varepsilon = \varepsilon_0/2^3$	3.10E-1	8.22E-2	2.09E-2	5.24E-3	1.31E-3	3.28E-4	8.17E-5
Order	-	1.91	1.98	1.99	2.00	2.00	2.00
$\varepsilon = \varepsilon_0/2^4$	1.51	5.75E-1	1.60E-1	4.06E-2	1.02E-2	2.55E-3	6.35E-4
Order	-	1.39	1.85	1.98	2.00	2.00	2.00
$\varepsilon = \varepsilon_0/2^5$	3.04	2.00	9.85E-1	3.11E-1	8.05E-2	2.02E-2	5.04E-3
Order	-	6.01E-1	1.02	1.66	1.95	1.99	2.00

Table 3.9: Spatial errors for second-order semi-implicit finite difference scheme at $t = 1$ of Case III initial data with $\varepsilon = \frac{1}{2^5}$.

h	h_0	$h_0/2$	$h_0/2^2$	$h_0/2^3$	$h_0/2^4$	$h_0/2^5$	$h_0/2^6$	$h_0/2^7$
$e^{\varepsilon}_{H^1}(t=1)$	3.74E-1	**9.90E-2**	2.71E-2	**6.88E-3**	1.72E-3	**4.31E-4**	1.08E-4	**2.69E-5**
Order	-	1.92	1.87	1.98	2.00	2.00	2.00	2.00
CPU time (s)	3.72	**9.02**	2.35E1	**6.59E1**	2.01E2	**5.39E2**	1.40E3	**4.47E3**

Table 3.10: Spatial errors for CSI-4cFD at $t = 1$ of Case III initial data with $\varepsilon = \frac{1}{2^5}$.

h	h_0	$h_0/2$	$h_0/2^2$	$h_0/2^3$	$h_0/2^4$	$h_0/2^5$	$h_0/2^6$	$h_0/2^7$
$e^{\varepsilon}_{H^1}(t=1)$	**9.97E-2**	**8.61E-3**	**5.59E-4**	**3.48E-5**	2.18E-6	1.36E-7	8.46E-9	4.98E-10
Order	-	3.53	3.95	4.00	4.00	4.00	4.01	4.08
CPU time (s)	**3.08**	**7.48**	**2.14E1**	**5.59E1**	1.58E2	4.04E2	1.20E3	3.96E3

Table 3.9 and 3.10 provide a comparison between the second-order semi-implicit finite difference scheme in [32] and our CSI-4cFD. From last rows of the two tables, we can see the computation cost at a fixed mesh are the same for both methods. Comparing two consecutive time consumptions in both tables, we find that a spatial mesh refining will increase the CPU time by a factor around 2.7 for both methods. The bold cases in two tables are four groups of experiments that achieve same numerical error for both methods respectively. The CSI-4cFD reduces the computational cost a lot to achieve an aimed accuracy comparing to the second order method since the CSI-4cFD methods has higher spatial convergence rate.

Chapter 4

Uniform Error Estimate of a 4cFD for ZS

4.1 An asymptotic consistent formulation

Consider the Zakharov system (ZS) in d dimensions describing the propagation of Langmuir waves in plasma,

$$\begin{cases} i\partial_t E^\varepsilon(\boldsymbol{x},t) + \Delta E^\varepsilon(\boldsymbol{x},t) - N^\varepsilon(\boldsymbol{x},t)E^\varepsilon(\boldsymbol{x},t) = 0, \quad \boldsymbol{x}\in\mathbb{R}^d,\ t>0, \\ \varepsilon^2\partial_{tt}N^\varepsilon(\boldsymbol{x},t) - \Delta N^\varepsilon(\boldsymbol{x},t) - \Delta\left|E^\varepsilon(\boldsymbol{x},t)\right|^2 = 0, \quad \boldsymbol{x}\in\mathbb{R}^d,\ t>0, \\ E^\varepsilon(\boldsymbol{x},0) = E_0(\boldsymbol{x}),\ N^\varepsilon(\boldsymbol{x},0) = N_0^\varepsilon(\boldsymbol{x}),\ \partial_t N^\varepsilon(\boldsymbol{x},0) = N_1^\varepsilon(\boldsymbol{x}),\ \boldsymbol{x}\in\mathbb{R}^d, \end{cases} \tag{4.1.1}$$

where $E^\varepsilon(\boldsymbol{x},t)$ is a complex function describing the slowly varying envelope of a high-frequency plasma field, $N^\varepsilon(\boldsymbol{x},t)$ is a real function representing the plasma ion density fluctuation from its equilibrium position, $\boldsymbol{x}$ is the spatial coordinate, t is the time coordinate, and $\varepsilon\in(0,1]$ is a dimensionless parameter inversely proportional to the ion acoustic speed. $E_0(\boldsymbol{x})$, $N_0^\varepsilon(\boldsymbol{x})$ and $N_1^\varepsilon(\boldsymbol{x})$ are given initials with $N_1^\varepsilon(\boldsymbol{x})$ satisfying $\int_{\mathbb{R}^d} N_1^\varepsilon(\boldsymbol{x})\mathrm{d}\boldsymbol{x}{=}0$. The asymptotic expansion [32] of the solution $(E^\varepsilon(\boldsymbol{x},t), N^\varepsilon(\boldsymbol{x},t))$ as $\varepsilon\downarrow 0$ is

$$\begin{aligned} E^\varepsilon(\boldsymbol{x},t) =& E(\boldsymbol{x},t) + \varepsilon^2 E^{(1)}(\boldsymbol{x},t) + \varepsilon^3 E^{(2)}(\boldsymbol{x},t) + \cdots \\ &+ \varepsilon^{1+\alpha^\dagger}U^{(0)}(\boldsymbol{x},t/\varepsilon) + \varepsilon^{1+\alpha^*}U^{(1)}(\boldsymbol{x},t/\varepsilon) + \cdots, \end{aligned} \tag{4.1.2}$$

$$\begin{aligned} N^\varepsilon(\boldsymbol{x},t) =& -|E(\boldsymbol{x},t)|^2 + \varepsilon^2 N^{(1)}(\boldsymbol{x},t) + \varepsilon^3 N^{(2)}(\boldsymbol{x},t) + \cdots \\ &+ \varepsilon^{\alpha}V^{(1)}(\boldsymbol{x},t/\varepsilon) + \varepsilon^{\beta}V^{(2)}(\boldsymbol{x},t/\varepsilon) + \varepsilon^{\alpha^*}V^{(3)}(\boldsymbol{x},t/\varepsilon) + O(\varepsilon^2), \end{aligned} \tag{4.1.3}$$

with $V^{(1)}, V^{(2)}$ satisfying

$$\begin{cases} \partial_{ss}V^{(1)}(\boldsymbol{x},s) - \Delta V^{(1)}(\boldsymbol{x},s) = 0, \\ V^{(1)}(\boldsymbol{x},0) = w_0(\boldsymbol{x}), \\ \partial_s V^{(1)}(\boldsymbol{x},0) = 0, \end{cases} \qquad \begin{cases} \partial_{ss}V^{(2)}(\boldsymbol{x},s) - \Delta V^{(2)}(\boldsymbol{x},s) = 0, \\ V^{(2)}(\boldsymbol{x},0) = 0, \\ \partial_s V^{(2)}(\boldsymbol{x},0) = w_1(\boldsymbol{x}). \end{cases} \tag{4.1.4}$$

The initial data can be classified into well and less-ill prepared ($\alpha, \beta \geq 1$) and ill prepared ($\min\{\alpha, \beta\} \in [0, 1)$) cases through considering the leading oscillation in the density N^ε as [2, 17, 32, 82] did. Inspired by the fitting corrector adopted by [2], we introduce the following asymptotic consistent formulation for the incompatible initial data as in [16]. Solve a linear wave function $G^\varepsilon(\boldsymbol{x}, t)$ from

$$\begin{cases} \partial_{ss}G^\varepsilon(\boldsymbol{x},s) - \frac{1}{\varepsilon^2}\Delta G^\varepsilon(\boldsymbol{x},s) = 0, & \boldsymbol{x} \in \mathbb{R}^d,\ s > 0, \\ G^\varepsilon(\boldsymbol{x},0) = \varepsilon^\alpha w_0(\boldsymbol{x}), & \boldsymbol{x} \in \mathbb{R}^d, \\ \partial_s G^\varepsilon(\boldsymbol{x},0) = \varepsilon^{\beta-1} w_1(\boldsymbol{x}), & \boldsymbol{x} \in \mathbb{R}^d, \end{cases} \tag{4.1.5}$$

and let

$$F^\varepsilon(\boldsymbol{x},t) = |E^\varepsilon(\boldsymbol{x},t)|^2 + N^\varepsilon(\boldsymbol{x},t) - G^\varepsilon(\boldsymbol{x},t), \quad \boldsymbol{x} \in \mathbb{R}^d, t \geq 0. \tag{4.1.6}$$

Substituting (4.1.6) into ZS (4.1.1), we get the asymptotic consistent formulation of ZS:

$$\begin{cases} i\partial_t E^\varepsilon(\boldsymbol{x},t) + \Delta E^\varepsilon(\boldsymbol{x},t) + [|E^\varepsilon(\boldsymbol{x},t)|^2 - G^\varepsilon(\boldsymbol{x},t) - F^\varepsilon(\boldsymbol{x},t)]E^\varepsilon(\boldsymbol{x},t) = 0, \\ \varepsilon^2 \partial_{tt}F^\varepsilon(\boldsymbol{x},t) - \Delta F^\varepsilon(\boldsymbol{x},t) - \varepsilon^2 \partial_{tt}|E^\varepsilon(\boldsymbol{x},t)|^2 = 0, \quad \boldsymbol{x} \in \mathbb{R}^d, t > 0, \\ E^\varepsilon(\boldsymbol{x},0) = E_0(\boldsymbol{x}),\ F^\varepsilon(\boldsymbol{x},0) = 0,\ \partial_t F^\varepsilon(\boldsymbol{x},0) = 0,\ \boldsymbol{x} \in \mathbb{R}^d. \end{cases} \tag{4.1.7}$$

Note that the fitting corrector term $G^\varepsilon(\boldsymbol{x}, t)$ is exactly the union of the first and second initial layers of $N^\varepsilon(\boldsymbol{x}, t)$ arising in (4.1.2). It can be solved exactly as long as the initial data w_0 and w_1 are given. When $\varepsilon \downarrow 0$, the convergence to NLSE (1.2.10) can be depicted by higher order approximation: $E^\varepsilon(\boldsymbol{x}, t) \to \tilde{E}^\varepsilon(\boldsymbol{x}, t)$ with $\tilde{E}^\varepsilon(\boldsymbol{x}, t)$ satisfying a nonlinear Schrödinger equation with an oscillatory potential $G^\varepsilon(\boldsymbol{x}, t)$ (NLS-OP):

$$\begin{cases} i\partial_t \tilde{E}^\varepsilon(\boldsymbol{x},t) + \Delta \tilde{E}^\varepsilon(\boldsymbol{x},t) + \left(|\tilde{E}^\varepsilon(\boldsymbol{x},t)|^2 - G^\varepsilon(\boldsymbol{x},t)\right)\tilde{E}^\varepsilon(\boldsymbol{x},t) = 0, \\ E^\varepsilon(\boldsymbol{x},0) = E_0(\boldsymbol{x}). \end{cases} \tag{4.1.8}$$

[16] proposed a uniform accurate finite difference method for the Zakharov system with asymptotic consistent form. They achieved uniform second order spatial convergence independent of the dimensionless parameter ε. Due to the high speed outgoing wave from the initial layer [2, 17, 91], the numerical method needs a large spatial domain of size $O(\frac{T}{\varepsilon})$, which arouses large computational cost if we need small h to achieve a required accuracy. Fortunately, the high oscillation in ZS wavelength of ZS is $O(1)$ on spatial direction provided non-oscillatory initials [16, 32]. and we are not restrict to use tiny h for spatial resolutions. Therefore, we adopt the 4th order compact scheme to ZS, by approximating the spatial derivatives at a point with the same number of nodes as the second order method needs to achieve a higher accuracy. The computational cost can be reduced a lot with a coarser grid partition than the second order method for an aimed error.

In this chapter, we apply the fourth order compact finite difference schemes to the asymptotic preserving formulation. For simplicity, we only show the schemes and analysis in one spatial dimension. Generalizations to higher dimensions are straightforward. For numerical computation, we truncate our computational domain into an interval $\Omega = (a, b)$ with zero Dirichlet boundary conditions. The asymptotic consistent form of ZS (4.1.7) is

$$\begin{cases} i\partial_t E^\varepsilon(x,t) + \partial_{xx}E^\varepsilon(x,t) + [|E^\varepsilon(x,t)|^2 - G^\varepsilon(x,t) - F^\varepsilon(x,t)]E^\varepsilon(x,t) = 0, \\ \varepsilon^2\partial_{tt}F^\varepsilon(x,t) - \partial_{xx}F^\varepsilon(x,t) - \varepsilon^2\partial_{tt}\left|E^\varepsilon(x,t)\right|^2 = 0, \quad x \in \Omega,\ t > 0, \end{cases} \tag{4.1.9}$$

with boundary condition

$$\begin{cases} E^\varepsilon(x,0) = E_0(x),\ F^\varepsilon(x,0) = 0,\ \partial_t F^\varepsilon(x,0) = 0, & x \in \Omega, \\ E^\varepsilon(x,t)|_{\partial\Omega} = 0,\ F^\varepsilon(x,t)|_{\partial\Omega} = 0, & t \geq 0, \end{cases} \tag{4.1.10}$$

where $G^\varepsilon(x,t)$ solves

$$\begin{cases} \partial_{ss}G^\varepsilon(x,s) - \frac{1}{\varepsilon^2}\partial_{xx}G^\varepsilon(x,s) = 0, & x \in \Omega,\ s > 0, \\ G^\varepsilon(x,0) = \varepsilon^\alpha\omega_0(x),\ \partial_s G^\varepsilon(x,0) = \varepsilon^{\beta-1}\omega_1(x), & x \in \Omega, \\ G^\varepsilon(x,s)|_{\partial\Omega} = 0, & s \geq 0. \end{cases} \tag{4.1.11}$$

The rest of this chapter is organized as follows. In Section 4.2, we introduced the uniform accurate fourth order compact scheme (UA-4cFD) for the asymptotic consistent formulation. The solvability, stability, and main results on error estimation are also presented. In Section 4.3, the uniform accurate error estimates of the UA-4cFD, combined by the optimal dependence of spatial and temporal errors on the small parameter ε, and error bounds through the biased error function are analysed rigorously. Several numerical simulations are reported in Section 4.4 to test the convergence rate from the theoretical analysis.

4.2 A uniform accurate 4cFD (UA-4cFD)

4.2.1 The numerical scheme

For mesh size $h := (b-a)/J$ and time step $\tau := T/N$, with J, N positive integers and $T > 0$ a fixed time less than the maximum common existence time for the solutions of (4.1.9). Denote the grid points and time steps as:

$x_j := a + jh, j = 0, 1, \ldots, J; \quad t_n := n\tau,\ n = 0, 1, \ldots, N.$

Let $\mathcal{T}_J = \{1, 2, \cdots, J-1\}$ and $\mathcal{T}_J^0 = \{0, 1, 2, \cdots, J\}$ be the index sets of grid points; let $E_j^{\varepsilon,n}$ and $F_j^{\varepsilon,n}$ be the numerical approximation of $E^\varepsilon(x_j, t_n)$ and $F^\varepsilon(x_j, t_n)$ for $j \in \mathcal{T}_J^0$; and denote the possible solution space as

$$X_J = \{u = (u_j)_{j\in\mathcal{T}_J^0} : u_0 = u_J = 0\} \subset \mathbb{C}^{J+1}. \tag{4.2.1}$$

Apart from the standard finite difference operators as noted in Section 3.2.1, we introduce two more finite difference operators:

$$\delta_t u_j^n = \frac{u_j^{n+1} - u_j^{n-1}}{2\tau},\ \delta_x u_j^n = \frac{u_{j+1}^n - u_{j-1}^n}{2h},$$

for $u_j^n = E_j^{\varepsilon,n}$ or $N_j^{\varepsilon,n}$. Let $\mathcal{A}_h$ be the standard fourth order approximation of the second order derivative as

$$\mathcal{A}_h u_j^n = u_j^n + \frac{h^2}{12}\delta_x^2 u_j^n, \tag{4.2.2}$$

then we have the uniform accurate fourth-order compact scheme (UA-4cFD) [124] of form:

$$i\delta_t E_j^{\varepsilon,n} = \left[-\mathcal{A}_h^{-1}\delta_x^2 + \frac{F_j^{\varepsilon,n-1}+F_j^{\varepsilon,n+1}}{2} + G_j^{\varepsilon,n} - \left|E_j^{\varepsilon,n}\right|^2\right]\frac{E_j^{\varepsilon,n-1}+E_j^{\varepsilon,n+1}}{2}, \quad (4.2.3)$$

$$\varepsilon^2\delta_t^2 F_j^{\varepsilon,n} = \frac{1}{2}\mathcal{A}_h^{-1}\delta_x^2\left(F_j^{\varepsilon,n-1}+F_j^{\varepsilon,n+1}\right) + \varepsilon^2\delta_t^2\left|E_j^{\varepsilon,n}\right|^2, \ j\in\mathcal{T}_J, n\geq 1, \quad (4.2.4)$$

with boundary and initial conditions

$$E_j^{\varepsilon,0} = E_0\left(x_j\right), \quad F_j^{\varepsilon,0} = 0, \quad j\in\mathcal{T}_J^0,$$
$$E_0^{\varepsilon,n} = E_J^{\varepsilon,n} = 0, \quad F_0^{\varepsilon,n} = F_J^{\varepsilon,n} = 0, \quad n\geq 0,$$

and first step discretization from the Taylor expansion of (4.1.9) at $t=0$:

$$E_j^{\varepsilon,1} = E_0(x_j) + \tau\phi_2(x_j) + \frac{\tau^2}{2}\phi_3(x_j), \ F_j^{\varepsilon,1} = \frac{\tau^2}{2}\phi_4(x_j), \ j\in\mathcal{T}_J, \quad (4.2.5)$$

where

$$\begin{cases} \phi_1(x) := \partial_t N^\varepsilon(x,0) = 2\,\mathrm{Im}(E_0''(x)\overline{E_0(x)}), \\ \phi_2(x) := \partial_t E^\varepsilon(x,0) = i\left(E_0''(x) - N_0^\varepsilon(x)E_0(x)\right), \\ \phi_3(x) := \partial_{tt} E^\varepsilon(x,0) = i\left(\phi_2''(x) - N_1^\varepsilon(x)E_0(x) - N_0^\varepsilon(x)\phi_2(x)\right), \\ \phi_4(x) := \partial_{tt} F^\varepsilon(x,0) = 2\,\mathrm{Im}\left(\phi_2(x)\overline{E_0''(x)} + E_0(x)\overline{\phi_2''(x)}\right), \end{cases} x\in\Omega. \quad (4.2.6)$$

In order to ensure the boundedness of $N^{\varepsilon,1}$ constructed from $N^{\varepsilon,1} = G^{\varepsilon,1} - |E^{\varepsilon,1}|^2 - F^{\varepsilon,1}$ for $\alpha,\beta\geq 0$, we adopt the method in [32] and [16] to bound the terms containing $\varepsilon^{\beta-1}$ in (4.2.5) originating from (1.2.12): using the trigonometric function $\sin(\tau/\varepsilon)$ which is uniformly bounded for $\varepsilon\in(0,1]$. Then, the first equation of (4.2.5) becomes:

$$\begin{aligned} E_j^{\varepsilon,1} =& E_0(x_j) + \tau\phi_2(x_j) + \frac{i\tau^2}{2}\left(\phi_2''(x_j) - \phi_1(x_j)E_0(x_j) - N_0^\varepsilon(x_j)\phi_2(x_j)\right) \\ &- \frac{i\tau\varepsilon^\beta}{2}\sin(\frac{\tau}{\varepsilon})E_0(x_j)w_1(x_j). \end{aligned} \quad (4.2.7)$$

The $G_j^{\varepsilon,n}$ can be solved directly by the sine pseudo-spectral method. After sine transform of the initial values, the amplitude of each mode in time can be integrated exactly in the phase space. We have

$$G_j^{\varepsilon,n} = \sum_{k=1}^{J-1} \sin\left(\frac{jk\pi}{J}\right)\left(\varepsilon^\alpha \widetilde{w_{0k}} \cos\left(\frac{\mu_k}{\varepsilon} t_n\right) + \frac{\varepsilon^\beta}{\mu_k}\widetilde{w_{1k}} \sin\left(\frac{\mu_k}{\varepsilon} t_n\right)\right), \tag{4.2.8}$$

where

$$\mu_k = \frac{k\pi}{b-a}, \; \widetilde{w_{0k}} = \frac{2}{J}\sum_{k=1}^{J-1} w_0(x_j)\sin\left(\frac{jk\pi}{J}\right), \; \tilde{w}_{1k} = \frac{2}{J}\sum_{k=1}^{J-1} w_1(x_j)\sin\left(\frac{jk\pi}{J}\right).$$

We treat the $G^{\varepsilon,n}$ as a source term in the iteration solver of (4.2.3) and (4.2.4). For simplicity, we introduce time average symbols at time $t = t_n$ for a grid function $u^n \in X_J$ (with $n \geq 0$) and a continuous function $v(x,t)$ on Ω_T :

$$[\![u]\!]_j^n = \frac{u_j^{n-1} + u_j^{n+1}}{2}, \; n \geq 1, j \in \mathcal{T}_J;$$
$$(\!|v|\!)(x,t_n) = \frac{v(x,t_{n-1}) + v(x,t_{n+1})}{2}, \; x \in \Omega.$$

Then, the 4th-order compact schemes (4.2.3) and (4.2.4) become

$$i\delta_t E_j^{\varepsilon,n} = \left(-\mathcal{A}_h^{-1}\delta_x^2 + [\![F^\varepsilon]\!]_j^n + G_j^{\varepsilon,n} - \left|E_j^{\varepsilon,n}\right|^2\right)[\![E^\varepsilon]\!]_j^n, \tag{4.2.9}$$

$$\varepsilon^2\delta_t^2 F_j^{\varepsilon,n} = \mathcal{A}_h^{-1}\delta_x^2[\![F^\varepsilon]\!]_j^n + \varepsilon^2\delta_t^2\left|E_j^{\varepsilon,n}\right|^2, \; j \in \mathcal{T}_J, n \geq 1. \tag{4.2.10}$$

4.2.2 Solvability of the difference equations

As in Lemma 2.1, the solvability of (4.2.3) and (4.2.4) can be proved by the Brouwer fixed point theorem as in [9, 115].

Lemma 4.1. (Solvability for the UA-4cFD) *For any given initial data $E^{\varepsilon,0}, F^{\varepsilon,0}$, $E^{\varepsilon,1}, F^{\varepsilon,1} \in X_J$, there exists a unique set of solutions $E^{\varepsilon,n}$ and $F^{\varepsilon,n}$ to the UA-4cFD (4.2.3) and (4.2.4) for $n > 1$.*

Proof. Firstly, we will show the solvability of the UA-4cFD. For every $j \in \mathcal{T}_J$, we can rewrite (4.2.9) and (4.2.10) as

$$[\![E^\varepsilon]\!]_j^n = E_j^{\varepsilon,n-1} + i\tau\left(\mathcal{A}_h^{-1}\delta_x^2 + \left|E_j^{\varepsilon,n}\right|^2 - [\![F^\varepsilon]\!]_j^n - G_j^{\varepsilon,n}\right)[\![E^\varepsilon]\!]_j^n, \tag{4.2.11}$$

$$[\![F^\varepsilon]\!]_j^n = F_j^{\varepsilon,n} + \frac{\tau^2}{\varepsilon^2}\mathcal{A}_h^{-1}\delta_x^2[\![F^\varepsilon]\!]_j^n + [\![|E^\varepsilon|^2]\!]_j^n - \left|E_j^{\varepsilon,n}\right|^2. \tag{4.2.12}$$

Define a continuous map $\psi^n : X_J \times Y_J \to X_J \times Y_J$ by

$$\psi^n(u,v) = (\psi_1^n(u,v), \psi_2^n(u,v)) \tag{4.2.13}$$

with

$$(\psi_1^n(u,v))_j = u_j - E_j^{\varepsilon,n-1} - i\tau\left(\mathcal{A}_h^{-1}\delta_x^2 + \left|E_j^{\varepsilon,n}\right|^2 - v_j - G_j^{\varepsilon,n}\right)u_j,$$

$$(\psi_2^n(u,v))_j = v_j - \frac{\tau^2}{\varepsilon^2}\mathcal{A}_h^{-1}\delta_x^2 v_j + \left|E_j^{\varepsilon,n}\right|^2 - F_j^{\varepsilon,n} - 2|u_j|^2 + 2\,\mathrm{Re}(u_j\overline{E_j^{\varepsilon,n}}) - 2\left|E_j^{\varepsilon,n}\right|^2,$$

for $u \in X_J$, $v \in Y_J = \{v = (v_0, v_1, \cdots, v_J) \in \mathbb{R}^{J+1} : v_0 = v_J = 0\}$. Thus, we can express (4.2.11) and (4.2.12) by

$$\psi^n([\![E^\varepsilon]\!]^n, [\![F^\varepsilon]\!]^n) = 0. \tag{4.2.14}$$

Note that

$$\lim_{\|u\|_{\ell^2}\to\infty} \frac{\mathrm{Re}\langle\psi_1^n(u,v),u\rangle}{\|u\|_{\ell^2}} = +\infty \tag{4.2.15}$$

since

$$\mathrm{Re}\langle\psi_1^n(u,v),u\rangle = \|u\|_{\ell^2}^2 - \mathrm{Re}\langle E^{\varepsilon,n-1},u\rangle \geq \frac{1}{2}\left(\|u\|_{\ell^2}^2 - \left\|E^{\varepsilon,n-1}\right\|_{\ell^2}^2\right). \tag{4.2.16}$$

Similarly, we have

$$\langle\psi_2^n(u,v),v\rangle \geq \|v\|_{\ell^2}^2 + \frac{\tau^2}{\varepsilon^2}|v|_{1,*}^2 - C(u)\|v\|_{\ell^2} \tag{4.2.17}$$

and

$$\lim_{\|v\|_{\ell^2}\to\infty} \frac{\langle\psi_2^n(u,v),v\rangle}{\|v\|_{\ell^2}} = +\infty. \tag{4.2.18}$$

Combine (4.2.15) and (4.2.18) together, we have

$$\lim_{\|u\|_{\ell^2},\|v\|_{\ell^2}\to\infty} \frac{|\langle\psi^n(u,v),(u,v)\rangle|}{\|u\|_{\ell^2} + \|v\|_{\ell^2}} = +\infty. \tag{4.2.19}$$

Since ψ^n is a continuous self mapping on finite dimensional space $X_J \times Y_J$, we know ψ^n is a surjection from [57]. The Brouwer fixed point theorem [7,66] indicates that ψ^n has a preimage (u^*, v^*) for 0, i.e., $\psi^n(u^*, v^*) = 0$. Then $2u^* - E^{\varepsilon,n-1}$ and $2v^* - F^{\varepsilon,n-1}$ are solutions to (4.2.3) and (4.2.4) respectively. $\square$

4.3 Uniform error bounds

Let T^* be the maximum common existence time for the solution $(E^\varepsilon(x,t), F^\varepsilon(x,t))$ to the ZS (4.1.9) and the solution $\tilde{E}^\varepsilon(x,t)$ to the corresponding NLS-OP (4.1.8). For any $T \in (0, T^*]$, as the asymptotic analysis showed, we may assume the exact solution $(E^\varepsilon(x,t), F^\varepsilon(x,t))$ of the ZS (4.1.9) and the exact solution $\tilde{E}^\varepsilon(x,t)$ of the NLS-OP (4.1.8) are smooth enough and satisfying the homogeneous Dirichlet boundary conditions with the following assumptions:

$$
\begin{aligned}
&\|E^\varepsilon\|_{L^\infty([0,T];W^{7,\infty}(\Omega))} + \|E^\varepsilon\|_{W^{1,\infty}([0,T];W^{3,\infty}(\Omega))} + \varepsilon\,\|E^\varepsilon\|_{W^{2,\infty}([0,T];W^{4,\infty}(\Omega))} \\
&+ \varepsilon^2\,\|E^\varepsilon\|_{W^{3,\infty}([0,T];W^{4,\infty}(\Omega))} \lesssim 1, \\
&\left\|\tilde{E}^\varepsilon\right\|_{L^\infty([0,T];W^{7,\infty}(\Omega))} + \left\|\tilde{E}^\varepsilon\right\|_{W^{1,\infty}([0,T];W^{3,\infty}(\Omega))} + \varepsilon^{1-\alpha*}\left\|\tilde{E}^\varepsilon\right\|_{W^{2,\infty}([0,T];W^{4,\infty}(\Omega))} \lesssim 1, \\
&\|F^\varepsilon\|_{L^\infty([0,T];W^{7,\infty}(\Omega))} \lesssim \varepsilon^2, \;\; \|F^\varepsilon\|_{W^{1,\infty}([0,T];W^{2,\infty}(\Omega))} \lesssim \varepsilon, \\
&\|F^\varepsilon\|_{W^{2,\infty}([0,T];W^{3,\infty}(\Omega))} + \varepsilon\,\|F^\varepsilon\|_{W^{3,\infty}([0,T];W^{2,\infty}(\Omega))} + \varepsilon^2\,\|F^\varepsilon\|_{W^{4,\infty}([0,T];W^{3,\infty}(\Omega))} \lesssim 1,
\end{aligned}
\tag{4.A}
$$

where

$$
\alpha^* = \min(1, \alpha, \beta). \tag{4.3.1}
$$

Under a good initial data assumption

$$
\|E_0\|_{H^6(\Omega)} + \|w_0\|_{H^4(\Omega)} + \|w_1\|_{H^4(\Omega)} \lesssim 1, \tag{4.B}
$$

we can obtain

$$
\|G^\varepsilon\|_{W^{m,\infty}([0,T],W^{3,\infty}(\Omega))} \lesssim \varepsilon^{\alpha^*-m}, \;\; m = 0, 1, 2, 3. \tag{4.3.2}
$$

Define the error functions $e^{\varepsilon,n}, f^{\varepsilon,n} \in X_J$ for $n \geq 0$ as

$$
e_j^{\varepsilon,n} = E^\varepsilon(x_j, t_n) - E_j^{\varepsilon,n}, \;\; f_j^{\varepsilon,n} = F^\varepsilon(x_j, t_n) - F_j^{\varepsilon,n}, \;\; j \in \mathcal{T}_J^0, \tag{4.3.3}
$$

and we have the following error estimates.

4.3.1 Main results

Theorem 4.1. (Error estimates for well-prepared and ill-prepared initial data) *Assume $\tau \lesssim h$ and under the assumption (4.A), there exist $\tau_0, h_0 > 0$ sufficiently* *small and independent of ε such that for any $\varepsilon \in (0,1]$, we have the following error estimate of the UA-4cFD for any $\tau \in (0,\tau_0], h \in (0,h_0]$:*

$$\|e^{\varepsilon,n}\|_{\ell^2} + |e^{\varepsilon,n}|_1 + \|f^{\varepsilon,n}\|_{\ell^2} \lesssim h^4 + \frac{\tau^2}{\varepsilon}, \quad 0 \le n \le \frac{T}{\tau}, \tag{4.3.4}$$

$$\|e^{\varepsilon,n}\|_{\ell^2} + |e^{\varepsilon,n}|_1 + \|f^{\varepsilon,n}\|_{\ell^2} \lesssim h^4 + \tau^2 + \tau\varepsilon^{\alpha^*} + \varepsilon^{1+\alpha^*}, \quad 0 \le n \le \frac{T}{\tau}. \tag{4.3.5}$$

Furthermore, combining (4.3.4) and (4.3.5) together, we have the following uniform error estimate independent of ε:

for well-prepared and less-ill-prepared initial data ($\alpha, \beta \in [1,+\infty)$),

$$\|e^{\varepsilon,n}\|_{\ell^2} + |e^{\varepsilon,n}|_1 + \|f^{\varepsilon,n}\|_{\ell^2} \lesssim h^4 + \min\{\tau^2 + \tau\varepsilon^{\alpha^*} + \varepsilon^2, \frac{\tau^2}{\varepsilon}\} \lesssim h^4 + \tau^{4/3}; \tag{4.3.6}$$

for ill-prepared initial data ($\alpha, \beta \in [0,1)$),

$$\|e^{\varepsilon,n}\|_{\ell^2} + |e^{\varepsilon,n}|_1 + \|f^{\varepsilon,n}\|_{\ell^2} \lesssim h^4 + \min\{\tau^2 + \varepsilon^{\alpha^*}(\tau+\varepsilon), \frac{\tau^2}{\varepsilon}\} \lesssim h^4 + \tau^{1+\frac{\alpha^*}{2+\alpha^*}}, \tag{4.3.7}$$

for $0 \le n \le \frac{T}{\tau}$.

In order to get theorem 4.1, we use the energy method and cut-off technique to prove the optimal error bound (4.3.4) and use the NLS-OP as a middle term to prove the error bound (4.3.5). The diagram below shows the two approaches to estimate the error between $(E^{\varepsilon,n}, F^{\varepsilon,n})$ and $(E^\varepsilon, F^\varepsilon)$ with the error scales labelled on each arrow. The first path gives the error bound in (4.3.4) while the second path gives (4.3.5).

$$\begin{tikzcd}
(E^{\varepsilon,n},F^{\varepsilon,n}) \arrow[rr, "O(h^4+\frac{\tau^2}{\varepsilon})"] \arrow[dr, "O(h^4+\tau^2+\tau\varepsilon^{\alpha^*}+\varepsilon^{1+\alpha^*})"'] & & (E^\varepsilon,F^\varepsilon) \\
& (\tilde{E}^\varepsilon,0) \arrow[ur, "O(\varepsilon^2)"'] &
\end{tikzcd}$$

Define the local truncation error $\eta^{\varepsilon,n}, \xi^{\varepsilon,n} \in X_J$ of UA-4cFD (4.2.3) and (4.2.4) as

$$\begin{aligned}
\eta_j^{\varepsilon,n} =& i\delta_t E^\varepsilon(x_j,t_n) \\
&+ \left[\mathcal{A}_h^{-1}\delta_x^2 + |E^\varepsilon(x_j,t_n)|^2 - G_j^{\varepsilon,n} - [\![F^\varepsilon]\!](x_j,t_n)\right][\![E^\varepsilon]\!](x_j,t_n),
\end{aligned} \tag{4.3.8}$$

$$\xi_j^{\varepsilon,n} = \varepsilon^2\delta_t^2 F^\varepsilon(x_j,t_n) - \mathcal{A}_h^{-1}\delta_x^2[\![F^\varepsilon]\!](x_j,t_n) - \varepsilon^2\delta_t^2\left|E^\varepsilon(x_j,t_n)\right|^2, \tag{4.3.9}$$

for $j \in \mathcal{T}_J$, $n \geq 1$.

Lemma 4.2. *Under assumption* (4.A), *we have*

$$\|\eta^{\varepsilon,n}\|_{\ell^2} + |\eta^{\varepsilon,n}|_1 \lesssim h^4 + \frac{\tau^2}{\varepsilon}, \tag{4.3.10}$$

$$\|\xi^{\varepsilon,n}\|_{\ell^2} \lesssim \varepsilon^2 h^4 + \tau, \tag{4.3.11}$$

$$\|\delta_t \xi^{\varepsilon,n}\|_{\ell^2} \lesssim \varepsilon h^4 + \frac{\tau^2}{\varepsilon}. \tag{4.3.12}$$

Proof. For each $n \geq 1$ and $j \in \mathcal{T}_J$, take Taylor expansion of $E^\varepsilon(x,t)$ at point (x_j, t_n), and, $E^\varepsilon_{xx}(x,t)$ at points (x_j, t_{n+1}) and (x_j, t_{n-1}) we have

$$\begin{aligned}
\eta_j^{\varepsilon,n} =& \frac{i}{2\tau}\int_{t_{n-1}}^{t_{n+1}} \partial_t E^\varepsilon(x_j,s)\,\mathrm{d}s \\
&+ \left[\mathcal{A}_h^{-1}\delta_x^2 + |E^\varepsilon(x_j,t_n)|^2 - G_j^{\varepsilon,n} - [\![F^\varepsilon]\!](x_j,t_n)\right][\![E^\varepsilon]\!](x_j,t_n) \\
=& \frac{i}{2\tau}\int_{t_{n-1}}^{t_{n+1}} [(-\partial_x^2 E^\varepsilon - |E^\varepsilon|^2 E^\varepsilon + E^\varepsilon F^\varepsilon)(x_j,s) + E^\varepsilon(x_j,s)\,G^\varepsilon(x_j,s)]\mathrm{d}s \\
&+ \left[\mathcal{A}_h^{-1}\delta_x^2 + |E^\varepsilon(x_j,t_n)|^2 - [\![F^\varepsilon]\!](x_j,t_n) - G_j^{\varepsilon,n}\right][\![E^\varepsilon]\!](x_j,t_n) \\
=& -\frac{\tau^2}{4}\int_{-1}^{1}(1-|s|)^2\partial_t^2\partial_x^2 E^\varepsilon(x_j, s\tau+t_n)\,\mathrm{d}s \\
&+ \left(\mathcal{A}_h^{-1}\delta_x^2[\![E^\varepsilon]\!](x_j,t_n) - [\![\partial_x^2 E^\varepsilon]\!](x_j,t_n)\right) \\
&+ \frac{\tau^2}{4}\int_{-1}^{1}(1-|s|)^2\partial_t^2(E^\varepsilon F^\varepsilon - |E^\varepsilon|^2 E^\varepsilon)(x_j, s\tau+t_n)\,\mathrm{d}s \\
&+ \frac{\tau^2}{2}\left(|E^\varepsilon(x_j,t_n)|^2 - G_j^{\varepsilon,n} - [\![F^\varepsilon]\!](x_j,t_n)\right)\int_{-1}^{1}(1-|s|)^2\partial_t^2 E^\varepsilon(x_j, s\tau+t_n)\,\mathrm{d}s \\
&- \frac{\tau^2}{2}E^\varepsilon(x_j,t_n)\int_{-1}^{1}(1-|s|)^2\partial_t^2 F^\varepsilon(x_j, s\tau+t_n)\,\mathrm{d}s \\
&+ \frac{1}{2\tau}\int_{t_{n-1}}^{t_{n+1}} E^\varepsilon(x_j,s)\,G^\varepsilon(x_j,s)\,\mathrm{d}s - E^\varepsilon(x_j,t_n)\,G_j^{\varepsilon,n}.
\end{aligned} \tag{4.3.13}$$

For the second term in the last part of (4.3.13), we have

$$\begin{aligned}
&\mathcal{A}_h\left(\mathcal{A}_h^{-1}\delta_x^2 E^\varepsilon(x_j,t_n) - \partial_x^2 E^\varepsilon(x_j,t_n)\right) \\
&\quad = \delta_x^2 E^\varepsilon(x_j,t_n) - \mathcal{A}_h\partial_x^2 E^\varepsilon(x_j,t_n) = -\frac{h^4}{240}\frac{\partial^6 E^\varepsilon(\zeta_j,t_n)}{\partial x^6},
\end{aligned} \tag{4.3.14}$$

for some $\zeta_j \in (x_{j-1}, x_{j+1})$. Therefore, we have the following bound

$$\left|\mathcal{A}_h^{-1}\delta_x^2[\![E^\varepsilon]\!](x_j,t_n) - [\![\partial_x^2 E^\varepsilon]\!](x_j,t_n)\right| \lesssim h^4\left\|\partial_x^6 E^\varepsilon\right\|_{L^\infty(\Omega_T)}. \tag{4.3.15}$$

Under assumption (4.A), we have

$$
\begin{aligned}
|\eta_j^{\varepsilon,n}| \lesssim & h^4\left\|\partial_x^6 E^\varepsilon\right\|_\infty + \tau^2\left(\left\|\partial_t^2\partial_x^2 E^\varepsilon\right\|_\infty + \left\|\partial_t^2(|E^\varepsilon|^2 E^\varepsilon)\right\|_\infty + \|E^\varepsilon\|_\infty\left\|\partial_t^2 F^\varepsilon\right\|_\infty\right. \\
& \left. + \left(\|\partial_t G^\varepsilon\|_\infty + \|\partial_t F^\varepsilon\|_\infty\right)\|\partial_t E^\varepsilon\|_\infty + \left(\|E^\varepsilon\|_\infty^2 + \|G^\varepsilon\|_\infty + \|F^\varepsilon\|_\infty\right)\left\|\partial_t^2 E^\varepsilon\right\|_\infty\right) \\
\lesssim & h^4 + \frac{\tau^2}{\varepsilon},
\end{aligned}
\tag{4.3.16}
$$

for $j \in \mathcal{T}_J, 1 \leq n \leq T/\tau - 1$. Similarly, we have

$$
\begin{aligned}
|\xi_j^{\varepsilon,n}| \lesssim & h^4\left\|\partial_x^6 F^\varepsilon\right\|_\infty + \tau^2\left(\varepsilon^2\left\|\partial_t^4 F^\varepsilon\right\|_\infty + \varepsilon^2\left\|\partial_t^4 E^\varepsilon\right\|_\infty + \left\|\partial_t^2\partial_x^2 F^\varepsilon\right\|_\infty\right) \\
\lesssim & \varepsilon^2 h^4 + \tau^2,
\end{aligned}
\tag{4.3.17}
$$

for $j \in \mathcal{T}_J, 1 \leq n \leq T/\tau - 1$. Apply δ_x^+ and δ_t to (4.3.8) and (4.3.9) respectively, we have

$$
\begin{aligned}
|\delta_x^+\eta_j^{\varepsilon,n}| \lesssim & h^4\left\|\partial_x^7 E^\varepsilon\right\|_\infty + \tau^2\left(\left\|\partial t^2\partial_x^3 E^\varepsilon\right\|_\infty + \left\|\partial_t^2\partial_x(|E^\varepsilon|^2 E^\varepsilon)\right\|_\infty + \|\partial_x E^\varepsilon\|_\infty\left\|\partial_t^2 F^\varepsilon\right\|_\infty\right. \\
& + \left(\|\partial_t G^\varepsilon\|_\infty + \|\partial_t F^\varepsilon\|_\infty\right)\|\partial_t\partial_x E^\varepsilon\|_\infty + \left(\|E^\varepsilon\|_\infty^2 + \|G^\varepsilon\|_\infty + \|F^\varepsilon\|_\infty\right)\left\|\partial_t^2\partial_x E^\varepsilon\right\|_\infty \\
& + \|E^\varepsilon\|_\infty\left\|\partial_t^2\partial_x F^\varepsilon\right\|_\infty + \left(\|\partial_t\partial_x G^\varepsilon\|_\infty + \|\partial_t\partial_x F^\varepsilon\|_\infty\right)\|\partial_t E^\varepsilon\|_\infty \\
& \left. + \left(\|\partial_x E^\varepsilon\|_\infty^2 + \|\partial_x G^\varepsilon\|_\infty + \|\partial_x F^\varepsilon\|_\infty\right)\left\|\partial_t^2 E^\varepsilon\right\|_\infty\right) \\
\lesssim & h^4 + \frac{\tau^2}{\varepsilon},
\end{aligned}
$$

for $j \in \mathcal{T}_J, 1 \leq n \leq T/\tau - 1$.

$$
\begin{aligned}
|\delta_t\xi_j^{\varepsilon,n}| \lesssim & h^4\left\|\partial_t\partial_x^6 F^\varepsilon\right\|_\infty + \tau^2\left(\varepsilon^2\left\|\partial_t^5 F^\varepsilon\right\|_\infty + \varepsilon^2\left\|\partial_t^5 E^\varepsilon\right\|_\infty + \left\|\partial_t^3\partial_x^2 F^\varepsilon\right\|_\infty\right) \\
\lesssim & \varepsilon h^4 + \frac{\tau^2}{\varepsilon},
\end{aligned}
$$

for $j \in \mathcal{T}_J, 2 \leq n \leq T/\tau - 2$. □

Lemma 4.3. *Under assumptions (4.A) and (4.B), we have the following estimates for the first step errors:*

$$
\begin{aligned}
e^{\varepsilon,0} = 0,\ \left|e^{\varepsilon,1}\right| + \left|\delta_x^+ e^{\varepsilon,1}\right| \lesssim \frac{\tau^2}{\varepsilon},\ \left|e^{\varepsilon,1}\right| \lesssim \frac{\tau^3}{\varepsilon^2},\ \left|\delta_t^+ e^{\varepsilon,0}\right| \lesssim \frac{\tau^2}{\varepsilon^2}, \\
f^{\varepsilon,0} = 0,\ \left|f^{\varepsilon,1}\right| \lesssim \frac{\tau^3}{\varepsilon},\ \left|\delta_t^+ f^{\varepsilon,0}\right| \lesssim \frac{\tau^2}{\varepsilon}.
\end{aligned}
\tag{4.3.18}
$$

The first row estimation in (4.3.18) is from a direct Taylor expansion of $E^\varepsilon(x,t)$ at $(x_j, 0)$ for (4.2.7); the second row is from the fact $\hat{f}^{\varepsilon,0} = 0$ and the Taylor expansion of $F^\varepsilon(x,t)$ at $(x_j, 0)$.

4.3.2 An error bound via the energy method

In order to give the error bound without prior assumptions on the boundedness of our numerical solutions, we adopt the cut-off technique to the nonlinear terms in ZS (4.1.9) as [5, 16] did. We apply the cut-off function onto E^ε for the nonlinear terms $|E^\varepsilon|^2$ and $F^\varepsilon E^\varepsilon$ in (4.1.9) as in [16] and [32]. Choose a sooth function $\rho(s) \in C^\infty([0, +\infty))$ such that

$$\rho(s) = \begin{cases} 1, & 0 \le s \le 1, \\ \in (0,1), & 1 < s < 2, \\ 0, & s \ge 2. \end{cases} \tag{4.3.19}$$

Let M_0 be a uniform upper bound of $E(x,t)$ and $E^\varepsilon(x,t)$ for ε on $\Omega_T = \Omega \times (0, T)$. For example, choose

$$M_0 = \max\{\|E(x,t)\|_{L^\infty(\Omega_T)}, \sup_{\varepsilon\in(0,1]} \left\|\tilde{E}^\varepsilon(x,t)\right\|_{L^\infty(\Omega_T)}\}, \tag{4.3.20}$$

Define the cut-off function for norms

$$\rho_B(s) = s\rho(s/B), \quad s \ge 0, \tag{4.3.21}$$

where $B = (1 + M_0)^2$. Let

$$g(u, v) = \int_0^1 \rho_B'(\theta|u|^2 + (1-\theta)|v|^2)\mathrm{d}\theta = \frac{\rho_B(|u|^2) - \rho_B(|v|^2)}{|u|^2 - |v|^2}. \tag{4.3.22}$$

Let $\hat{E}^{\varepsilon,0} = E^{\varepsilon,0}$, $\hat{F}^{\varepsilon,0} = F^{\varepsilon,0}$, $\hat{E}^{\varepsilon,1} = E^{\varepsilon,1}$ and $\hat{F}^{\varepsilon,1} = F^{\varepsilon,1}$. Choose $(\hat{E}^{\varepsilon,n}, \hat{F}^{\varepsilon,n})$ to be the solution of a variation of the UA-4cFD (4.2.3) and (4.2.4) with cut-off nonlinearity:

$$i\delta_t \hat{E}_j^{\varepsilon,n} = \left[-\mathcal{A}_h^{-1}\delta_x^2 + G_j^{\varepsilon,n} + \left(-\rho_B\left(|\hat{E}_j^{\varepsilon,n}|^2\right) + [\![\hat{F}^\varepsilon]\!]_j^n\right) g(\hat{E}_j^{\varepsilon,n-1}, \hat{E}_j^{\varepsilon,n+1})\right] [\![\hat{E}_j^{\varepsilon,n}]\!], \tag{4.3.23}$$

$$\varepsilon^2\delta_t^2 \hat{F}_j^{\varepsilon,n} = \mathcal{A}_h^{-1}\delta_x^2[\![\hat{F}^\varepsilon]\!]_j^n + \varepsilon^2\delta_t^2\rho_B\left(|\hat{E}_j^{\varepsilon,n}|^2\right), \tag{4.3.24}$$

for $j \in \mathcal{T}_J, n \ge 1$. Notice that $(\hat{E}^{\varepsilon,n}, \hat{F}^{\varepsilon,n})$ is another approximation of $(E^\varepsilon(x_j, t_n)$, $F^\varepsilon(x_j, t_n))$ and it is equal to $(E^{\varepsilon,n}, F^{\varepsilon,n})$ if the function $g(\hat{E}_j^{\varepsilon,n-1}, \hat{E}_j^{\varepsilon,n+1}) = 1$ in

(4.3.23) and $\rho_B\left(|\hat{E}_j^{\varepsilon,n}|^2\right)=|\hat{E}_j^{\varepsilon,n}|^2$ in (4.3.24) for all j,n. Since $\rho'(s)$ is bounded, we know ρ_B and g are Lipschitz functions. Therefore the system composed by (4.3.23) and (4.3.24) is uniquely solvable for small time step τ. In the following context, we will prove (3.3.3) type error estimates for $(\hat{E}^{\varepsilon,n},\hat{F}^{\varepsilon,n})$ at first. Define the error functions $\hat{e}^{\varepsilon,n},\hat{f}^{\varepsilon,n}\in X_J$ for $n\geq 0$ as

$$\hat{e}_j^{\varepsilon,n}=E^\varepsilon(x_j,t_n)-\hat{E}_j^{\varepsilon,n},\ \hat{f}_j^{\varepsilon,n}=F^\varepsilon(x_j,t_n)-\hat{F}_j^{\varepsilon,n},\ j\in\mathcal{T}_J^0, \tag{4.3.25}$$

then we have the following error estimate.

Theorem 4.2. (Error estimates from the standard energy method) *Assume $\tau\lesssim h$ and under the assumption (4.A), there exist $\tau_1,h_1>0$ sufficiently small and independent of ε such that for any $\varepsilon\in(0,1]$, we have the following error estimate of the UA-4cFD for any $\tau\in(0,\tau_1],h\in(0,h_1]$:*

$$\|\hat{e}^{\varepsilon,n}\|_{\ell^2}+|\hat{e}^{\varepsilon,n}|_1+\left\|\hat{f}^{\varepsilon,n}\right\|_{\ell^2}\lesssim h^4+\frac{\tau^2}{\varepsilon},\quad 0\leq n\leq\frac{T}{\tau}. \tag{4.3.26}$$

Subtracting (4.3.23) from (4.3.8) and (4.3.24) from (4.3.9), we get the following error equations:

$$i\delta_t\hat{e}_j^{\varepsilon,n}=\left(-\mathcal{A}_h^{-1}\delta_x^2+G_j^{\varepsilon,n}\right)[\![\hat{e}^\varepsilon]\!]_j^n+\hat{R}_j^n+\hat{\eta}_j^{\varepsilon,n}, \tag{4.3.27}$$

$$\varepsilon^2\delta_t^2\hat{f}_j^{\varepsilon,n}=\mathcal{A}_h^{-1}\delta_x^2[\![\hat{f}^\varepsilon]\!]_j^n+\varepsilon^2\delta_t^2\hat{P}_j^n+\hat{\xi}_j^{\varepsilon,n}, \tag{4.3.28}$$

for $j\in\mathcal{T}_J,n\geq 1$, with

$$\begin{aligned}\hat{R}_j^n=&\left((\![F^\varepsilon]\!)(x_j,t_n)-|E^\varepsilon(x_j,t_n)|^2\right)(\![E^\varepsilon]\!)(x_j,t_n)\\&+\left(\rho_B(|\hat{E}_j^{\varepsilon,n}|^2)-[\![\hat{F}^\varepsilon]\!]_j^n\right)g\left(\hat{E}_j^{\varepsilon,n+1},\hat{E}_j^{\varepsilon,n-1}\right),\end{aligned} \tag{4.3.29}$$

$$\hat{P}_j^n=\rho_B(|E^\varepsilon(x_j,t_n)|^2)-\rho_B(|\hat{E}_j^{\varepsilon,n}|^2). \tag{4.3.30}$$

In order to bound $\hat{R}_j^n$ by $|\hat{e}_j^{\varepsilon,n}|$ and $|\hat{f}_j^{\varepsilon,n}|$'s, we rewrite $\hat{R}_j^n$ as summation differences:

$$\hat{R}_j^n=q_1^n+q_2^n, \tag{4.3.31}$$

with $q_1^n,q_2^n\in X_J$ defined by

$$\begin{aligned}q_{1,j}^n&=\left((\![F^\varepsilon]\!)(x_j,t_n)-|E^\varepsilon(x_j,t_n)|^2\right)\left((\![E^\varepsilon]\!)(x_j,t_n)-g\left(\hat{E}_j^{\varepsilon,n+1},\hat{E}_j^{\varepsilon,n-1}\right)\right),\\q_{2,j}^n&=-\left(\hat{P}_j^n-[\![\hat{F}^\varepsilon]\!]_j^n\right)g\left(\hat{E}_j^{\varepsilon,n+1},\hat{E}_j^{\varepsilon,n-1}\right),\quad j\in\mathcal{T}_J.\end{aligned}$$

From the construction of ρ and g, we know $\|\rho_B'\|_\infty, \|\rho_B''\|_\infty$ are bounded. Therefore we have

$$|\rho_B(|E^\varepsilon(x_j,t_n)|^2)-\rho_B(|E_j^{\varepsilon,n}|^2)| \le \sqrt{C_B}|\hat{e}_j^n|, \tag{4.3.32}$$

$$|g(E^\varepsilon(x_j,t_{n+1}),E^\varepsilon(x_j,t_{n-1}))-g(\hat{E}_j^{\varepsilon,n+1},\hat{E}_j^{\varepsilon,n-1})| \lesssim |\hat{e}_j^{n+1}|+|\hat{e}_j^{n-1}|, \tag{4.3.33}$$

$$|g_e(E^\varepsilon(x_j,t_{n+1}),E^\varepsilon(x_j,t_{n-1}))-g_e(\hat{E}_j^{\varepsilon,n+1},\hat{E}_j^{\varepsilon,n-1})| \le |\hat{e}_j^{n+1}|+|\hat{e}_j^{n-1}|, \tag{4.3.34}$$

$$\begin{aligned}&|\delta_x^+(g_e(E^\varepsilon(x_j,t_{n+1}),E^\varepsilon(x_j,t_{n-1}))-g_e(\hat{E}_j^{\varepsilon,n+1},\hat{E}_j^{\varepsilon,n-1}))|\\ &\qquad\lesssim \sum_{m=n\pm1}(|\hat{e}_j^m|+|\hat{e}_{j+1}^m|+|\delta_x^+\hat{e}_j^m|),\end{aligned} \tag{4.3.35}$$

where $g_e(u,v)=g(u,v)(u+v)$, and C_B is a number depending on B and $\rho(\cdot)$. Then, combining (4.3.31), (4.3.33) and (4.3.34) and using Cauchy inequality, we have

$$\left|\hat{R}_j^n\right| \lesssim \left|\hat{e}_j^{\varepsilon,n+1}\right|+\left|\hat{e}_j^{\varepsilon,n}\right|+\left|\hat{e}_j^{\varepsilon,n-1}\right|+\left|\hat{f}_j^{\varepsilon,n+1}\right|+\left|\hat{f}_j^{\varepsilon,n-1}\right|. \tag{4.3.36}$$

In order to bound the $\|\hat{e}_j^{\varepsilon,n}\|_{\ell^2}$ term, multiplying $2h\tau(\bar{\hat{e}}_j^{\varepsilon,n+1}+\bar{\hat{e}}_j^{\varepsilon,n-1})$ on both side of (4.3.27), summing up for all j, and taking the imaginary part, we have:

$$\|\hat{e}^{\varepsilon,n+1}\|_{\ell^2}-\|\hat{e}^{\varepsilon,n-1}\|_{\ell^2}=4\tau\,\mathrm{Im}\langle\hat{R}^n+\hat{\eta}^{\varepsilon,n},[\![\hat{e}^\varepsilon]\!]^n\rangle; \tag{4.3.37}$$

In order to bound the $|\hat{e}_j^{\varepsilon,n}|_1$ term, which is equivalent to $|\hat{e}_j^{\varepsilon,n}|_{1,*}$ as argued in (2.2.16), multiplying $2h(\bar{\hat{e}}_j^{\varepsilon,n+1}-\bar{\hat{e}}_j^{\varepsilon,n-1})$ on both side of (4.3.27), summing up for all j, and taking the real part, we have:

$$|\hat{e}^{\varepsilon,n+1}|_{1,*}-|\hat{e}^{\varepsilon,n-1}|_{1,*}=-2\,\mathrm{Re}\langle G^{\varepsilon,n}[\![\hat{e}^\varepsilon]\!]^n+\hat{R}^n+\hat{\eta}^{\varepsilon,n},\hat{e}^{\varepsilon,n+1}-\hat{e}^{\varepsilon,n-1}\rangle; \tag{4.3.38}$$

In order to bound the $\|\hat{\nu}_j^{\varepsilon,n}\|_{\ell^2}$ term, multiplying $h\tau(\hat{u}_j^{\varepsilon,n+\frac12}+\hat{u}_j^{\varepsilon,n-\frac12})$ on both side of (4.3.27) and summing up for all j, we have:

$$\begin{aligned}&\varepsilon^2\left(|\hat{u}^{\varepsilon,n+\frac12}|_{1,*}-|\hat{u}^{\varepsilon,n-\frac12}|_{1,*}\right)+\frac12\left(\|\hat{f}^{\varepsilon,n+1}\|_{\ell^2}-\|\hat{f}^{\varepsilon,n-1}\|_{\ell^2}\right)\\ &\quad=\langle[\![\hat{f}^\varepsilon]\!],2\tau\delta_t\hat{P}^n\rangle+\tau\langle\hat{\xi}^{\varepsilon,n},\hat{u}^{\varepsilon,n+\frac12}+\hat{u}^{\varepsilon,n-\frac12}\rangle.\end{aligned} \tag{4.3.39}$$

Here, $\hat{u}_j^{\varepsilon,n+\frac12}$ is the solution of

$$-\mathcal{A}_h^{-1}\delta_x^2\hat{u}_j^{\varepsilon,n+\frac12}=\delta_t^+(\hat{f}_j^{\varepsilon,n}-\hat{P}_j^n). \tag{4.3.40}$$

For energy $\hat{S}^n$ defined by

$$\begin{aligned}\hat{S}^n =& C_B\left(\|\hat{e}^{\varepsilon,n}\|_{\ell^2}^2 + \left\|\hat{e}^{\varepsilon,n+1}\right\|_{\ell^2}^2\right) + |\hat{e}^{\varepsilon,n}|_{1,*}^2 + |\hat{e}^{\varepsilon,n+1}|_{1,*}^2 \\ &+ \varepsilon^2|\hat{u}^{\varepsilon,n+\frac{1}{2}}|_{1,*}^2 + \frac{1}{2}\|\hat{f}^{\varepsilon,n+1}\|_{\ell^2}^2 + \frac{1}{2}\|\hat{f}^{\varepsilon,n}\|_{\ell^2}^2,\end{aligned} \tag{4.3.41}$$

C_B(4.3.37) + 4(4.3.38) + (4.3.39) indicates

$$\begin{aligned}\hat{S}^n - \hat{S}^{n-1} =& 4\tau\,\mathrm{Im}\langle \hat{R}^n + \hat{\eta}^{\varepsilon,n}, [\![\hat{e}^\varepsilon]\!]^n\rangle - 2\,\mathrm{Re}\langle G^{\varepsilon,n}[\![\hat{e}^\varepsilon]\!]^n + \hat{R}^n + \hat{\eta}^{\varepsilon,n}, \hat{e}^{\varepsilon,n+1} - \hat{e}^{\varepsilon,n-1}\rangle \\ &+ \langle [\![\hat{f}^\varepsilon]\!], 2\tau\delta_t\hat{P}^n\rangle + \tau\langle \hat{\xi}^{\varepsilon,n}, \hat{u}^{\varepsilon,n+\frac{1}{2}} + \hat{u}_j^{\varepsilon,n-\frac{1}{2}}\rangle.\end{aligned} \tag{4.3.42}$$

Note that the C_B coefficient in $\hat{S}^n$ is designed to make sure

$$\hat{S}^n \geq \frac{C_B}{2}\left(\|\hat{e}^{\varepsilon,n}\|_{\ell^2}^2 + \left\|\hat{e}^{\varepsilon,n+1}\right\|_{\ell^2}^2\right) \geq \langle \hat{P}^n, \hat{P}^{n+1}\rangle.$$

We have the following lemma to bound each term on the RHS of (4.3.42).

Lemma 4.4. *Under assumption (4.A), we have the following estimates*

$$\left|\mathrm{Im}\langle \hat{R}^n, [\![\hat{e}^\varepsilon]\!]^n\rangle\right| \lesssim S^n + S^{n-1}, \tag{4.3.43}$$

$$|\mathrm{Im}\langle \hat{\eta}^{\varepsilon,n}, [\![\hat{e}^\varepsilon]\!]^n\rangle| \lesssim \|\hat{\eta}^{\varepsilon,n}\|_{\ell^2}^2 + S^n + S^{n-1}, \tag{4.3.44}$$

$$4\,\mathrm{Re}\langle G^{\varepsilon,n}[\![\hat{e}^\varepsilon]\!]^n + \hat{R}^n + \hat{\eta}^{\varepsilon,n}, \tau\delta_t\hat{e}^{\varepsilon,n}\rangle \lesssim |\hat{\eta}^{\varepsilon,n}|_{1,*}^2 + \|\hat{\eta}^{\varepsilon,n}\|_{\ell^2}^2 + S^n + S^{n-1}, \tag{4.3.45}$$

$$\mathrm{Re}\langle \hat{R}^n, 4\tau\delta_t\hat{e}^{\varepsilon,n}\rangle \lesssim \tau(\|\hat{\eta}^{\varepsilon,n}\|_{\ell^2}^2 + S^n + S^{n-1}), \tag{4.3.46}$$

$$\left|\mathrm{Re}\langle \hat{R}^n, 4\tau\delta_t\hat{e}^{\varepsilon,n}\rangle - \langle [\![\hat{f}^\varepsilon]\!], 2\tau\delta_t\hat{P}^n\rangle\right| \lesssim \tau(\|\hat{\eta}^{\varepsilon,n}\|_{\ell^2}^2 + S^n + S^{n-1}), \tag{4.3.47}$$

and

$$\begin{aligned}&\left|-\frac{\hat{S}^n}{4} + \tau\sum_{m=1}^{n}\langle \hat{\xi}^{\varepsilon,m}, \hat{u}^{\varepsilon,m+\frac{1}{2}} + \hat{u}^{\varepsilon,m-\frac{1}{2}}\rangle\right| \lesssim \hat{S}^0 + \tau\sum_{m=2}^{n-1}\left(\left\|\delta_t\hat{\xi}^{\varepsilon,m}\right\|_{\ell^2}^2 + \hat{S}^m\right) \\ &+ \sum_{m=1}^{2}\left(\left\|\hat{\xi}^{\varepsilon,m}\right\|_{\ell^2}^2 + \left\|\hat{\xi}^{\varepsilon,n+1-m}\right\|_{\ell^2}^2\right),\end{aligned} \tag{4.3.48}$$

The proof is mainly based on Cauchy inequality as in Lemma 3.4. (4.3.48) used the technique of summation by part. Summing up (4.3.42) for time steps from 1 to $n < \frac{T}{\tau}$ and applying the estimations in Lemma 4.4, we obtain

$$\begin{aligned}\hat{S}^n \lesssim & \hat{S}^0 + \tau \sum_{m=1}^{n-1} \hat{S}^m + \sum_{m=0}^{2} \left(\left\| \hat{\xi}^{\varepsilon,m} \right\|_{\ell^2}^2 + \left\| \hat{\xi}^{\varepsilon,n+1-m} \right\|_{\ell^2}^2 \right) \\ & + \tau \sum_{m=1}^{n} \left(\|\hat{\eta}^{\varepsilon,n}\|_{\ell^2}^2 + |\hat{\eta}^{\varepsilon,n}|_{1,*}^2 \right) + \tau \sum_{m=2}^{n-1} \left\| \delta_t \hat{\xi}^{\varepsilon,n} \right\|_{\ell^2}^2 \\ \lesssim & \left(h^4 + \frac{\tau^2}{\varepsilon} \right)^2 + \tau \sum_{m=1}^{n} \hat{S}^m,\end{aligned} \tag{4.3.49}$$

The last inequality above depends on

$$\begin{aligned}\hat{S}^0 = & |\hat{e}^{\varepsilon,0}|_{1,*}^2 + \varepsilon^2 |\hat{u}^{\varepsilon,\frac{1}{2}}|_{1,*}^2 + \frac{1}{2} \|\hat{f}^{\varepsilon,1}\|_{\ell^2}^2 \\ \lesssim & \left(h^4 + \frac{\tau^2}{\varepsilon} \right)^2.\end{aligned} \tag{4.3.50}$$

From the discrete Gronwall's inequality, there exists $\tau_1 > 0$ such that for $0 < \tau \leq \tau_1$, we have

$$\hat{S}^n \lesssim \left(h^4 + \frac{\tau^2}{\varepsilon} \right)^2. \tag{4.3.51}$$

Combine (2.2.16) and (4.3.51) , we get

$$\|\hat{e}^{\varepsilon,n}\|_{\ell^2} + \left\|\delta_x^+ \hat{e}^{\varepsilon,n}\right\|_{\ell^2} + \left\| \hat{f}^{\varepsilon,n} \right\|_{\ell^2} \lesssim \|\hat{e}^{\varepsilon,n}\|_{\ell^2} + |\hat{e}^{\varepsilon,n}|_{1,*} + \left\| \hat{f}^{\varepsilon,n} \right\|_{\ell^2} \lesssim h^4 + \frac{\tau^2}{\varepsilon}. \tag{4.3.52}$$

4.3.3 Another error bound via the limiting equation

We will show (4.3.5) type error estimate for $(\hat{E}^{\varepsilon,n}, \hat{F}^{\varepsilon,n})$ in this subsection. Define the biased error function as

$$\tilde{e}_j^{\varepsilon,n} = E(x_j, t_n) - \hat{E}_j^{\varepsilon,n},\ \tilde{f}_j^{\varepsilon,n} = 0 - \hat{F}_j^{\varepsilon,n}, \quad j \in \mathcal{T}_J^0, n \geq 1, \tag{4.3.53}$$

Theorem 4.3. (Error bound from limiting equation) *Assume $\tau \lesssim h$ and under the assumption (4.A), there exist $\tau_2, h_2 > 0$ sufficiently small and independent of ε such that for any $\varepsilon \in (0, 1]$, we have the following error estimate of the UA-4cFD for any $\tau \in (0, \tau_2], h \in (0, h_2]$:*

$$\|\tilde{e}^{\varepsilon,n}\|_{\ell^2} + \left|\delta_x^+ \tilde{e}^{\varepsilon,n}\right|_1 + \left\| \tilde{f}^{\varepsilon,n} \right\|_{\ell^2} \lesssim h^4 + \tau^2 + \tau\varepsilon^{\alpha^*} + \varepsilon^{1+\alpha^*}, \quad 0 \leq n \leq \frac{T}{\tau}. \tag{4.3.54}$$

Define the discrete potential $\tilde{u}^{\varepsilon,n-\frac{1}{2}} \in X_J$ satisfying $\tilde{u}^{\varepsilon,n-\frac{1}{2}} = -(\delta_x^2)^{-1}\mathcal{A}_h\delta_t^-(\tilde{f}_j^{\varepsilon,n} - p_j^n)$ and define local truncation errors $\tilde{\eta}^{\varepsilon,n}, \tilde{\xi}^{\varepsilon,n} \in X_J$:

$$
\begin{aligned}
\tilde{\eta}_j^{\varepsilon,n} =& i\delta_t^c \tilde{E}^\varepsilon(x_j,t_n) + \left(\mathcal{A}_h^{-1}\delta_x^2 - G_j^{\varepsilon,n}\right)[\![\tilde{E}^\varepsilon]\!](x_j,t_n) \\
&+ \rho_B\left(\left|\tilde{E}^\varepsilon(x_j,t_n)\right|^2\right) g\left(\tilde{E}^\varepsilon(x_j,t_{n+1}), \tilde{E}^\varepsilon(x_j,t_{n-1})\right) \\
=& i\delta_t^c \tilde{E}^\varepsilon(x_j,t_n) + \left(\mathcal{A}_h^{-1}\delta_x^2 + \left|\tilde{E}^\varepsilon(x_j,t_n)\right|^2 - G_j^{\varepsilon,n}\right)[\![\tilde{E}^\varepsilon]\!](x_j,t_n) \qquad (4.3.55) \\
\tilde{\xi}_j^{\varepsilon,n} =& -\varepsilon^2\delta_t^2\rho_B\left(\left|\tilde{E}^\varepsilon(x_j,t_n)\right|^2\right) = -\varepsilon^2\delta_t^2\left(\left|\tilde{E}^\varepsilon(x_j,t_n)\right|^2\right), \quad j \in \mathcal{T}_J \qquad (4.3.56)
\end{aligned}
$$

As proved in Lemma 4.2 and 4.3, under assumption (A) and (B), we have the following local truncation errors

$$
\|\tilde{\eta}^{\varepsilon,n}\|_{\ell^2} + |\tilde{\eta}^{\varepsilon,n}|_1 \lesssim h^4 + \tau^2 + \tau\varepsilon^*, \ \left\|\tilde{\xi}^{\varepsilon,n}\right\|_{\ell^2} \lesssim \varepsilon^2, \ \left\|\delta_t\tilde{\xi}^{\varepsilon,n}\right\|_{\ell^2} \lesssim \varepsilon^{1+\alpha^*}, \qquad (4.3.57)
$$

and

$$
\left\|\tilde{f}^{\varepsilon,1}\right\|_{\ell^2} \lesssim \tau^2, \ \left\|\tilde{u}^{\varepsilon,\frac{1}{2}}\right\|_{\ell^2} \lesssim \left\|\delta_t^-\tilde{f}^{\varepsilon,1}\right\|_{\ell^2} \lesssim h^4 + \tau + \varepsilon^{\alpha-1} + \varepsilon^{\beta-1}. \qquad (4.3.58)
$$

The differences between (4.3.55),(4.3.56) and (4.3.23),(4.3.24) yield the error functions

$$
\begin{aligned}
i\delta_t^-\tilde{e}_j^{\varepsilon,n} &= (-\mathcal{A}_h^{-1}\delta_x^2 + G_j^{\varepsilon,n})[\![\tilde{e}^\varepsilon]\!]_j^n + \tilde{R}_j^n + \tilde{\eta}_j, \qquad (4.3.59) \\
\varepsilon^2\delta_t^2\tilde{f}_j^{\varepsilon,n} &= \mathcal{A}_h^{-1}\delta_x^2[\![\tilde{f}^\varepsilon]\!]_j^n + \varepsilon^2\delta_t^2\tilde{P}_j^n + \tilde{\xi}_j, \qquad (4.3.60)
\end{aligned}
$$

for $j \in \mathcal{T}_J, n \geq 1$, with $\tilde{R}_j^n$ and $\tilde{P}_j^n$ defined similar as $\hat{R}_j^n$ and $\hat{P}_j^n$ in Section 3.3.2:

$$
\begin{aligned}
\tilde{R}_j^n =& -\left|\tilde{E}^\varepsilon(x_j,t_n)\right|^2[\![\tilde{E}^\varepsilon]\!](x_j,t_n) \\
&+ \left(\rho_B(|\hat{E}_j^{\varepsilon,n}|^2) - [\![\hat{F}^\varepsilon]\!]_j^n\right) g\left(\hat{E}_j^{\varepsilon,n+1}, \hat{E}_j^{\varepsilon,n-1}\right), \qquad (4.3.61) \\
\tilde{P}_j^n =& |\tilde{E}^\varepsilon(x_j,t_n)|^2 - \rho_B(|\hat{E}_j^{\varepsilon,n}|^2). \qquad (4.3.62)
\end{aligned}
$$

Define a discrete energy function

$$
\begin{aligned}
\tilde{S}^n =& C_B\left(\|\tilde{e}^{\varepsilon,n}\|_{\ell^2}^2 + \left\|\tilde{e}^{\varepsilon,n+1}\right\|_{\ell^2}^2\right) + |\tilde{e}^{\varepsilon,n}|_{1,*}^2 + |\tilde{e}^{\varepsilon,n+1}|_{1,*}^2 \\
&+ \varepsilon^2|\tilde{u}^{\varepsilon,n+\frac{1}{2}}|_{1,*}^2 + \frac{1}{2}\|\tilde{f}^{\varepsilon,n+1}\|_{\ell^2}^2 + \frac{1}{2}\|\tilde{f}^{\varepsilon,n}\|_{\ell^2}^2, \qquad (4.3.63)
\end{aligned}
$$

Similar to the procedure in Section 3.3.2, with the discrete Gronwall's inequality, we have

$$\left(\|\tilde{e}^{\varepsilon,n}\|_{\ell^2} + |\tilde{e}^{\varepsilon,n}|_{1,*} + \left\|\tilde{f}^{\varepsilon,n}\right\|_{\ell^2}\right)^2 \lesssim \tilde{S}^n \lesssim (h^4 + \tau^2 + \tau\varepsilon^{\alpha^*} + \varepsilon^{1+\alpha^*})^2. \tag{4.3.64}$$

Combining (4.3.64) with assumption (4.B) and (4.3.2), we have

$$\begin{aligned} &\|\hat{e}^{\varepsilon,n}\|_{\ell^2} + |\hat{e}^{\varepsilon,n}|_{1,*} + \left\|\hat{f}^{\varepsilon,n}\right\|_{\ell^2} \\ \leq &\|\tilde{e}^{\varepsilon,n}\|_{\ell^2} + |\tilde{e}^{\varepsilon,n}|_{1,*} + \left\|\hat{E}(\cdot,t_n) - E^{\varepsilon}(\cdot,t_n)\right\|_{H^1} + \|F^{\varepsilon}(\cdot,t_n)\|_{L^2} \\ \lesssim &h^4 + \tau^2 + \varepsilon^{\alpha^*}(\tau+\varepsilon). \end{aligned} \tag{4.3.65}$$

4.3.4 Proof of the main results

Based on the above analysis, we now give the proof of (4.3.6) and (4.3.7) in Theorem 4.1. For any $u \in X_J$, from the discrete Sobolev inequality, there exist a constant C_Ω depending on the domain Ω such that

$$\|u\|_\infty \leq C_\Omega |u|_1. \tag{4.3.66}$$

Under assumption (4.A) and (4.B) and from (4.3.52), we have

$$\left\|\hat{E}^{\varepsilon,n}\right\|_\infty \leq \|E^{\varepsilon}(x,t)\|_\infty + \|\hat{e}^{\varepsilon,n}\|_\infty \leq M_0 + 1, \tag{4.3.67}$$

for small enough h and τ. Then we have $\hat{E}^{\varepsilon,n} = E^{\varepsilon,n}$ and $\hat{F}^{\varepsilon,n} = F^{\varepsilon,n}$, since the equations for $\hat{E}^{\varepsilon,n}$ and $\hat{F}^{\varepsilon,n}$ collapse to (4.2.3) and (4.2.4). Thus, we have the boundedness of the original numerical solutions $(E^{\varepsilon,n}, F^{\varepsilon,n})$. Applying the whole estimating procedure of Section 3.3.2 to $e^{\varepsilon,n}$ and $f^{\varepsilon,n}$, we have the error bounds (4.3.6) and (4.3.7).

Applying the procedure in Section 4.3.2 to $e^{\varepsilon,n}$ and $f^{\varepsilon,n}$ as above, we have the error bound (4.3.5) in Theorem 4.1 as (4.3.65) with an extra assumption (B). Taking the minimum of (4.3.4) and (4.3.5), we have

$$\|e^{\varepsilon,n}\|_{\ell^2} + \left|\delta_x^+ e^{\varepsilon,n}\right|_1 + \|f^{\varepsilon,n}\|_{\ell^2} \lesssim h^4 + \min\{\tau^2 + \varepsilon^{\alpha^*}(\tau+\varepsilon), \frac{\tau^2}{\varepsilon}\}, \tag{4.3.68}$$

for $0 \leq n \leq \frac{T}{\tau}$. Take a common upper bound of RHS independent of ε gives (4.3.7). When $\alpha, \beta \geq 1$, α^* is 1 and we get (4.3.6).

4.4 Numerical results

In this section, we present numerical results of the UA-4cFD (4.2.3, 4.2.4) for ZS (4.1.9). The initial data is chosen as [32]:

$$E_0(x) = \mathrm{e}^{-x^2/2}, w_0(x) = \mathrm{e}^{-x^2/4}, w_1(x) = \sin(x)\mathrm{e}^{-x^2/3}. \tag{4.4.1}$$

The parameter α and β are taken several typical cases:

Case I. A well-prepared initial data, $\alpha = 2$ and $\beta = 2$;

Case II. A less-ill-prepared initial data, $\alpha = 1$ and $\beta = 1$;

Case III. An ill-prepared initial data, $\alpha = 0$ and $\beta = 0$;

During our numerical simulation, the computational domain is fixed to $\Omega = (200, 200)$, such that the error due to the truncation with homogeneous Dirichlet boundary condition is negligible. The 'exact solution' is computed by a finer mesh or by the time splitting spectral method introduced in [18] with a fine enough mesh $h = 1/32, \tau = 10^{-7}$.

In order to quantify the convergence, we use following standard error functions as in [32] for the discrete ℓ^2-error and H^1-error at $t_n = n\tau$:

$$e^{\varepsilon}_{L^2}(t_n) = \|e^{\varepsilon,n}\|_{\ell^2},\ e^{\varepsilon}_{H^1}(t_n) = \|e^{\varepsilon,n}\|_{\ell^2} + |e^{\varepsilon,n}|_1,\ \nu^{\varepsilon}_{L^2}(t_n) = \|\nu^{\varepsilon,n}\|_{\ell^2}. \tag{4.4.2}$$

Tables 4.1-4.3 show the spatial errors of the 3 cases all converge at 4-th order. As showed in each column of the three table, the error does not increasing when ε decreases, which means the spatial convergence rate is independent of the dimensionless parameter ε for all the initial data, which is exact as in Theorem 4.1. Table 4.4 to 4.6 have second order time convergence rate for τ much smaller than ε, which coincide with the error bound in (4.3.4). Although the convergence in time is disturbed in the resonance region of the temporal error tables, the error scale is unchanged when $\varepsilon \downarrow 0$ with τ fixed, especially for the cases where ε decreases near to $\varepsilon_0/2^9$. This shows that the temporal error of UA-4cFD is uniform for ε.

As in the analysis for (3.3.76), the resonance regions for ZS in subsonic regime is from the matching $\tau^2 + \varepsilon^{\alpha^*}(\tau + \varepsilon) \sim \frac{\tau^2}{\varepsilon}$ raised in (4.3.68). For the well-prepared and less-ill prepared initial data, the resonance region is $\tau = O(\varepsilon^{3/2})$ from $\varepsilon^3 \sim \tau^2$ for $\alpha^* = 1$. For the ill prepared initial data, the resonance region is $\tau = O(\varepsilon^{(2+\alpha^*)/2})$ from $\varepsilon^{2+\alpha^*} \sim \tau^2$. We show the convergence rate in the resonance direction in Table 4.7 - 4.9 for the Case I-III initial data. Corresponding convergence rates in these tables coincide well with the uniform temporal error bounds stated in Theorem 4.1. For the well-prepared and less-ill-prepared cases, the numerical convergence rates in Table 4.7 and 4.8 for resonance region are nearly equal to 4/3; for the ill-prepared case, the numerical convergence rates in Table 4.9 for resonance region are approximately equal to 1. The errors in Table 4.7 - 4.9 are from the bold case errors in Table 4.4-4.6.

Table 4.1: Spatial errors of UA-4cFD at $t = 1$ for the well-prepared initial data Case I with $\varepsilon_0 = 1, h_0 = 0.8$ at $t = 1$.

$e^{\varepsilon}_{H^1}(t=1)$	$h_0 = 0.8$	$h_0/2$	$h_0/2^2$	$h_0/2^3$	$h_0/2^4$	$h_0/2^5$
$\varepsilon = \varepsilon_0$	6.69E-2	9.18E-3	6.15E-4	3.84E-5	2.39E-6	1.40E-7
Order	-	2.87	3.90	4.00	4.01	4.09
$\varepsilon = \varepsilon_0/2$	5.49E-2	8.44E-3	5.61E-4	3.50E-5	2.18E-6	1.28E-7
Order	-	2.70	3.91	4.00	4.01	4.09
$\varepsilon = \varepsilon_0/2^2$	9.88E-2	7.85E-3	5.28E-4	3.29E-5	2.05E-6	1.20E-7
Order	-	3.65	3.90	4.00	4.01	4.09
$\varepsilon = \varepsilon_0/2^3$	1.01E-1	8.43E-3	5.42E-4	3.38E-5	2.10E-6	1.23E-7
Order	-	3.59	3.96	4.00	4.01	4.09
$\varepsilon = \varepsilon_0/2^7$	9.99E-2	8.65E-3	5.61E-4	3.50E-5	2.18E-6	1.28E-7
Order	-	3.53	3.95	4.00	4.01	4.09
$\varepsilon = \varepsilon_0/2^9$	9.99E-2	8.65E-3	5.61E-4	3.50E-5	2.18E-6	1.28E-7
Order	-	3.53	3.95	4.00	4.01	4.09

$\nu^{\varepsilon}_{L^2}(t=1)$	$h_0 = 0.8$	$h_0/2$	$h_0/2^2$	$h_0/2^3$	$h_0/2^4$	$h_0/2^5$
$\varepsilon = \varepsilon_0$	4.46E-2	1.67E-3	9.87E-5	6.09E-6	3.78E-7	2.38E-8
Order	-	4.74	4.08	4.02	4.01	3.99
$\varepsilon = \varepsilon_0/2$	4.37E-2	2.60E-3	1.51E-4	9.27E-6	5.75E-7	3.29E-8
Order	-	4.07	4.11	4.03	4.01	4.13
$\varepsilon = \varepsilon_0/2^2$	3.84E-2	2.73E-3	1.61E-4	9.81E-6	6.07E-7	3.64E-8
Order	-	3.81	4.09	4.03	4.01	4.06
$\varepsilon = \varepsilon_0/2^3$	1.85E-2	8.66E-4	5.98E-5	3.65E-6	2.25E-7	1.56E-8
Order	-	4.42	3.86	4.03	4.02	3.85
$\varepsilon = \varepsilon_0/2^7$	1.53E-2	3.85E-4	2.35E-5	1.46E-6	9.08E-8	5.75E-9
Order	-	5.31	4.03	4.01	4.01	3.98
$\varepsilon = \varepsilon_0/2^9$	1.53E-2	3.84E-4	2.34E-5	1.45E-6	9.04E-8	5.34E-9
Order	-	5.31	4.04	4.01	4.01	4.08

Table 4.2: Spatial errors of UA-4cFD at $t = 1$ for the less-ill-prepared initial data Case II with $\varepsilon_0 = 1, h_0 = 0.8$ at $t = 1$.

$e^{\varepsilon}_{H^1}(t=1)$	$h_0 = 0.8$	$h_0/2$	$h_0/2^2$	$h_0/2^3$	$h_0/2^4$	$h_0/2^5$
$\varepsilon = \varepsilon_0$	6.69E-2	9.18E-3	6.15E-4	3.84E-5	2.39E-6	1.40E-7
Order	-	2.87	3.90	4.00	4.01	4.09
$\varepsilon = \varepsilon_0/2$	5.56E-2	8.66E-3	5.78E-4	3.60E-5	2.24E-6	1.32E-7
Order	-	2.68	3.91	4.00	4.01	4.09
$\varepsilon = \varepsilon_0/2^2$	1.01E-1	8.02E-3	5.40E-4	3.37E-5	2.10E-6	1.23E-7
Order	-	3.65	3.89	4.00	4.01	4.09
$\varepsilon = \varepsilon_0/2^3$	1.03E-1	8.57E-3	5.51E-4	3.44E-5	2.14E-6	1.25E-7
Order	-	3.58	3.96	4.00	4.01	4.09
$\varepsilon = \varepsilon_0/2^7$	9.99E-2	8.65E-3	5.61E-4	3.50E-5	2.18E-6	1.28E-7
Order	-	3.53	3.95	4.00	4.01	4.09
$\varepsilon = \varepsilon_0/2^9$	9.99E-2	8.65E-3	5.61E-4	3.50E-5	2.18E-6	1.28E-7
Order	-	3.53	3.95	4.00	4.01	4.09

$\nu^{\varepsilon}_{L^2}(t=1)$	$h_0 = 0.8$	$h_0/2$	$h_0/2^2$	$h_0/2^3$	$h_0/2^4$	$h_0/2^5$
$\varepsilon = \varepsilon_0$	4.46E-2	1.67E-3	9.87E-5	6.09E-6	3.78E-7	2.38E-8
Order	-	4.74	4.08	4.02	4.01	3.99
$\varepsilon = \varepsilon_0/2$	4.60E-2	2.64E-3	1.53E-4	9.41E-6	5.84E-7	3.30E-8
Order	-	4.12	4.11	4.03	4.01	4.14
$\varepsilon = \varepsilon_0/2^2$	3.93E-2	2.73E-3	1.60E-4	9.80E-6	6.07E-7	3.59E-8
Order	-	3.85	4.09	4.03	4.01	4.08
$\varepsilon = \varepsilon_0/2^3$	1.90E-2	8.73E-4	6.01E-5	3.68E-6	2.26E-7	1.52E-8
Order	-	4.44	3.86	4.03	4.02	3.89
$\varepsilon = \varepsilon_0/2^7$	1.53E-2	3.85E-4	2.35E-5	1.46E-6	9.08E-8	5.75E-9
Order	-	5.31	4.03	4.01	4.01	3.98
$\varepsilon = \varepsilon_0/2^9$	1.53E-2	3.84E-4	2.34E-5	1.45E-6	9.04E-8	5.34E-9
Order	-	5.31	4.04	4.01	4.01	4.08

Table 4.3: Spatial errors of UA-4cFD at $t = 1$ for the ill-prepared initial data Case III with $\varepsilon_0 = 1, h_0 = 0.8$ at $t = 1$.

$e^{\varepsilon}_{H^1}(t=1)$	$h_0 = 0.8$	$h_0/2$	$h_0/2^2$	$h_0/2^3$	$h_0/2^4$	$h_0/2^5$
$\varepsilon = \varepsilon_0$	6.69E-2	9.18E-3	6.15E-4	3.84E-5	2.39E-6	1.40E-7
Order	-	2.87	3.90	4.00	4.01	4.09
$\varepsilon = \varepsilon_0/2$	7.45E-2	9.51E-3	6.35E-4	3.96E-5	2.47E-6	1.45E-7
Order	-	2.97	3.91	4.00	4.01	4.09
$\varepsilon = \varepsilon_0/2^2$	1.82E-1	1.10E-2	7.20E-4	4.49E-5	2.79E-6	1.66E-7
Order	-	4.05	3.93	4.00	4.01	4.07
$\varepsilon = \varepsilon_0/2^3$	3.13E-1	1.83E-2	1.14E-3	7.12E-5	4.43E-6	2.61E-7
Order	-	4.09	4.01	4.00	4.01	4.09
$\varepsilon = \varepsilon_0/2^7$	9.97E-2	8.56E-3	5.55E-4	3.46E-5	2.15E-6	1.27E-7
Order	-	3.54	3.95	4.00	4.01	4.09
$\varepsilon = \varepsilon_0/2^9$	9.99E-2	8.64E-3	5.61E-4	3.50E-5	2.18E-6	1.28E-7
Order	-	3.53	3.95	4.00	4.01	4.09

$\nu^{\varepsilon}_{L^2}(t=1)$	$h_0 = 0.8$	$h_0/2$	$h_0/2^2$	$h_0/2^3$	$h_0/2^4$	$h_0/2^5$
$\varepsilon = \varepsilon_0$	4.46E-2	1.67E-3	9.87E-5	6.09E-6	3.78E-7	2.38E-8
Order	-	4.74	4.08	4.02	4.01	3.99
$\varepsilon = \varepsilon_0/2$	5.33E-2	2.89E-3	1.67E-4	1.03E-5	6.37E-7	3.80E-8
Order	-	4.20	4.11	4.03	4.01	4.07
$\varepsilon = \varepsilon_0/2^2$	7.05E-2	3.21E-3	1.89E-4	1.16E-5	7.19E-7	4.45E-8
Order	-	4.46	4.08	4.03	4.01	4.01
$\varepsilon = \varepsilon_0/2^3$	6.99E-2	2.37E-3	1.43E-4	8.86E-6	5.50E-7	3.13E-8
Order	-	4.88	4.05	4.02	4.01	4.14
$\varepsilon = \varepsilon_0/2^7$	1.51E-2	3.94E-4	2.40E-5	1.49E-6	9.29E-8	5.84E-9
Order	-	5.27	4.04	4.01	4.01	3.99
$\varepsilon = \varepsilon_0/2^9$	1.52E-2	3.85E-4	2.34E-5	1.46E-6	9.05E-8	5.35E-9
Order	-	5.31	4.04	4.01	4.01	4.08

Table 4.4: Temporal errors of UA-4cFD at $t = 1$ for the well-prepared initial data Case I with $\varepsilon_0 = 1, \tau_0 = 0.05$ at $t = 1$.

$e^{\varepsilon}_{H^1}(t=1)$	$\tau_0 = 0.05$	$\tau_0/2$	$\tau_0/2^2$	$\tau_0/2^3$	$\tau_0/2^4$	$\tau_0/2^5$	$\tau_0/2^6$
$\varepsilon = \varepsilon_0$	4.45E-2	1.64E-2	4.82E-3	1.25E-3	3.14E-4	7.77E-5	1.85E-5
Order	-	1.44	1.77	1.95	1.99	2.01	2.07
$\varepsilon = \varepsilon_0/2$	3.47E-2	1.40E-2	4.14E-3	1.08E-3	2.70E-4	6.69E-5	1.59E-5
Order	-	1.30	1.76	1.95	1.99	2.01	2.07
$\varepsilon = \varepsilon_0/2^2$	2.96E-2	1.22E-2	3.70E-3	9.66E-4	2.43E-4	6.01E-5	1.43E-5
Order	-	1.28	1.72	1.94	1.99	2.01	2.07
$\varepsilon = \varepsilon_0/2^3$	3.63E-2	1.33E-2	3.71E-3	9.55E-4	2.40E-4	5.93E-5	1.41E-5
Order	-	1.45	1.84	1.96	1.99	2.01	2.07
$\varepsilon = \varepsilon_0/2^7$	3.63E-2	1.36E-2	3.87E-3	9.97E-4	2.50E-4	6.19E-5	1.47E-5
Order	-	1.42	1.81	1.96	1.99	2.01	2.07
$\varepsilon = \varepsilon_0/2^9$	3.63E-2	1.36E-2	3.87E-3	9.97E-4	2.50E-4	6.19E-5	1.47E-5
Order	-	1.42	1.81	1.96	1.99	2.01	2.07

$\nu^{\varepsilon}_{L^2}(t=1)$	$\tau_0 = 0.05$	$\tau_0/2$	$\tau_0/2^2$	$\tau_0/2^3$	$\tau_0/2^4$	$\tau_0/2^5$	$\tau_0/2^6$
$\varepsilon = \varepsilon_0$	2.67E-3	6.73E-4	1.70E-4	4.28E-5	1.07E-5	2.65E-6	6.33E-7
Order	-	1.99	1.98	1.99	2.00	2.01	2.07
$\varepsilon = \varepsilon_0/2$	**5.67E-3**	1.51E-3	3.85E-4	9.71E-5	2.43E-5	6.01E-6	1.43E-6
Order	-	1.91	1.97	1.99	2.00	2.01	2.07
$\varepsilon = \varepsilon_0/2^2$	1.23E-2	4.15E-3	1.13E-3	2.89E-4	7.25E-5	1.80E-5	4.28E-6
Order	-	1.56	1.88	1.97	1.99	2.01	2.07
$\varepsilon = \varepsilon_0/2^3$	5.72E-3	2.46E-3	1.19E-3	**3.55E-4**	9.15E-5	2.28E-5	5.44E-6
Order	-	1.21	1.05	1.74	1.96	2.01	2.07
$\varepsilon = \varepsilon_0/2^5$	1.61E-3	9.33E-4	7.05E-4	3.81E-4	1.40E-4	6.06E-5	**1.62E-5**
Order	-	7.87E-1	4.04E-1	8.89E-1	1.44	1.21	1.91
$\varepsilon = \varepsilon_0/2^7$	1.39E-3	3.45E-4	1.04E-4	6.68E-5	5.91E-5	4.60E-5	2.37E-5
Order	-	2.01	1.73	6.40E-1	1.77E-1	3.61E-1	9.57E-1
$\varepsilon = \varepsilon_0/2^9$	1.39E-3	3.28E-4	8.28E-5	2.08E-5	6.44E-6	4.31E-6	4.21E-6
Order	-	2.09	1.99	2.00	1.69	5.79E-1	3.49E-2

Table 4.5: Temporal errors of UA-4cFD at $t = 1$ for the less-ill-prepared initial data Case II with $\varepsilon_0 = 1, \tau_0 = 0.05$ at $t = 1$.

$e^{\varepsilon}_{H^1}(t=1)$	$\tau_0 = 0.05$	$\tau_0/2$	$\tau_0/2^2$	$\tau_0/2^3$	$\tau_0/2^4$	$\tau_0/2^5$	$\tau_0/2^6$
$\varepsilon = \varepsilon_0$	4.45E-2	1.64E-2	4.82E-3	1.25E-3	3.14E-4	7.77E-5	1.85E-5
Order	-	1.44	1.77	1.95	1.99	2.01	2.07
$\varepsilon = \varepsilon_0/2$	3.63E-2	1.45E-2	4.31E-3	1.12E-3	2.81E-4	6.96E-5	1.66E-5
Order	-	1.32	1.75	1.95	1.99	2.01	2.07
$\varepsilon = \varepsilon_0/2^2$	3.07E-2	1.25E-2	3.80E-3	9.94E-4	2.50E-4	6.19E-5	1.47E-5
Order	-	1.30	1.72	1.94	1.99	2.01	2.07
$\varepsilon = \varepsilon_0/2^3$	3.72E-2	1.36E-2	3.80E-3	9.78E-4	2.45E-4	6.07E-5	1.45E-5
Order	-	1.46	1.83	1.96	1.99	2.01	2.07
$\varepsilon = \varepsilon_0/2^7$	3.63E-2	1.36E-2	3.87E-3	9.97E-4	2.50E-4	6.19E-5	1.47E-5
Order	-	1.42	1.81	1.96	1.99	2.01	2.07
$\varepsilon = \varepsilon_0/2^9$	3.63E-2	1.36E-2	3.87E-3	9.97E-4	2.50E-4	6.19E-5	1.47E-5
Order	-	1.42	1.81	1.96	2.00	2.01	2.07

$\nu^{\varepsilon}_{L^2}(t=1)$	$\tau_0 = 0.05$	$\tau_0/2$	$\tau_0/2^2$	$\tau_0/2^3$	$\tau_0/2^4$	$\tau_0/2^5$	$\tau_0/2^6$
$\varepsilon = \varepsilon_0$	2.67E-3	6.73E-4	1.70E-4	4.28E-5	1.07E-5	2.65E-6	6.33E-7
Order	-	1.99	1.98	1.99	2.00	2.01	2.07
$\varepsilon = \varepsilon_0/2$	**6.20E-3**	1.65E-3	4.20E-4	1.06E-4	2.65E-5	6.57E-6	1.56E-6
Order	-	1.91	1.97	1.99	2.00	2.01	2.07
$\varepsilon = \varepsilon_0/2^2$	1.26E-2	4.21E-3	1.14E-3	2.92E-4	7.33E-5	1.81E-5	4.33E-6
Order	-	1.58	1.88	1.97	1.99	2.01	2.07
$\varepsilon = \varepsilon_0/2^3$	6.09E-3	2.52E-3	1.18E-3	**3.53E-4**	9.10E-5	2.27E-5	5.41E-6
Order	-	1.27	1.09	1.75	1.96	2.01	2.07
$\varepsilon = \varepsilon_0/2^5$	1.63E-3	9.47E-4	7.14E-4	3.86E-4	1.41E-4	6.05E-5	**1.62E-5**
Order	-	7.85E-1	4.07E-1	8.86E-1	1.45	1.22	1.91
$\varepsilon = \varepsilon_0/2^7$	1.40E-3	3.48E-4	1.05E-4	6.71E-5	5.93E-5	4.62E-5	2.38E-5
Order	-	2.00	1.73	6.45E-1	1.78E-1	3.62E-1	9.57E-1
$\varepsilon = \varepsilon_0/2^9$	1.39E-3	3.30E-4	8.34E-5	2.10E-5	6.48E-6	4.32E-6	4.21E-6
Order	-	2.08	1.98	1.99	1.69	5.86E-1	3.60E-2

Table 4.6: Temporal errors of UA-4cFD at $t = 1$ for the ill-prepared initial data Case III with $\varepsilon_0 = 1, \tau_0 = 0.05$ at $t = 1$.

$e^{\varepsilon}_{H^1}(t=1)$	$\tau_0 = 0.05$	$\tau_0/2$	$\tau_0/2^2$	$\tau_0/2^3$	$\tau_0/2^4$	$\tau_0/2^5$	$\tau_0/2^6$
$\varepsilon = \varepsilon_0$	4.45E-2	1.64E-2	4.82E-3	1.25E-3	3.14E-4	7.77E-5	1.85E-5
Order	-	1.44	1.77	1.95	1.99	2.01	2.07
$\varepsilon = \varepsilon_0/2$	4.56E-2	1.66E-2	4.86E-3	1.26E-3	3.16E-4	7.83E-5	1.87E-5
Order	-	1.46	1.77	1.95	1.99	2.01	2.07
$\varepsilon = \varepsilon_0/2^2$	5.47E-2	1.74E-2	5.00E-3	1.29E-3	3.25E-4	8.04E-5	1.91E-5
Order	-	1.65	1.80	1.95	1.99	2.01	2.07
$\varepsilon = \varepsilon_0/2^3$	1.08E-1	3.04E-2	7.94E-3	2.01E-3	5.01E-4	1.24E-4	2.95E-5
Order	-	1.84	1.94	1.98	2.00	2.02	2.07
$\varepsilon = \varepsilon_0/2^7$	5.72E-2	3.40E-2	6.15E-3	1.63E-3	4.19E-4	1.05E-4	2.50E-5
Order	-	7.49E-1	2.47	1.92	1.96	2.00	2.07
$\varepsilon = \varepsilon_0/2^9$	5.60E-2	4.48E-2	1.33E-2	8.19E-3	1.27E-3	3.25E-4	8.01E-5
Order	-	3.22E-1	1.75	7.00E-1	2.69	1.96	2.02

$\nu^{\varepsilon}_{L^2}(t=1)$	$\tau_0 = 0.05$	$\tau_0/2$	$\tau_0/2^2$	$\tau_0/2^3$	$\tau_0/2^4$	$\tau_0/2^5$	$\tau_0/2^6$
$\varepsilon = \varepsilon_0$	2.67E-3	6.73E-4	1.70E-4	4.28E-5	1.07E-5	2.65E-6	6.33E-7
Order	-	1.99	1.98	1.99	2.00	2.01	2.07
$\varepsilon = \varepsilon_0/2$	7.66E-3	2.03E-3	5.18E-4	1.31E-4	3.27E-5	8.09E-6	1.93E-6
Order	-	1.92	1.97	1.99	2.00	2.01	2.07
$\varepsilon = \varepsilon_0/2^2$	1.64E-2	**5.07E-3**	1.35E-3	3.45E-4	8.65E-5	2.14E-5	5.10E-6
Order	-	1.69	1.90	1.97	2.00	2.01	2.07
$\varepsilon = \varepsilon_0/2^3$	1.27E-2	4.32E-3	**1.46E-3**	4.10E-4	1.05E-4	2.60E-5	6.21E-6
Order	-	1.56	1.57	1.83	1.97	2.01	2.07
$\varepsilon = \varepsilon_0/2^5$	7.04E-3	2.92E-3	1.43E-3	6.94E-4	**2.37E-4**	7.45E-5	1.90E-05
Order	-	1.27	1.03	1.04	1.55	1.67	1.97
$\varepsilon = \varepsilon_0/2^7$	1.29E-2	6.02E-3	1.50E-3	4.86E-4	1.99E-4	9.38E-5	**4.31E-5**
Order	-	1.10	2.01	1.62	1.29	1.09	1.12
$\varepsilon = \varepsilon_0/2^9$	1.24E-2	1.29E-2	3.12E-3	1.49E-3	3.63E-4	1.02E-4	3.01E-5
Order	-	-6.59E-2	2.05	1.06	2.04	1.84	1.75

Table 4.7: Temporal errors of UA-4cFD at $t = 1$ for the well-prepared initial data Case I with $\varepsilon_0 = 1, \tau_0 = 0.05$ in resonance regions at $t = 1$.

τ	τ_0	$\tau_0/2^3$	$\tau_0/2^6$
ε	$\varepsilon_0/2$	$\varepsilon_0/2^3$	$\varepsilon_0/2^5$
$\nu^{\varepsilon}_{L^2}(t=1)$	5.67E-3	3.55E-4	1.62E-5
Order	-	1.33	1.48

Table 4.8: Temporal errors of UA-4cFD at $t = 1$ for the less-ill-prepared initial data Case II with $\varepsilon_0 = 1, \tau_0 = 0.05$ in resonance regions at $t = 1$.

τ	τ_0	$\tau_0/2^3$	$\tau_0/2^6$
ε	$\varepsilon_0/2$	$\varepsilon_0/2^3$	$\varepsilon_0/2^5$
$\nu^{\varepsilon}_{L^2}(t=1)$	6.20E-3	3.53E-4	1.62E-5
Order	-	1.38	1.48

Table 4.9: Temporal errors of UA-4cFD at $t = 1$ for the ill-prepared initial data Case III with $\varepsilon_0 = 1, \tau_0 = 0.05$ in resonance regions at $t = 1$.

τ	$\tau_0/2$	$\tau_0/2^2$	$\tau_0/2^3$	$\tau_0/2^4$	$\tau_0/2^5$	$\tau_0/2^6$
ε	$\varepsilon_0/2^2$	$\varepsilon_0/2^3$	$\varepsilon_0/2^4$	$\varepsilon_0/2^5$	$\varepsilon_0/2^6$	$\varepsilon_0/2^7$
$\nu^{\varepsilon}_{L^2}(t=1)$	5.07E-3	1.46E-3	5.51E-4	2.37E-4	1.06E-4	4.31E-5
Order	-	1.80	1.40	1.22	1.16	1.30

Chapter 5

Quantized Vortex Interactions in NLSE with Periodic BCs

In this chapter, we will study the interaction of quantized vortices under the nonlinear Schrödinger equation with periodic boundary conditions (BCs). An efficient way of initial setups is proposed and the numerical simulation results coincide well with the reduced dynamical laws under the zero initial momentum limit assumption on flat torus. We also simulate the non-vanishing momentum cases as well as general rectangle domain cases, which provide us some extending guesses on the reduced dynamical laws. Some interesting vortex interaction configurations, such as periodic vortex trajectories, vortex merging, and leapfrogging type motions, are also studied.

5.1 The NLSE in two dimensions

Consider the two-dimensional nonlinear Schrödinger equation (NLSE) or the Gross–Pitaevskii equation under the periodic BCs with a dimensionless parameter $\varepsilon > 0$:

$$i\partial_t\psi^\varepsilon(\boldsymbol{x},t) = \Delta\psi^\varepsilon + \frac{1}{\varepsilon^2}(1-|\psi^\varepsilon|^2)\psi^\varepsilon, \qquad \boldsymbol{x} = (x,y) \in \Omega, t > 0, \tag{5.1.1}$$

with initial condition

$$\psi^\varepsilon(\boldsymbol{x},0) = \psi_0^\varepsilon(\boldsymbol{x}), \quad \boldsymbol{x} \in \Omega, \tag{5.1.2}$$

and periodic BCs on rectangular domain

$$\Omega = (0, a) \times (0, b),$$

i.e.,

$$\begin{cases} \psi^\varepsilon(x, 0, t) = \psi^\varepsilon(x, b, t), \partial_y \psi^\varepsilon(x, 0, t) = \partial_y \psi^\varepsilon(x, b, t), \ \text{for } x \in [0, a], t \geq 0; \\ \psi^\varepsilon(0, y, t) = \psi^\varepsilon(a, y, t), \partial_x \psi^\varepsilon(0, y, t) = \partial_x \psi^\varepsilon(a, y, t), \ \text{for } y \in [0, b], t \geq 0. \end{cases} \tag{5.1.3}$$

As mentioned in [36], the NLSE (5.1.1) with periodic BCs has properties of mass conservation, energy conservation and momentum conservation. With mass, energy and momentum defined as

$$M(t) := M(\psi^\varepsilon(\cdot, t)) = \int_\Omega |\psi^\varepsilon(\boldsymbol{x}, t)|^2 \mathrm{d}\boldsymbol{x}, \tag{5.1.4}$$

$$E(t) := E(\psi^\varepsilon(\cdot, t)) = \int_\Omega [\frac{1}{2}|\nabla \psi^\varepsilon(\boldsymbol{x}, t)|^2 + \frac{1}{4\varepsilon^2}(1 - |\psi^\varepsilon(\boldsymbol{x}, t)|^2)^2] \mathrm{d}\boldsymbol{x}, \tag{5.1.5}$$

$$\mathbf{P}(t) := \mathbf{P}(\psi^\varepsilon(\cdot, t)) = \mathrm{Im}\left(\int_\Omega \bar{\psi}^\varepsilon(\boldsymbol{x}, t) \nabla \psi^\varepsilon(\boldsymbol{x}, t) \mathrm{d}\boldsymbol{x}\right), \tag{5.1.6}$$

we have

$$M(t) \equiv M(0), E(t) \equiv E(0), \text{ and } \mathbf{P}(t) \equiv \mathbf{P}(0). \tag{5.1.7}$$

Note that for the current $\mathbf{j}$ defined by

$$\mathbf{j}(\psi^\varepsilon(\boldsymbol{x}, t)) = \mathrm{Im}\left(\bar{\psi}^\varepsilon(\boldsymbol{x}, t) \nabla \psi^\varepsilon(\boldsymbol{x}, t)\right), \tag{5.1.8}$$

we have

$$\mathbf{P}(\psi^\varepsilon(\cdot, t)) = \int_\Omega \mathbf{j}(\psi^\varepsilon(\boldsymbol{x}, t)) \mathrm{d}\boldsymbol{x}, \tag{5.1.9}$$

and conservation of mass flow

$$\frac{\mathrm{d}}{\mathrm{d}t}|\psi^\varepsilon(\boldsymbol{x}, t)|^2 + 2\nabla \cdot \mathbf{j}(\psi^\varepsilon(\boldsymbol{x}, t)) = 0. \tag{5.1.10}$$

These three conserved quantities in (5.1.7) can be used to validate our numerical simulations, since they should to be kept in acceptable numerical errors. The NLSE is also unchanged under the rescaling $\boldsymbol{x} \to C\boldsymbol{x}, t \to C^2 t$, and $\varepsilon \to C\varepsilon$ with $C > 0$ a positive constant. Therefore, without loss of generality, we can assume the edge lengths of Ω are $O(1)$ and then study the influence of ε and vortex center distances on vortex dynamics.

5.2 Quantized vortices and setups of initial data

A quantum vortex of the 2D NLSE (5.1.1) is a topological defect of the solution $\psi^\varepsilon(\boldsymbol{x}, t)$, where the density is zero at the vortex center and the phase change along any closed curve enclosing the vortex center is a nonzero integral multiple of 2π. And the integer is called degree or winding number of the quantized vortex [21, 42]. A simple vortex refers to a vortex with winding numbers ± 1 and it is the only kind of stable vortex under small disturbance of initial data or the potential function in NLSE [85, 128]. Therefore, we only consider simple vortices in following context.

A special property from periodic BCs is that the summation of all winding numbers is zero: let $\arg(z)$ be the argument of complex number z, and $\mathrm{Arg}(z)$ be the principle argument (between 0 and 2π), then from the periodicity of initial data (5.1.3), we have

$$\int_{\partial\Omega} \nabla \arg(\psi_0^\varepsilon) \cdot \boldsymbol{\tau} \mathrm{d}s = 0, \tag{5.2.1}$$

where $\boldsymbol{\tau}$ is the unit tangent vector along $\partial\Omega$, and s is the arc length parameter of $\partial\Omega$.

This exerts a restriction on the vortex configuration of the initial data of our numerical simulation: we need even number of initial vortices and half of them have winding number 1 while the other half have winding number -1. We can assume that the initial data $\psi_0^\varepsilon(\boldsymbol{x})$ has $2M$ distinct simple vortices with center located at $\boldsymbol{x}_j^0$ and winding number $d_j \in \{-1, 1\}$ for $j = 1, 2, \cdots, 2M$. For easy description, let $\boldsymbol{x}_j^\varepsilon(t)$ denote the location of j-th vortex center at time t.

We set up the initial profile by multiplying the profile of several simple vortex in steady state with proper phase tune. The initial value is of form

$$\psi_0^\varepsilon(\boldsymbol{x}) = \exp(iq(\boldsymbol{x})) \prod_{j=1}^{2M} \phi_{d_j}^\varepsilon(\boldsymbol{x} - \boldsymbol{x}_j^0), \tag{5.2.2}$$

where $\phi_{d_j}^\varepsilon(\boldsymbol{x} - \boldsymbol{x}_j^0)$ is a single steady vortex profile with winding number d_j and center $\boldsymbol{x}_j^0$ for Dirichlet BCs on domain Ω, which has constant modulus near $\partial\Omega$. And $q(\boldsymbol{x}) \in \mathbb{R}$ is a phase tune for $\psi_0^\varepsilon(\boldsymbol{x})$ that satisfies

- $\Delta q(\boldsymbol{x}) = 0$;
- $\psi_0^\varepsilon(\boldsymbol{x})$ is periodic on Ω.

5.2.1 A single vortex profile under Dirichlet BCs

In [21], there are detailed descriptions of setting initial data $\phi^\varepsilon_{d_j}(\boldsymbol{x}-\boldsymbol{x}_j^0)$ for Dirichlet BCs. At first, we can assume that the single steady solution has radial symmetric form

$$\phi_d^\varepsilon(\boldsymbol{x}) = f^\varepsilon(|\boldsymbol{x}|)e^{id\theta(\boldsymbol{x})} \tag{5.2.3}$$

with $\theta(\boldsymbol{x}) = \mathrm{Arg}(x+iy)$, $d=\pm1$, and $f^\varepsilon(r)$ chosen as

$$f^\varepsilon(r) = \begin{cases} 1, \ \text{for } r > R_0, \\ f_v(\frac{r}{\varepsilon}), \ \text{for } 0 \le r \le R_0, \end{cases} \tag{5.2.4}$$

where f_v is the solution of

$$\begin{cases} [\frac{1}{r}\frac{\mathrm{d}}{\mathrm{d}r}(r\frac{\mathrm{d}}{\mathrm{d}r}) - \frac{1}{r^2} + (1-(f_v(r))^2)]f_v(r) = 0, \quad 0 < r < \tilde{R}_0, \\ f_v(0) = 0, \ f_v(\tilde{R}_0) = 1. \end{cases} \tag{5.2.5}$$

Here R_0 is the maximum radius for computing the modulus profile of an initial vortex and should be less than the distance between initial vortex centers and $\partial\Omega$. $\tilde{R}_0$ is a truncate radius that is far greater than 1 and makes sure that each single vortex profile $\phi^\varepsilon_{d_j}(\boldsymbol{x}-\boldsymbol{x}_j^0)$ has constant modulus near $\partial\Omega$ ($\tilde{R}_0 \le R_0/\varepsilon$). The proposition of $f_v(r)$ is for calculating (5.2.5) once and working for all initial single vortex profiles with smaller ε. Equation (5.2.5) is derived from substituting single vortex profile ϕ_d^ε into NLSE (5.1.1) with the time derivative term eliminated:

$$\Delta\phi_d^\varepsilon + \frac{1}{\varepsilon^2}(1-|\phi_d^\varepsilon|^2)\phi_d^\varepsilon = 0. \tag{5.2.6}$$

This is a common handling procedure of the initialization for vortex simulations as in [3, 20, 23, 65, 127, 128]. ϕ_d in (5.2.6) is called a steady state of a single vortex since its modulus is time independent. We can discretize (5.2.5) into a finite difference scheme and then use Newton iteration to get numerical solutions to (5.2.5) with a proper initial guess from asymptotic analysis [90, 128]. Here is a plot of $f^\varepsilon(r)$ for different ε's in Figure 5.1, which shows that the core size of our initial setups is $O(\varepsilon)$ clearly.

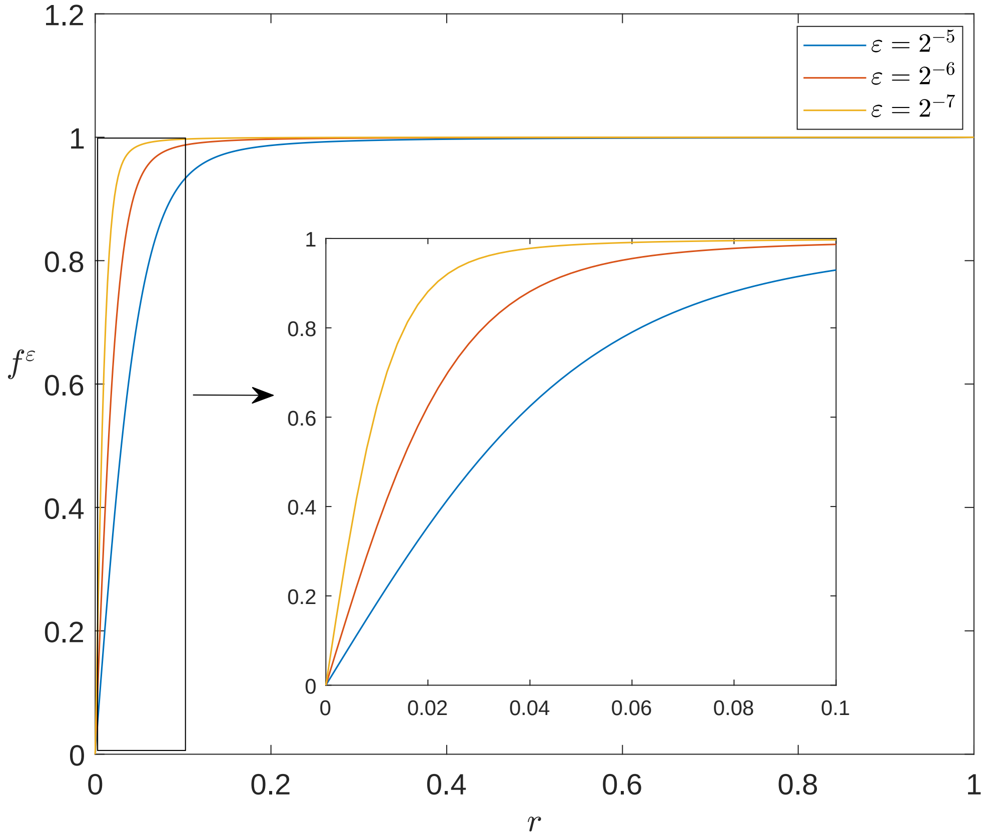

Figure 5.1: Plot of $f^\varepsilon(r)$ for different ε's.

5.2.2 Conditions on initial data satisfying periodic BCs

After acquiring the Dirichlet boundary type initial value $\psi^\varepsilon_{DC}(\boldsymbol{x}) = \prod_{j=1}^{2M} \phi^\varepsilon_{d_j}(\boldsymbol{x} - \boldsymbol{x}_j^0)$, we can construct a periodic initial value ψ_0^ε through (5.2.2) with solving

$$\begin{cases} \Delta q(\boldsymbol{x}) = 0; \\ q(\boldsymbol{x}) + \mathrm{Arg}(\psi^\varepsilon_{DC}(\boldsymbol{x})) \text{ is periodic up to first-order derivatives on } \Omega. \end{cases} \tag{5.2.7}$$

Note that the solution of $q(\boldsymbol{x})$ is only unique up to a constant and the periodicity of phase is up to 2π. Without lost of generality, we may assume $\int_\Omega q(\boldsymbol{x})\mathrm{d}\boldsymbol{x} = 0$.

Since the initial data satisfies $\sum_{j=1}^{2M} d_j = 0$, we can view the initial data as multiplication of M vortex dipoles (a dipole means a system of two single vortices with opposite winding numbers). Without loss of generality, we may assume the M dipole has initial profile $\Psi^\varepsilon_{D,j} = \phi^\varepsilon_1(|\boldsymbol{x} - \boldsymbol{x}_{2j-1}|)\phi^\varepsilon_{-1}(|\boldsymbol{x} - \boldsymbol{x}_{2j}|)$. Since every dipole satisfies the Dirichlet boundary conditions, we can choose the segment with endpoints at vortex centers as a branch cut of their phase.

5.2.3 Some setups with zero initial momentum limit

Another observation from our numerical simulation is that without applying phase in-painting, when the vortex core size converges to zero, the limit of the initial momentum relies on the weighted mass center [23, 121]

$$\bar{\boldsymbol{x}} = \sum_{j=1}^{2M} d_j \boldsymbol{x}_j^0. \tag{5.2.8}$$

Theorem 5.1 (Initial momentum limit)**.** *For a set of initial data $\psi_0^\varepsilon(\boldsymbol{x})$ with vortices centered at $\boldsymbol{x}_j^0$'s, $O(\varepsilon)$ core sizes and $\mathrm{Arg}(\psi_0^\varepsilon(\boldsymbol{x}))$ continuous on $\partial\Omega$, their initial momentum satisfies*

$$\lim_{\varepsilon\to 0} \mathbf{P}(\psi_0^\varepsilon) = 2\pi \mathbf{J}\bar{\boldsymbol{x}}, \tag{5.2.9}$$

where $\mathbf{J} = \begin{pmatrix} 0 & 1 \\ -1 & 0 \end{pmatrix}$.

Proof. At first, let us consider the limit momentum of a vortex dipole as $\varepsilon \downarrow 0$. As noted in [42], it is easy to verify that if initial value ψ_0^ε is written in polar form

$$\psi_0^\varepsilon(\boldsymbol{x}) = \rho(\boldsymbol{x})e^{i\Theta(\boldsymbol{x})}$$

with ρ and Θ real functions on Ω, then the current $\mathbf{j}$ defined in (5.1.8) has expression

$$\mathbf{j}(\psi_0^\varepsilon(\boldsymbol{x})) = \rho^2(\boldsymbol{x})\nabla\Theta(\boldsymbol{x}). \tag{5.2.10}$$

For the vortex dipole centered at $\boldsymbol{x}_1^0 = (x_1^0, y_1^0)$ and $\boldsymbol{x}_2^0 = (x_2^0, y_2^0)$ with winding number $d_1 = 1$ and $d_2 = -1$, The module and phase of the initial data in polar form can have expression

$$\rho(\boldsymbol{x}) = f^\varepsilon(|\boldsymbol{x} - \boldsymbol{x}_1^0|) f^\varepsilon(|\boldsymbol{x} - \boldsymbol{x}_2^0|), \tag{5.2.11}$$

$$\Theta(\boldsymbol{x}) = q(\boldsymbol{x}) + \theta(\boldsymbol{x} - \boldsymbol{x}_1^0) - \theta(\boldsymbol{x} - \boldsymbol{x}_2^0), \tag{5.2.12}$$

where $\theta(\boldsymbol{x}) = \mathrm{Arg}(x + iy)$, $\lim\limits_{\varepsilon\to 0} \inf\limits_{\boldsymbol{x}\in B_{r_0}^c} |f^\varepsilon(\boldsymbol{x})| = 1$ for some fixed $r_0 > 0$, where $B_{r_0}^c = \Omega \backslash B_{r_0}(\mathbf{0})$ with $B_{r_0}(\mathbf{0})$ the ball centered at $\mathbf{0}$ with radius r_0, and $q(\boldsymbol{x})$ denotes a continuous differentiable function inside Ω.

Then from (5.2.10) and (5.2.11), we have

$$\lim_{\varepsilon\to 0} \mathbf{P}(\psi_0^\varepsilon) = \int_\Omega \nabla\Theta \mathrm{d}\boldsymbol{x}, \tag{5.2.13}$$

provided that the integrands on right hand are integrable.

Note that (5.2.10) is defined locally, we have

$$\nabla\Theta(\boldsymbol{x}) = \nabla\theta(\boldsymbol{x} - \boldsymbol{x}_1^0) - \nabla\theta(\boldsymbol{x} - \boldsymbol{x}_2^0) + \nabla q(\boldsymbol{x}) \tag{5.2.14}$$

at place where $\theta(\boldsymbol{x} - \boldsymbol{x}_1^0) - \theta(\boldsymbol{x} - \boldsymbol{x}_2^0) + q(\boldsymbol{x})$ is continuously differentiable. On the other hand, from the periodic BCs (5.1.3) and small initial momentum condition we know

$$q(a, y) + \mathrm{Arg}(\psi_{DC}^\varepsilon(a, y)) = q(0, y) + \mathrm{Arg}(\psi_{DC}^\varepsilon(0, y)), \tag{5.2.15}$$

$$q(x, b) + \mathrm{Arg}(\psi_{DC}^\varepsilon(x, b)) = q(x, 0) + \mathrm{Arg}(\psi_{DC}^\varepsilon(x, 0)), \tag{5.2.16}$$

for $\psi_{DC}^\varepsilon(\boldsymbol{x}) = f^\varepsilon(|\boldsymbol{x} - \boldsymbol{x}_1^0|) f^\varepsilon(|\boldsymbol{x} - \boldsymbol{x}_2^0|) e^{i(\theta(\boldsymbol{x}-\boldsymbol{x}_1^0) - \theta(\boldsymbol{x}-\boldsymbol{x}_2^0))}$.

Denote $I = \{\lambda \boldsymbol{x}_1^0 + (1-\lambda)\boldsymbol{x}_2^0 : \lambda \in (0, 1)\}$, then

$$\begin{aligned}
\lim_{\varepsilon\to 0} \mathbf{P}(\psi_0^\varepsilon) &= \int_\Omega \nabla\theta(\boldsymbol{x} - \boldsymbol{x}_1^0) - \nabla\theta(\boldsymbol{x} - \boldsymbol{x}_2^0) + \nabla q(\boldsymbol{x}) \mathrm{d}\boldsymbol{x} \\
&= \int_{\Omega\backslash I} \nabla\theta(\boldsymbol{x} - \boldsymbol{x}_1^0) - \nabla\theta(\boldsymbol{x} - \boldsymbol{x}_2^0) + \nabla q(\boldsymbol{x}) \mathrm{d}\boldsymbol{x} \\
&= \int_{\Omega\backslash I} \nabla\theta(\boldsymbol{x} - \boldsymbol{x}_1^0) - \nabla\theta(\boldsymbol{x} - \boldsymbol{x}_2^0) \mathrm{d}\boldsymbol{x} + \int_\Omega \nabla q(\boldsymbol{x}) \mathrm{d}\boldsymbol{x}.
\end{aligned} \tag{5.2.17}$$

Due to a phase jump on the segment I, the second component of the last term in (5.2.17) can be computed by following integration by part:

$$
\begin{aligned}
&\int_0^a \int_0^b \partial_y q(\boldsymbol{x}) \mathrm{d}y \mathrm{d}x \\
=& \int_0^a q(x,y)|_{y=0}^{b} \mathrm{d}x \\
=& \int_0^a \mathrm{Arg}(\psi_{DC}^{\varepsilon}(x,y))|_{y=b}^{0} \mathrm{d}x \\
=& -\int_0^a \Bigg(\Bigg(\int_0^l \frac{\mathrm{d}}{dy} \mathrm{Arg}(\psi_{DC}^{\varepsilon}(x,y)) \mathrm{d}y + \big(\theta(\boldsymbol{x}-\boldsymbol{x}_1^0) - \theta(\boldsymbol{x}-\boldsymbol{x}_2^0)\big) |_{y=l-}^{l+} \\
&\quad + \int_l^a \frac{\mathrm{d}}{dy} \mathrm{Arg}(\psi_{DC}^{\varepsilon}(x,y)) \mathrm{d}y \Bigg) \mathrm{d}x \\
=& -\int_{\Omega \backslash I} \partial_y \theta(\boldsymbol{x}-\boldsymbol{x}_1^0) - \partial_y \theta(\boldsymbol{x}-\boldsymbol{x}_2^0) \mathrm{d}\boldsymbol{x} - \int_0^a \big(\theta(\boldsymbol{x}-\boldsymbol{x}_1^0) - \theta(\boldsymbol{x}-\boldsymbol{x}_2^0)\big) |_{y=l-}^{l+} \mathrm{d}x \\
=& -\int_{\Omega \backslash I} \partial_y \theta(\boldsymbol{x}-\boldsymbol{x}_1^0) - \partial_y \theta(\boldsymbol{x}-\boldsymbol{x}_2^0) \mathrm{d}\boldsymbol{x} + 2\pi(x_1^0 - x_2^0),
\end{aligned}
\tag{5.2.18}
$$

with l satisfying that (x,l) lies on the segment I, i.e.,

$$
(x_2^0 - x_1^0)(l - y_1^0) = (y_2^0 - y_1^0)(x - x_1^0). \tag{5.2.19}
$$

With similar procedure, we can get

$$
\int_0^a \int_0^b \partial_x q(\boldsymbol{x}) \mathrm{d}y \mathrm{d}x = -\int_{\Omega \backslash I} \partial_x \theta(\boldsymbol{x}-\boldsymbol{x}_1^0) - \partial_x \theta(\boldsymbol{x}-\boldsymbol{x}_2^0) \mathrm{d}\boldsymbol{x} - 2\pi(y_1^0 - y_2^0), \tag{5.2.20}
$$

Therefore,

$$
\lim_{\varepsilon \to 0} \mathbf{P} = 2\pi \mathbf{J} \bar{\boldsymbol{x}}. \tag{5.2.21}
$$

It is easy to extend the calculation above to any general case of vortex configuration by considering more vortex dipoles instead of one. And the momentum value comes from the phase jump on all the segments, each of which links the two vortex centers in a dipole like I inside Ω. $\square$

5.3 The reduced dynamical laws under zero initial momentum limit

5.3.1 The reduced dynamical laws (RDLs)

In [41, 42], Colliander and Jerrard gave the reduced dynamical laws (RDLs) for vortex interactions of the NLSE under periodic BCs, which provides a set of ODEs describing the motion of vortex centers for $\varepsilon \downarrow 0$.

Take $\Omega = (0,1)^2$ to be the computational domain and $\mathbb{T}^2 = S^1 \times S^1$ to be the unitary flat torus. Under three assumptions on the initial conditions [42] including the zero initial momentum limit condition, i.e.,

$$\lim_{\varepsilon \to 0^+} \int_\Omega \mathbf{j}(\psi_0^\varepsilon) \mathrm{d}\boldsymbol{x} = 0, \tag{5.3.1}$$

the trajectories of vortex centers converge to solutions of the following ODEs as $\varepsilon \downarrow 0$:

$$\begin{cases} \dfrac{\mathrm{d}\boldsymbol{x}_j(t)}{\mathrm{d}t} &= -2\mathbf{J} \sum\limits_{\substack{k=1\\k\neq j}}^{2M} d_k \nabla F(\boldsymbol{x}_k - \boldsymbol{x}_j), \\ \boldsymbol{x}_j(0) &= \boldsymbol{x}_j^0, \end{cases} \tag{5.3.2}$$

where $\nabla F(\boldsymbol{x}) = \begin{pmatrix} \partial_x F(\boldsymbol{x}) \\ \partial_y F(\boldsymbol{x}) \end{pmatrix}$, and $F(\boldsymbol{x})$ is the Green function on the unitary flat torus that solves

$$\Delta F(\boldsymbol{x}) = 2\pi(\delta(\boldsymbol{x}) - 1), \;\; \boldsymbol{x} \in \mathbb{T}^2, \tag{5.3.3}$$

with $\delta(\boldsymbol{x})$ the Dirac function. The Green function $F(\boldsymbol{x})$ has an analytical expression by theta function $\theta_1(z)$ [71]:

$$F(x,y) = \ln|\theta_1(x+iy)| - \pi y^2, \tag{5.3.4}$$

where $\theta_1(z)$ is an exponentially convergent series

$$\theta_1(z) = 2\sum_{n=0}^{\infty} (-1)^n e^{-\pi(n+1/2)^2} \sin((2n+1)\pi z), \tag{5.3.5}$$

which benefits the numerical computation a lot.

From (5.3.4) and Figure 5.2 we can see that the $F(\boldsymbol{x})$ is singular at the origin. Since $\ln(\boldsymbol{x})$ satisfies

$$\Delta \ln|\boldsymbol{x}| = 2\pi\delta(\boldsymbol{x}), \tag{5.3.6}$$

the difference between $\ln|\boldsymbol{x}|$ and $F(\boldsymbol{x})$ (left part of Figure 5.2) is a smooth function whose Laplacian equals to -2π in Ω . Therefore $\nabla F(\boldsymbol{x})$ has almost the same direction as $\nabla \ln(\boldsymbol{x}) = \boldsymbol{x}/|\boldsymbol{x}|^2$ where $|\boldsymbol{x}|$ is small. As in [121], we can have the following qualitative description on vortex dynamics from the interaction terms of two vortices in (5.3.2): two vortices in a vortex dipole move parallelly and two vortices in a vortex pair (two single vortices with same winding number) rotate about each other.

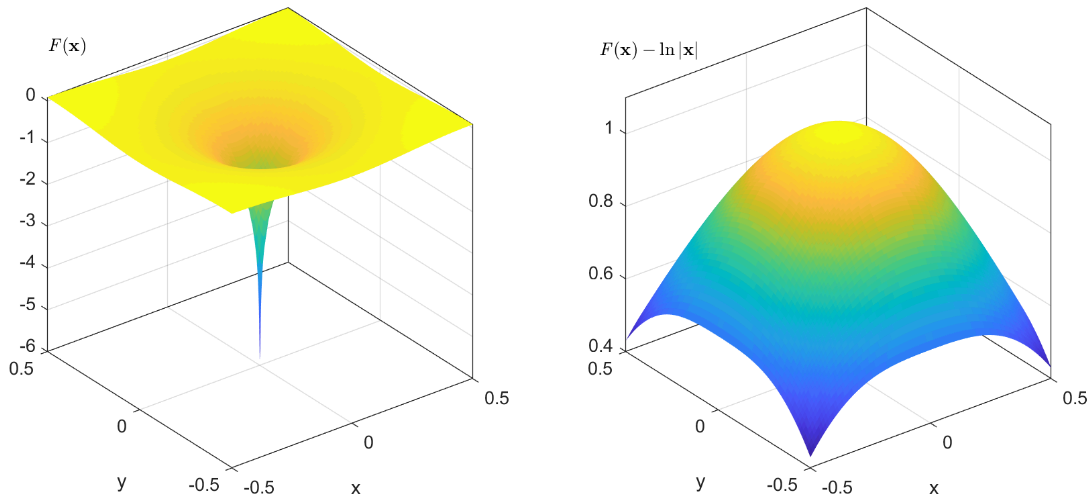

Figure 5.2: Plot of $F(\boldsymbol{x})$ (left); plot of $F(\boldsymbol{x}) - \ln|\boldsymbol{x}|$ (right).

5.3.2 Several analytical solutions under specific setups

The ODE system from RDLs is an autonomous system. From considering the first integral of the system, we can find several analytical solutions. In this part, we will discuss several periodical analytical solutions for the ODEs from RDLs. For more general cases, we adopt the standard fourth order Runge-Kutta method (RK4) to solve the ODEs, which can provide comparison with numerical simulation results from solving the NLSE.

Define the Case I initial vortex setup as $\boldsymbol{x}_1^0 = C_\Omega + (-\alpha^0, -\beta^0)^T$, $\boldsymbol{x}_2^0 = C_\Omega + (\alpha^0, -\beta^0)^T$, $\boldsymbol{x}_3^0 = C_\Omega + (\alpha^0, \beta^0)^T$, $\boldsymbol{x}_4^0 = C_\Omega + (-\alpha^0, \beta^0)^T$, $d_1 = d_3 = 1, d_2 = d_4 = -1$, with $C_\Omega = (\frac{1}{2}, \frac{1}{2})^T$ the center of Ω. Note the initial vortex configurations are symmetric about C_Ω with the considerations of vortex locations and winding numbers.

Lemma 5.1 (A vortex polygon type periodic solution of the RDLs). *For initial value chosen as the Case I setup on $\Omega = (0,1)^2$, the solution of (5.3.2) is $\boldsymbol{x}_1 = (\frac{1}{2} - \alpha(t), \frac{1}{2} - \beta(t))^T$, $\boldsymbol{x}_2 = (\frac{1}{2} + \alpha(t), \frac{1}{2} - \beta(t))^T$, $\boldsymbol{x}_3 = (\frac{1}{2} + \alpha(t), \frac{1}{2} + \beta(t))^T$, $\boldsymbol{x}_4 = (\frac{1}{2} - \alpha(t), \frac{1}{2} + \beta(t))^T$, with $(\alpha(t), \beta(t))$ satisfies*

$$f_1(\alpha(t), \beta(t)) = f_1(\alpha^0, \beta^0), \tag{5.3.7}$$

where

$$f_1(x, y) = F(2x, 2y) - F(2x, 0) - F(0, 2y). \tag{5.3.8}$$

Proof. Substituting the initial data into (5.3.2), we get an ODE system:

$$\begin{cases} \dot{\boldsymbol{x}}_1 = -2\mathbf{J}\nabla(-F(\boldsymbol{x}_2 - \boldsymbol{x}_1) + F(\boldsymbol{x}_3 - \boldsymbol{x}_1) - F(\boldsymbol{x}_4 - \boldsymbol{x}_1)), \\ \dot{\boldsymbol{x}}_2 = -2\mathbf{J}\nabla(F(\boldsymbol{x}_1 - \boldsymbol{x}_2) + F(\boldsymbol{x}_3 - \boldsymbol{x}_2) - F(\boldsymbol{x}_4 - \boldsymbol{x}_2)), \\ \dot{\boldsymbol{x}}_3 = -2\mathbf{J}\nabla(F(\boldsymbol{x}_1 - \boldsymbol{x}_3) - F(\boldsymbol{x}_2 - \boldsymbol{x}_3) - F(\boldsymbol{x}_4 - \boldsymbol{x}_3)), \\ \dot{\boldsymbol{x}}_4 = -2\mathbf{J}\nabla(F(\boldsymbol{x}_1 - \boldsymbol{x}_4) - F(\boldsymbol{x}_2 - \boldsymbol{x}_4) + F(\boldsymbol{x}_3 - \boldsymbol{x}_4)), \\ \boldsymbol{x}_1(0) = \boldsymbol{x}_1^0,\ \boldsymbol{x}_2(0) = \boldsymbol{x}_2^0,\ \boldsymbol{x}_3(0) = \boldsymbol{x}_3^0,\ \boldsymbol{x}_4(0) = \boldsymbol{x}_4^0. \end{cases} \tag{5.3.9}$$

From the symmetry of the initial setting, we can see that the solution is of form $\boldsymbol{x}_1 = (\frac{1}{2} - \alpha(t), \frac{1}{2} - \beta(t))^T$, $\boldsymbol{x}_2 = (\frac{1}{2} + \alpha(t), \frac{1}{2} - \beta(t))^T$, $\boldsymbol{x}_3 = (\frac{1}{2} + \alpha(t), \frac{1}{2} + \beta(t))^T$, $\boldsymbol{x}_4 = (\frac{1}{2} - \alpha(t), \frac{1}{2} + \beta(t))^T$, and the ODE system (5.3.9) can be reduced to a system with two variables $\alpha(t), \beta(t)$.

As in [71], we know the Green function $F(x, y)$ in (5.3.3) is unique up to a constant, then we get $F(\pm x, \pm y) = F(x, y)$ for the F in (5.3.4). Consequently, we have

$$\begin{aligned}
\nabla F(-x,-y) &= -\nabla F(x,y),\\
\partial_x F(-x,y) &= -\partial_x F(x,y),\\
\partial_y F(-x,y) &= \partial_y F(x,y),\\
\partial_x F(x,-y) &= \partial_x F(x,y),\\
\partial_y F(x,-y) &= -\partial_y F(x,y).
\end{aligned}$$

Substituting the above equalities into (5.3.2) and adding up the equations of $\dot{\boldsymbol{x}}_1$ and $\dot{\boldsymbol{x}}_2$ yields

$$\dot{\beta} = 2F_x(2\alpha,0) - 2F_x(2\alpha,2\beta); \tag{5.3.10}$$

and adding up the equations of $\dot{\boldsymbol{x}}_2$ and $\dot{\boldsymbol{x}}_3$ gives us

$$\dot{\alpha} = 2F_y(2\alpha,2\beta) - 2F_y(0,2\beta). \tag{5.3.11}$$

Thus we have

$$\begin{aligned}
&\frac{\mathrm{d}}{\mathrm{d}t}\left(F(2\alpha,2\beta) - F(2\alpha,0) - F(0,2\beta)\right)\\
=&2(F_y(2\alpha,2\beta) - F_y(0,2\beta))\dot{\beta} - 2(F_x(2\alpha,0) - F_x(2\alpha,2\beta))\dot{\alpha}\\
=&\dot{\alpha}\dot{\beta} - \dot{\beta}\dot{\alpha} = 0.
\end{aligned} \tag{5.3.12}$$

The solution of $(\alpha(t),\beta(t))$ falls on a level set of function f_1 in (5.3.8), which is called the first integral of the system composed by (5.3.11) and (5.3.10). □

We solve (5.3.2) with Case I setup for $\alpha^0 = \beta^0 = 1/8$ by RK4 method up to time $T = 0.2$. The numerical trajectories with time step $\tau = 10^{-4}$ is showed in the left part of Figure 5.3, where '+' and '−' sign indicate the position of initial vortex with winding numbers +1 and −1 respectively. A contour plot of f_1 in (5.3.8) is showed on the middle graph. A orbit of a single vortex from the left picture is one of the level sets of f_1. The last picture shows the convergence of the numerical solution of (5.3.2) through RK4 to a level set of f_1 as τ decreases.

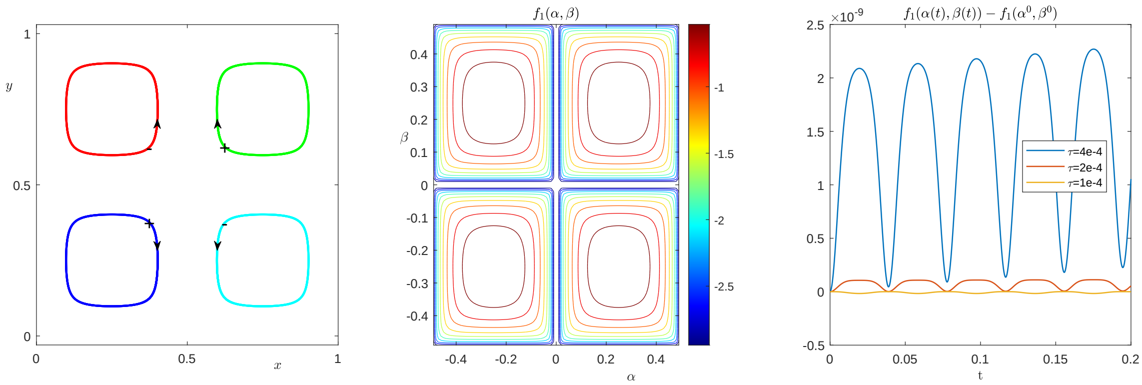

Figure 5.3: Vortex trajectories of Case I with $\alpha^0 = \beta^0 = 1/8$ (left); contour lines of f_1 (middle); value of $f_1(\alpha(t), \beta(t))$ with (α, β) solved form $\boldsymbol{x}_1$ in (5.3.9) for different time step τ (right).

Define Case II initial vortex setup as two vortex dipoles located on the same straight line: $\boldsymbol{x}_1^0 = C_\Omega + (-L_1 - L_2, 0)^T$, $\boldsymbol{x}_2^0 = C_\Omega + (-L_1 + L_2, 0)^T$, $\boldsymbol{x}_3^0 = C_\Omega + (L_1 - L_2, 0)^T$, $\boldsymbol{x}_4^0 = C_\Omega + (L_1 + L_2, 0)^T$, for $L_1, L_2 \in (0, \frac{1}{2})$ satisfying $L_1 + L_2 < \frac{1}{2}$, $d_1 = d_4 = 1$, and $d_2 = d_3 = -1$.

Lemma 5.2 (A periodic solution with collinear initial vortex centers)**.** *For the Case II type setup with $L_1 = 1/4, L_2 = \alpha^0$, the periodic solution of (5.3.2) is of form $\boldsymbol{x}_1 = (\frac{1}{4} - \alpha(t), \frac{1}{2} - \beta(t))^T$, $\boldsymbol{x}_2 = (\frac{1}{4} + \alpha(t), \frac{1}{2} - \beta(t))^T$, $\boldsymbol{x}_3 = (\frac{3}{4} - \alpha(t), \frac{1}{2} + \beta(t))^T$, $\boldsymbol{x}_4 = (\frac{3}{4} + \alpha(t), \frac{1}{2} + \beta(t))^T$ with $(\alpha(t), \beta(t))$ on the level set of*

$$f_2(x, y) = F(2x, 0) + F(\frac{1}{2}, 2y) - F(\frac{1}{2} - 2x, 2y). \tag{5.3.13}$$

Remark: The proof is quite similar to Lemma 5.1 and we omit it here. Not like Case I, the Figure 5.4 shows that the orbits in Lemma 5.2 have two types. One crosses the boundaries and the other is closed cycle inside Ω. When considered on $\mathbb{T}^2$, a loop for one period in the left chart of Figure 5.4 corresponds to the unitary element of the fundamental group of $\mathbb{T}^2$ while a one-period loop from the middle chart corresponds to the zero element. Based on numerical solution and binary search algorithm, we can detect that the bifurcation point for these two kinds of trajectories is $\alpha_0 = \alpha^* \approx 0.138621$.

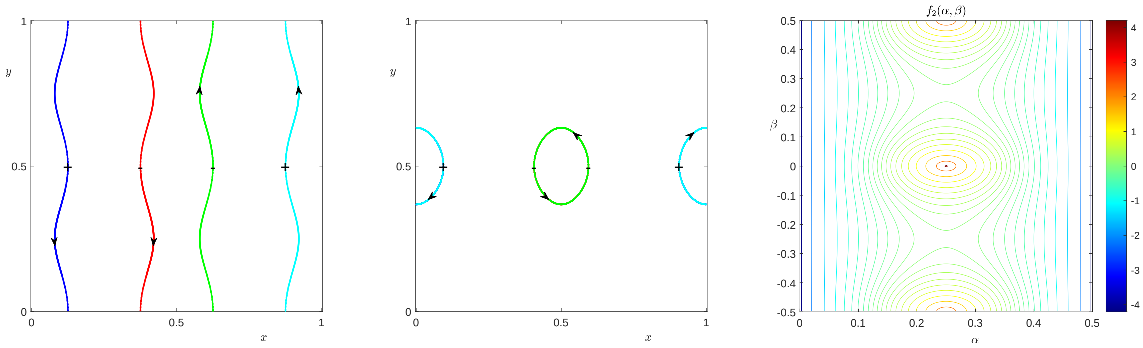

Figure 5.4: Two different kinds of trajectories for RDLs and contour lines plots of $f_2(x, y)$ in (5.3.13).

Define an initial setup (Case III) with vortices centered at a regular 2N-side polygon:

$$\boldsymbol{x}_j^0 = C_\Omega + L\left(\cos(\frac{(2j-1)\pi}{2N}), \sin(\frac{(2j-1)\pi}{2N})\right), d_j = (-1)^{j-1}, \tag{5.3.14}$$

for $j = 1, 2, \cdots, 2N$ and $L \in (0, 1/2)$.

Lemma 5.3 (A vortex octagon type periodic solution of the RDLs). *For initial value chosen as the Case III setup with $N = 4$, the solution of (5.3.2) is $\boldsymbol{x}_1 = C_\Omega + (-\alpha(t), -\beta(t))^T$, $\boldsymbol{x}_2 = C_\Omega + (-\beta(t), -\alpha(t))^T$, $\boldsymbol{x}_3 = C_\Omega + (\beta(t), -\alpha(t))^T$, $\boldsymbol{x}_4 = C_\Omega + (\alpha(t), -\beta(t))^T$, $\boldsymbol{x}_5 = C_\Omega + (\alpha(t), \beta(t))^T$, $\boldsymbol{x}_6 = C_\Omega + (\beta(t), \alpha(t))^T$, $\boldsymbol{x}_7 = C_\Omega + (-\beta(t), \alpha(t))^T$, $\boldsymbol{x}_8 = C_\Omega + (-\alpha(t), \beta(t))^T$, and $d_j = (-1)^{j-1}$, with $(\alpha(t), \beta(t))$ satisfies*

$$f_3(\alpha(t), \beta(t)) = f_3(\alpha^0, \beta^0), \tag{5.3.15}$$

where

$$\begin{aligned} f_3(x, y) =& F(2x, 2y) - F(2x, 0) - F(0, 2y) - F(x+y, x+y) \\ &- (F(x-y, x-y) - F(x+y, x-y) - F(x-y, x+y)). \end{aligned} \tag{5.3.16}$$

For the general rectangular domain, there still exist periodic solutions as stated in Lemma 5.1 and Lemma 5.2. Inspired by the periodic boundary conditions of the PDE problem, there should be periodic solutions if we duplicate the initial vortex configuration several times. If the total vortex number equals to $4N$ for some $N \in \mathbb{N}^+$, there exists some configuration of initial vortices to assure periodic solutions for the RDLs. One example is stated in following theorem.

Theorem 5.2 (A periodic solution of the RDLs with 4N initial vortices)**.** *If the initial configuration of the* $4N$ *vortices are* $\boldsymbol{x}^0_{4k-3} = C_k + (-\alpha^0, -\beta^0)$, $\boldsymbol{x}^0_{4k-2} = C_k + (\alpha^0, -\beta^0)$, $\boldsymbol{x}^0_{4k-1} = C_k + (\alpha^0, \beta^0)$, $\boldsymbol{x}^0_{4k} = C_k + (-\alpha^0, \beta^0)$, $d_{4k-3} = d_{4k-1} = 1$ *and* $d_{4k-2} = d_{4k} = -1$ *with* $C_k = (1/2, \frac{2k-1}{2N})$, *for* $k = 1, 2, \cdots N$, *then the vortices trajectories from the RDLs are of form* $\boldsymbol{x}_{4k-3} = C_k + (-\alpha(t), -\beta(t))$, $\boldsymbol{x}_{4k-2} = C_k + (\alpha(t), -\beta(t))$, $\boldsymbol{x}_{4k-1} = C_k + (\alpha(t), \beta(t))$, *and* $\boldsymbol{x}_{4k} = C_k + (-\alpha(t), \beta(t))$, *with* $\alpha(t)$ *and* $\beta(t)$ *on the level set of function*

$$f_p(\alpha, \beta) = \sum_{k=1}^{N} \left(F(0, \frac{k-1}{N} - 2\beta) - F(2\alpha, \frac{k-1}{N} - 2\beta) + F(2\alpha, \frac{k-1}{N}) \right). \quad (5.3.17)$$

The proof is similar to 5.1. Figure 5.5 shows an example for $N = 3$. The vortex orbits in the left figure are of the same shape as the level sets of f_p in the middle picture, also the numerical value of $f_p(\alpha(t), \beta(t))$ corresponding to the orbits converges to a constant when the time step decreasing.

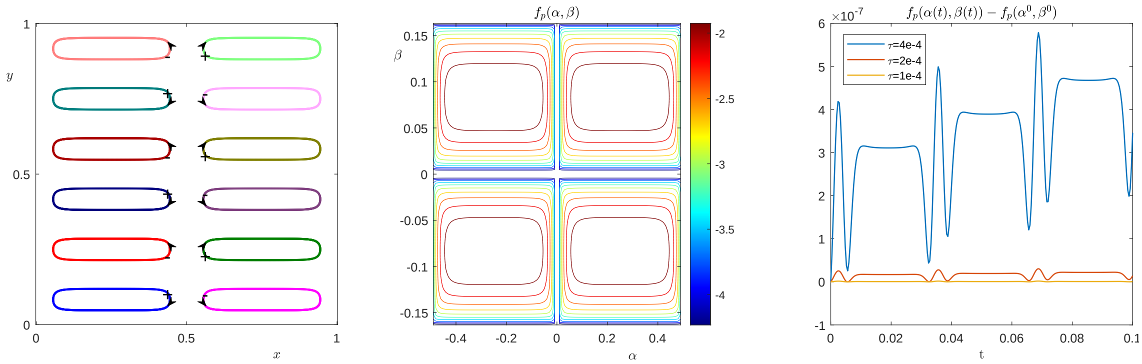

Figure 5.5: Vortex trajectories of duplicated initial data with $N = 3$ (left); contour line plot of the f_p (middle); values of $f_p(\alpha(t), \beta(t))$ corresponding to the numerical solutions of the RDLs with different time step sizes (right).

5.4 Numerical methods

5.4.1 A time splitting Fourier spectral method for NLSE

Since we have periodic boundary condition, Fourier pseudo-spectral method in space is the first choice for its computational efficiency [13,15,102]. In time direction, we adopt the standard Strang splitting method as in [4,14,27,83] as follows.

Let $\tau > 0$ be the time step for numerical simulations and for each $(n+1)$-th time step evolution ($n \in \mathbb{N}$), split the NLSE (5.1.1) into the following two equations:

$$i\partial_t \psi^\varepsilon(\boldsymbol{x}, t) = \frac{1}{\varepsilon^2}(1 - |\psi^\varepsilon|^2)\psi^\varepsilon, \;\; \boldsymbol{x} \in \Omega, \tag{5.4.1}$$

$$i\partial_t \psi^\varepsilon(\boldsymbol{x}, t) = \Delta\psi^\varepsilon, \;\; \boldsymbol{x} \in \Omega. \tag{5.4.2}$$

In each time step evolution, we do following three steps:

1. solve (5.4.1) with initial data $\psi^\varepsilon(\boldsymbol{x}, t_n) = \psi^\varepsilon_n(\boldsymbol{x})$ to $t = t_n + \frac{\tau}{2}$, and denote the solution at time $t_n + \frac{\tau}{2}$ as $\psi^\varepsilon_*(\boldsymbol{x})$;

2. solve (5.4.2) with initial data $\psi^\varepsilon(\boldsymbol{x}, t_n) = \psi^\varepsilon_*(\boldsymbol{x})$ to time $t = t_{n+1}$ by Fourier spectral method, and denote the solution at time t_{n+1} as $\psi^\varepsilon_{**}(\boldsymbol{x})$;

3. solve (5.4.1) from $t = t_n + \frac{\tau}{2}$ to $t = t_{n+1}$ with initial data $\psi^\varepsilon(\boldsymbol{x}, t_n + \frac{\tau}{2}) = \psi^\varepsilon_{**}(\boldsymbol{x})$ and take the solution at time t_{n+1} as $\psi^\varepsilon_{n+1}(\boldsymbol{x})$.

Remarks:

- For the first time evolution step, $\psi^\varepsilon_0(\boldsymbol{x})$ is the initial data; for the subsequent $(n+1)$-th step, the $\psi^\varepsilon_n(\boldsymbol{x})$ is the result of n-th step.

- As the splitting operation in [21] pointed out, the special structure of the nonlinear terms in (5.1.1) determine that the solution ψ^ε of (5.4.1) satisfies

$$\partial_t |\psi^\varepsilon(\boldsymbol{x}, t)|^2 = 0, \tag{5.4.3}$$

and that there is an analytical solution of (5.4.1):

$$\psi^\varepsilon(\boldsymbol{x}, t) = \psi^\varepsilon(\boldsymbol{x}, t_n) \exp\left(-\frac{i(t - t_n)}{\varepsilon^2}(1 - |\psi^\varepsilon(\boldsymbol{x}, t_n)|^2)\right), \quad \text{for } t \geq t_n, \boldsymbol{x} \in \Omega. \tag{5.4.4}$$

This unchanged density of (5.4.1) gives us a convenient to combine the last step in n-th iteration together with the first step in the $(n+1)$-th to save some computational resources.

5.4.2 A 4cFD method to prepare the initial data

In the numerical discretization of initial data, we use fourth-order compact finite difference to approximate $\Delta q(\boldsymbol{x}) = 0$. After rearranging the numerical value of $q(\boldsymbol{x})$ on grid points into a vector $\mathbf{q}$, combining the boundary condition in (5.2.7), we can formulate a linear system of form

$$A\mathbf{q} = \mathbf{b}. \tag{5.4.5}$$

The matrix A is one rank lower than full rank. Combined with an additional requirement $\sum_l q_l = 0$, we can get a unique $\mathbf{q}$. This is consistent with the continuous case in (5.2.7) where $q(\boldsymbol{x})$ is only unique up to a constant. In the following part of this section, the detailed construction of A and $\mathbf{q}$ is presented.

Here we give the numerical scheme for calculating the $q(x)$ on $\Omega = (0, a) \times (0, b)$ [22]. For two positive integers J and K, let space-steps be $h_1 = a/J$ and $h_2 = b/K$. Denote $x_j = jh_1$, for $j \in \mathcal{T}_J^0 = \{0, 1, \cdots, J\}$, $y_k = kh_2$, for $k \in \mathcal{T}_K^0 = \{0, 1, \cdots, K\}$, and the spatial grid points $\Omega_h = \{(x_j, y_k) : j \in \mathcal{T}_J^0, k \in \mathcal{T}_K^0\}$. For simplicity, denote $\Phi(x, y) = \mathrm{Arg}(\psi_{DC}^{\varepsilon}(x, y))$, $\Phi^1(x, y) = \partial_x \Phi(x, y)$ and $\Phi^2(x, y) = \partial_y \Phi(x, y)$. Let $q_{j,k}$ be the numerical approximation of $q(x_j, y_k)$ and denote $\Phi_{j,k} = \Phi(x_j, y_k)$, $\Phi_{j,k}^1$ and $\Phi_{j,k}^2$ are defined similarly. We introduce the finite difference operator as in formal sections

$$\delta_x^+ u_{j,k} = \frac{u_{j+1,k} - u_{j,k}}{h_1}, \quad \delta_x^- u_{j,k} = \frac{u_{j,k} - u_{j-1,k}}{h_1},$$
$$\delta_x^2 u_{j,k} = \delta_x^- \delta_x^+ u_{j,k} = \frac{u_{j+1,k} - 2u_{j,k} + u_{j-1,k}}{h_1^2}.$$

The spatial 4th-order compact finite difference operator $\mathcal{A}_{h1}$ is defined as

$$\mathcal{A}_{h1} u_j^n = (I + \frac{h_1^2}{12}\delta_x^2) u_{j,k} = \frac{1}{12}(u_{j-1,k} + 10u_{j,k} + u_{j+1,k}), \quad j \in \mathcal{T}_J. \tag{5.4.6}$$

Notations of δ_y^+, δ_y^-, δ_y^2 and $\mathcal{A}_{h2}$ are denoted similarly. Then, the compact finite difference discretization of (5.2.7) is

$$\mathcal{A}_{h1}^{-1}\delta_x^2 q_{j,k} + \mathcal{A}_{h2}^{-1}\delta_y^2 q_{j,k} = 0, \quad j \in \mathcal{T}_J, k \in \mathcal{T}_K, \tag{5.4.7}$$

with equations from the periodic boundary condition

$$q_{0,k} + \Phi_{0,k} = q_{J,k} + \Phi_{J,k}, k \in \mathcal{T}_K^0, \tag{5.4.8}$$

$$q_{j,0} + \Phi_{j,0} = q_{j,K} + \Phi_{j,K},\ j \in \mathcal{T}_J^0, \tag{5.4.9}$$

$$q_{0,k}^1 + \Phi_{0,k}^1 = q_{J,k}^1 + \Phi_{J,k}^1, k \in \mathcal{T}_K^0, \tag{5.4.10}$$

$$q_{j,0}^2 + \Phi_{j,0}^2 = q_{j,K}^2 + \Phi_{j,K}^2,\ j \in \mathcal{T}_J^0, \tag{5.4.11}$$

where $q_{0,k}^1 = \frac{1}{h_1}\left(-\frac{11}{6}q_{0,k} + 3q_{1,k} - \frac{3}{2}q_{2,k} + \frac{1}{3}q_{3,k}\right)$ that comes from a one-side Taylor expansion for $q(\boldsymbol{x})$ at $(0, y_k)$ to approximate $\partial_x q(0, y_k)$. Similarly, we have $q_{J,k}^1 = \frac{1}{h_1}\left(\frac{11}{6}q_{J,k} - 3q_{J-1,k} + \frac{3}{2}q_{J-2,k} - \frac{1}{3}q_{J-3,k}\right)$, $q_{j,0}^2 = \frac{1}{h_2}\left(-\frac{11}{6}q_{j,0} + 3q_{j,1} - \frac{3}{2}q_{j,2} + \frac{1}{3}q_{j,3}\right)$, $q_{j,K}^2 = \frac{1}{h_2}\left(\frac{11}{6}q_{j,K} + 3q_{j,K-1} - \frac{3}{2}q_{j,K-2} + \frac{1}{3}q_{j,K-3}\right)$. Note that we have $(J+1)\times(K+1)$ unknowns of $q_{j,k}$ and we have $(J-1)\times(K-1)$ equations of form (5.4.7) and $2J+2K$ equations from (5.4.8)-(5.4.11). Therefore, we can rearrange (5.4.7)-(5.4.11) into a linear system of form (5.4.5) with A a squared matrix having $(J+1)\times(K+1)$ rows. Since $(1, 1, \cdots, 1)$ is an eigenvector of A with corresponding eigenvalue 0, we know $\text{rank}(A) = (J+1)\times(K+1) - 1$. Form the construction of our $\psi_{DC}^{\varepsilon}(x, y)$ for periodic initials, we know $\int_{\partial\Omega} \nabla\Phi d\mathbf{n} = 0$ and the summation of elements of $\mathbf{b}$ in (5.4.5) converges to zero as $h \downarrow 0$. Thus we can solve (5.4.5) by least square method and get a periodic initial phase for vortex dynamics simulations.

5.5 Verification for the RDLs

In our numerical simulation of the NLSE with periodic BCs, we use phase transition along grid points combined with the convexity of module to detect the position of vortex centers. Since we have second order accuracy in time and spectral accuracy in space, our vortex centers position can achieve higher accuracy than the mesh-size in space h. We can apply linear interpolation to the numerical value of ψ^ε on grid points and then apply the detecting rules [20, 21, 127] to the interpolated numerical values. In practice, we detect the vortex center to $O(h^2)$ accuracy. In following context, we use $\boldsymbol{x}_j^\varepsilon(t)$ and $\boldsymbol{x}_j(t)$ to denote the j-th vortex center corresponding to the NLSE and the RDLs respectively. Let $\delta_j^\varepsilon(t) = |\boldsymbol{x}_j^\varepsilon(t) - \boldsymbol{x}_j(t)|$ and define

$$\delta^\varepsilon(t) = \max_j \delta_j^\varepsilon(t) \tag{5.5.1}$$

as a measurement of the difference of trajectories between the RDLs and numerical solutions of the NLSE.

5.5.1 Vortex interactions of 4 vortices

As in section 5.2.3, the simplest configuration of zero initial momentum of simple vortices needs four vortices with zero weighted mass center (5.2.8). There is a list of phase and density plot of $\psi^\varepsilon(\boldsymbol{x}, t)$ for Case I setup in Figure 5.6. The mesh size is chosen as $h = \frac{1}{512}$ and $\tau = 5 \times 10^{-7}$. From $t = 0$ to $t = 0.12$, each vortex moves on a loop with the shape of a square with round corners. The four snapshots are corresponding to the times when vortices are in corners of each loops.

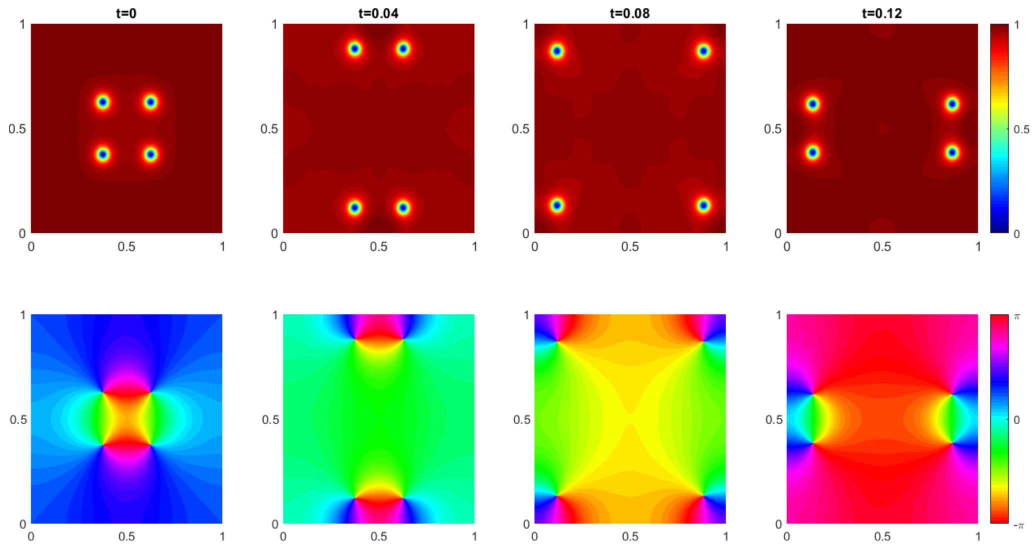

Figure 5.6: Contour plots of the density (first row) and phase (second row) of $\psi^\varepsilon(\boldsymbol{x}, t)$ with Case I initials and $(\alpha^0, \beta^0) = (\frac{1}{8}, \frac{1}{8})$ at time $t = 0, 0.04, 0.08, 0.12$ for $\varepsilon = \frac{1}{64}$.

We show the convergence test of Case I setups in Figure 5.7. The left picture of the first row depicts the vortex center trajectories from the RDLs on Ω. Since there are some overlaps after one period, we plot the coordinates of 2 representative vortices w.r.t. time t in the right side picture. The points denoted by $\circ$, $\triangle$ and $\Diamond$ are corresponding to the positions of vortex centers in Figure 5.6 for $t = 0.04, 0.08$, and 0.12 respectively. The last row shows the convergence of vortex trajectories from numerical simulations to RDLs: as $\varepsilon \downarrow 0$, δ^ε in (5.5.1) decreases to zero.

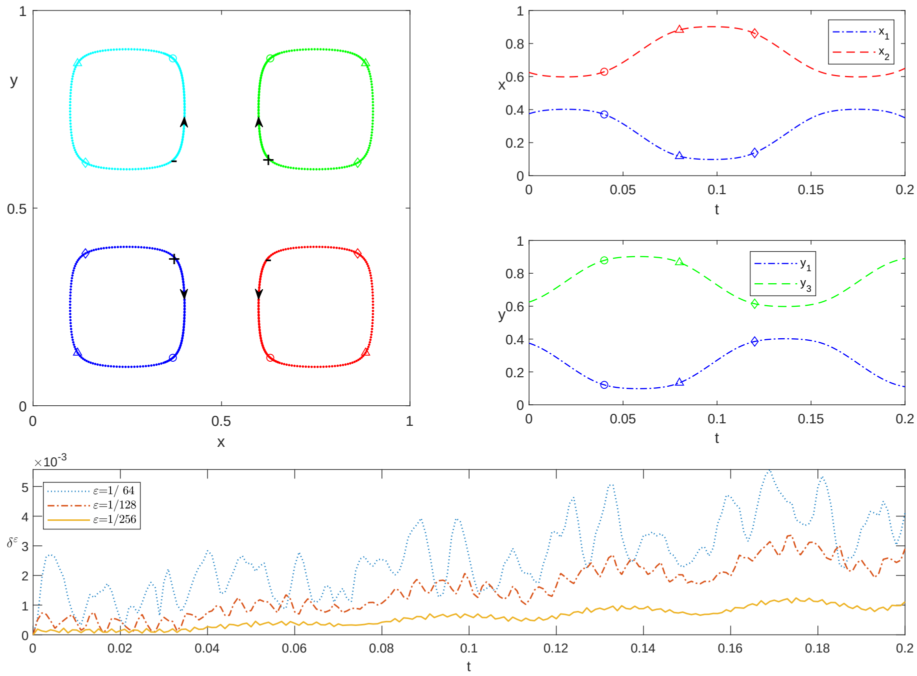

Figure 5.7: Convergence test for the Case I setup with $(\alpha^0, \beta^0) = (\frac{1}{8}, \frac{1}{8})$.

The three charts in Figure 5.8 are vortex trajectories form numerical simulation with Case I setups with $(\alpha^0, \beta^0) = (\frac{1}{16}, \frac{1}{16}), (\frac{1}{8}, \frac{1}{8})$ and $(\frac{3}{16}, \frac{3}{16})$.

Although we have periodic orbits for solutions of the RDLs, the numerical simulation will not preserve the periodic pattern for a long time simulation. The reason is that the periodic orbits come from symmetry and they are not stable. We can see this by solving (5.3.2) with initial values $\boldsymbol{x}_j^0$'s perturbed a little bit. The corresponding trajectories are showed in Figure 5.9.

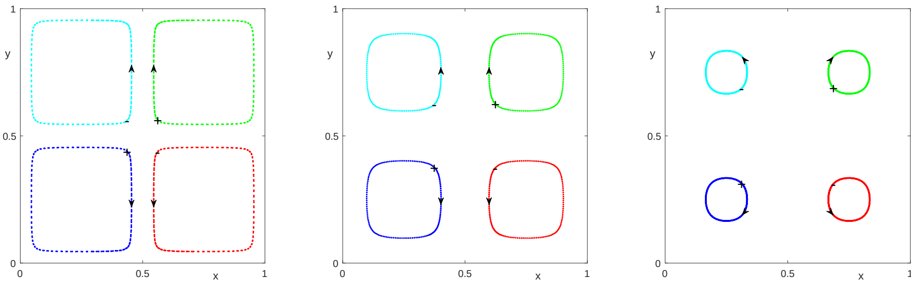

Figure 5.8: Vortex trajectories detected form numerical simulation for $\varepsilon = \frac{1}{128}$.

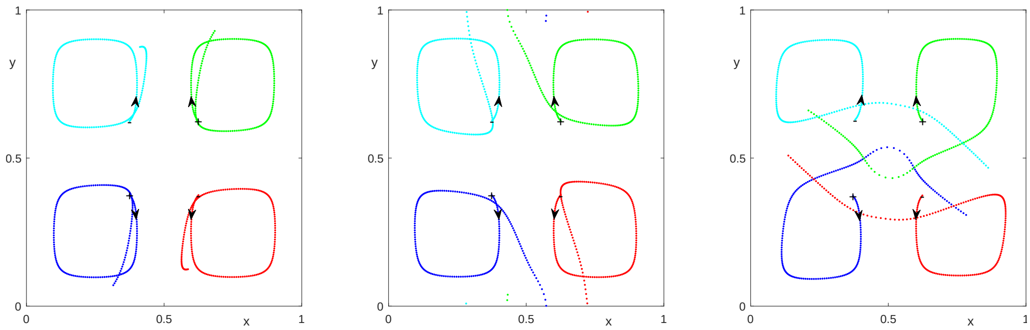

Figure 5.9: Trajectories from the RDLs with $O(\frac{1}{1000}), O(\frac{1}{500})$, and $O(\frac{1}{100})$ perturbations on the initial position of vortices in Case I setup with $(\alpha^0, \beta^0) = (\frac{1}{8}, \frac{1}{8})$.

Numerical simulations on Case II setups

We simulate vortex interactions with collinear initial data of Case II setups and show the convergence test in Figure 5.12. The first row shows the periodicity solution of RDLs and the trajectory plots coincide well with the level sets in Figure 5.7. The second row shows the convergence of vortex trajectories from numerical simulations to RDLs very well. In Figure 5.10 and 5.11, snapshots of density plots are listed to show a period of vortex motions with Case II setups. Artificial lines of vortex center trajectories are added to the density plots for a good understanding of vortex center motions.

As mentioned in Section 5.3.2, the solution of the RDLs has two topological types for $L_1 = \frac{1}{4}$. One kind has orbits crossing the boundary $y = 1, y = 0$ and the other kind does not. If we view the two kinds of orbits on $\mathbb{T}^2$, they belong to different

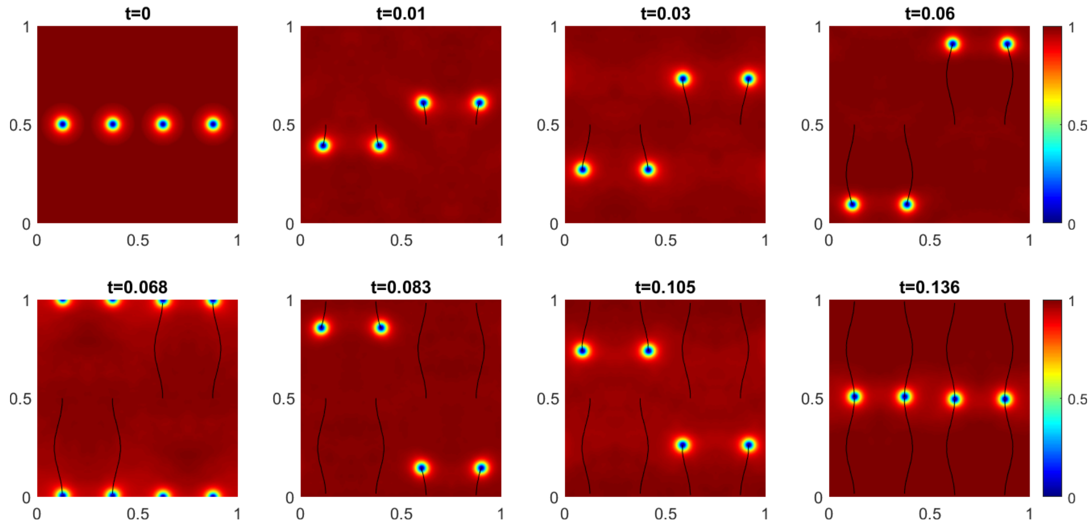

Figure 5.10: Density plots of Case II type setups with $(L_1, L_2) = (\frac{1}{4}, \frac{1}{8}), \varepsilon = \frac{1}{64}$.

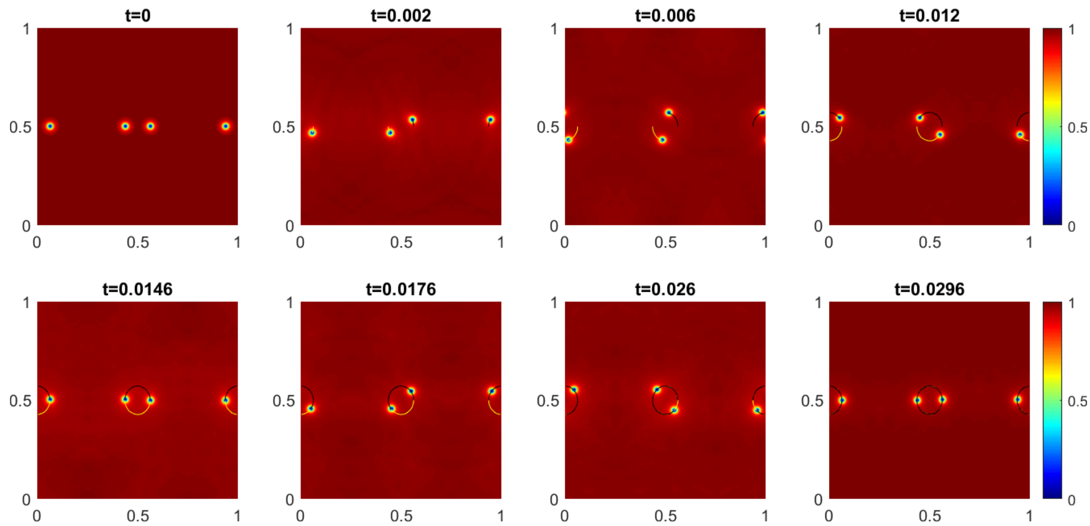

Figure 5.11: Density plots of Case II type setups with $(L_1, L_2) = (\frac{1}{4}, \frac{3}{16}), \varepsilon = \frac{1}{128}$.

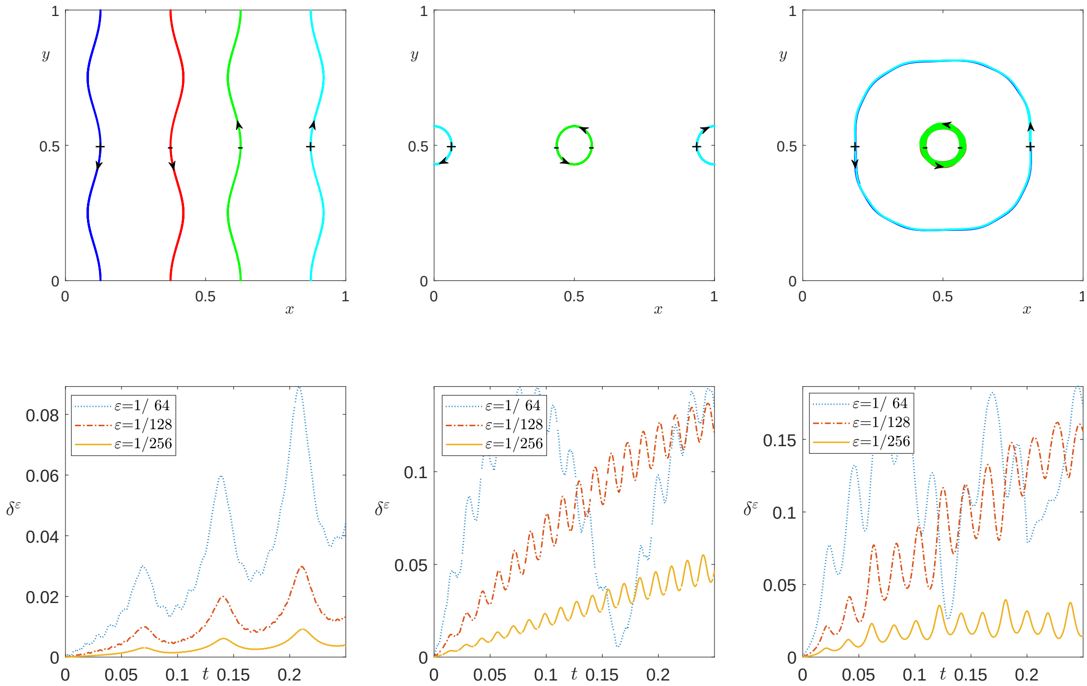

Figure 5.12: Convergence test on some Case II type setups with $(L_1, L_2) = (\frac{1}{4}, \frac{1}{8}), (\frac{1}{4}, \frac{3}{16})$ and $(\frac{3}{16}, \frac{1}{8})$ (from left to right).

homotopy classes of loops. A loop moves through an orbit in the first picture of Figure 5.12 once is isomorphic to $(1, 0)$ of the fundamental group of $\mathbb{T}^2$, and a loop moves through an orbit in the second picture is isomorphic to 0. When L_2 is small, the vortex dipole interaction effect takes control and the trajectories are almost two paralleling moving vortex dipoles; when L_2 is large, the vortex pair interaction effect dominates and the trajectories are almost two rotated vortex pairs. Since ODEs are easier to solve rather than PDEs, we can study the critical L_2 as a parameter for bifurcation. We get the critical $L_2 = 18169/2^{17}$ with accuracy $O(\frac{1}{2^{17}})$ using bisection method and this result coincides well with the result from the saddle point of f_2 in (5.3.13) up to the fourth decimal place. Two kinds of orbits near the bifurcation parameter is drawn in Figure 5.13. The left column of the figure plots the axes of vortex centers w.r.t. time t. For the first case, L_2 is less than the critical value and $x_2(t)$ does not intersect with $x_3(t)$; the second case has L_2 greater than the critical value and vortices $\boldsymbol{x}_2$ and $\boldsymbol{x}_3$ rotate about each other.

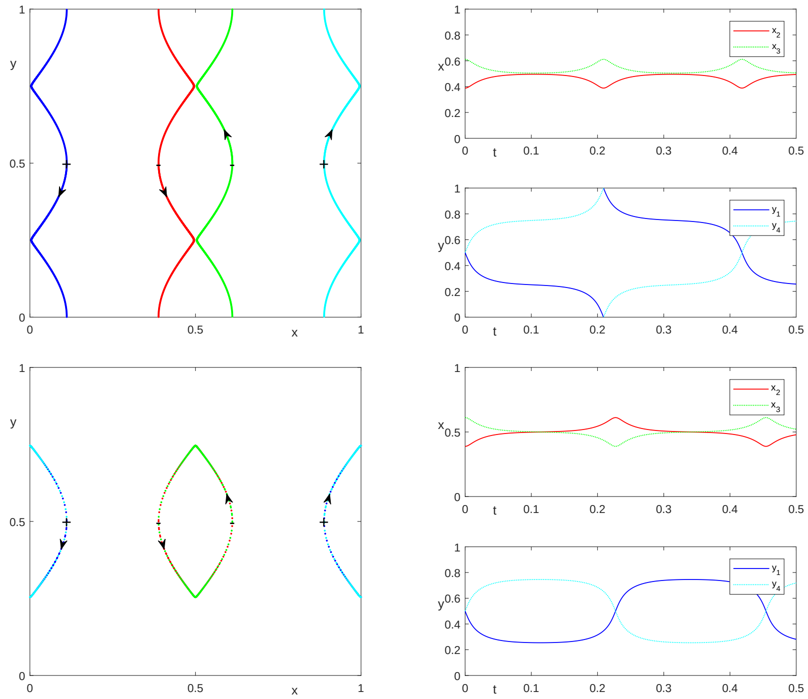

Figure 5.13: Trajectories from the RDLs of Case II setups with $(L_1, L_2) = (\frac{1}{4}, \frac{4541}{2^{15}})$ (first row) and $(L_1, L_2) = (\frac{1}{4}, \frac{4543}{2^{15}})$ (second row).

We do one challenging simulation to see how the vortex moves if the L_2 is near the bifurcation point. Trajectories of vortex centers detected form the solution of NLSE and relating convergence test are in Figure 5.14. The trajectories in Figure 5.14 are pretty different from solutions of the RDLs in Figure 5.13. $\delta^\varepsilon(t)$'s increase rapidly This is also reflected from the plots of δ^ε's which increase a lot after $t = 0.1$. This sharp change is due to the intrinsic bifurcation of (5.3.2) with intentionally constructed initial data we discussed before.

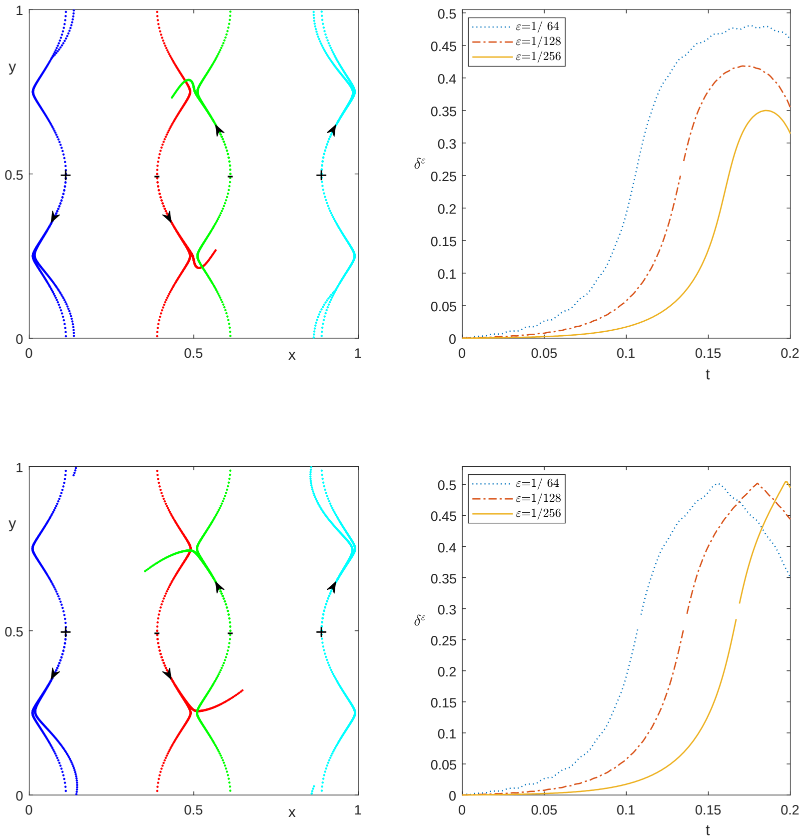

Figure 5.14: Trajectories from numerical simulations with the same initial setups as Figure 5.13 for $\varepsilon = \frac{1}{256}$ (left); corresponding convergence test (right).

5.5.2 Vortex interactions of 6 vortices and beyond

In this section, let us consider vortex interactions of polygonal distributed vortices as the Case III mentioned in Section 5.3.2 with initial vortex profiles satisfying (5.3.14). For the motion of vortex hexagon of Case III setups with $N = 3$ and $L = 1/3$, we show a series of density plots for the vortex interactions with $\varepsilon = \frac{1}{128}$ in Figure 5.15. The black dot lines in the density plots are artificial lines to indicate the continuous motion of vortex centers, which provides better understanding of the dynamics of vortices, especially for the cases with complex vortex interactions. The convergence to RDLs as $\varepsilon \downarrow 0$ is show in Figure 5.16: the trajectories of vortex centers converges to the RDLs as $\varepsilon \downarrow 0$. Note the discontinuity of $\delta^\varepsilon(t)$ is due to the failure detection of vortex centers who are crossing the boundaries.

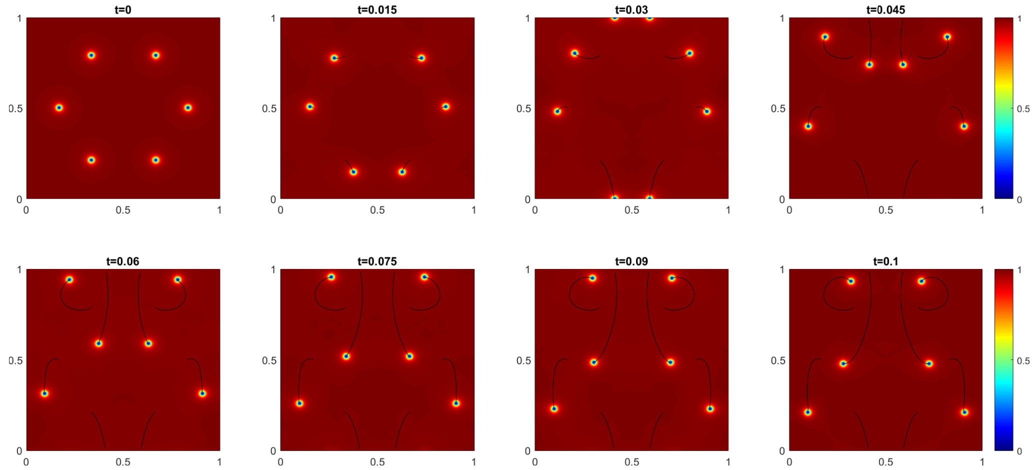

Figure 5.15: Density plots of $\psi^\varepsilon(\boldsymbol{x}, t)$ for a vortex hexagon with $\varepsilon = \frac{1}{128}$ at different instants.

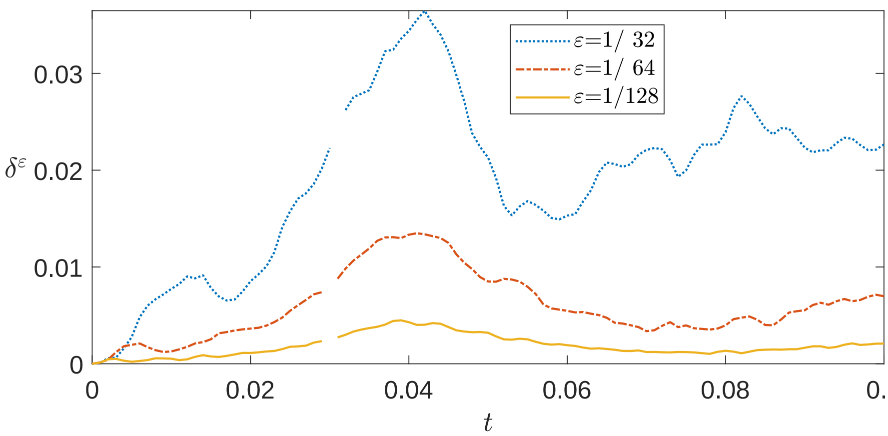

Figure 5.16: Convergence test on Case III initials of vortex hexagon with $L = \frac{1}{3}$.

To compare with periodic trajectories from RDLs of Case III setup with eight vortices in Lemma 5.3, we carry a simulation on the interaction of vortex octagons. Figure 5.17 shows eight snapshots of the density distribution for almost one period.

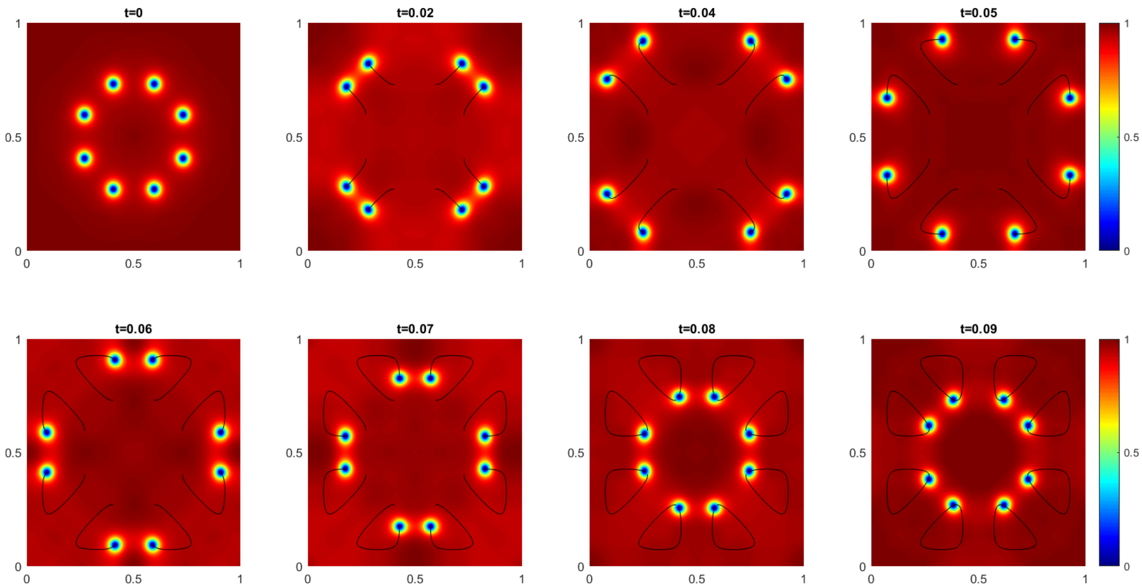

Figure 5.17: Density plots of $\psi^\varepsilon(\boldsymbol{x}, t)$ for a vortex octagon with $\varepsilon = \frac{1}{64}$ at different instants.

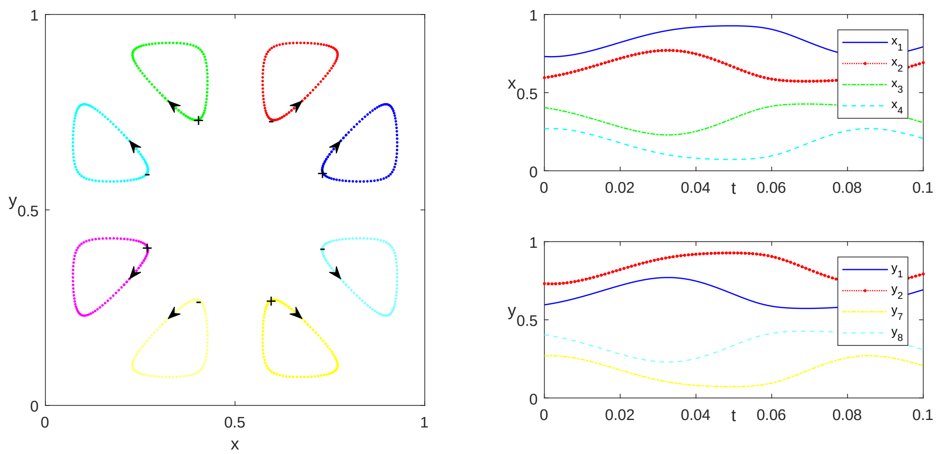

Figure 5.18: Trajectories of the vortex octagon from RDLs up to $T = 0.1$.

5.6 Numerical results for the nonzero initial momentum limit

5.6.1 Numerical results for 2 vortices

As mentioned in section 5.2, a vortex dipole is the most simple configuration of vortices for periodic BCs. We fist start our simulation of vortex interactions of a dipole with $\boldsymbol{x}_1^0 = (\frac{1}{2} - \alpha^0, \frac{1}{2} - \beta^0), \boldsymbol{x}_2^0 = (\frac{1}{2} + \alpha^0, \frac{1}{2} + \beta^0), d_1 = 1, d_2 = -1$ (Case IV) on $\Omega = (0,1)^2$. The ODE for the limiting case of vortex motion is simple due to less vortex interaction. Based on our numerical simulations, we observed that the vortex center for the limiting case ($\varepsilon \downarrow 0$) is paralleling moving with a fixed speed:

$$\dot{\boldsymbol{x}}_1 = \dot{\boldsymbol{x}}_2 = -2\left(\nabla \times \mathbf{F}(2\alpha^0, 2\beta^0) + \mathbf{P}_0\right). \tag{5.6.1}$$

We do the numerical simulation of the NLSE under Case IV setup with $(\alpha^0, \beta^0) = (0, \frac{1}{8})$ for $\varepsilon = \frac{1}{64}, \frac{1}{128}$ and $\frac{1}{256}$ up to $T = 0.06$. Here is a list of snapshots of a vortex dipole with initial vortex center distance $\frac{1}{4}$ on y-axis in Figure 5.19. The vortex centers move parallelly to the direction of x-axis, and they can cross the boundary near t=0.052 due to the periodic BCs. In another view, the dipole moves out through the right boundary and then a new dipole generates from the opposite boundary. For simplicity, we regard the disappeared vortex dipole and the newly generated as a same one.

The mass, momentum and energy are showed in the first row of Figure 5.20, which affirms that the three quantities were well preserved during our simulation. Since the second component of the momentum is always 0, we only plot the first component of it. The third chart shows the relative energy define by $\mathcal{E}(t) = E(t)/E(0)$ for $\varepsilon = \frac{1}{64}$. Although the relative kinetic and potential energies ($\mathcal{E}_K$ and $\mathcal{E}_p$ respectively) vary a little bit, they are in a steady state during the motion which differs a lot with the merging case. The second row of Figure 5.20 shows the trajectories of limiting vortex centers from our observation in Ω (left) and w.r.t. time t (middle), and the last chart shows the maximum distance between $\boldsymbol{x}_j^\varepsilon(t)$'s and $\boldsymbol{x}_j(t)$'s. The

$\delta^\varepsilon(t)$ decreases as ε decreases, which shows the converges to (5.6.1) clearly.

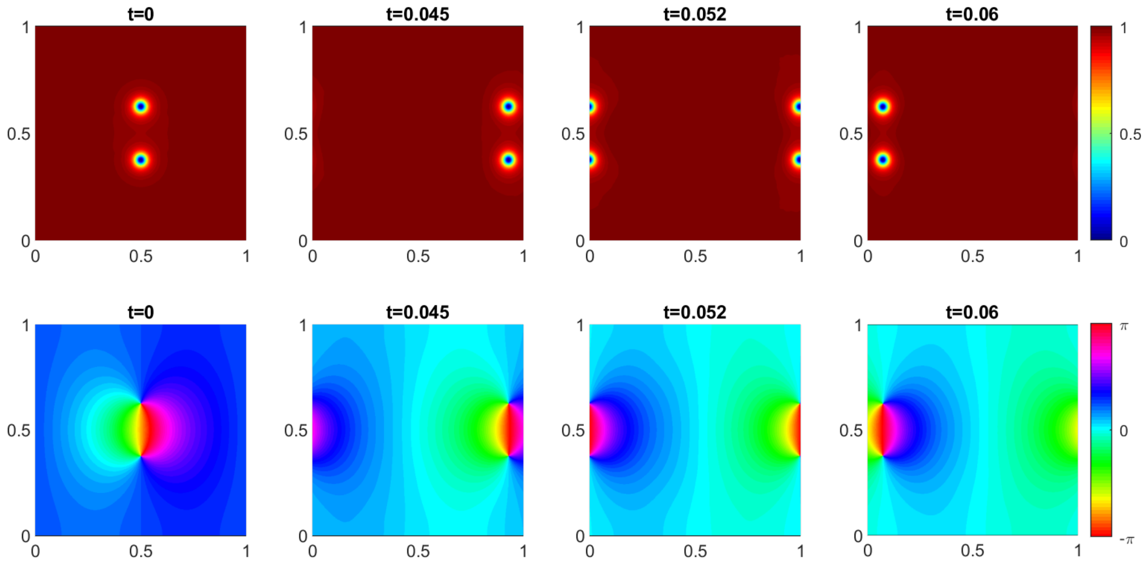

Figure 5.19: Contour plots of the density (first row) and phase (second row) of $\psi^\varepsilon(\boldsymbol{x}, t)$ at 4 moments with $\varepsilon = \frac{1}{64}$.

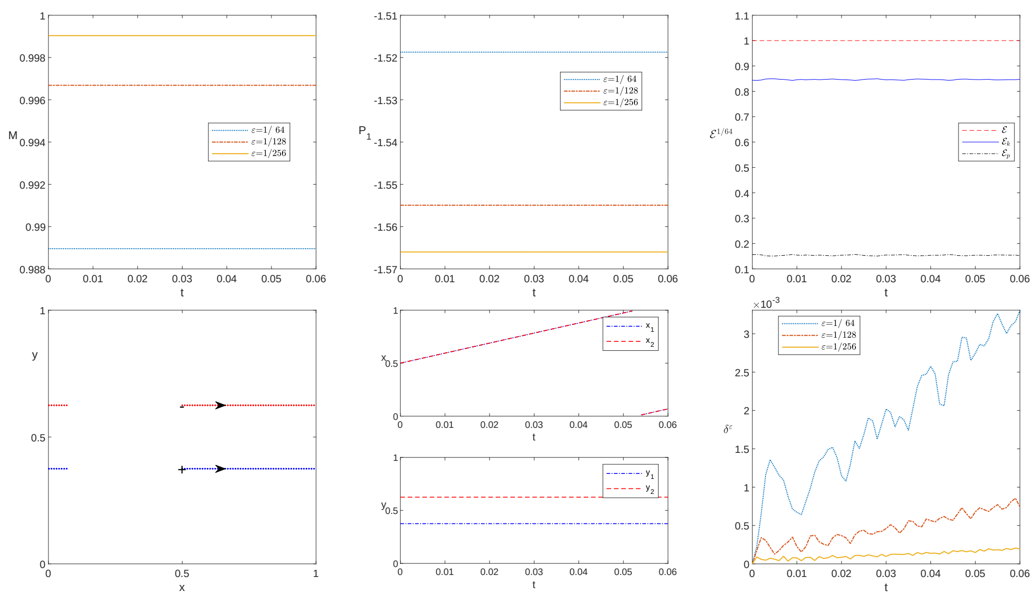

Figure 5.20: Mass, momentum and relative energy plots for Case IV initial setups with initial vortices distance $\frac{1}{4}$ (first row); limiting vortex center trajectories from (5.6.1) and convergence test (second row).

RDLs describe the limiting case of vortex center motions as $\varepsilon \downarrow 0$ only suitable for well separated initial vortices. There are notations about merger of vortices both in physical experiment [25,29,101] and theoretical studies [67]. Figure 5.21 presents an example of merging dipole snapshots for Case IV initials with $\varepsilon = 1/16$ and vortex center distance 3ε. The two vortices are overlapped at the initial moment. As time involved, the vortex dipole moves right as the well separated case in Figure 5.19 but with vortex centers moving toward each other. Finally, the two vortices merged at $t = 0.0125$, which can be see from the fourth phase plot. Vortex trajectories from numerical detection are showed in Figure 5.22. The critical merger distance denoted as δ_c, i.e. the maximum distance for vortices in a dipole that can merge, depends on ε [21] and the shape of vortex [96]. We studied the critical distance numerically and got a the relation between δ_c and ε: $\delta_c \approx 3.55\varepsilon$. From the plot of δ_c w.r.t. ε showed in Figure 5.23, the linear dependency of δ_c on ε is clear.

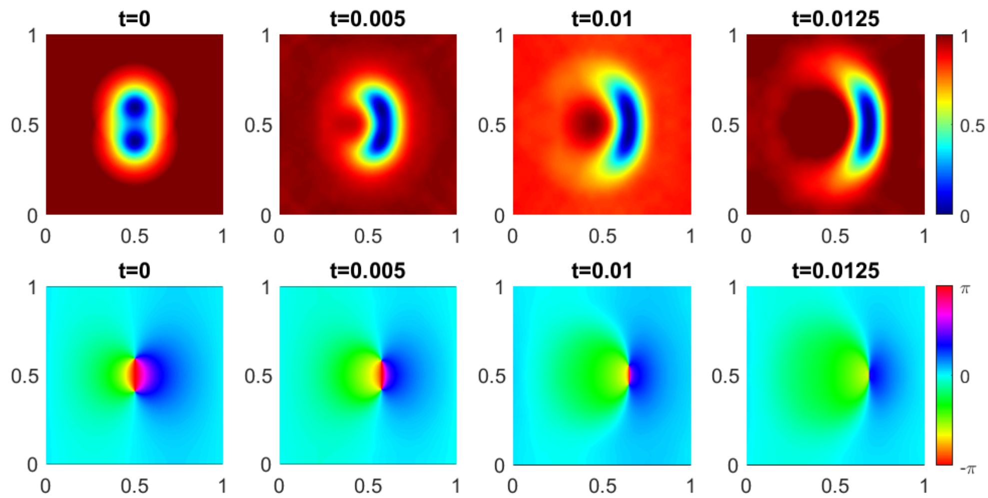

Figure 5.21: Contour plots of the density (first row) and phase (second row) of a merging dipole with $\varepsilon = \frac{1}{16}$ at 4 moments.

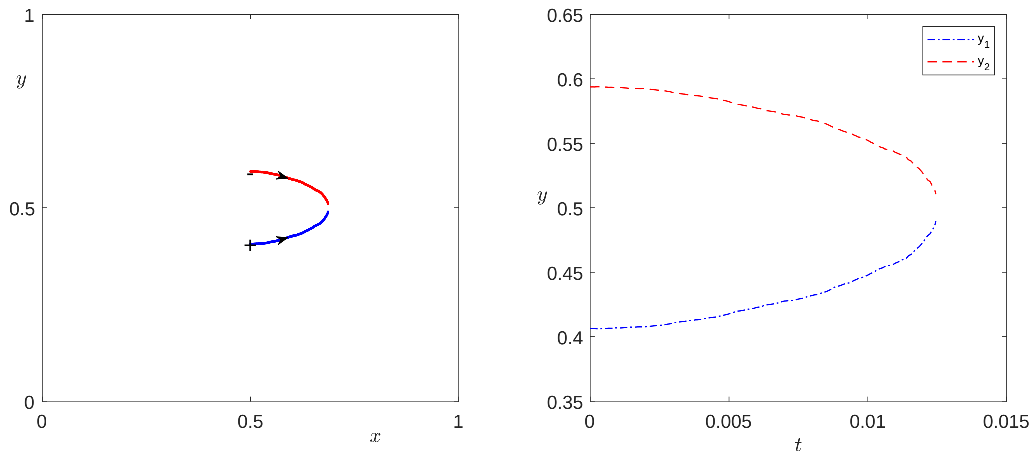

Figure 5.22: Plot of trajectories of a merging dipole in Ω (left); plot of corresponding y coordinates w.r.t. t.

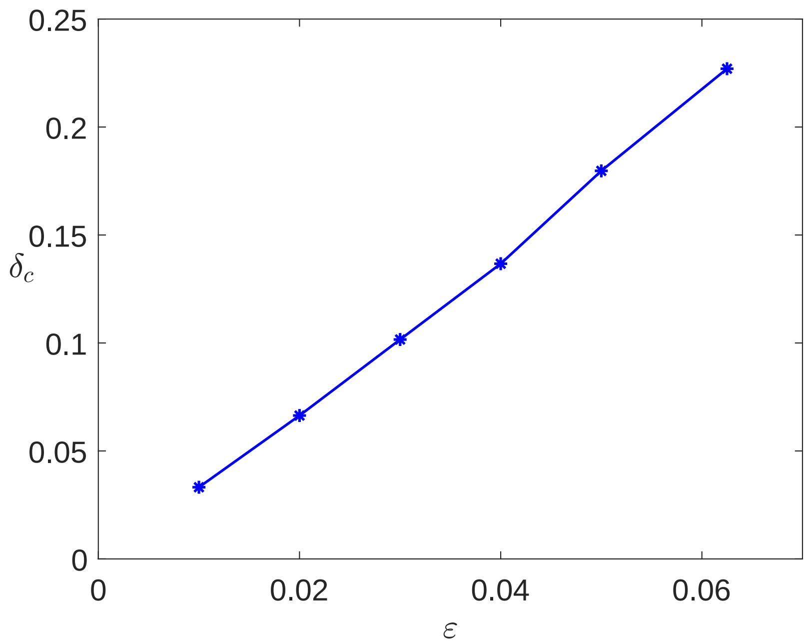

Figure 5.23: Plot of δ_c in dipole configurations w.r.t. ε.

5.6.2 Numerical results for 4 vortices

If we put two vortex dipoles parallel to each other as an initial configuration, they will do the famous leapfrogging type motion [47, 60, 94, 95]: the smaller dipole (the dipole with smaller vortex center distance) has larger speed and it will pass through the larger dipole. Later, the larger dipole will shrink into a smaller one and then move fast and experience the same motion pattern of smaller dipole again.

Let us define the Case V initial vortex configuration as $\boldsymbol{x}_1^0 = (x_1^0, \frac{1}{2} - L_1/2)^T$, $\boldsymbol{x}_2^0 = (x_2^0, \frac{1}{2} - L_2/2)^T$, $\boldsymbol{x}_3^0 = (x_1^0, \frac{1}{2} + L_1/2)^T$, $\boldsymbol{x}_4^0 = (x_2^0, \frac{1}{2} + L_2/2)^T$, with $d_1 = d_2 = 1$ and $d_3 = d_4 = -1$. Several snapshots for different moments are in Figure 5.24 and the crossing happens at around $t = 0.02$. We plot the vortex trajectories detected from the NLSE of Case V initials with $(x_1^0, x_2^0) = (\frac{1}{8}, \frac{3}{8}), L_1 = L_2 = \frac{1}{2}$ in Figure 5.25.

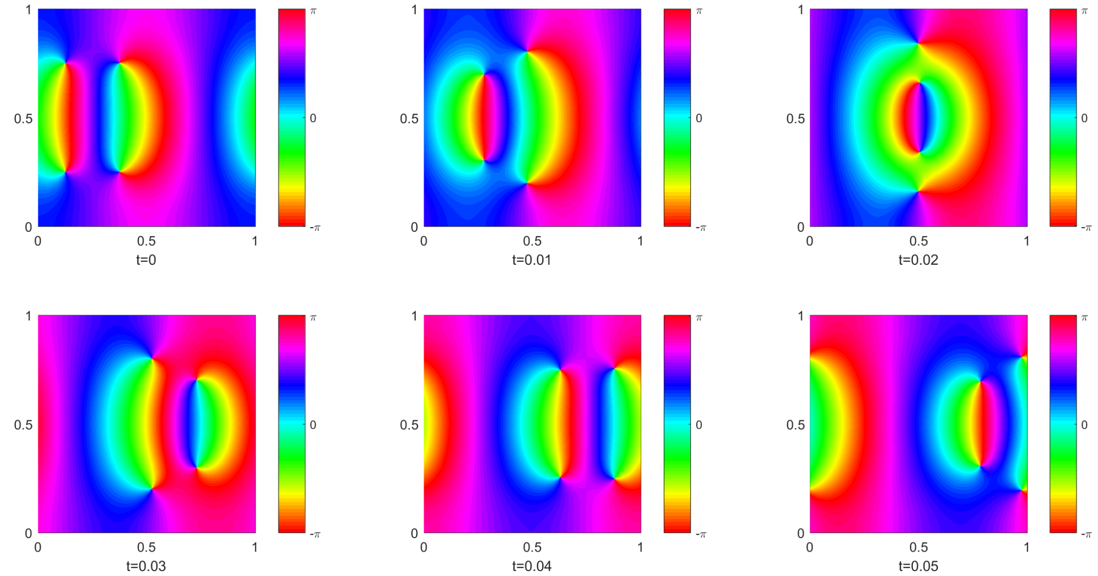

Figure 5.24: Phase snapshots of Case V with $(x_1^0, x_2^0) = (\frac{1}{8}, \frac{3}{8}), L_1 = L_2 = \frac{1}{2}$ and $\varepsilon = \frac{1}{128}$.

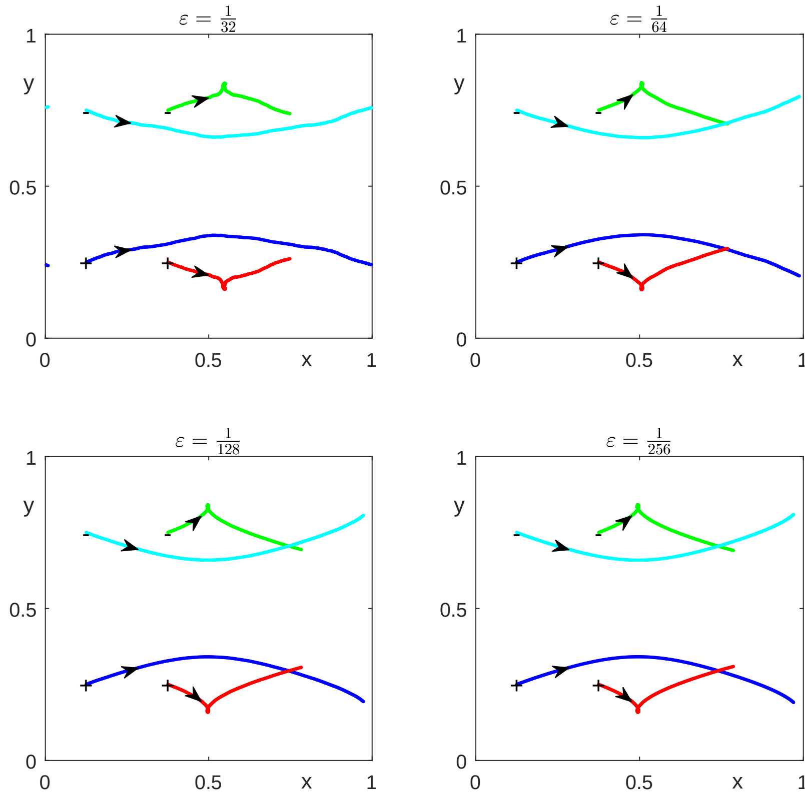

Figure 5.25: Detected vortex trajectories for Case V initials with different ε's.

5.6.3 Numerical results for 6 vortices and beyond

We carry a numerical simulation of three parallel dipoles on $\Omega = (0,2) \times (0,1)$. Let the Case VI vortex configuration be $\boldsymbol{x}_1^0 = (-L1, -L2) + C_{\boldsymbol{x}}$, $\boldsymbol{x}_2^0 = (-L1, L2) + C_{\boldsymbol{x}}$, $\boldsymbol{x}_3^0 = (0, -L2) + C_{\boldsymbol{x}}$, $\boldsymbol{x}_4^0 = (0, L2) + C_{\boldsymbol{x}}$, $\boldsymbol{x}_5^0 = (L1, -L2) + C_{\boldsymbol{x}}$, $\boldsymbol{x}_6^0 = (L1, L2) + C_{\boldsymbol{x}}$, with $d_j = (-1)^{j-1}$ and $C_{\boldsymbol{x}} = (\frac{1}{2}, \frac{1}{2})$ the mass center of all six vortices. In the first 5 snapshots of Figure 5.26, one period of leapfrogging type motion of three dipoles are shown. The vortices with the same winding number rotate about each other and the three dipoles are always parallel to $y-$axis. The ending configuration of next period is shown in the sixth snapshot.

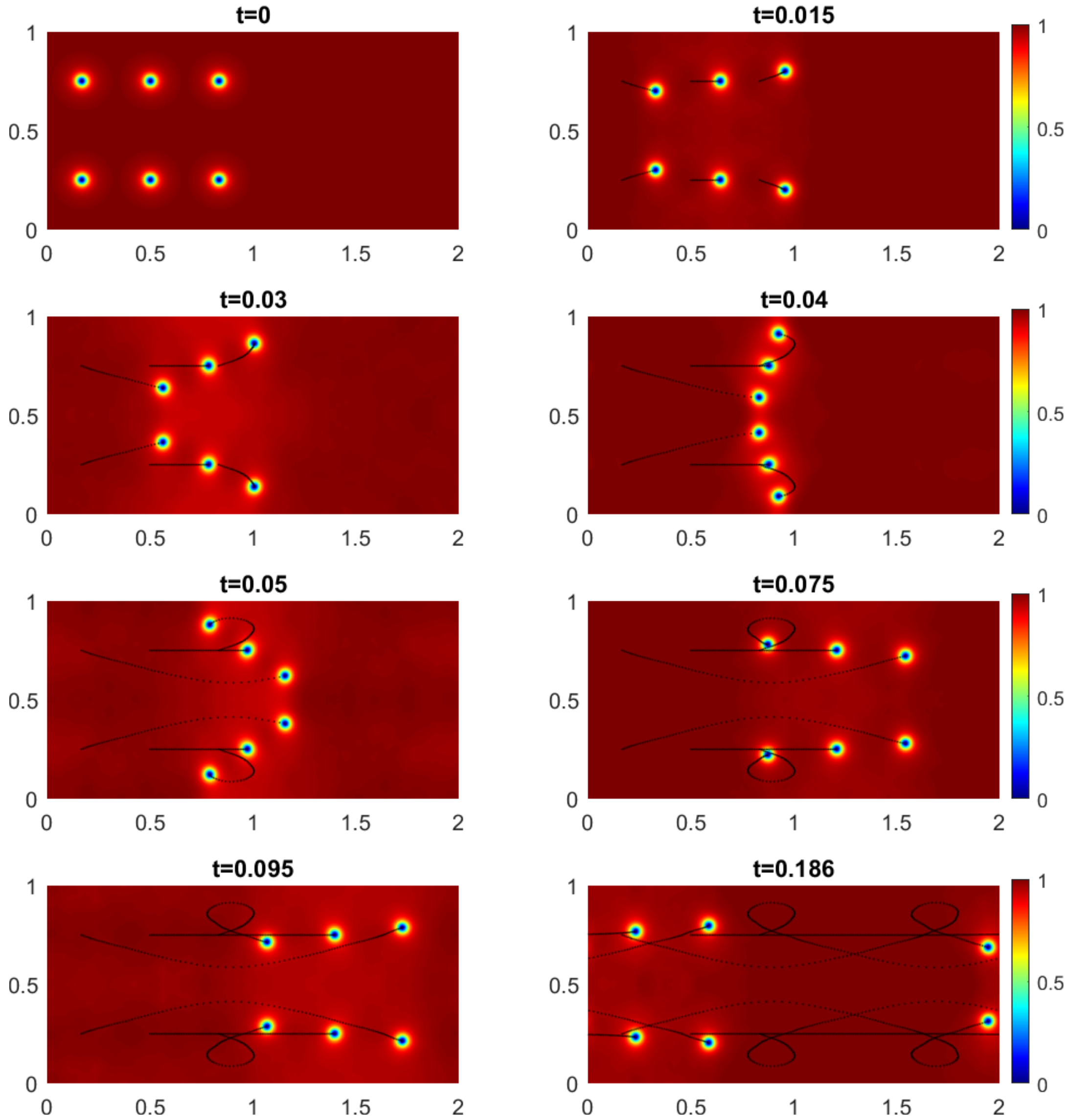

Figure 5.26: Phase snapshots of Case VI with $C_{\boldsymbol{x}} = (\frac{1}{2}, \frac{1}{2}), L_1 = \frac{1}{3}, L_2 = \frac{1}{4}$ and $\varepsilon = \frac{1}{64}$.

5.7 A conjecture on the RDLs for NLSE under periodic BCs

The sufficient conditions for periodical initial data in section 5.2.2 indicate that there are many initial setups with non-zero initial momentum limits. Therefore, we proposed our generalized reduced laws based on our numerical observations. For generality, we consider the NLSE on a rectangle domain $\Omega = (0,a) \times (0,b)$.

Conjecture 1 (Generalized reduced dynamical laws (GRDLs))**.** *For initial data ψ_0^ε satisfies the conditions of the RDLs without vanishing initial momentum limit assumption on $\Omega = (0,a)\times(0,b)$, the governing ODEs for the limit vortex trajectories are*

$$\begin{cases} \dfrac{\mathrm{d}\boldsymbol{x}_j(t)}{\mathrm{d}t} & = -2\mathbf{J}\sum\limits_{\substack{k=1\\k\neq j}}^{M} d_k \nabla F_{ab}(\boldsymbol{x}_k - \boldsymbol{x}_j) - \dfrac{2}{a^2b^2}\begin{pmatrix} b^2 & 0 \\ 0 & a^2 \end{pmatrix}\mathbf{P}_0, \\ \boldsymbol{x}_j(0) & = \boldsymbol{x}_j^0, \end{cases} \tag{5.7.1}$$

with $\mathbf{P}_0$ the limiting initial momentum and F_{ab} the periodic Green function on $\mathbb{T}_{ab}^2 = (\mathbb{R}/a\mathbb{Z}) \times (\mathbb{R}/b\mathbb{Z})$ that solves

$$\Delta F_{ab}(\boldsymbol{x}) = 2\pi(\delta(\boldsymbol{x}) - \frac{1}{ab}), \text{for } \boldsymbol{x} \in \mathbb{T}_{ab}^2. \tag{5.7.2}$$

Note that for initial data ψ_0^ε of the form in section 5.1, we have $\mathbf{P}_0 = 2\pi\mathbf{J}\bar{\boldsymbol{x}}$. The corresponding numerical test is in section 4 and 5.

Figure 5.27 presents a verification on the convergence of the GRDLs. The trajectories from GRDLs are in first row of Figure 5.27 and the plot of δ^ε in the second row shows the convergence of vortex trajectories clearly. In the trajectories plots w.r.t t, we can also see that the crossing time (when $x_1 = x_2$) of two vortex dipoles is approximate $t = 0.02$, this coincides well with the simulation in Figure 5.24. The plots of $\delta^\varepsilon(t)$ show the convergence of vortex center trajectories to GRDLs as $\varepsilon \downarrow 0$. Figure 5.28 gives a verification for GRDLs on general rectangle domain. Comparing the trajectories from GRDLs (first chart of Figure 5.28) with vortex center detected from simulation of Case VI setups (the artificial dot line in Figure 5.26), we can see they have the same shape quantitatively. The second chart in Figure 5.28 shows that the trajectories of vortex centers converge to the GRDLs in (5.7.1) as $\varepsilon \downarrow 0$.

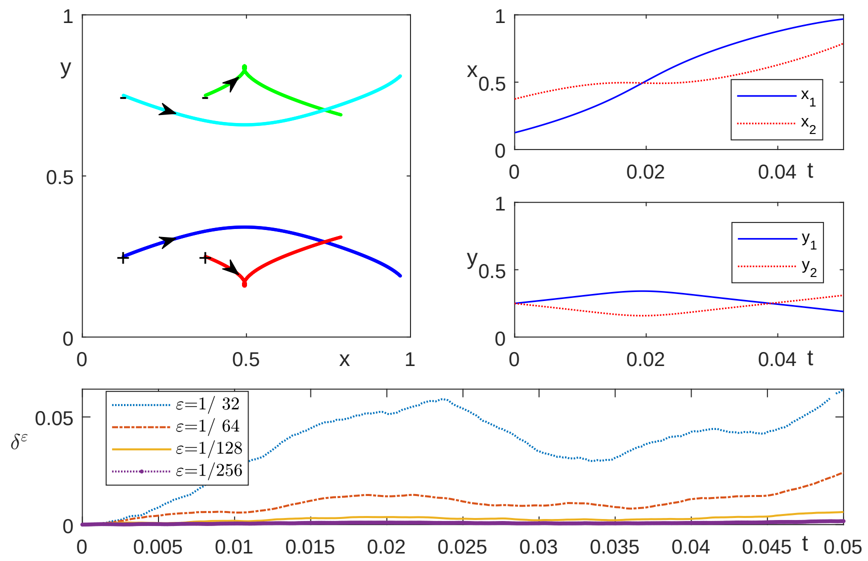

Figure 5.27: Vortex trajectories of a leapfrogging motion (Case V) from GRDLs (first row); corresponding convergence test (second row).

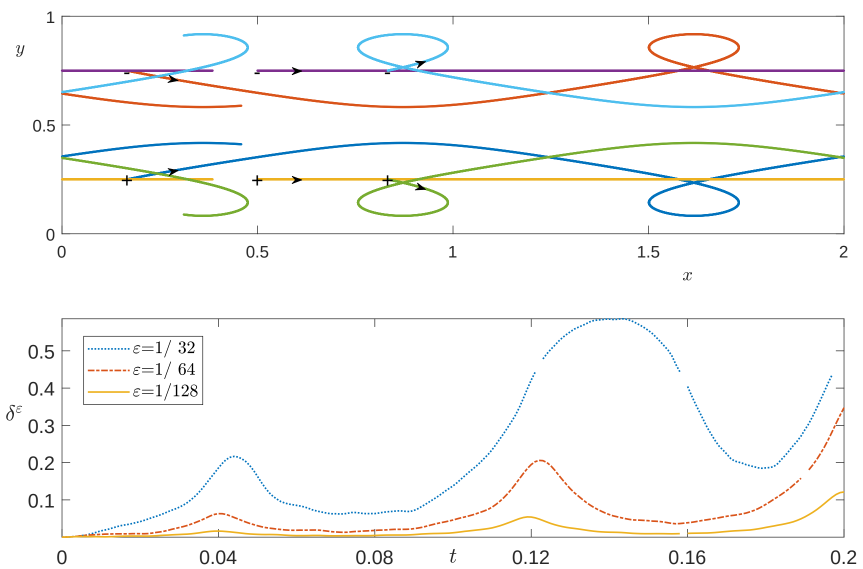

Figure 5.28: Vortex trajectories of a leapfrogging motion (Case VI) from GRDLs (first row); corresponding convergence test (second row).

Chapter 6

Conclusions and Perspectives

This thesis proposed several fourth-order compact finite difference schemes (4cFD-s) for some highly oscillatory dispersive PDEs, including the nonlinear Klein-Gordon equitation (NKGE), Zakharov system (ZS), and nonlinear Schrödinger equation (NLSE). Both conservative and efficient 4cFDs were considered, and rigorous error bounds of these schemes were established.

For NKGE in the nonrelativistic regime, two 4cFDs including a Crank-Nicolson one and a semi-implicit one were derived. The optimal error estimates for the two 4cFDs were rigorously analysed through energy methods and cut-off techniques. The conservation of discrete energy of CN-4cFD was also proved. Under proper boundedness and smoothness assumptions on the analytical solutions, the error bounds of the two schemes are both at $O(h^4 + \tau^2/\varepsilon^6)$.

For ZS in the subsonic regime, with a dimensionless parameter ε inversely proportional to the acoustic speed, the solutions oscillate with $O(\varepsilon)$ wavelength in time, $O(1/\varepsilon)$ speed in space, and $O(\varepsilon^2)$ and $O(1)$ amplitudes for well-prepared and ill-prepared initial data respectively. For CSI-4cFD, a uniform error bound at $O(h^4 + \tau^{2\alpha^\dagger/3})$ for the well- and less-ill-prepared initial data and an error bound at $O(h^4/\varepsilon^{1-\alpha^*} + \tau^2/\varepsilon^{3-\alpha^*})$ for the ill-prepared initial data were proved, where $\alpha^\dagger \in [1, 2]$ and $\alpha^* \in [0, 1)$ are parameters independent of ε that describe the illness of initial data. For UA-4cFD, the uniform error bound independent of ε for the well- and less-ill-prepared initial data is at $O(h^4 + \tau^{4/3})$; and the uniform error bound for the ill-prepared initial data is at $O(h^4 + \tau^{(1+\alpha^*)/(2+\alpha^*)})$. The uniform error bounds were achieved by taking a minimum of two errors depending on ε, an error from standard energy method and an error between ZS and its limiting equation. The compact schemes provide much better spatial resolution than general second order methods and reduce the computational cost a lot, and these techniques can easily be generalized. Therefore, we can extend this asymptotic consistent formulation of ZS to other coupled Zakharov system such as Klein-Gordon-Zakharov system and get some uniform error bounds in the future.

Last but not least, we studied systematically the quantized vortex interactions in two dimensional NLSE with periodic boundary conditions (BCs). Here, we adopt the 4cFD method to discretize the Laplace's equation with non-standard BCs in order to prepare accurate initial data satisfying the periodic BCs. We verified the convergence to the reduced dynamical laws under the zero initial momentum limit assumption, which confirmed the analytical results in the literature. In addition, based on our numerical results for nonzero initial momentum limit cases, we formalized a conjecture on generalized reduced dynamical laws. Further simulations on general cases of vortex dynamics such as vortex dynamics of NLSE with non-local interaction and quantum turbulence simulations are worth considering for future works.

Bibliography

[1] M. J. Ablowitz, *Nonlinear Dispersive Waves: Asymptotic Analysis and Solitons*, vol. 47, Cambridge University Press, 2011.

[2] H. Added and S. Added, *Equations of Langmuir turbulence and nonlinear Schrödinger equation: smoothness and approximation*, J. Funct. Anal., 79 (1988), pp. 183–210.

[3] S. K. Adhikari and L. Salasnich, *Nonlinear Schrödinger equation for a superfluid Bose gas from weak coupling to unitarity: Study of vortices*, Phys. Rev. A, 77 (2008), article 033618.

[4] X. Antoine, W. Bao, and C. Besse, *Computational methods for the dynamics of the nonlinear Schrödinger/Gross-Pitaevskii equations*, Comput. Phys. Commun., 184 (2013), pp. 2621–2633.

[5] W. Bao and Y. Cai, *Uniform error estimates of finite difference methods for the nonlinear Schrödinger equation with wave operator*, SIAM J. Numer. Anal., 50 (2012), pp. 492–521.

[6] ——, *Mathematical theory and numerical methods for Bose-Einstein condensation*, Kinet. Relat. Models, 6 (2013), pp. 1–135.

[7] ——, *Optimal error estimates of finite difference methods for the Gross-Pitaevskii equation with angular momentum rotation*, Math. Comp., 82 (2013), pp. 99–128.

[8] W. Bao, Y. Cai, and X. Zhao, *A uniformly accurate multiscale time integrator pseudospectral method for the Klein-Gordon equation in the nonrelativistic limit regime*, SIAM J. Numer. Anal., 52 (2014), pp. 2488–2511.

[9] W. Bao and X. Dong, *Analysis and comparison of numerical methods for the Klein-Gordon equation in the nonrelativistic limit regime*, Numer. Math., 120 (2012), pp. 189–229.

[10] W. Bao, X. Dong, and X. Zhao, *An exponential wave integrator sine pseudospectral method for the Klein-Gordon-Zakharov system*, SIAM J. Sci. Comput., 35 (2013), pp. A2903–A2927.

[11] ——, *Uniformly accurate multiscale time integrators for highly oscillatory second order differential equations*, J. Math. Study, 47 (2014), pp. 111–150.

[12] W. Bao, Y. Feng, and W. Yi, *Long time error analysis of finite difference time domain methods for the nonlinear Klein-Gordon equation with weak nonlinearity*, Commun. Comput. Phys., 26 (2019), pp. 1307–1334.

[13] W. Bao, D. Jaksch, and P. A. Markowich, *Numerical solution of the Gross-Pitaevskii equation for Bose-Einstein condensation*, J. Comput. Phys., 187 (2003), pp. 318–342.

[14] W. Bao, S. Jin, and P. A. Markowich, *On time-splitting spectral approximations for the Schrödinger equation in the semiclassical regime*, J. Comput. Phys., 175 (2002), pp. 487–524.

[15] ——, *Numerical study of time-splitting spectral discretizations of nonlinear Schrödinger equations in the semiclassical regimes*, SIAM J. Sci. Comput., 25 (2003), pp. 27–64.

[16] W. Bao and C. Su, *Uniform error bounds of a finite difference method for the Zakharov system in the subsonic limit regime via an asymptotic consistent formulation*, Multiscale Model. Simul., 15 (2017), pp. 977–1002.

[17] ——, *A uniformly and optimally accurate method for the Zakharov system in the subsonic limit regime*, SIAM J. Sci. Comput., 40 (2018), pp. A929–A953.

[18] W. Bao and F. Sun, *Efficient and stable numerical methods for the generalized and vector Zakharov system*, SIAM J. Sci. Comput., 26 (2005), pp. 1057–1088.

[19] W. Bao, F. Sun, and G. W. Wei, *Numerical methods for the generalized Zakharov system*, J. Comput. Phys., 190 (2003), pp. 201–228.

[20] W. Bao and Q. Tang, *Numerical study of quantized vortex interaction in the Ginzburg-Landau equation on bounded domains*, Commun. Comput. Phys., 14 (2013), pp. 819–850.

[21] ——, *Numerical study of quantized vortex interactions in the nonlinear Schrödinger equation on bounded domains*, Multiscale Model. Simul., 12 (2014), pp. 411–439.

[22] W. Bao, Q. Tang, and T. Zhang, *Numerical simulations of vortex interactions in the nonlinear Schrödinger equation with periodic boundary condition*, in preparation.

[23] W. Bao, R. Zeng, and Y. Zhang, *Quantized vortex stability and interaction in the nonlinear wave equation*, Phys. D, 237 (2008), pp. 2391–2410.

[24] W. Bao and X. Zhao, *Comparison of numerical methods for the nonlinear Klein-Gordon equation in the nonrelativistic limit regime*, J. Comput. Phys., 398 (2019), article 108886.

[25] C. F. Barenghi, R. J. Donnelly, and W. Vinen, *Quantized Vortex Dynamics and Superfluid Turbulence*, vol. 571, Springer Science & Business Media, 2001.

[26] G. Berikelashvili, M. M. Gupta, and M. Mirianashvili, *Convergence of fourth order compact difference schemes for three-dimensional convection-diffusion equations*, SIAM J. Numer. Anal., 45 (2007), pp. 443–455.

[27] C. Besse, B. Bidgaray, and S. Descombes, *Order estimates in time of splitting methods for the nonlinear Schrödinger equation*, SIAM J. Numer. Anal., 40 (2002), pp. 26–40.

[28] C. Besse, R. Carles, and F. Mhats, *An asymptotic preserving scheme based on a new formulation for NLS in the semiclassical limit*, Multiscale Model. Simul., 11 (2013), pp. 1228–1260.

[29] G. P. Bewley, M. S. Paoletti, K. R. Sreenivasan, and D. P. Lathrop, *Characterization of reconnecting vortices in superfluid helium*, Proc. Natl. Acad. Sci., 105 (2008), pp. 13707–13710.

[30] J. Bourgain and J. Colliander, *On wellposedness of the Zakharov system*, Int. Math. Res. Not. IMRN, (1996), pp. 515–546.

[31] A. Bratsos, *On the numerical solution of the Klein-Gordon equation*, Numer. Methods Partial Differential Eq., 25 (2009), pp. 939–951.

[32] Y. Cai and Y. Yuan, *Uniform error estimates of the conservative finite difference method for the Zakharov system in the subsonic limit regime*, Math. Comp., 87 (2018), pp. 1191–1225.

[33] W.-M. Cao and B.-Y. Guo, *Fourier collocation method for solving nonlinear Klein-Gordon equation*, J. Comput. Phys., 108 (1993), pp. 296–305.

[34] R. Carles, R. Danchin, and J.-C. Saut, *Madelung, Gross-Pitaevskii and Korteweg*, Nonlinearity, 25 (2012), pp. 2843–3873.

[35] M. H. Carpenter, D. Gottlieb, and S. Abarbanel, *Time-stable boundary conditions for finite-difference schemes solving hyperbolic systems: methodology and application to high-order compact schemes*, J. Comput. Phys., 111 (1994), pp. 220–236.

[36] T. Cazenave, *Semilinear Schrödinger Equations*, vol. 10, American Mathematical Soc., 2003.

[37] Q. Chang, E. Jia, and W. Sun, *Difference schemes for solving the generalized nonlinear Schrödinger equation*, J. Comput. Phys., 148 (1999), pp. 397–415.

[38] Q. S. Chang, B. L. Guo, and H. Jiang, *Finite difference method for generalized Zakharov equations*, Math. Comp., 64 (1995), pp. 537–553.

[39] S. J. Chapman and G. Richardson, *Motion of vortices in type II superconductors*, SIAM J. Appl. Math., 55 (1995), pp. 1275–1296.

[40] D. S. Clark, *Short proof of a discrete Gronwall inequality*, Discrete Appl. Math., 16 (1987), pp. 279–281.

[41] J. Colliander and R. Jerrard, *Vortex dynamics for the Ginzburg-Landau-Schrödinger equation*, Int. Math. Res. Not. IMRN, 1998 (1998), pp. 333–358.

[42] ——, *Ginzburg-Landau vortices: weak stability and Schrödinger equation dynamics*, J. Anal. Math., 77 (1999), pp. 129–205.

[43] M. Dehghan and A. Shokri, *Numerical solution of the nonlinear Klein–Gordon equation using radial basis functions*, J. Comput. Appl. Math., 230 (2009), pp. 400–410.

[44] M. Dehghan and A. Taleei, *A compact split-step finite difference method for solving the nonlinear Schrödinger equations with constant and variable coefficients*, Comput. Phys. Comm., 181 (2010), pp. 43–51.

[45] R. O. Dendy, *Plasma Dynamics*, Clarendon Press, 1990.

[46] X. Dong, Z. Xu, and X. Zhao, *On time-splitting pseudospectral discretization for nonlinear Klein-Gordon equation in nonrelativistic limit regime*, Commun. Comput. Phys., 16 (2014), pp. 440–466.

[47] R. J. Donnelly, *Quantized Vortices in Helium II*, vol. 2, Cambridge University Press, 1991.

[48] E. Faou and K. Schratz, *Asymptotic preserving schemes for the Klein-Gordon equation in the non-relativistic limit regime*, Numer. Math., 126 (2014), pp. 441–469.

[49] Y. Feng, *Long time error analysis of the fourth-order compact finite difference methods for the nonlinear Klein-Gordon equation with weak nonlinearity*, Numer. Methods Partial Differential Eq., 37 (2021), pp. 897–914.

[50] G. Fibich, *The Nonlinear Schrödinger Equation*, Springer, 2015.

[51] J. Ginibre, Y. Tsutsumi, and G. Velo, *On the Cauchy problem for the Zakharov system*, J. Funct. Anal., 151 (1997), pp. 384–436.

[52] J. Ginibre and G. Velo, *The global Cauchy problem for the nonlinear Klein-Gordon equation*, Math. Z., 189 (1985), pp. 487–505.

[53] ——, *The global Cauchy problem for the nonlinear Klein-Gordon equation. II*, Ann. Inst. H. Poincaré Anal. Non Linéaire, 6 (1989), pp. 15–35.

[54] L. Glangetas and F. Merle, *Existence of self-similar blow-up solutions for Zakharov equation in dimension two. I*, Comm. Math. Phys., 160 (1994), pp. 173–215.

[55] R. T. Glassey, *Approximate solutions to the Zakharov equations via finite differences*, J. Comput. Phys., 100 (1992), pp. 377–383.

[56] ——, *Convergence of an energy-preserving scheme for the Zakharov equations in one space dimension*, Math. Comp., 58 (1992), pp. 83–102.

[57] E. Heinz, *An elementary analytic theory of the degree of mapping in n-dimensional space*, J. Math. Mech., 8 (1959), pp. 231–247.

[58] R. S. Hirsh, *Higher order accurate difference solutions of fluid mechanics problems by a compact differencing technique*, J. Comput. Phys., 19 (1975), pp. 90–109.

[59] K. Huang, C. Xiong, and X. Zhao, *Scalar-field theory of dark matter*, Internat. J. Modern Phys. A, 29 (2014), article 1450074.

[60] M. Ikuta, Y. Sugano, and H. Saito, *Symmetry-breaking instability of leapfrogging vortex rings in a Bose-Einstein condensate*, Phys. Rev. A, 99 (2019), article 043610.

[61] R. L. Jerrard and D. Spirn, *Refined Jacobian estimates and Gross-Pitaevsky vortex dynamics*, Arch. Ration. Mech. Anal., 190 (2008), pp. 425–475.

[62] A. J. Jerri, *The Shannon sampling theoremits various extensions and applications: A tutorial review*, Proc. IEEE, 65 (1977), pp. 1565–1596.

[63] S. Jin, P. A. Markowich, and C. Zheng, *Numerical simulation of a generalized Zakharov system*, J. Comput. Phys., 201 (2004), pp. 376–395.

[64] J.-L. Joly, G. Métivier, and J. Rauch, *Diffractive nonlinear geometric optics with rectification*, Indiana Univ. Math. J., (1998), pp. 1167–1241.

[65] M. Kobayashi, P. Parnaudeau, F. Luddens, C. Lothod, L. Danaila, M. Brachet, and I. Danaila, *Quantum turbulence simulations using the GrossPitaevskii equation: High-performance computing and new numerical benchmarks*, Comput. Phys. Commun, 258 (2020), article 107579.

[66] R. Landes, *On Galerkin's method in the existence theory of quasilinear elliptic equations*, J. Funct. Anal., 39 (1980), pp. 123–148.

[67] O. Lange and B. Schroers, *Unstable manifolds and Schrödinger dynamics of Ginzburg-Landau vortices*, Nonlinearity, 15 (2002), p. 1471.

[68] S. K. Lele, *Compact finite difference schemes with spectral-like resolution*, J. Comput. Phys., 103 (1992), pp. 16–42.

[69] M. Li, T. Tang, and B. Fornberg, *A compact fourth-order finite difference scheme for the steady incompressible Navier-Stokes equations*, Internat. J. Numer. Methods Fluids, 20 (1995), pp. 1137–1151.

[70] X. Li and B. Guo, *A Legendre pseudospectral method for solving nonlinear Klein-Gordon equation*, J. Comput. Math., (1997), pp. 105–126.

[71] C.-S. Lin and C.-L. Wang, *Elliptic functions, Green functions and the mean field equations on tori*, Ann. of Math., (2010), pp. 911–954.

[72] F. H. Lin, *Some dynamical properties of Ginzburg-Landau vortices*, Comm. Pure Appl. Math., 49 (1996), pp. 323–360.

[73] ——, *Complex Ginzburg-Landau equations and dynamics of vortices, filaments, and codimension-2 submanifolds*, Comm. Pure Appl. Math., 51 (1998), pp. 385–441.

[74] F.-H. Lin and Q. Du, *Ginzburg-Landau vortices: Dynamics, pinning, and hysteresis*, SIAM J. Math. Anal., 28 (1997), pp. 1265–1293.

[75] F.-H. Lin and J. Xin, *On the incompressible fluid limit and the vortex motion law of the nonlinear Schrödinger equation*, Comm. Math. Phys., 200 (1999), pp. 249–274.

[76] F. Linares and G. Ponce, *Introduction to Nonlinear Dispersive Equations*, Springer, New York, 2015.

[77] Y. Luo, X. Li, and C. Guo, *Fourth-order compact and energy conservative scheme for solving nonlinear Klein-Gordon equation*, Numer. Methods Partial Differential Eq., 33 (2017), pp. 1283–1304.

[78] Y. Ma and C. Su, *A uniformly and optimally accurate multiscale time integrator method for the Klein-Gordon-Zakharov system in the subsonic limit regime*, Comput. Math. Appl., 76 (2018), pp. 602–619.

[79] S. Machihara, *The nonrelativistic limit of the nonlinear Klein-Gordon equation*, Funkcial. Ekvac., 44 (2001), pp. 243–252.

[80] S. Machihara, K. Nakanishi, and T. Ozawa, *Nonrelativistic limit in the energy space for nonlinear Klein-Gordon equations*, Math. Ann., 322 (2002), pp. 603–621.

[81] N. Masmoudi and K. Nakanishi, *From nonlinear Klein-Gordon equation to a system of coupled nonlinear Schrödinger equations*, Math. Ann., 324 (2002), pp. 359–389.

[82] N. Masmoudi and K. Nakanishi, *Energy convergence for singular limits of Zakharov type systems*, Invent. Math., 172 (2008), pp. 535–583.

[83] R. I. McLachlan and G. R. W. Quispel, *Splitting methods*, Acta Numer., 11 (2002), pp. 341–434.

[84] F. Merle, *Blow-up results of viriel type for Zakharov equations*, Comm. Math. Phys., 175 (1996), pp. 433–455.

[85] P. Mironescu, *On the stability of radial solutions of the Ginzburg-Landau equation*, J. Funct. Anal., 130 (1995), pp. 334–344.

[86] A. Mohebbi and M. Dehghan, *High-order compact solution of the one-dimensional heat and advection–diffusion equations*, Appl. Math. Model., 34 (2010), pp. 3071–3084.

[87] K. W. Morton and D. F. Mayers, *Numerical Solution of Partial Differential Equations*, Cambridge University Press, Cambridge, second ed., 2005.

[88] B. Najman, *The nonrelativistic limit of the nonlinear Klein-Gordon equation*, Nonlinear Anal., 15 (1990), pp. 217–228.

[89] M. Nakamura and T. Ozawa, *The Cauchy problem for nonlinear Klein-Gordon equations in the Sobolev spaces*, Publ. Res. Inst. Math. Sci., 37 (2001), pp. 255–293.

[90] J. C. Neu, *Vortices in complex scalar fields*, Phys. D, 43 (1990), pp. 385–406.

[91] T. Ozawa, Y. Tsutsumi, and H. Brezis, *The nonlinear Schrödinger limit and the initial layer of the Zakharov equations*, Differ. Integral Equ., 5 (1992), pp. 721–745.

[92] J. A. Pava, *Nonlinear Dispersive Equations: Existence and Stability of Solitary and Periodic Travelling Wave Solutions*, no. 156, American Mathematical Soc., 2009.

[93] V. Penna, *Quantum dynamics of two-dimensional vortex pairs with arbitrary total vorticity*, Phys. Rev. B, 59 (1999), p. 7127.

[94] A. Péntek, T. Tél, and T. Toroczkai, *Chaotic advection in the velocity field of leapfrogging vortex pairs*, J. Phys. Math. Gen., 28 (1995), pp. 2191–2216.

[95] N. Riley and D. P. Stevens, *A note on leapfrogging vortex rings*, Fluid Dyn. Res., 11 (1993), pp. 235–244.

[96] C. Rorai, K. Sreenivasan, and M. E. Fisher, *Propagating and annihilating vortex dipoles in the Gross-Pitaevskii equation*, Phys. Rev. B, 88 (2013), article 134522.

[97] J. Sanz-Serna and J. Verwer, *Conerservative and nonconservative schemes for the solution of the nonlinear Schrödinger equation*, IMA J. Numer. Anal., 6 (1986), pp. 25–42.

[98] S. H. Schochet and M. I. Weinstein, *The nonlinear Schrödinger limit of the Zakharov equations governing Langmuir turbulence*, Comm. Math. Phys., 106 (1986), pp. 569–580.

[99] K. Schratz and X. Zhao, *On comparison of asymptotic expansion techniques for nonlinear Klein-Gordon equation in the nonrelativistic limit regime*, Discrete Contin. Dyn. Syst. Ser. B, 25 (2020), pp. 2841–2865.

[100] I. Segal, *The global Cauchy problem for a relativistic scalar field with power interaction*, Bulletin de la S. M. F., 91 (1963), pp. 129–135.

[101] S. Serafini, L. Galantucci, E. Iseni, T. Bienaimé, R. N. Bisset, C. F. Barenghi, F. Dalfovo, G. Lamporesi, and G. Ferrari, *Vortex reconnections and rebounds in trapped atomic Bose-Einstein condensates*, Phys. Rev. X, 7 (2017), article 021031.

[102] J. Shen, T. Tang, and L.-L. Wang, *Spectral Methods: Algorithms, Analysis and Applications*, vol. 41, Springer Science & Business Media, 2011.

[103] J. C. Simon and E. Taflin, *The Cauchy problem for non-linear Klein-Gordon equations*, Comm. Math. Phys., 152 (1993), pp. 433–478.

[104] G. Smith, *Numerical Solution of Partial Differential Equations: Finite Difference Methods*, Oxford university press, 1985.

[105] W. Strauss and L. Vazquez, *Numerical solution of a nonlinear Klein-Gordon equation*, J. Comput. Phys., 28 (1978), pp. 271–278.

[106] C. Su, *Comparison of numerical methods for the Zakharov system in the subsonic limit regime*, J. Comput. Appl. Math., 330 (2018), pp. 441–455.

[107] T. Tao, *Nonlinear Dispersive Equations: Local and Global Analysis*, no. 106, American Mathematical Soc., 2006.

[108] B. Texier, *Derivation of the Zakharov equations*, Arch. Ration. Mech. Anal., 184 (2007), pp. 121–183.

[109] V. Thomée, *Galerkin Finite Element Methods for Parabolic Problems*, vol. 1054, Springer, 1984.

[110] Z. Tian and Y. Ge, *A fourth-order compact finite difference scheme for the steady stream function-vorticity formulation of the Navier-Stokes/Boussinesq equations*, Internat. J. Numer. Methods Fluids, 41 (2003), pp. 495–518.

[111] M. Tsutsumi, *Nonrelativistic approximation of nonlinear Klein-Gordon equations in two space dimensions*, Nonlinear Anal., 8 (1984), pp. 637–643.

[112] J. Wang, *Multisymplectic numerical method for the Zakharov system*, Comput. Phys. Comm., 180 (2009), pp. 1063–1071.

[113] T. Wang and B. Guo, *Unconditional convergence of two conservative compact difference schemes for non-linear Schrödinger equation in one dimension*, Sci. Sin. Math., 41 (2011), pp. 207–233.

[114] T. Wang, B. Guo, and Q. Xu, *Fourth-order compact and energy conservative difference schemes for the nonlinear Schrödinger equation in two dimensions*, J. Comput. Phys., 243 (2013), pp. 382–399.

[115] T. Wang and X. Zhao, *Optimal l^∞ error estimates of finite difference methods for the coupled Gross-Pitaevskii equations in high dimensions*, Sci. China Math., 57 (2014), pp. 2189–2214.

[116] T. Wang and X. Zhao, *Unconditional L^∞-convergence of two compact conservative finite difference schemes for the nonlinear Schrödinger equation in multi-dimensions*, Calcolo, 55 (2018), p. 34.

[117] Y. Wang and X. Zhao, *Symmetric high order Gautschi-type exponential wave integrators pseudospectral method for the nonlinear Klein-Gordon equation in the nonrelativistic limit regime*, Int. J. Numer. Anal. Model., 15 (2018), pp. 405–427.

[118] Y. Xia, Y. Xu, and C.-W. Shu, *Local discontinuous Galerkin methods for the generalized Zakharov system*, J. Comput. Phys., 229 (2010), pp. 1238–1259.

[119] S.-S. Xie, G.-X. Li, and S. Yi, *Compact finite difference schemes with high accuracy for one-dimensional nonlinear Schrödinger equation*, Comput. Methods Appl. Mech. Engrg., 198 (2009), pp. 1052–1060.

[120] C. Xiong, M. R. Good, Y. Guo, X. Liu, and K. Huang, *Relativistic superfluidity and vorticity from the nonlinear Klein-Gordon equation*, Phys. Rev. D, 90 (2014), article 125019.

[121] Z. Xu, W. Bao, and S. Shi, *Quantized vortex dynamics and interaction patterns in superconductivity based on the reduced dynamical law*, Discrete Contin. Dyn. Syst. Ser. B, 23 (2018), pp. 2265–2297.

[122] V. E. Zakharov et al., *Collapse of Langmuir waves*, Sov. Phys. JETP, 35 (1972), pp. 908–914.

[123] J. Zhang, *An explicit fourth-order compact finite difference scheme for three-dimensional convection-diffusion equation*, Comm. Numer. Methods Engrg., 14 (1998), pp. 209–218.

[124] T. Zhang and Q. Tang, *Uniform error bounds of a 4th-order compact finite difference methods for the Zakharov system of an asymptotic consistent formulation in the subsonic regime*, in preparation.

[125] T. Zhang and T. Wang, *Uniform error bounds of 4th-order compact finite difference methods for the Zakharov system in the subsonic regime*, preprint.

[126] ——, *Optimal error estimates of fourth-order compact finite difference methods for the nonlinear Klein-Gordon equation in the nonrelativistic regime*, Numer. Methods Partial Differential Eq., 37 (2021), pp. 2089–2108.

[127] Y. Zhang, W. Bao, and Q. Du, *The dynamics and interaction of quantized vortices in the Ginzburg–Landau–Schrödinger equation*, SIAM J. Appl. Math., 67 (2007), pp. 1740–1775.

[128] ——, *Numerical simulation of vortex dynamics in Ginzburg-Landau-Schrödinger equation*, European J. Appl. Math., 18 (2007), pp. 607–630.

[129] X. Zhou and L. Zhang, *A conservative compact difference scheme for the Zakharov equations in one space dimension*, Int. J. Comput. Math., 95 (2018), pp. 279–302.

[130] D. W. Zingg, *Comparison of high-accuracy finite-difference methods for linear wave propagation*, SIAM J. Sci. Comput., 22 (2000), pp. 476–502.

List of Publications

1. T. Zhang and T. Wang, *Optimal error estimates of fourth-order compact finite difference methods for the nonlinear Klein-Gordon equation in the non-relativistic regime*, Numer. Methods Partial Differential Eq., 37 (2021), pp. 2089–2108.

2. T. Zhang and T. Wang, *Uniform error bounds of 4th-order compact finite difference methods for the Zakharov system in the subsonic regime*, preprint.

3. T. Zhang and Q. Tang, *Uniform error bounds of a 4th-order compact finite difference methods for the Zakharov system of an asymptotic consistent formulation in the subsonic regime*, In preparation.

4. W. Bao and Q. Tang and T. Zhang, *Numerical simulations of vortex interactions in the nonlinear Schrödinger equation with periodic boundary condition*, In preparation.

Error bounds of 4th-order compact finite difference methods for some dispersive partial differential equations and their applications **Teng Zhang** **2021**